WOMEN IN SCIENCE - PATHOLOGY 2021

EDITED BY: Sabrina Battista and Wei Jiang
PUBLISHED IN: Frontiers in Medicine

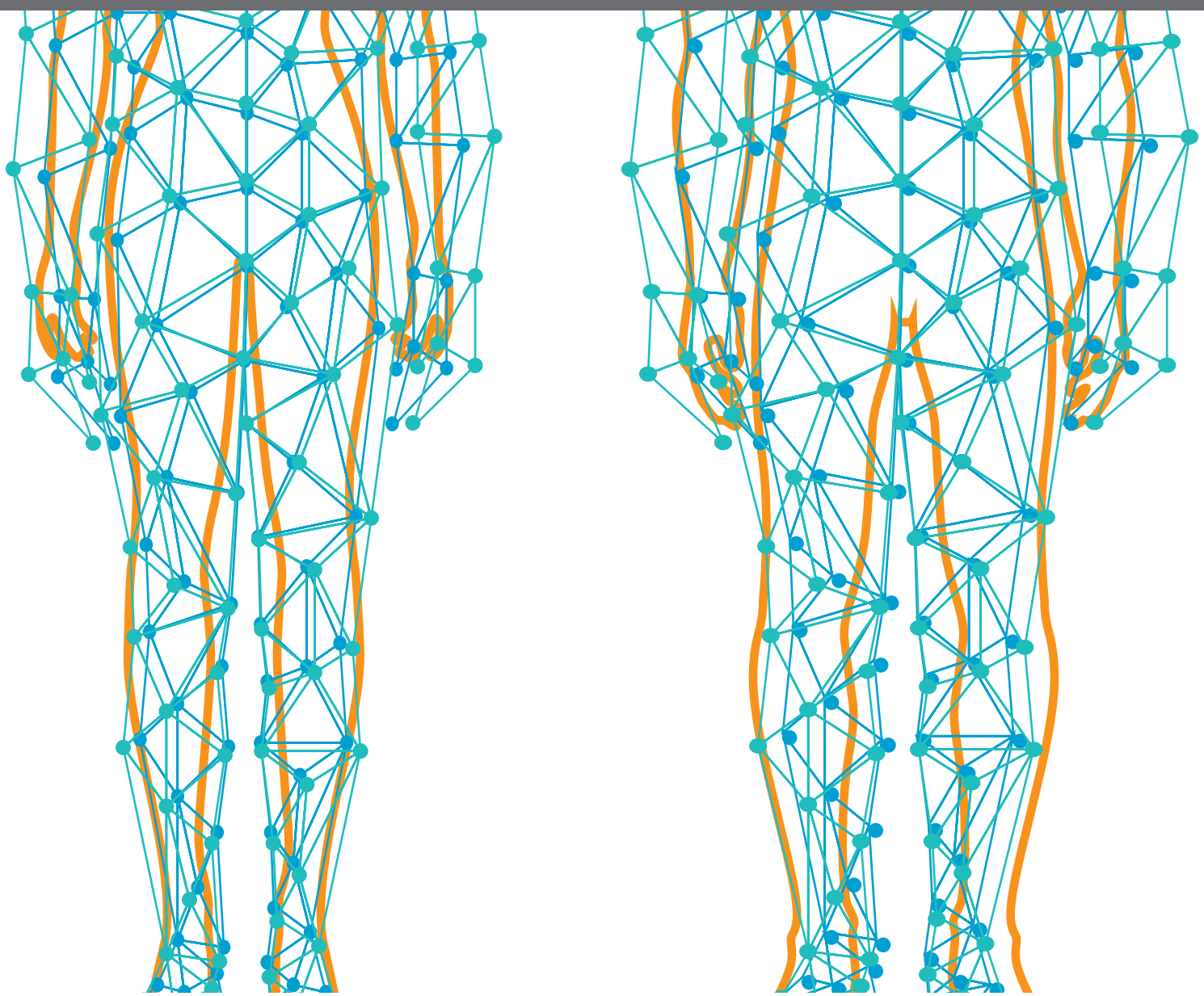

frontiers Research Topics

ISSN 1664-8714
ISBN 978-2-83250-218-1
DOI 10.3389/978-2-83250-218-1

About Frontiers

Frontiers is more than just an open-access publisher of scholarly articles: it is a pioneering approach to the world of academia, radically improving the way scholarly research is managed. The grand vision of Frontiers is a world where all people have an equal opportunity to seek, share and generate knowledge. Frontiers provides immediate and permanent online open access to all its publications, but this alone is not enough to realize our grand goals.

Frontiers Journal Series

The Frontiers Journal Series is a multi-tier and interdisciplinary set of open-access, online journals, promising a paradigm shift from the current review, selection and dissemination processes in academic publishing. All Frontiers journals are driven by researchers for researchers; therefore, they constitute a service to the scholarly community. At the same time, the Frontiers Journal Series operates on a revolutionary invention, the tiered publishing system, initially addressing specific communities of scholars, and gradually climbing up to broader public understanding, thus serving the interests of the lay society, too.

Dedication to Quality

Each Frontiers article is a landmark of the highest quality, thanks to genuinely collaborative interactions between authors and review editors, who include some of the world's best academicians. Research must be certified by peers before entering a stream of knowledge that may eventually reach the public - and shape society; therefore, Frontiers only applies the most rigorous and unbiased reviews.
Frontiers revolutionizes research publishing by freely delivering the most outstanding research, evaluated with no bias from both the academic and social point of view. By applying the most advanced information technologies, Frontiers is catapulting scholarly publishing into a new generation.

What are Frontiers Research Topics?

Frontiers Research Topics are very popular trademarks of the Frontiers Journals Series: they are collections of at least ten articles, all centered on a particular subject. With their unique mix of varied contributions from Original Research to Review Articles, Frontiers Research Topics unify the most influential researchers, the latest key findings and historical advances in a hot research area! Find out more on how to host your own Frontiers Research Topic or contribute to one as an author by contacting the Frontiers Editorial Office: frontiersin.org/about/contact

WOMEN IN SCIENCE - PATHOLOGY 2021

Topic Editors:
Sabrina Battista, Institute for Endocrinology and Experimental Oncology Gaetano Salvatore, National Research Council (CNR), Italy
Wei Jiang, Medical University of South Carolina, United States

Citation: Battista, S., Jiang, W., eds. (2022). Women in Science - Pathology 2021. Lausanne: Frontiers Media SA. doi: 10.3389/978-2-83250-218-1

Table of Contents

frontiers in Medicine

CASE REPORT
published: 24 June 2021
doi: 10.3389/fmed.2021.689895

Case Report: Analysis of Circulating Tumor Cells in a Triple Negative Spindle-Cell Metaplastic Breast Cancer Patient

Tania Rossi[1], Michela Palleschi[2], Davide Angeli[3], Michela Tebaldi[3], Giovanni Martinelli[4], Ivan Vannini[1], Maurizio Puccetti[5], Francesco Limarzi[6], Roberta Maltoni[7], Giulia Gallerani[1†] and Francesco Fabbri[1†]*

[1] Biosciences Laboratory, IRCCS Istituto Romagnolo per lo Studio dei Tumori (IRST) "Dino Amadori", Meldola, Italy, [2] Department of Medical Oncology, IRCCS Istituto Romagnolo per lo Studio dei Tumori (IRST) "Dino Amadori", Meldola, Italy, [3] Unit of Biostatistics and Clinical Trials, IRCCS Istituto Romagnolo per lo Studio dei Tumori (IRST) "Dino Amadori", Meldola, Italy, [4] Scientific Directorate, IRCCS Istituto Scientifico Romagnolo per lo Studio dei Tumori (IRST) "Dino Amadori", Meldola, Italy, [5] Azienda Unità Sanitaria Locale Imola, Imola, Italy, [6] Pathology Unit, Morgagni-Pierantoni Hospital, Forlì, Italy, [7] Healthcare Administration, IRCCS Istituto Romagnolo per lo Studio dei Tumori (IRST) "Dino Amadori", Meldola, Italy

OPEN ACCESS

Edited by:
Dario de Biase, University of Bologna, Italy

Reviewed by:
Ivonne Nel, Leipzig University, Germany
Liubov A. Tashireva, Tomsk Cancer Research Institute (RAS), Russia

***Correspondence:**
Tania Rossi
tania.rossi@irst.emr.it

† These authors have contributed equally to this work and share last authorship

Specialty section:
This article was submitted to Pathology, a section of the journal Frontiers in Medicine

Received: *01 April 2021*
Accepted: *17 May 2021*
Published: *24 June 2021*

Citation:
Rossi T, Palleschi M, Angeli D, Tebaldi M, Martinelli G, Vannini I, Puccetti M, Limarzi F, Maltoni R, Gallerani G and Fabbri F (2021) Case Report: Analysis of Circulating Tumor Cells in a Triple Negative Spindle-Cell Metaplastic Breast Cancer Patient. Front. Med. 8:689895. doi: 10.3389/fmed.2021.689895

Circulating tumor cells (CTCs) are a rare population of cells found in the bloodstream and represent key players in the metastatic cascade. Their analysis has proved to provide further core information concerning the tumor. Herein, we aim at investigating CTCs isolated from a 32-year-old patient diagnosed with triple negative spindle-shaped metaplastic breast cancer (MpBC), a rare tumor poorly responsive to therapies and with a dismal prognosis. The molecular analysis performed on the primary tumor failed to underline effective actionable targets to address the therapeutic strategy. Besides the presence of round-shaped CTCs, cells with a spindle shape were present as well, and through molecular analysis, we confirmed their malignant nature. This aspect was coherent with the primary tumor histology, proving that CTCs are released regardless of their morphology. Copy number aberration (CNA) profiling and variant analysis using next-generation sequencing (NGS) showed that these cells did not harbor the alterations exhibited by the primary tumor (*PIK3CA* G1049A mutation, *MYC* copy number gain). However, despite the great heterogeneity observed, the amplification of regions involved in metastasis emerged (8q24.22–8q24.23). Our findings support the investigation of CTCs to identify alterations that could have a role in the metastatic process. To the best of our knowledge, this is the first examination of CTCs in an MpBC patient.

Keywords: metaplastic breast cancer, circulating tumor cells, next generation sequencing, copy number aberration, metastasis, liquid biopsy

INTRODUCTION

Among all the breast malignancies, metaplastic breast cancer (MpBC) accounts for <1% and has a dismal prognosis, worse than the other BC types. Pathologically, MpBCs are ductal carcinomas composed by one or more cell populations that have undergone metaplastic transformation into a non-glandular pattern, leading to the presence of epithelial (e.g., squamous cells) and sarcomatous (e.g., chondroid, spindle cell, and osseous) elements. The World Health Organization (WHO)

further divides MpBCs in subgroups, resulting in a plethora of chemorefractory and aggressive MpBC variants (1–3).

Despite the paucity of MpBC cases, some studies in literature have detected epithelial-to-mesenchymal transition (EMT), phosphoinositide 3-kinase (PI3K) signaling, epidermal growth factor receptor (EGFR) signaling, and others as the major altered pathways in this disease (3). Nevertheless, the lack of actionable targets remains a matter of concern, and conventional regimens of chemotherapy mainstay are the gold standards for treatment together with surgery and radiation therapy (4, 5). However, the poor survival and the high recurrence rates further emphasize the inadequacy of the available treatment options and the imperative need to individuate appropriate therapeutic strategies.

Genetic and phenotypic heterogeneity is a hallmark of MpBC and has important reflections for cancer treatment as the presence of multiple clones may hide cells responsible for relapse (6, 7). In this context, the characterization of circulating tumor cells (CTCs), a rare population of cells considered as pro-metastasis precursors (8), may be helpful in the unraveling of tumor heterogeneity (9).

We report a case of a patient diagnosed with triple negative spindle-cell MpBC for which molecular analysis of the primary tumor failed to highlight valid actionable alterations. We decided to characterize CTCs at both morphological and molecular levels, as they may bring out new alterations to be explored. To the best of our knowledge, this is the first examination of CTCs in a MpBC patient.

CASE PRESENTATION

Here we report the case of a 32-year-old patient (**Figure 1**) who presented, on December 20, 2018, during breastfeeding, a clinical onset of a right breast lump. Ultrasound-guided core biopsy of this right breast mass was performed with histological diagnosis of metaplastic spindle-cell infiltrating carcinoma of the breast, estrogen receptor (ER) = 0%, progesterone receptor (PgR) = 0%, HER2-neu negative (score 0), and Ki-67 = 90%. She had a past history of Crohn's disease, at the time of MpBC diagnosis during treatment with mesalamine. Positron emission tomography-computed tomography (PET-CT) revealed a 40-mm lesion in the right breast without bone or visceral involvement. In January 2019, treatment began with neoadjuvant chemotherapy (NAC) with adryamicin (60 mg/m^2) and cyclophosphamide (600 mg/m^2) intravenous for one cycle. Due to local progression, NAC was switched to docetaxel for one cycle (January 23, 2019), but the patient experienced further local progression.

In February 2019, she underwent right mastectomy with axillary node dissection; the histopathology exam describes a lesion of 65-mm maximum diameter, ypT3 ypN0 M0, ER = 0%, PgR = 0%, HER2-neu negative (score 0), and Ki-67 = 90%. The microscopic photograph (10× magnification) of hematoxylin and eosin staining of the resected tumor is reported in **Figure 2**. On immunostains, the tumor cells were strongly positive for vimentin and showed weak positivity for p63. Cytokeratins (AE1/AE3 clone) and E-cadherin were positive in scattered cells. Moreover, CAM5.2, calponin, SMA, GATA-3, ALK, ER, PR, and Her2-neu were negative. Expression of programmed death-ligand 1 (PD-L1) was <1%.

From March to June 2019, she received adjuvant weekly paclitaxel (80 mg/m^2) for 12 cycles. From July to August 2019 right chest radiotherapy (total dose 50 Gy) was performed.

In November 2019, PET-CT scan revealed the presence of a 40 × 37-mm lung lesion and other sub-centimeter bilateral lung nodules. Further analyses on primary tumor revealed no *BRCA1*/*BRCA2* alterations.

From November to December 2019, she received two cycles of cisplatin (60 mg/m^2; day 1), vinorelbine (20 mg/m^2; days 1 and 3), and capecitabine (500 mg thrice a day).

In January 2020, PET-CT showed lung, bone, and bilateral ovarian progression. The NGS Oncomine Focus Assay (Thermo Fisher Scientific) on the primary tumor exposed the G1049A *PIK3CA* mutation and amplification of the *MYC* locus (copy number: 26 copies).

In January 2020, she received two cycles of eribulin (1.23 mg/m^2), and in February, she underwent bilateral ovariectomy and wedge liver resection. The histopathology exam described triple negative metaplastic BC metastases. Moreover, several subcutaneous metastases on the scalp, neck, and chest arise, other than bilateral lung nodules. After multidisciplinary meeting, in consideration of the absence of valid therapeutic alternatives, physicians decided to start an "off-label" treatment regimen: doxorubicin (30 mg/m^2) plus bevacizumab (15 mg/kg every 3 weeks) plus everolimus (7.5 mg daily) (10).

In February 2020, she started the first cycle (without bevacizumab due to recent surgery), with a clinically stable disease, improvement on pain, and reduction of all subcutaneous nodules. Before chemotherapy administration, CTC investigation was performed.

In March 2020, she received the second cycle (including bevacizumab). She had a clinical benefit in terms of the disappearance of most subcutaneous metastases, no pain, and a good quality of life until April 2020 when she complained of fever, cough, and low blood pressure. Therefore, she was hospitalized for the appropriate treatment with antibiotics and steroids without benefit, and she died on April 21, 2020 due to respiratory failure.

ISOLATION OF CIRCULATING TUMOR CELLS AND ANALYSES

To investigate the features of CTCs, approximately 9 ml of peripheral blood was collected in a PAXGene Blood ccfDNA tube before the administration of the off-label therapy. CTCs were enriched from whole blood by immunomagnetic negative selection. In order to identify the highest number of CTCs, we opted for antibody cocktails for the detection of each phenotype, instead of a single target for each channel. EpCAM, CKs, and E-cadherin antibodies were used to identify epithelial phenotype (phycoerythrin, PE channel), and N-cadherin, ABCG2, CD44v6, and CD133 were used to identify stem/mesenchymal phenotype (allophycocyanin, APC channel). Hoechst 33342 (DAPI channel) was used for nuclear staining

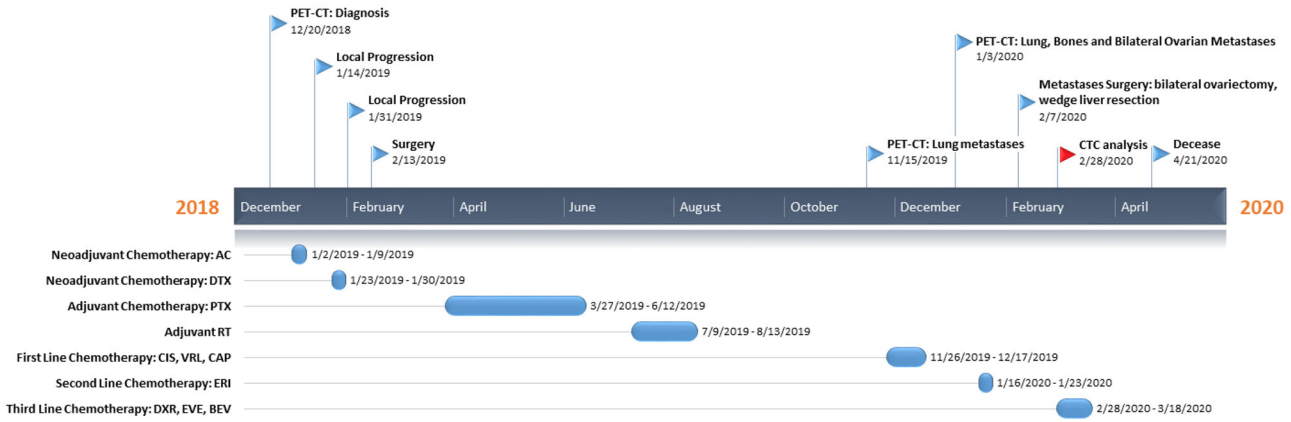

FIGURE 1 | Patient's timeline. At the top, we reported the milestones of her clinical course, while on the bottom the treatment regimens administered to the patient. PET-CT, positron emission tomography-computed tomography; AC, adryamicin-cyclophosphamide; DTX, docetaxel; PTX, paclitaxel; CIS, cisplatin; VRL, vinorelbine; CAP, capecitabine; ERI, eribulin; DXR, doxorubicin; EVE, everolimus; BEV, bevacizumab; CTC, circulating tumor cell.

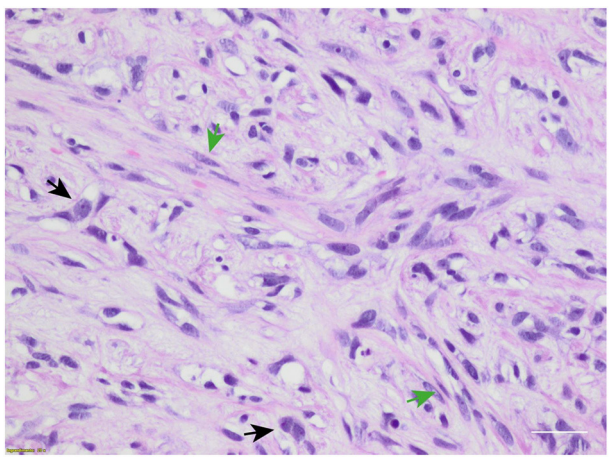

FIGURE 2 | Microscopic hematoxylin and eosin photograph of metaplastic breast carcinoma (MpBC) with coexisting spindled (green arrows) and oval (black arrows) cells. Scale bar: 50 μm.

and anti-CD45 Alexafluor488 antibody (FITC channel) as leukocyte marker for CTC negative selection. CTC identification and analysis were performed by DEPArray NxT platform (**Figure 3A**). To set up the auto-fluorescence signal detected in FITC channel, we used MCF7 cell line (CD45–) and leukocytes (CD45+) (**Supplementary Figure 1**).

We identified non-canonical cells positive for both epithelial and stem/mesenchymal targets with a spindle-shaped morphology ($n = 14$) and CTCs with a round-shaped morphology ($n = 184$). CTC clusters ($n = 5$) were present as well (**Supplementary Figure 2**). Due to the high amount of debris into the sample, we successfully sorted one single spindle-shaped cell (ID: 793) and two 10-CTC pools (Pool 1 and Pool 2).

Next, we aimed at assessing the molecular characteristics of the MpBC patient's CTCs isolated through DEPArray and to establish the nature of the spindle-shaped cell. To do this, we massively amplified the genome of the samples using Ampli1 WGA kit (Menarini-Silicon Biosystems) to obtain evaluable genetic material, then we proceeded with library construction and sequencing for copy number aberrations (CNAs) and single nucleotide variant (SNV) analyses.

For CNAs, libraries were prepared using the Ampli1 LowPass kit for Ion Torrent (Menarini-Silicon Biosystems).

After Ion 520 chip loading was performed on Ion Torrent Chef (Thermo Fisher Scientific), sequencing was carried out on an Ion S5 System (Thermo Fisher Sc.), and CNAs were called with Control-FREEC (11). Through this technique, we were able to unequivocally establish the tumor nature of the unconventional spindle-shaped CTC (ID: 793), since it was characterized by an aneuploid genome with an altered CNA profile (**Figure 3B**). Through intersection bioinformatic analysis, we observed that the greatest part of the entire genome was not comparable among the three samples, suggesting high heterogeneity levels. We detected only three mutual aberrant regions (4p16.1, 8q24.22–8q24.23, and 22q12.3) shared among the samples, which were always in gain. The genes within the mentioned regions are reported in **Supplementary Table 1**. We did not observe the gain of *MYC* gene, which was observed in the primary tumor molecular characterization. Moreover, after whole genome amplification, we assessed the mutational status of 60 cancer-related genes. Libraries were prepared using the Ampli1 OncoSeek kit (Menarini Silicon Biosystems) and run on a 300-cycle V2 cartridge on the miSeq instrument (Illumina Inc.). We did not observe the *PIK3CA* mutation G1049A, which emerged at primary tumor NGS analysis. The single CTC 793 harbored the homozygous *RET* I602V and heterozygous M249V variant of gene *MAP2K1*. Interestingly, we also found a heterozygous synonymous C50C variant of *TP53* that, although not responsible for the amino acid change in protein structure, may be associated with gene expression regulation as it occurs in the noncoding exon 1 (12). Concerning the 10-CTC pools, in Pool 1, we found the variants *KRAS* S17I (frequency 80%),

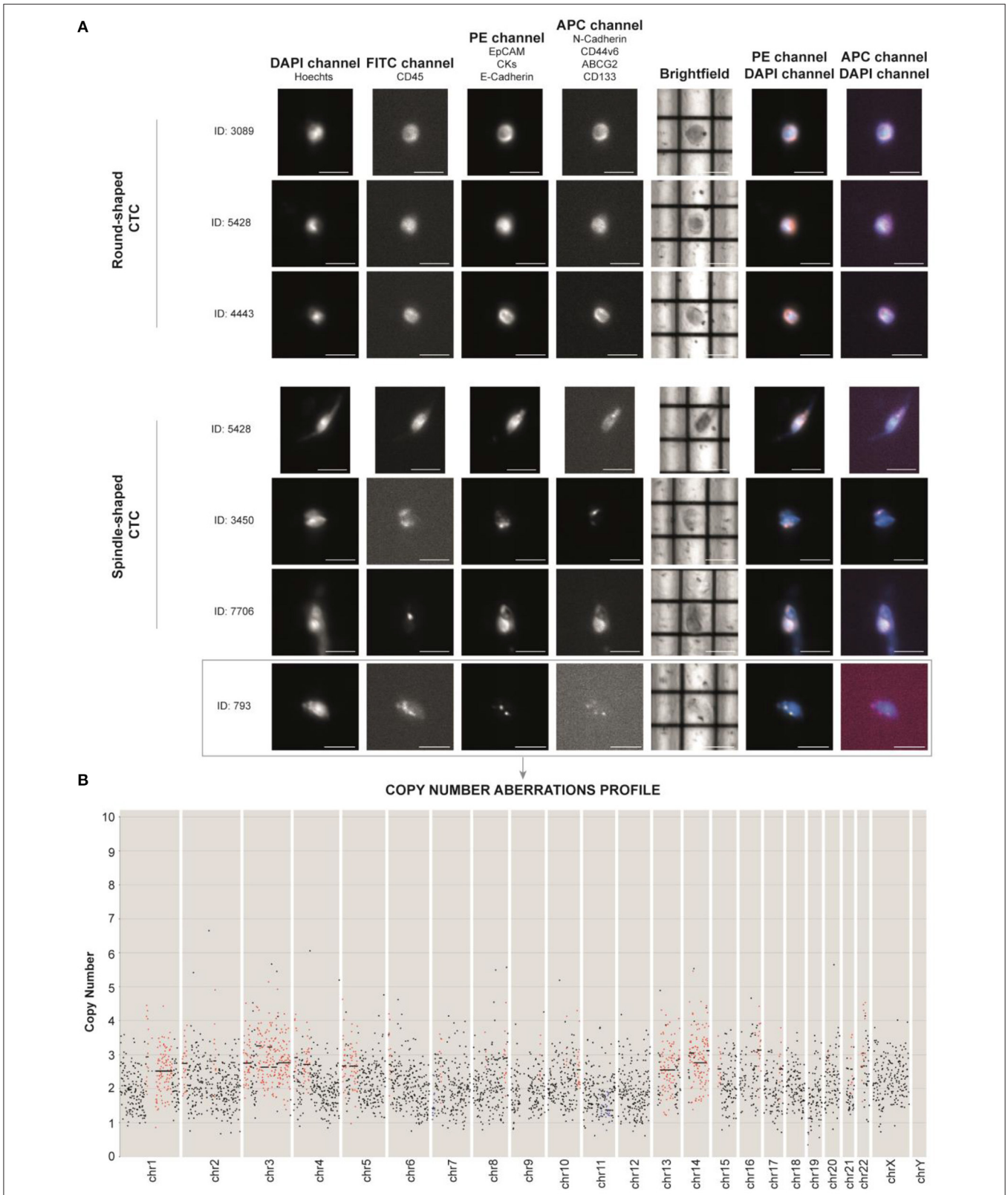

FIGURE 3 | (A) DEPArray images of the most representative single circulating tumor cells (CTCs) of the patient based on their shape (round- and spindle-shaped). The DAPI channel was used for nuclear staining using Hoechst 33342, PE channel for epithelial tag [anti-EPCAM, anti-cytokeratins (CKs) and anti-E-cadherin antibodies],

(Continued)

FIGURE 3 | and APC channel for mesenchymal tag (anti-N-cadherin, anti-CD44v6, anti-ABCG2, and anti-CD133 antibodies). Anti-CD45 (FITC channel) was used for CTC negative selection (**Supplementary Figure 1**). Scale bar: 30 μm. **(B)** Profiling of the CTC ID: 793 reveals the presence of aberrant regions, consistent with tumor nature. Chromosomes (Chr) and number of copies are reported along the *x*- and *y*-axis, respectively. Black dots in the figure represent chromosome regions with a normal diploid copy number. Conversely, red dots and blue dots indicate, respectively, significant copy number gains (copies > 2) and losses (copies < 2), called by Control-FREEC (11).

PIK3CA W498C (20%), *PTEN* A34T (16%), *MET* T835N (14%), *PIK3CA* L1026I (14%), *SMAD4* Q249R (10%), *KIT* G534V (10%), *MAP2K1* G131A and N122K (10%), and *PTEN* M35T (10%). Pool 2 harbored the *HRAS* frameshift deletion I46fs (20%) and the non-synonymous SNV of *RB1* R556G (10%). None of the detected variants were already described as pathogenic in literature, and no variants were identified in common among the samples. However, frequencies of some alterations found in samples Pool 1 and Pool 2 reveal that more than one cell within each pool harbor certain mutations.

DISCUSSION

Here, we report a case of a 32-year-old patient diagnosed with triple-negative spindle-cell MpBC, a rare disease with marked tendency to metastasize to secondary organs. Because of the paucity of cases, few is known about the molecular mechanisms underlying its aggressiveness, and no druggable targets have been identified yet.

Investigation of the primary tumor performed through an NGS-based approach detected alterations that are not uniquely ascribable to MpBC and failed to underline effective actionable targets to address the therapeutic strategy. Indeed, *MYC* copy number gain (13, 14) and *PIK3CA* mutation (15, 16) are widely described in the literature to be involved in many cancer types, including BC (17, 18). Herein, by exploiting a liquid biopsy approach, we emphasize that the characterization of CTCs, rare cells with a crucial role in the metastatic cascade, could be worthwhile to guide the investigation of the molecular mechanisms underlying rare tumors. However, this study has some weaknesses. First, due to the high amount of debris in the sample, it was not possible for us to recover, for downstream analysis, all the CTCs found. Moreover, the primary tumor and metastatic tissue specimens were not available, making impossible the comparison with CTCs, except for clinical reports. Conversely, to the best of our knowledge, this is the first investigation of CTCs in an MpBC case and could have a strong impact in the improvement of personalized medicine in the future. In fact, the investigation of CTCs has the potential to unmask the intra-tumor heterogeneity of MpBC, revealing the presence of under-represented clones from the primary tumor. Simultaneously, longitudinal molecular profiling of CTCs could reveal acquired resistance mechanism, helping to address the therapeutic strategy (19).

Our analysis revealed a high count of CTCs expressing both epithelial and mesenchymal markers in the peripheral blood of the MpBC patient. CTC enumeration and evaluation have been performed in a delayed period after removal of the primary tumor. Therefore, in the absence of their major source, CTCs are likely to come from secondary homing sites such as bone marrow or other occult niches (9, 20).

The first criterion concerned the different morphology of CTCs retrieved in the bloodstream of the patient. Along with the canonical round CTCs, we found unconventional cells characterized by a spindle morphology, whose nature was confirmed to be cancerous due to the presence of CNAs along the genome. A study by Yu et al., conducted on non-metaplastic BC patients, demonstrates that besides the presence of round-shaped CTCs with unconventional morphology associated with EMT initiation, therapy failure and tumor progression were present as well (21). However, it is not clear whether the presence of both round- and spindle-shaped CTCs in this MpBC case assumes the same meaning as in non-metaplastic BC, or is consistent with tumor histology solely. Indeed, the cytopathology of CTCs detected in this MpBC case is coherent with primary tumor histology, in which oval and spindle-shaped cells were shown to coexist. Thorough analysis on the metastatic site specimens would provide further information about the role of CTC morphology in MpBC tumor progression.

Concerning molecular analyses, we found that CTCs did not harbor primary tumor-specific alterations (*MYC* copy number gain and G1049A *PIK3CA* mutation). In addition, CTC samples had discordant CNAs and SNVs compared with each other, suggesting molecular heterogeneity as well. These results are consistent with the presence of circulating heterogeneous subclones with a potential role in tumor progression and resistance to therapies. Accordingly, in the HR-positive metastatic BC patient, CTCs could circulate as heterogeneous subclones and harbor molecular alterations that could drive to different mechanisms of resistance to endocrine therapies (22). Together with our data, these findings support the need to increase the application of CTCs in the clinical practice to gain further complementary information concerning the tumor evolution, including therapy resistance.

CNA profiling revealed the existence of three amplified genomic regions (4p16.1, 8q24.22–8q24.23, and 22q12.3) shared among the CTC samples. Among these, region 8q24.22–8q24.23 turned out to be highly attractive.

Amplification of chromosome 8q regions has been described in numerous cancer types, such as hepatocellular carcinoma (23), gastric cancer (24), clear cell renal carcinoma (25), and BC (26). In particular, in BC, 8q is considered a hotspot site of amplification associated with unfavorable prognosis (27) and, accordingly in our study, poor response to NAC (28), in part due to the location of c-myc locus in 8q24.1, near 8q24.22–8q24.23. However, the tendency to drive metastasis is not only imputable to *MYC* solely, but other genes have been hypothesized to enhance the

metastatic process, as reported by Han and collaborators (28). Accordingly, investigation of CTCs revealed that several cancer-associated genes were found altered, but not *MYC*.

For instance, *WISP1* codifies for WNT1-inducible signaling pathway protein 1 (WISP1/CCN4), a member of the CCN family that acts as an oncogene in BC. It has been shown to stimulate EMT and metastasis, and to modulate the expression of the tumor suppressor N-myc downstream-regulated gene 1 (NDRG1) in BC cell lines. This modulation occurs through the NDGR1 gene promoter, which is located within the 8q24.23 site (29). However, the role of this tumor-suppressor protein is controversial, as recent data highlighted that NDRG1 expression is a predictor of worse prognosis in inflammatory BC patients receiving adjuvant radiotherapy (30). Both *WISP1* and *NDGR1* loci are included within the regions that we found in gain in all the CTC samples.

Another gene located in the 8q22.2 locus that recently emerged as a metastasis driver is the Otoconin 90 (*OC90*) gene. Although it is normally expressed in the cochlea for appropriate otolith development, its expression and gene amplification were observed in different cancer types, such as breast, prostate, and lung cancer. In TNBC cell lines, *OC90* overexpression was shown to increase invasion, and knockdown reduced cellular viability and invasiveness (31).

Taken together, despite high levels of heterogeneity, we observed that the analysis of CTCs at the molecular level can potentially drive to the discovery of chromosomal regions that may have a role in the metastatic cascade. In the future, this aspect could be helpful to deepen the knowledge regarding MpBC and to address new therapeutic strategies.

DATA AVAILABILITY STATEMENT

The datasets presented in this article are not readily available for ethical and privacy reasons. Requests to access the datasets should be directed to the corresponding author.

ETHICS STATEMENT

Ethical review and approval was not required for the study on human participants in accordance with the local legislation and institutional requirements. The patients/participants provided their written informed consent to participate in this study. Written informed consent was obtained from the individual(s) for the publication of any potentially identifiable images or data included in this article.

AUTHOR CONTRIBUTIONS

TR, MPa, GM, IV, GG, and FF contributed to the conceptualization and design of the study. TR and MPa wrote the first draft. DA and MT performed bioinformatic analysis. TR, MPa, MPu, FL, RM, and GG contributed to data collection. GG and FF reviewed the final draft before submission. All authors contributed to the manuscript revision, and read and approved the submitted version.

SUPPLEMENTARY MATERIAL

The Supplementary Material for this article can be found online at: https://www.frontiersin.org/articles/10.3389/fmed.2021.689895/full#supplementary-material

REFERENCES

1. Pezzi CM, Patel-Parekh L, Cole K, Franko J, Klimberg VS, Bland K. Characteristics and treatment of metaplastic breast cancer: analysis of 892 cases from the national cancer data base. *Ann Surg Oncol.* (2006) 14:166–73. doi: 10.1245/s10434-006-9124-7
2. Tray N, Taff J, Adams S. Therapeutic landscape of metaplastic breast cancer. *Cancer Treat Rev.* (2019) 79:101888. doi: 10.1016/j.ctrv.2019.08.004
3. Reddy TP, Rosato RR, Li X, Moulder S, Piwnica-Worms H, Chang JC. A comprehensive overview of metaplastic breast cancer: clinical features and molecular aberrations. *Breast Cancer Res.* (2020) 22:121. doi: 10.1186/s13058-020-01353-z
4. Chen IC, Lin CH, Huang CS, Lien HC, Hsu C, Kuo WH, et al. Lack of efficacy to systemic chemotherapy for treatment of metaplastic carcinoma of the breast in the modern era. *Breast Cancer Res Treat.* (2011) 130:345–51. doi: 10.1007/s10549-011-1686-9
5. Al-Hilli Z, Choong G, Keeney MG, Visscher DW, Ingle JN, Goetz MP, et al. Metaplastic breast cancer has a poor response to neoadjuvant systemic therapy. *Breast Cancer Res Treat.* (2019) 176:709–16. doi: 10.1007/s10549-019-05264-2
6. Geyer FC, Weigelt B, Natrajan R, Lambros MB, de Biase D, Vatcheva R, et al. Molecular analysis reveals a genetic basis for the phenotypic diversity of metaplastic breast carcinomas. *J Pathol.* (2010) 220:562–73. doi: 10.1002/path.2675
7. Kim C, Gao R, Sei E, Brandt R, Hartman J, Hatschek T, et al. Chemoresistance evolution in triple-negative breast cancer delineated by single-cell sequencing. *Cell.* (2018) 173:879–93.e13. doi: 10.1016/j.cell.2018.03.041
8. Yu T, Wang C, Xie M, Zhu C, Shu Y, Tang J, et al. Heterogeneity of CTC contributes to the organotropism of breast cancer. *Biomed Pharmacother.* (2021) 137:111314. doi: 10.1016/j.biopha.2021.111314
9. Rossi T, Gallerani G, Angeli D, Cocchi C, Bandini E, Fici P, et al. Single-cell NGS-based analysis of copy number alterations reveals new insights in circulating tumor cells persistence in early-stage breast cancer. *Cancers.* (2020) 12:2490. doi: 10.3390/cancers12092490
10. Basho RK, Yam C, Gilcrease M, Murthy RK, Helgason T, Karp DD, et al. Comparative effectiveness of an mTOR-based systemic therapy regimen in advanced, metaplastic and nonmetaplastic triple-negative breast cancer. *Oncologist.* (2018) 23:1300–9. doi: 10.1634/theoncologist.2017-0498
11. Boeva V, Popova T, Bleakley K, Chiche P, Cappo J, Schleiermacher G, et al. Control-FREEC: a tool for assessing copy number and allelic content using next-generation sequencing data. *Bioinformatics.* (2012) 28:423–5. doi: 10.1093/bioinformatics/btr670
12. Hainaut P, Pfeifer GP. Somatic TP53 mutations in the era of genome sequencing. *Cold Spring Harb Perspect Med.* (2016) 6:a026179. doi: 10.1101/cshperspect.a026179
13. Lee KS, Kwak Y, Nam KH, Kim D-W, Kang S-B, Choe G, et al. c-MYC copy-number gain is an independent prognostic factor in patients with colorectal cancer. *PLoS ONE.* (2015) 10:e0139727. doi: 10.1371/journal.pone.0139727
14. Ribeiro FR, Henrique R, Martins AT, Jerónimo C, Teixeira MR. Relative copy number gain of MYC in diagnostic needle biopsies is an independent prognostic factor for prostate cancer patients. *Eur Urol.* (2007) 52:116–25. doi: 10.1016/j.eururo.2006.09.018

15. Mei ZB, Duan CY, Li CB, Cui L, Ogino S. Prognostic role of tumor PIK3CA mutation in colorectal cancer: a systematic review and meta-analysis. *Ann Oncol.* (2016) 27:1836–48. doi: 10.1093/annonc/mdw264
16. Seo AN, Kang BW, Bae HI, Kwon OK, Park KB, Lee SS, et al. Exon 9 mutation of PIK3CA associated with poor survival in patients with Epstein-Barr virus-associated gastric cancer. *Anticancer Res.* (2019) 39:2145–54. doi: 10.21873/anticanres.13328
17. Nedeljković M, Tanić N, Dramićanin T, Milovanović Z, Šušnjar S, Milinković V, Vujović I, et al. Importance of copy number alterations of FGFR1 and C-MYC genes in triple negative breast cancer. *J Med Biochem.* (2019) 38:63–70. doi: 10.2478/jomb-2018-0012
18. Keraite I, Alvarez-Garcia V, Garcia-Murillas I, Beaney M, Turner NC, Bartos C, et al. PIK3CA mutation enrichment and quantitation from blood and tissue. *Sci Rep.* (2020) 10:17082. doi: 10.1038/s41598-020-74086-w
19. Alix-Panabières C, Pantel K. Clinical applications of circulating tumor cells and circulating tumor DNA as liquid biopsy. *Cancer Discov.* (2016) 6:479–91. doi: 10.1158/2159-8290.CD-15-1483
20. Banys M, Krawczyk N, Becker S, Jakubowska J, Staebler A, Wallwiener D, et al. The influence of removal of primary tumor on incidence and phenotype of circulating tumor cells in primary breast cancer. *Breast Cancer Res Treat.* (2012) 132:121–9. doi: 10.1007/s10549-011-1569-0
21. Yu M, Bardia A, Wittner BS, Stott SL, Smas ME, Ting DT, et al. Circulating breast tumor cells exhibit dynamic changes in epithelial and mesenchymal composition. *Science.* (2013) 339:580–4. doi: 10.1126/science.1228522
22. Paoletti C, Cani AK, Larios JM, Hovelson DH, Aung K, Darga EP, et al. Comprehensive mutation and copy number profiling in archived circulating breast cancer tumor cells documents heterogeneous resistance mechanisms. *Cancer Res.* (2018) 78:1110–22. doi: 10.1158/0008-5472.CAN-17-2686
23. Zhao K, Zhao Y, Zhu J-Y, Dong H, Cong W-M, Yu Y, et al. A panel of genes identified as targets for 8q24.13-24.3 gain contributing to unfavorable overall survival in patients with hepatocellular carcinoma. *Curr Med Sci.* (2018) 38:590–6. doi: 10.1007/s11596-018-1918-x
24. Kang JU. Chromosome 8q as the most frequent target for amplification in early gastric carcinoma. *Oncol Lett.* (2014) 7:1139–43. doi: 10.3892/ol.2014.1849
25. Klatte T, Kroeger N, Rampersaud EN, Birkhäuser FD, Logan JE, Sonn G, et al. Gain of chromosome 8q is associated with metastases and poor survival of patients with clear cell renal cell carcinoma. *Cancer.* (2012) 118:5777–82. doi: 10.1002/cncr.27607
26. Ching HC, Naidu R, Seong MK, Har YC, Taib NAM. Integrated analysis of copy number and loss of heterozygosity in primary breast carcinomas using high-density SNP array. *Int J Oncol.* (2011) 39:621–33. doi: 10.3892/ijo.2011.1081
27. Zhang Y, Martens JWM, Yu JX, Jiang J, Sieuwerts AM, Smid M, et al. Copy number alterations that predict metastatic capability of human breast cancer. *Cancer Res.* (2009) 69:3795–801. doi: 10.1158/0008-5472.CAN-08-4596
28. Han S, Park K, Shin E, Kim H-J, Kim JY, Kim JY, et al. Genomic change of chromosome 8 predicts the response to taxane-based neoadjuvant chemotherapy in node-positive breast cancer. *Oncol Rep.* (2010) 24:121–8. doi: 10.3892/or_00000836
29. Chiang K-C, Yeh C-N, Chung L-C, Feng T-H, Sun C-C, Chen M-F, et al. WNT-1 inducible signaling pathway protein-1 enhances growth and tumorigenesis in human breast cancer. *Sci Rep.* (2015) 5:8686. doi: 10.1038/srep08686
30. Villodre ES, Gong Y, Hu X, Huo L, Yoon EC, Ueno NT, et al. NDRG1 expression is an independent prognostic factor in inflammatory breast cancer. *Cancers.* (2020) 12:3711. doi: 10.3390/cancers12123711
31. Pearlman A, Rahman MT, Upadhyay K, Loke J, Ostrer H. Ectopic Otoconin 90 expression in triple negative breast cancer cell lines is associated with metastasis functions. *PLoS ONE.* (2019) 14:e0211737. doi: 10.1371/journal.pone.0211737

Conflict of Interest: The authors declare that the research was conducted in the absence of any commercial or financial relationships that could be construed as a potential conflict of interest.

frontiers in Medicine

ORIGINAL RESEARCH
published: 23 September 2021
doi: 10.3389/fmed.2021.746909

Dedifferentiated Central Chondrosarcoma: A Clinical, Histopathological, and Immunohistochemical Analysis of 57 Cases

Li-Hua Gong[1], Yong-Bin Su[2], Wen Zhang[1], Wei-Feng Liu[3], Rong-Fang Dong[1], Xiao-Qi Sun[1], Ming Zhang[1] and Yi Ding[1]**

[1] Department of Pathology, Beijing Jishuitan Hospital, The Fourth Medical College of Peking University, Beijing, China, [2] Department of Radiology, Beijing Jishuitan Hospital, The Fourth Medical College of Peking University, Beijing, China, [3] Department of Orthopedic Oncology Surgery, Beijing Jishuitan Hospital, Fourth Medical College of Peking University, Beijing, China

OPEN ACCESS

Edited by:
Andrey Bychkov,
Kameda Medical Center, Japan

Reviewed by:
Thiyaphat Laohawetwanit,
Thammasat University, Thailand
Kris Lami,
Nagasaki University, Japan

***Correspondence:**
Li-Hua Gong
lhgong2005@126.com
Yi Ding
jst_blk@126.com

Specialty section:
This article was submitted to Pathology, a section of the journal Frontiers in Medicine

Received: 25 July 2021
Accepted: 31 August 2021
Published: 23 September 2021

Citation:
Gong L-H, Su Y-B, Zhang W, Liu W-F, Dong R-F, Sun X-Q, Zhang M and Ding Y (2021) Dedifferentiated Central Chondrosarcoma: A Clinical, Histopathological, and Immunohistochemical Analysis of 57 Cases. Front. Med. 8:746909. doi: 10.3389/fmed.2021.746909

Dedifferentiated central chondrosarcoma (DCCS) is a rare cartilage tumor with invasive biological behavior and a poor prognosis. To better understand the morphological characteristics of this type of tumor and its internal mechanism of dedifferentiation, we retrospectively analyzed 57 cases of DCCS. A total of 29 female and 28 male patients were included, ranging in age from 20 to 76 years, with a median age of 54 years. Fifty-seven cases of DCCS occurred in the pelvis ($n = 29$), femur ($n = 17$), scapula ($n = 4$), tibia ($n = 2$), humerus ($n = 2$), metatarsals ($n = 1$), fibula ($n = 1$), and radius ($n = 1$). Radiologically, DCCS had two different appearances on imaging, with an area showing calcifications of the cartilage forming the tumor juxtaposed to a lytic area with a highly aggressive, non-cartilaginous component. Histopathologically, the distinctive morphological features consisted of two kinds of defined components: a well-differentiated cartilaginous tumor and non-cartilaginous sarcoma. The cartilaginous components included grade 1 ($n = 38$; 66.7%) and grade 2 ($n = 19$; 33.3%) cartilage. The sarcoma components included those of osteosarcoma ($n = 29$; 50.9%), undifferentiated pleomorphic sarcoma ($n = 20$; 35.1%), rhabdomyosarcoma ($n = 3$; 5.2%), fibrosarcoma ($n = 2$; 3.5%), spindle cell sarcoma ($n = 2$; 3.5%) and angiosarcoma ($n = 1$; 1.8%). Immunohistochemistry showed that the expression of p53 and RB in the sarcoma components was significantly higher than that in the cartilaginous components, suggesting that these factors play roles in the dedifferentiation process of chondrosarcoma. DCCS is a highly malignant tumor with a poor prognosis. Except for the patients who were lost to follow-up, most of our patients died.

Keywords: dedifferentiated, chondrosarcoma, central, imaging, immunohistochemistry

INTRODUCTION

Dedifferentiated chondrosarcoma (DCS) is a high-grade chondrosarcoma with the bimorphic histological appearance of a conventional chondrosarcoma with abrupt transition to non-cartilaginous sarcoma (1). In the literature, the reported incidence of DCS in chondrosarcoma cases is 10–15% (2). This type of tumor usually occurs between the ages of 50 and 60 years and occurs more frequently in males (3). It is most often located in the pelvis and long bones such as the proximal femur or humerus, the distal femur and the tibia. Dedifferentiation usually originates from either an enchondroma or a low-grade chondrosarcoma (dedifferentiated central chondrosarcoma, DCCS), but it can also originate from a low-grade peripheral chondrosarcoma secondary to a pre-existing osteochondrosarcoma or a solitary osteochondroma (dedifferentiated peripheral chondrosarcoma) (4). Histopathologically, the distinctive morphological features include two kinds of defined components, a well-differentiated cartilage tumor juxtaposed to a high-grade non-cartilaginous sarcoma, and the transition between the two is abrupt. The dedifferentiated components may be conventional osteosarcoma, telangiectatic osteosarcoma (5), undifferentiated pleomorphic sarcoma (UPS), or fibrosarcoma (6). Other rare histological subtypes of the differentiated components may include leiomyosarcoma (7), rhabdomyosarcoma (8), giant cell tumor-like (9–12), gastrointestinal stromal tumor (GIST)-like (13), or epithelial differentiation (14). To better understand the characteristics and dedifferentiation transformation mechanism underlying DCCS, we conducted a retrospective study to analyze the clinicopathological features of 57 patients with DCCS. Additionally, we carried out immunohistochemistry to explore the intrinsic mechanism involved in the process of dedifferentiation in these tumors.

METHODS

Patients and Surgical Specimens

With approval from the institutional ethics committee and following the research protocol, 57 DCCS cases were retrieved from surgical pathological records between January 2009 and December 2020 at the Department of Pathology, Beijing Jishuitan Hospital. All tissues were fixed in neutral buffered formalin and processed routinely *via* paraffin embedding, and then the sections were prepared and stained with hematoxylin and eosin (HE). Histopathological assessment was carried out according to the WHO Classification of Tumors of Soft Tissue and Bone and reviewed by three pathologists, while clinical and imaging information was obtained from online medical records and surgeons. All cases were treated by surgery, and 28 cases were treated with chemotherapy after surgery.

Imaging

Pre-operative imaging studies included plain radiographs, computed tomography (CT) and magnetic resonance imaging (MRI). As a routine examination protocol in our hospital, patients with bone tumors are assessed by contrast-enhanced CT or contrast-enhanced MRI. Fifty-one patients underwent plain radiographs with at least two positions; 45 patients were evaluated with CT scans, and 38 patients were assessed by MRI. The images were reviewed on our PACS (Picture Archiving and Communication Systems) by two experienced radiologists (YS, WL).

TABLE 1 | Antibodies used for immunohistochemical staining.

Antigen	Antibody	Source	Type	Dilution
Desmin	ZC18	Zymed	Monoclonal antibody	Prediluted
Myogenin	F5D	DAKO	Monoclonal antibody	1:200
RB	1FB	Zhongshan	Monoclonal antibody	Prediluted
CDK4	EP180	Zhongshan	Polyclonal antibody	Prediluted
Cyclin D1	SP4	Roch	Polyclonal antibody	Prediluted
p53	D0-7	Leica	Monoclonal antibody	1:100
p16	G175-405	Zymed	Monoclonal antibody	Prediluted
S-100	None	Leica	Polyclonal antibody	1:400
H3k27me3	None	Zhongshan	Polyclonal antibody	Prediluted
Ki-67	MM1	Leica	Monoclonal antibody	Prediluted

Tissue Samples and Immunohistochemistry

Formalin-fixed, paraffin-embedded specimens of DCCS were available for immunohistochemical analysis. Immunohistochemical staining was performed with an automated immunostainer (Autostainer 720, Labvision, San Diego, CA) according to standard heat-induced epitope retrieval and the avidin-biotin-peroxidase complex method. The following cytophenotypic markers were detected: desmin, S-100, p16, RB, p53, Cyclin D1, CDK4, H3k27me3, and Ki-67 (**Table 1**). Simultaneously, appropriate positive and negative control sections were used. Positive immunostaining was characterized by brown nuclear or cytoplasmic staining under a microscope. Cytoplasmic staining was considered positive for desmin, and nuclear staining was considered positive for S-100, p16, RB, p53, Cyclin D1, CDK4, H3k27me3, and Ki-67. All slides were evaluated independently by two pathologists who were not provided clinical information. The grade of immunoreactivity was defined as follows: negative (–); focal positive (+): fewer than 75% of tumor cells were positive; and diffuse positive (++): more than 75% of tumor cells were positive. The Ki67 proliferation index was defined 25% as the threshold value. Agreement was reached by careful discussion when the opinions of the two pathologists (LG, YD) were different.

RESULTS

Clinical Characteristics

The patients included 29 females and 28 males, ranging in age from 20 to 76 years, with a median age of 54 years. Fifty-seven cases of DCCS occurred in the pelvis ($n = 29$), femur ($n = 17$), scapula ($n = 4$), tibia ($n = 2$), humerus ($n = 2$), metatarsals ($n = 1$), fibula ($n = 1$), and radius ($n = 1$). In our study, 12 cases (21.1%) were secondary DCCS occurring after central low-grade

TABLE 2 | Clinical summary of DCCS.

Age	*n* (%)
≥50 years	34 (59.7)
<50 years	23 (40.3)
Sex	
Female	29 (50.9)
Male	28 (49.1)
Location	
Pelvis	29 (50.8)
Femur	17 (29.8)
Scapule	4 (7.0)
Tibia	2 (3.5)
Humerus	2 (3.5)
Fibula	1 (1.8)
Radius	1 (1.8)
Metatarsals	1 (1.8)
Classification	
Primary	45 (78.9)
Secondary	12 (21.1)
Grade of chondrogenic component	
G1	38 (66.7)
G2	19 (33.3)
Type of dedifferentiation	
Osteosarcoma	29 (50.9)
UPS	20 (35.1)
Rhabdomyosarcoma	3 (5.2)
Fibrosarcoma	2 (3.5)
Spindle cell sarcoma	2 (3.5)
Angiosarcoma	1 (1.8)
Prognosis	
Disease-free survival	27 (47.4)
Dead	23 (40.3)
Missed follow-up	7 (12.3)

G1, grade 1; G2, grade 2; UPS, undifferentiated pleomorphic sarcoma.

chondrosarcoma recurrence. The other cases involved primary dedifferentiation (**Table 2**).

Imaging Characteristics

Most of the tumors were located in the pelvis and femur. Lesions often exhibit ill-defined intramedullary destruction with calcific foci and associated cortical permeation and soft tissue masses and with heterogeneous contrast enhancement on imaging. The most characteristic features of images consist of two different appearances on imaging, with an area showing calcifications or hyperintense chondral component of the cartilage-forming tumor juxtaposed to a lytic area involving a highly aggressive, non-cartilaginous component with a soft tissue mass, which frequently reflects the presence of undifferentiated pleomorphic sarcoma or osteosarcoma (**Figures 1**, **2**). A total of 21.6% (11/51), 75.6% (34/45), and 50% (19/38) of lesions showed this biphasic pattern on plain radiograph, CT and MRI, respectively. This bimorphic pattern was characteristic and was appreciated more clearly on CT images than on radiography.

Gross Pathological Features

Grossly, the tumor was located in the medullary cavity. The cartilaginous and DCS components are distinct. The cartilaginous component was blue-gray, translucent and fragile, whereas the dedifferentiated components were fresh, pale, soft, tough or hard (**Figure 3A**). The sarcoma components could invade the cortex of bone, forming a soft tissue mass (**Figure 3B**).

Histopathological Features

Microscopically, the DCCS cases showed a typical chondrosarcoma structure and non-chondrogenic sarcoma structure. The types of chondrosarcoma include chondrosarcoma grade I and chondrosarcoma grade II. Grade I cartilage may mimic normal hyaline cartilage. In 38/57 cases, the cartilaginous component consisted of chondrosarcoma grade I, which is weakly to moderately cellular and hyperchromatic, with no mitoses (**Figure 4A**). Nineteen cases of chondrosarcoma grade II were found. Chondrosarcoma grade II is more cellular, with a greater degree of nuclear atypia, and mitoses can be found (**Figure 4B**). The perilobular and interlobular cells of chondrosarcoma grade II are rich and pleomorphic. Myxoid changes were found in 22 cases, primarily in chondrosarcoma grade II components.

The dedifferentiated components usually transition abruptly to distinct cartilaginous components. We observed an obvious line of demarcation as described in the WHO classification. Fiber bundles were present in some cases and absent in others (**Figure 4C**). Additionally, in some cases, sarcoma could be the major component, and the focal cartilaginous component was located in it, forming an island structure (**Figure 4D**). The dedifferentiated components showed multiple features, including those of high-grade sarcomas, namely, osteosarcoma ($n = 29$), UPS ($n = 20$), rhabdomyosarcoma ($n = 3$), fibrosarcoma ($n = 2$, the diagnostic criteria refer to adult fibrosarcoma in the WHO classification) and angiosarcoma ($n = 1$). Additionally, there were low-grade components, such as grade I or II spindle cell sarcoma ($n = 2$) (**Table 1**).

In the UPS, sarcoma showed high-grade cell pleomorphism and atypia, some zones with bizarre multinuclear tumorous giant cells (**Figure 5A**), and some zones with epithelioid morphology. The high-grade myxoid zone also existed, forming high-grade myxoid fibrosarcoma features. In two cases, pleomorphic rhabdomyosarcoma differentiation occurred. The cells were large, round or polygonal with abundant pink cytoplasm and unusual nuclei, similar to rhabdomyosarcoma (**Figure 5B**). In one case, the tumor invaded the lymph node. Only dedifferentiated components could be found in the lymph node without cartilaginous components.

In the osteosarcoma component, the cells were highly anaplastic and pleomorphic with enlarged and darkly stained nuclei (**Figure 5C**). A focal hemangiopericytoma-like pattern was also found (**Figure 5D**). The important and necessary characteristics for the diagnosis of osteosarcoma are the production of osteoids by malignant tumor cells. Osteoids

FIGURE 1 | Radiologic features of DCCS. **(A)** Anteroposterior view of the left femur. Radiographs show a large lytic lesion of the femur, with cortical remodeling and a poorly defined margin of the distal part. The proximal part of the lesion has popcorn-like matrix calcifications. **(B)** Coronal T1-weighted MR image of the left femur. MR imaging shows a large destruction in the medullary cavity of the femur, with low signal on the T1-weighted image. **(C)** Coronal fat-suppressed T2-weighted MR image of the left femur. On fat-saturated T2-weighted images, the existence of the two components is recognized. The proximal third of the lesion has areas of low signal representing matrix mineralization and areas of high signal representing the high water content of the cartilage matrix, but the distal two-thirds has a heterogeneous predominantly high signal and peritumoral edema, showing bimorphism of the lesion.

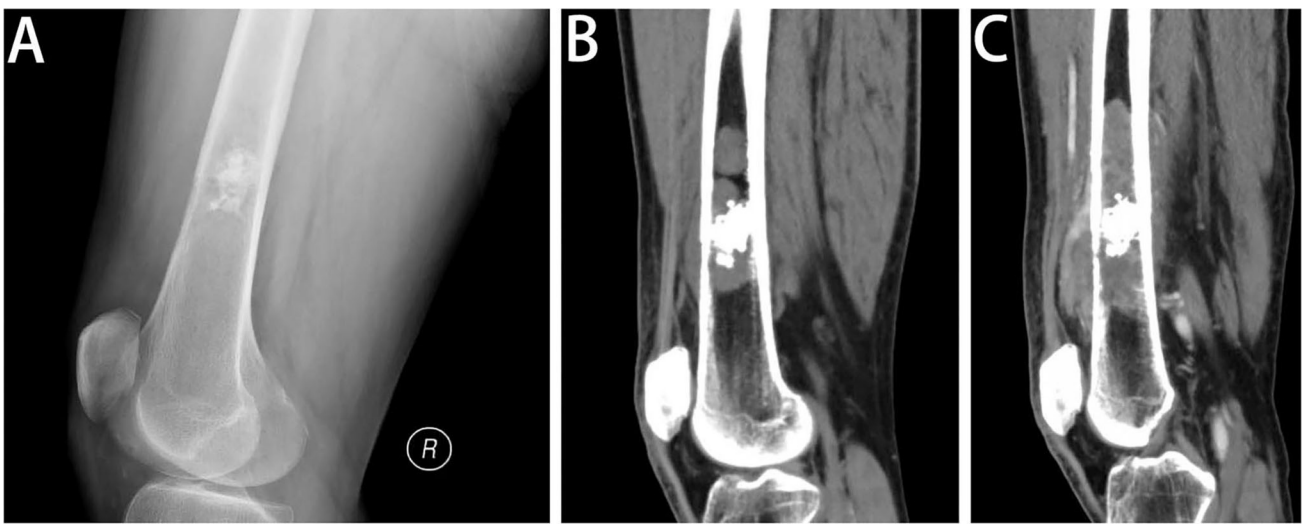

FIGURE 2 | Radiologic features of DCCS. **(A)** Lateral view of the left femur. Radiography of the distal femur shows a lesion in the medullary cavity with calcifications, with subtle destruction of the anterior cortex and anterior soft tissue mass. **(B)** Sagittal CT scan of the left femur in the soft tissue window. The sagittal CT images demonstrate that the lesion is multifocal, with penetration of the cortex and considerable soft tissue components. In addition to the calcific foci, the lesion contains more areas of lytic destructive changes. **(C)** Sagittal post-contrast CT scan of the left femur in the soft tissue window. One and a half months later, the sagittal post-contrast CT image in the soft tissue window shows the lesion expanding into a large area of bone destruction, with heterogeneous enhancement.

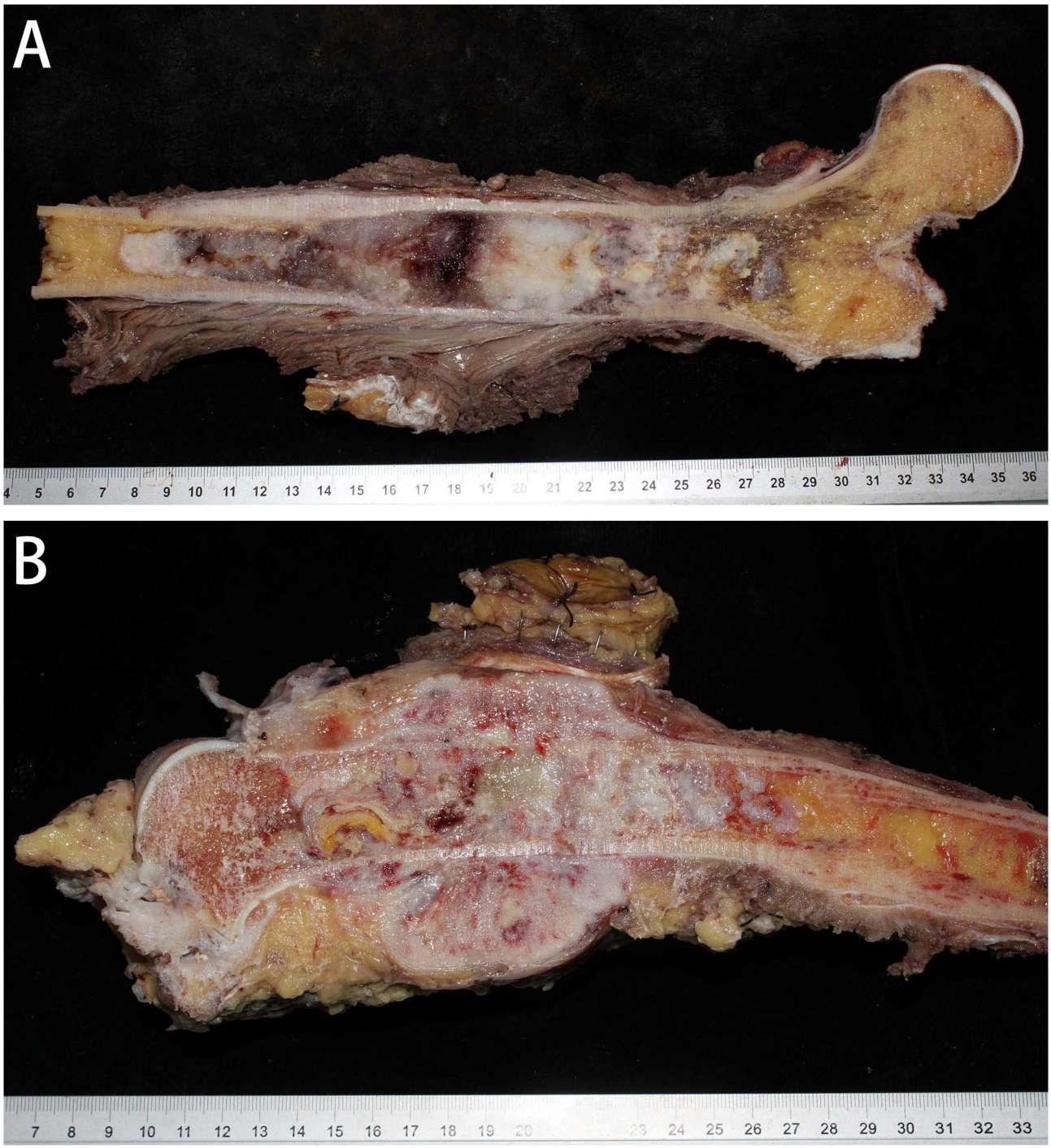

FIGURE 3 | Gross specimens of DCCS. **(A)** The tumor was located in the medullary cavity and was composed of porcelain white cartilage and red fish-like tissue. **(B)** The tumor in the marrow cavity was cartilage-like with invasion of the surrounding soft tissues, forming an osteosarcoma structure.

were dense, pink, and amorphous intercellular material with or without calcification. Osteosarcoma has a broad morphological spectrum. Small cell osteosarcoma had uniform small cells with scant cytoplasm, with little pink osteoid production. The nuclei were round to oval, and the chromatin was fine. The osteoclast-type giant cells scattered in the tumor cells formed the giant cell-enriched variant of osteosarcoma in one case. Additionally, in this case, blood vessel invasion could be found (**Figure 5E**). Two cases showed focal telangiectatic osteosarcoma features. The tumor was composed of cystic spaces simulating

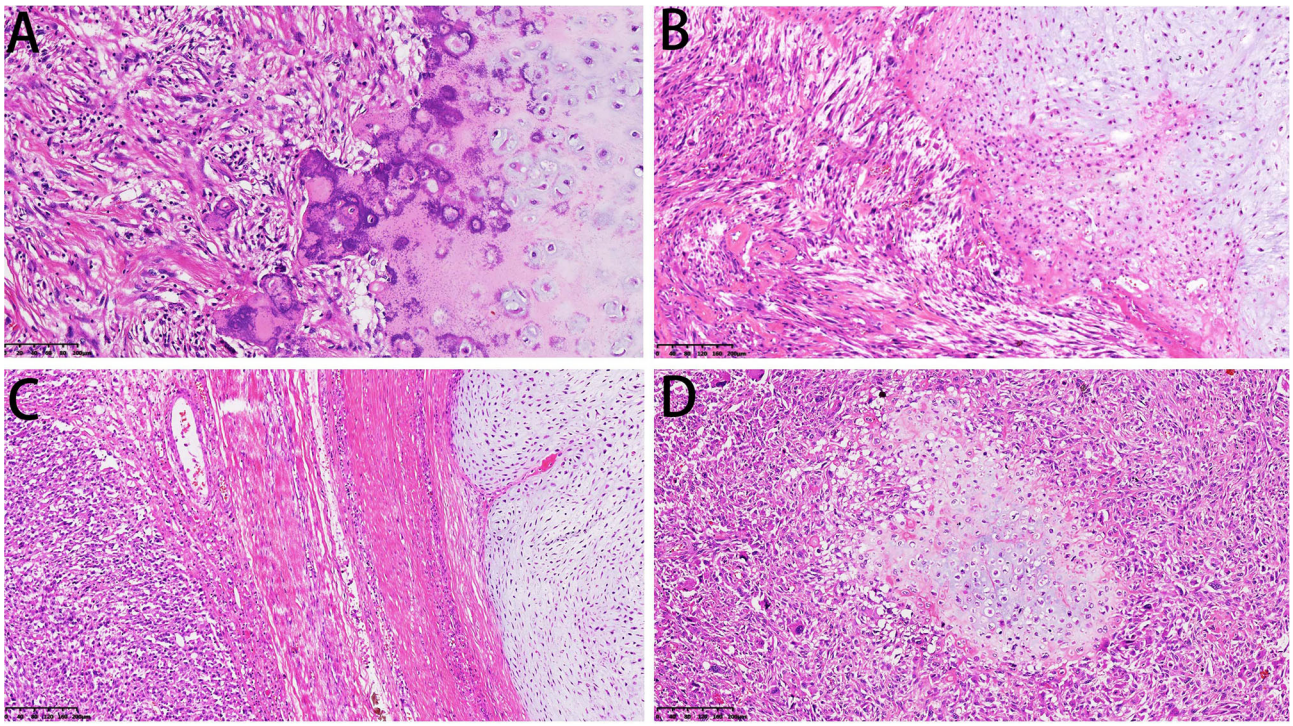

FIGURE 4 | Microscopical features of DCCS. **(A)** The cartilage component shows a grade I cartilage structure, and the sarcoma component shows a low-grade sarcoma morphology (HE, 200×). **(B)** The cartilage component shows a grade II cartilage structure, and the sarcoma component shows the morphology of myxofibrosarcoma (HE, 200×). **(C)** Thick fibrous separation was located between the cartilage component and the sarcoma component (HE, 100×). **(D)** Well-differentiated cartilage nodules surrounded by sarcoma components (HE, 100×).

an aneurysmal bone cyst, but pleomorphic tumor cells with focal osteoid formation were scattered in the septa-like structures.

One case showed epithelioid angiosarcoma features (**Figure 5F**). The fibrosarcoma was composed of relatively monomorphic spindle cells with a "herringbone" growth pattern and sometimes also formed a synovial sarcoma-like structure (**Figure 6A**). In some areas, the tumor cells were round and epithelioid with interstitial fiber formation, similar to sclerosing epithelioid fibrosarcoma features (**Figure 6B**). Two cases showed low-grade spindle cell sarcoma, with mild-moderate atypia, and some areas had storiform patterns, forming a benign fibrohistiocytoma structure (**Figure 6C**); some areas had a distinctive inflammatory infiltrate with aggregates of plasma cells and lymphocytes mimicking the inflammatory myofibroblastic tumor (**Figure 6D**).

Immunohistochemical Features

Immunohistochemical staining showed strong positivity for desmin in the rhabdomyosarcoma differentiation components in two cases (**Figure 7A**). The Ki-67 index revealed active cell proliferation in the sarcoma components; 79.3% cases showed a Ki-67 value >25%, with only individual cells in the cartilage portion showing proliferative activity, and the Ki-67 value was <25% in all cartilage portions (**Figure 7B**). Staining for p16 was negative in sarcoma and original cartilaginous lesions in most cases; only in some cases were both components positive, and the sarcoma component showed stronger and more diffuse staining than the cartilaginous components (**Figure 7C**). Staining for p53 was diffusely positive in the nuclei of tumor cells in the dedifferentiated components of 54.4% cases (**Figure 7D**) but almost undetectable in the chondrosarcoma component, except for one case with grade II cartilage. The expression pattern of Cyclin D1 was similar to that of p16. In 29.9% of cases, the sarcoma was focal positive, while in only 5.3% of cases, the cartilage was positive. The expression intensity of the sarcoma portion was much higher than that of the cartilage portion (**Figure 7E**). In some cases, although CDK4 was positive in both the cartilage and sarcoma portions, the cartilage portion showed focal positive expression, while the sarcoma portions showed mainly diffuse expression (**Figure 7F**). RB was not expressed in the cartilage portion of all cases, but it showed positivity (73.7%) in the sarcoma portion (**Figure 7G**). H3k27me3 was diffuse positive in the cartilage in all cases, and the sarcoma components were diffuse positive in 89.5% of cases; in only six cases, H3k27me3 showed focal expression (**Figure 7H**). The results of immunohistochemical staining are depicted in **Table 3**.

PROGNOSIS

The patients were followed up from 2 to 127 months. The median follow-up time was 59 months. Seven patients were lost to follow-up. Twenty-three patients died of DCCS. The remaining

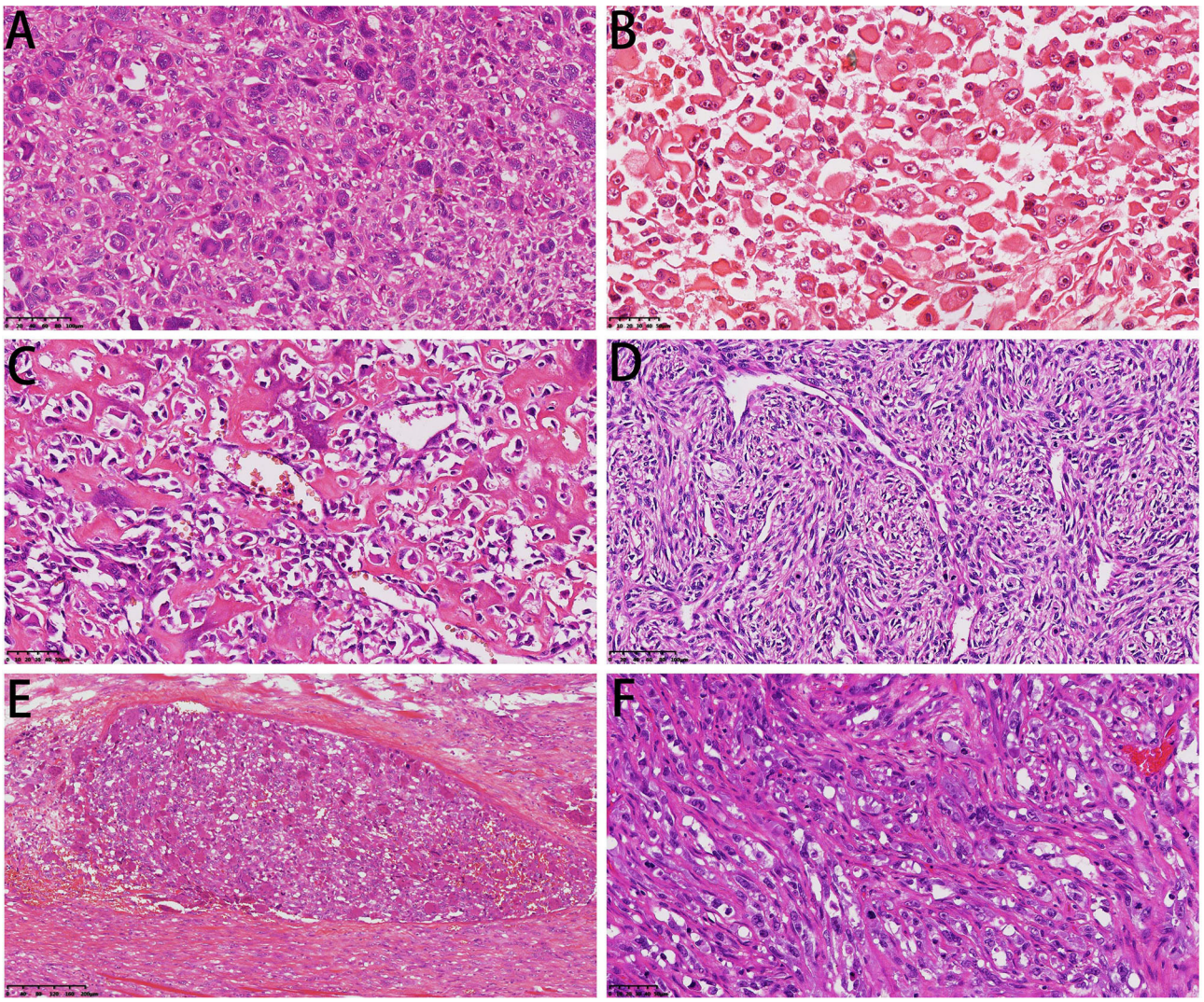

FIGURE 5 | Microscopical features of DCCS. **(A)** Diffuse multinuclear tumor giant cells were dispersed in sarcoma components (HE, 200×). **(B)** The tumor cells showed characteristics of striated muscle differentiation with enriched cytoplasm (HE, 300×). **(C)** The sarcoma component was conventional osteosarcoma (HE, 300×). **(D)** Osteosarcoma tissue showed perivascular arrangement (HE, 200×). **(E)** Intravascular emboli showed a giant cell-rich structure (HE, 100×). **(F)** The sarcoma component showed epithelioid angiosarcoma differentiation (HE, 300×).

27 patients showed no evidence of recurrence and survived disease free.

DISCUSSION

In 1971, Dalin and Beabout first fully described the dedifferentiation of low-grade chondrosarcomas, which is rare, and reported a combination of well-differentiated chondrosarcoma of the ordinary type and juxtaposed zones of anaplastic fibrosarcoma or osteogenic sarcoma. The incidence of peripheral DCS has ranged between 8.9 and 13.7% of all DCS cases (15). Staals et al. (16) found 109 central DCS cases out of 784 central chondrosarcomas (13.9%). In our hospital, from 2009 to 2019, 694 cases of chondrosarcoma were treated at our institution. Among them, 57 patients were diagnosed with DCCS, which accounts for an 8.2% dedifferentiation rate and does not include peripheral DCS. DCCS usually affects the long bones, such as the proximal femur, humerus and tibia. The femur was involved twice as often as the pelvis in DCCS, and there were slightly more males than females at the Razzoli Institute (17). However, in our series, the pelvis was a more common location than the femur, and there were more females than males. These differences may be explained by the selection bias associated with more complicated lesions at the Orthopedic Oncologic Center.

The biphasic pattern is the most characteristic feature of imaging and is appreciated more clearly on contrast-enhanced CT images and MRI than on radiography. Plain radiography has a poor ability to assess the soft tissue mass of the aggressive part. MRI has been investigated well in DCCS and proved to be a useful imaging modality. On MR fluid-sensitive sequences such as

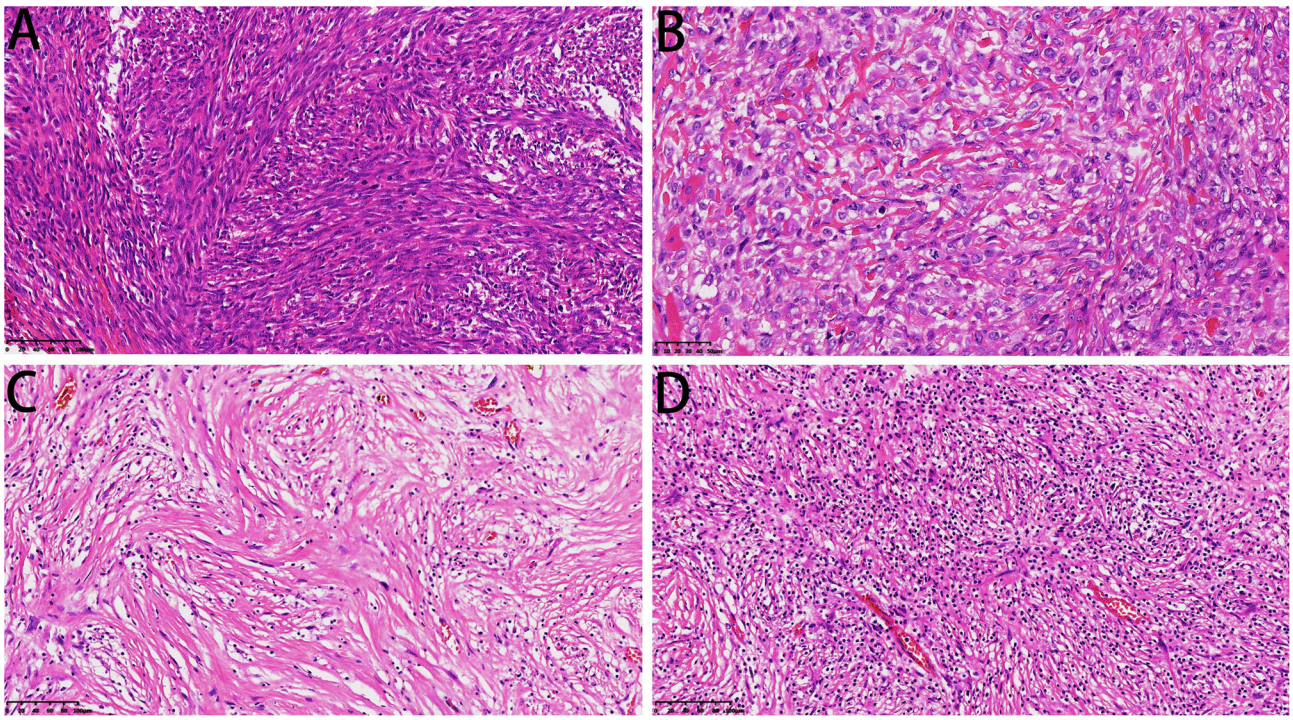

FIGURE 6 | Microscopic features of DCCS. **(A)** The spindle cells were arranged in a bundle-like fibrosarcoma (HE, 200×). **(B)** The sarcoma component resembled sclerotic epithelioid fibrosarcoma (HE, 300×). **(C)** Low-grade sarcoma components showed storiform structures (HE, 200×). **(D)** Low-grade areas showed inflammatory fibroblastoma morphology (HE, 200×).

T2-weighted or STIR images, chondral tumors are hyperintense, whereas dedifferentiated tumors have reduced signal intensity or heterogeneous signal intensity. Based on our results, CT is a good imaging technique to show matrix calcifications of the underlying chondral tumor and osteoid production by osteosarcoma, and with post-contrast images, the soft tissue mass of dedifferentiated tumors is clearly demonstrated with avid enhancement. Imaging findings of the biphasic pattern are important to help pathologists choose the appropriate areas to observe.

DCCS can take place at the first surgery for endochondroma or low-grade chondrosarcoma, which is called synchronous (primary) DCCS, and can also be found at recurrence after resection of these chondrogenic tumors, which is called metachronous (secondary) DCCS. When recurrence occurs at the same site of the chondrosarcoma, the lesion may include the chondrosarcoma structure, which must be combined with the previous pathology to make a precise diagnosis. In addition, the dedifferentiated component may be very small; therefore, pathologists should sample cartilaginous tumors thoroughly, paying special attention to zones that seem grossly abnormal. For the diagnosis of primary DCCS, due to limitations of biopsy, it is often difficult to obtain both cartilage and dedifferentiated components at the same time, which leads to errors in diagnosis. CT-guided puncture could greatly improve the accuracy of diagnosis. For the diagnosis of secondary DCCS, biopsy combined with history could be easier to diagnose.

The Evans grading system classifies chondrosarcoma into grades I, II, and III (low, intermediate and high grade, respectively) according to nuclear morphology, mitotic activity and the degree of cellularity (18). Similar to reports in the literature, the cartilage components in our case had grade I and II morphology, and no grade III morphology was observed. It should be noted that cells around the grade II cartilage lobules are often densely distributed and should be distinguished from grade III. Moreover, in cases of secondary dedifferentiation, the grade of cartilage components are higher than that in the original case. Myxoid degeneration of cartilage was also common, but it was not a criterion for grading. The dedifferentiation components may show multiple features, and UPS, fibrosarcoma and osteosarcoma were the main types. Rare types, such as small cell osteosarcoma, could also be seen. In many cases of osteosarcoma, osteoid production may occupy a small part and show multiple patterns. We also observed other rare types of histology, including angiosarcoma and rhabdomyosarcoma. Similar to Wick's description (19), in our cases, the dedifferentiated component also showed low-grade spindle cell tumor features, which existed in the form of a storiform structure, with focal lymphocyte infiltration, generating an inflammatory myofibroblastoma-like morphology. Consistent with literature reports of giant cell tumor-like morphology, there were indeed a large number of giant cells in our cases, in either

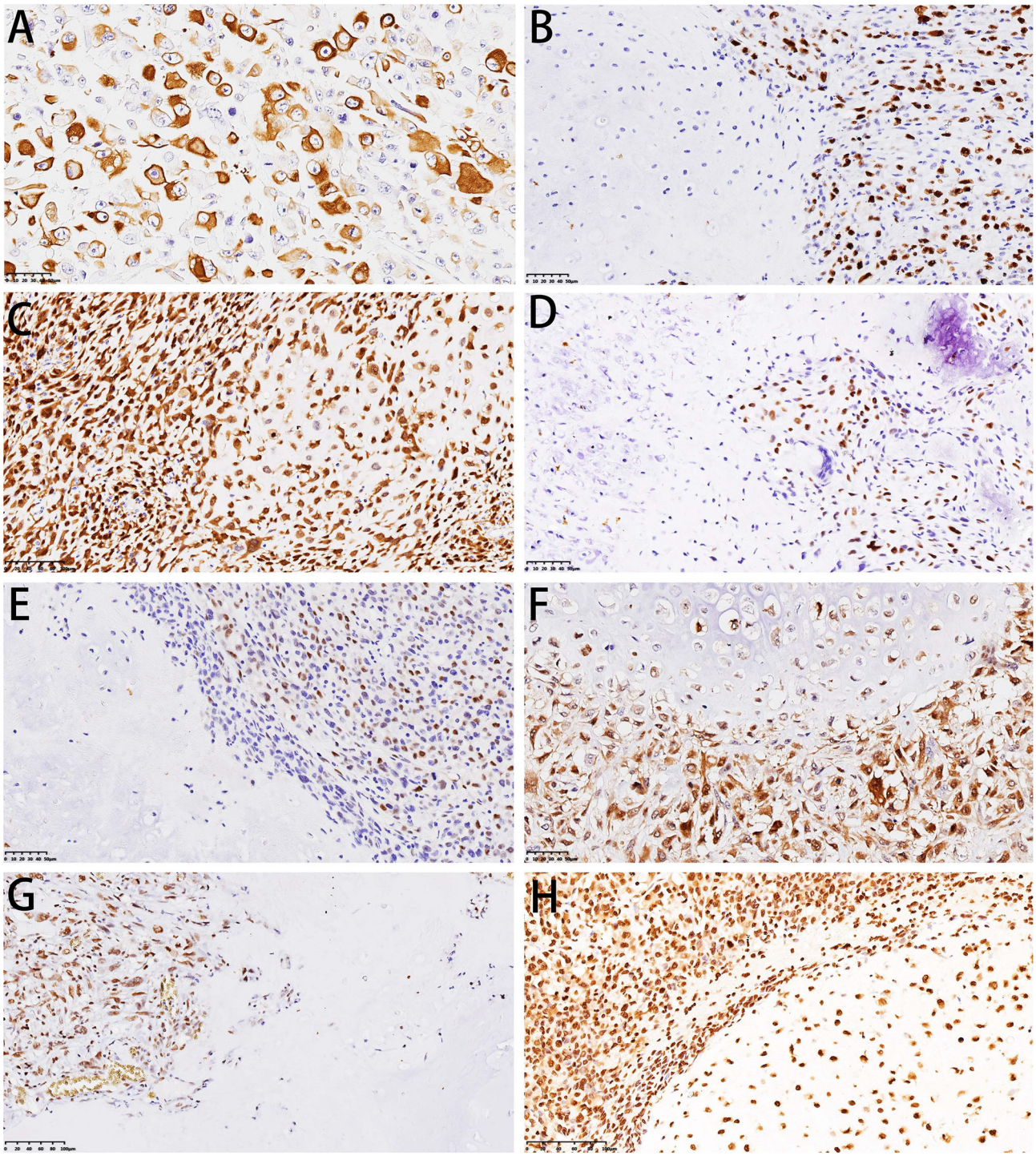

FIGURE 7 | Immunohistochemical features of DCCS. **(A)** Immunohistochemistry showed desmin positivity for striated muscle differentiation. **(B)** Immunohistochemistry showed that Ki-67 was highly expressed in sarcomas. **(C)** Immunohistochemistry showed dense expression of p16 in cartilage and sarcomas. **(D)** Immunohistochemistry showed p53 expression in sarcomas. **(E)** Immunohistochemistry showed Cyclin D1 expression in sarcomas. **(F)** Immunohistochemistry showed that both cartilage and sarcoma components expressed CDK4. **(G)** Immunohistochemistry showed RB expression in sarcoma. **(H)** Immunohistochemistry showed that H3K27me3 was expressed in both the cartilage and sarcoma components.

giant cell-rich undifferentiated sarcomas or giant cell-rich osteosarcomas, especially in the latter, where the focal lesion may present low-grade features similar to those of giant cell tumors of bone. These giant cells were all benign and behaved differently from tumor giant cells in undifferentiated pleomorphic sarcoma.

TABLE 3 | Immunohistochemical results of DCCS.

	Negative (–) *n* (%)		Focal positive (+) *n* (%)		Diffuse positive (++) *n* (%)	
	Chondrogenic	**Sarcoma**	**Chondrogenic**	**Sarcoma**	**Chondrogenic**	**Sarcoma**
Desmin	57 (100)	54 (94.7)	0	3 (5.3)	0	0
Myogenin	57 (100)	54 (94.7)	0	3 (5.3)	0	0
S-100	0	57 (100)	0	0	57 (100)	0
RB	57 (100)	15 (26.3)	0	23 (40.4)	0	19 (33.3)
CDK4	45 (78.9)	29 (50.9)	12 (21.1)	20 (35.1)	0	8 (14.0)
Cyclin D1	54 (94.7)	40 (70.2)	3 (5.3)	14 (24.6)	0	3 (5.3)
p53	56 (98.2)	31 (54.4)	1 (1.7)	19 (33.3)	0	7 (12.3)
p16	47 (82.4)	45 (78.9)	4 (7.0)	6 (10.5)	6 (10.5)	6 (10.5)
H3k27me3	0	0	0	6 (10.5)	57 (100)	51 (89.5)

The origin of the dedifferentiation component remains controversial. Sanerkin and Woods (20) suggested that two completely different tumor cell components developed from multipotent mesenchymal stem cells into different cell clones and then differentiated into different neoplastic cell components (collision tumor). In contrast to this theory, more evidence supports the monoclonal origin theory that genomic instability causes a common primitive mesenchymal cell progenitor, which possesses both the ability to develop into a differentiated (chondrocytic features) and a dedifferentiated cell population (high-grade sarcoma features) (21). The fact that chondrocytes were found to have the potential to differentiate into osteoblastic cells supports this theory. Therefore, chondrocyte transition to other tissues may also be possible. The molecular mechanisms of chondrosarcoma dedifferentiation transition also must be further explored.

Morphological observation shows that there is more active mitosis in the sarcoma component than in the cartilage component. Moreover, the Ki-67 proliferation index was significantly increased in sarcoma components by immunohistochemical staining. Therefore, we performed immunohistochemical analysis of cell cycle-related molecules. p53 plays a role in cell cycle regulation, apoptosis, genomic stability, and inhibition of angiogenesis. Studies have shown that p53 mutation is the main mutant gene in high-grade chondrosarcoma (22, 23) and DCS. In DCS, p53 mutation or loss of heterozygosity (LOH) was detected only in the advanced dedifferentiated components (24). It has been reported that p53 is overexpressed in dedifferentiated areas, while chondrosarcoma areas have only focal weakly positive or negative expression (25). Bovée et al. (26) found that p53 was expressed in both chondrosarcoma and dedifferentiated regions. These differences were thought to be due to the different cartilage grades; grade II cartilage is more likely to be p53 positive than grade I cartilage. According to these findings, in our one case, p53 was weakly positive in grade II cartilage; the other cases were negative in the cartilage area, but p53 was positive to varying degrees in the sarcoma area of 26 cases. Another study confirmed the role of the p53 pathway in the high-grade progression of chondrosarcoma (27). Therefore, we believe that p53 may be related to the malignant transformation of chondrosarcoma dedifferentiation.

The retinoblastoma (RB) protein controls E2F-mediated gene transcription activation and is a key factor for cells entering S phase and cell cycle progression. Loss of RB function is an essential step in tumorigenesis. The LOH of RB is associated with high-grade cartilage tumors and is thought to occur only in the anaplastic component (28, 29). We found that the expression of RB occurs in dedifferentiated components without exception and that the cartilage components are all negative. Therefore, we hypothesized that abnormal expression of RB could induce cartilage tumor stem cells to accelerate cell cycle progression and combine with p53 gene mutation to lead to the development of sarcoma.

Amary et al. (30) showed that p16 copy number variation could be found in high-grade chondrosarcoma (GII, GIII and dedifferentiated) and may be associated with tumor progression. Analysis of a DCS cell line suggests that deletion of the p16 gene plays a major role in the malignant phenotype of DCS (31). p16 regulates the cell cycle by inhibiting CDK4 and Cyclin D1. We found that in most cases, p16 showed a loss of expression in cartilage and dedifferentiated components, which may suggest that the inhibition of CDK4 and Cyclin D1 was reduced, prompting tumor cells to enter the cell cycle progression. Therefore, p16 may also play a role in the high-grade progression of chondrosarcoma.

Our immunohistochemical results showed that positive cells were often located at the junction of cartilage nodules and dedifferentiated components—that is, cells around the cartilage lobules. We believe that the cells surrounding the cartilage lobules are germinal cells or tumor stem cells of cartilage tumors, which could generate new chondrocytes and differentiate in different directions. This expression suggests that these cells terminally differentiate into dedifferentiated sarcoma components. In other words, the cartilage component and the sarcoma components are from the same source. However, the mechanism by which cartilage tumor stem cells differentiate into sarcoma cells remains unknown.

H3K27me3 deficiency was found in 34–75% of malignant peripheral nerve sheath tumors (MPNSTs), and the loss of H3K27me3 expression by immunohistochemical staining could provide a diagnostic clue for MPNSTs (32). The histology of DCS that was deficient in H3K27me3 was different from that of DCS that fully expressed H3K27me3 because the former exhibited characteristics of malignant peripheral nerve sheath tumors (33). In our study, six cases showed a dispersed reduction in H3K27me3 expression, and the morphologies were spindle cell tumors. Nevertheless, the basis for the diagnosis of MPNST is insufficient.

The tumors must be differentiated from other cartilaginous tumors and non-chondroid mesenchymal tumors, which may be confused on clinical and roentgenologic grounds. Occasional high-grade chondrosarcoma, which has dense spindle cells around the periphery of cartilaginous lobules, could be explained as the primitive multipotential stem cell of chondrosarcoma, but dedifferentiation does not occur. In mesenchymal chondrosarcoma, there is also relatively well-differentiated cartilage, but the compact proliferated cells adjacent to the cartilage are composed of round or oval primitive cells, and a perivascular structure may exist. However, in DCCS, the high-grade non-chondroid component showed more variable features. In chondroblastic osteosarcoma, the cartilage is usually grade II or grade III, and there is either a gradual rather than rapid transition between the cartilage and the high-grade osteosarcoma zones or a mixing of the two components. Other non-chondroid mesenchymal tumors, such as UPS or fibrosarcoma of bone, may be mixed with secondary DCS without cartilage areas. Therefore, careful sampling combined with patient history is important.

CONCLUSIONS

We reported histological and immunohistochemical characteristics of a large institutional series of DCCS. Immunohistochemical analysis showed that p53 and RB may be related to malignant transformation of DCCS. Because of its rareness, DCCS should be diagnosed carefully and differentiated from other primary malignant sarcomas. Recognizing DCCS is important because of its aggressive clinical behaviors, frequency of recurrence and poor prognosis.

DATA AVAILABILITY STATEMENT

The original contributions presented in the study are included in the article/supplementary material, further inquiries can be directed to the corresponding authors.

ETHICS STATEMENT

This study was approved by the Ethic Committee of Beijing JishuiTan Hospital. This retrospective study of formalin-fixed and paraffin-embedded specimen was waived of obtaining patient consent.

AUTHOR CONTRIBUTIONS

L-HG and YD conceived the study and designed the experiments. L-HG, WZ, and R-FD performed the experiments. Y-BS and W-FL collected and analyzed the radiology data. X-QS and MZ collected the immunohistochemical data. All authors read and approved the final manuscript.

REFERENCES

1. WHO Classification of Tumours Editorial Board eds. *World Health Organization Classification of Soft Tissue and Bone Tumours*. 5th ed. Lyon: IARC Press (2020).
2. Mitchell AD, Ayoub K, Mangham DC, Grimer RJ, Carter SR, Tillman RM. Experience in the treatment of dedifferentiated chondrosarcoma. *J Bone Joint Surg Br.* (2000) 82:55–61. doi: 10.1302/0301-620X.82B1.0820055
3. Pring ME, Weber KL, Unni KK, Sim FH. Chondrosarcoma of the pelvis. A review of sixty-four cases. *J Bone Joint Surg Am.* (2001) 83-A:1630–42. doi: 10.2106/00004623-200111000-00003
4. Franchi A, Baroni G, Sardi I, Giunti L, Capanna R, Campanacci D. Dedifferentiated peripheral chondrosarcoma: a clinicopathologic, immunohistochemical, and molecular analysis of four cases. *Virchows Arch.* (2012) 460:335–42. doi: 10.1007/s00428-012-1206-2
5. Okada K, Hasegawa T, Tateishi U, Endo M, Itoi E. Dedifferentiated chondrosarcoma with telangiectatic osteosarcoma-like features. *J Clin Pathol.* (2006) 59:1200–2. doi: 10.1136/jcp.2005.029629
6. Capanna R, Bertoni F, Bettelli G, Picci P, Bacchini P, Present D, et al. Dedifferentiated chondrosarcoma. *J Bone Joint Surg Am.* (1988) 70:60–9. doi: 10.2106/00004623-198870010-00010
7. Akahane T, Shimizu T, Isobe K, Yoshimura Y, Kato H. Dedifferentiated chondrosarcoma arising in a solitary osteochondroma with leiomyosarcomatous component: a case report. *Arch Orthop Trauma Surg.* (2008) 128:951–3. doi: 10.1007/s00402-008-0567-0
8. Bisceglia M, D'Angelo VA, Guglielmi G, Dor DB, Pasquinelli G. Dedifferentiated chordoma of the thoracic spine with rhabdomyosarcomatous differentiation. Report of a case and review of the literature. *Ann Diagn Pathol.* (2007) 11:262–73. doi: 10.1016/j.anndiagpath.2006.09.002
9. Ishida T, Dorfman HD, Habermann ET. Dedifferentiated chondrosarcoma of humerus with giant cell tumor-like features. *Skeletal Radiol.* (1995) 24:76–80. doi: 10.1007/BF02425959
10. Estrada EG, Ayala AG, Lewis V, Czerniak B. Dedifferentiated chondrosarcoma with a noncartilaginous component mimicking a conventional giant cell tumor of bone. *Ann Diagn Pathol.* (2002) 6:159–63. doi: 10.1053/adpa.2002.33905
11. Knösel T, Werner M, Jung A, Kirchner T, Dürr HR. Dedifferentiated chondrosarcoma mimicking a giant cell tumor. Is this low grade dedifferentiated chondrosarcoma? *Pathol Res Pract.* (2014) 210:194–7. doi: 10.1016/j.prp.2013.12.003
12. Huang J, Jiang Z, Yang Q, Zhang H. Benign looking giant cell component in dedifferentiated chondrosarcoma: benign or malignant? A case report. *Int J Surg Pathol.* (2013) 21:48–53. doi: 10.1177/1066896912451322
13. Akisue T, Kishimoto K, Kawamoto T, Hara H, Kurosaka M. Dedifferentiated chondrosarcoma with a high-grade mesenchymal component mimicking a gastrointestinal stromal tumor. *Open J Pathol.* (2012) 2:90–5. doi: 10.4236/ojpathology.2012.23017
14. Gambarotti M, Righi A, Frisoni T, Donati D, Vanel D, Sbaraglia M, et al. Dedifferentiated chondrosarcoma with "adamantinoma-like" features: a case report and review of literature. *Pathol Res Pract.* (2017) 213:698–701. doi: 10.1016/j.prp.2017.04.019
15. Bertoni F, Present D, Bacchini P, Picci P, Pignatti G, Gherlinzoni F,Campanacci M. Dedifferentiated peripheral chondrosarcomas. A

report of seven cases. *Cancer*. (1989) 63:2054–9. doi: 10.1002/1097-0142(19890515)63:10<2054::AID-CNCR2820631030>3.0.CO;2-V
16. Staals EL, Bacchini P, Mercuri M, Bertoni F. Dedifferentiated chondrosarcomas arising in preexisting osteochondromas. *J Bone Joint Surg Am*. (2007) 89:987–99. doi: 10.2106/JBJS.F.00288
17. Staals EL, Bacchini P, Bertoni F. Dedifferentiated central chondrosarcoma. *Cancer*. (2006) 106:2682–91. doi: 10.1002/cncr.21936
18. Evans HL, Ayala AG, Romsdahl MM. Prognostic factors in chondrosarcoma of bone. A clinicopathologic analysis with emphasis on histologicgrading. *Cancer*. (1977) 40 818-831 doi: 10.1002/1097-014240:2<818::AID--CNCR2820400234>3.0.CO;2-B
19. Wick MR, Siegal GP, Mills SE, Thompson RC, Sawhney D, Fechner RE. Dedifferentiated chondrosarcoma of bone. An immunohistochemical and lectin-histochemical study. *Virchows Arch A Pathol Anat Histopathol*. (1987) 411:23–32. doi: 10.1007/BF00734510
20. Sanerkin NG, Woods CG. Fibrosarcomata and malignant fibrous histiocytoma arising in relation to enchondromata. *J Bone Jt Surg*. (1979) 61B:366–72. doi: 10.1302/0301-620X.61B3.225333
21. Bridge JA, DeBoer J, Travis J, Johansson SL, Elmberger G, Noel SM, et al. Simultaneous interphase cytogenetic analysis and fluorescence immunophenotyping of dedifferentiated chondrosarcoma. Implications for histopathogenesis. *Am J Pathol*. (1994) 144:215–20.
22. Terek RM, Healey JH, Garin-Chesa P, Mak S, Huvos A, Albino AP. p53 mutations in chondrosarcoma. *Diagn Mol Pathol*. (1998) 7:51–6. doi: 10.1097/00019606-199802000-00009
23. Dobashi Y, Sugimura H, Sato A, Hirabayashi T, Kanda H, Kitagawa T, et al. Possible association of p53 overexpression and mutation with high-grade chondrosarcoma. *Diagn Mol Pathol*. (1993) 2:257–63. doi: 10.1097/00019606-199300020-00037
24. Simms WW, Ordóñez NG, Johnston D, Ayala AG, Czerniak B. p53 expression in dedifferentiated chondrosarcoma. *Cancer*. (1995) 76:223–7. doi: 10.1002/1097-0142(19950715)76:2<223::AID-CNCR2820760210>3.0.CO;2-4
25. Coughlan B, Feliz A, Ishida T, Czerniak B, Dorfman HD. p53 expression and DNA ploidy of cartilage lesions. *Hum Pathol*. (1995) 26:620–4. doi: 10.1016/0046-8177(95)90166-3
26. Bovée JV, Cleton-Jansen AM, Rosenberg C, Taminiau AH, Cornelisse CJ, Hogendoorn PC. Molecular genetic characterization of both components of a dedifferentiated chondrosarcoma, with implications for its histogenesis. *J Pathol*. (1999) 189:454-62. doi: 10.1002/(SICI)1096-9896(199912)189:4<454::AID-PATH467>3.0.CO;2-N
27. Meijer D, de Jong D, Pansuriya TC, van den Akker BE, Picci P, Szuhai K, et al. Genetic characterization of mesenchymal, clear cell, dedifferentiated chondrosarcoma. *Genes Chromosomes Cancer*. (2012) 51:899–909. doi: 10.1002/gcc.21974
28. Röpke M, Boltze C, Meyer B, Neumann HW, Roessner A, Schneider-Stock R. Rb-loss is associated with high malignancy in chondrosarcoma. *Oncol Rep*. (2006) 15:89–95. doi: 10.3892/or.15.1.89
29. Sakamoto A. The molecular pathogenesis of dedifferentiated chondrosarcoma *Indian J Orthop*. (2014) 48:262–5. doi: 10.4103/0019-5413.132506
30. Amary MF, Ye H, Forbes G, Damato S, Maggiani F, Pollock R, et al. M Flanagan (2015) isocitrate dehydrogenase 1 mutations (IDH1) and p16/CDKN2A copy number change in conventional chondrosarcomas. *Virchows Arch*. 466:217–22 doi: 10.1007/s00428-014-1685-4
31. Yang L, Chen Q, Zhang S, Wang X, Li W, Wen J, et al. A novel mutated cell line with characteristics of dedifferentiated chondrosarcoma. *Int J Mol Med*. (2009) 24:427–35. doi: 10.3892/ijmm_00000249
32. Prieto-Granada CN, Wiesner T, Messina JL, Jungbluth AA, Chi P, Antonescu CR. Loss of H3K27me3 expression is a highly sensitive marker for sporadic and radiation-induced MPNST. *Am J Surg Pathol*. (2016) 40:479–89. doi: 10.1097/PAS.0000000000000564
33. Makise N, Sekimizu M, Konishi E, Motoi T, Kubo T, Ikoma H, et al. H3K27me3 deficiency defines a subset of dedifferentiated chondrosarcomas with characteristic clinicopathological features. *Mod Pathol*. (2019) 32:435–5. doi: 10.1038/s41379-018-0140-5

Conflict of Interest: The authors declare that the research was conducted in the absence of any commercial or financial relationships that could be construed as a potential conflict of interest.

Publisher's Note: All claims expressed in this article are solely those of the authors and do not necessarily represent those of their affiliated organizations, or those of the publisher, the editors and the reviewers. Any product that may be evaluated in this article, or claim that may be made by its manufacturer, is not guaranteed or endorsed by the publisher.

frontiers in Medicine

ORIGINAL RESEARCH
published: 08 October 2021
doi: 10.3389/fmed.2021.734901

Delta-Like Protein 3 Expression in Paired Chemonaive and Chemorelapsed Small Cell Lung Cancer Samples

Christiane Kuempers[1], Tobias Jagomast[1], Rosemarie Krupar[2], Finn-Ole Paulsen[1,3], Carsten Heidel[1], Julika Ribbat-Idel[1], Christian Idel[4], Bruno Märkl[5], Martin Anlauf[6], Sabina Berezowska[7,8], Markus Tiemann[9], Hans Bösmüller[10], Falko Fend[10], Barbara Kalsdorf[11], Sabine Bohnet[12], Eva Dreyer[1], Verena Sailer[1], Jutta Kirfel[1] and Sven Perner[1,2,13]*

[1] Institute of Pathology, Luebeck, University Hospital Schleswig-Holstein, Luebeck, Germany, [2] Pathology, Research Center Borstel-Leibniz Lung Center, Borstel, Germany, [3] Department of Oncology, Hematology and Bone Marrow Transplantation With Division of Pneumology, University Medical Center Hamburg-Eppendorf, Hamburg, Germany, [4] Department of Otorhinolaryngology, Luebeck, University of Luebeck and University Hospital Schleswig-Holstein, Luebeck, Germany, [5] Medical Faculty, General Pathology and Molecular Diagnostics, University Augsburg, Augsburg, Germany, [6] Institute of Pathology, Cytology and Molecular Pathology Limburg, Limburg, Germany, [7] Department of Laboratory Medicine and Pathology, Institute of Pathology, Lausanne University Hospital and University of Lausanne, Lausanne, Switzerland, [8] Institute of Pathology, University of Bern, Bern, Switzerland, [9] Institute for Hematopathology, Hamburg, Germany, [10] Institute of Pathology and Neuropathology University Hospital Tuebingen, Tuebingen, Germany, [11] Medical Clinic, Research Center Borstel-Leibniz Lung Center, Borstel, Germany, [12] Department of Pulmonology, Luebeck, University Hospital Schleswig-Holstein, Luebeck, Germany, [13] Airway Research Center North (ARCN), Member of the German Center for Lung Research (DZL), Borstel, Germany

OPEN ACCESS

Edited by:
Gabriella Nesi,
University of Florence, Italy

Reviewed by:
Hyo Sup Shim,
Yonsei University College of Medicine, South Korea
Steven Christopher Smith,
Virginia Commonwealth University Health System, United States

***Correspondence:**
Christiane Kuempers
christiane.kuempers@uksh.de

Specialty section:
This article was submitted to Pathology, a section of the journal Frontiers in Medicine

Received: 01 July 2021
Accepted: 23 August 2021
Published: 08 October 2021

Citation:
Kuempers C, Jagomast T, Krupar R, Paulsen F-O, Heidel C, Ribbat-Idel J, Idel C, Märkl B, Anlauf M, Berezowska S, Tiemann M, Bösmüller H, Fend F, Kalsdorf B, Bohnet S, Dreyer E, Sailer V, Kirfel J and Perner S (2021) Delta-Like Protein 3 Expression in Paired Chemonaive and Chemorelapsed Small Cell Lung Cancer Samples. Front. Med. 8:734901. doi: 10.3389/fmed.2021.734901

Rovalpituzumab tesirine (Rova-T), an antibody-drug conjugate directed against Delta-like protein 3 (DLL3), is under development for patients with small cell lung cancer (SCLC). DLL3 is expressed on the majority of SCLC samples. Because SCLC is rarely biopsied in the course of disease, data regarding DLL3 expression in relapses is not available. The aim of this study was to investigate the expression of DLL3 in chemorelapsed (but untreated with Rova-T) SCLC samples and compare the results with chemonaive counterparts. Two evaluation methods to assess DLL3 expression were explored. Additionally, we assessed if DLL3 expression of chemorelapsed and/or chemonaive samples has prognostic impact and if it correlates with other clinicopathological data. The study included 30 paired SCLC samples, which were stained with an anti DLL3 antibody. DLL3 expression was assessed using tumor proportion score (TPS) and H-score and was categorized as DLL3 low (TPS $< 50\%$, H-score ≤ 150) and DLL3 high (TPS $\geq 50\%$, H-score > 150). Expression data were correlated with clinicopathological characteristics. Kaplan–Meier curves were used to illustrate overall survival (OS) depending on DLL3 expression in chemonaive and chemorelapsed samples, respectively, and depending on dynamics of expression during course of therapy. DLL3 was expressed in 86.6% chemonaive and 80% chemorelapsed SCLC samples without significant differences between the two groups. However, the extent of expression varied in a substantial proportion of pairs (36.6% with TPS, 43.3% with H-score), defined as a shift from low to high or high to low expression. TPS and H-score provided comparable results. There

were no profound correlations with clinicopathological data. Survival analysis revealed a trend toward a more favorable OS in DLL low-expressing chemonaive SCLC ($p = 0.57$) and, in turn, in DLL3 high-expressing chemorelapsed SCLC ($p = 0.42$) as well as in SCLC demonstrating a shift from low to high expression ($p = 0.56$) without being statistically significant. This is the first study to investigate DLL3 expression in a large cohort of rare paired chemonaive-chemorelapsed SCLC specimens. Comparative analysis revealed that DLL3 expression was not stable during the course of therapy, suggesting therapy-based alterations. Unlike in chemonaive samples, a high DLL3 expression in chemorelapsed samples indicated a trend for a more favorable prognosis. Our results highlight the importance to investigate DLL3 in latest chemorelapsed SCLC tumor tissue.

Keywords: delta-like protein 3, small cell lung cancer, paired, chemonaive, chemorelapsed

INTRODUCTION

Small cell lung cancer (SCLC) is known as a highly aggressive type of cancer with a miserable prognosis. It is the second most common lung cancer type and accounts for ∼15% of lung cancer cases. Therapy remained essentially unchanged in recent years and is usually based on chemotherapy with etoposide and a platinating agent (1), whereas, lately, clinical activity of immunotherapies has been observed in patients with refractory or metastatic SCLC. In a phase 3 trial conducted by Horn et al. it was shown that the addition of the anti PD-L1 antibody atezolizumab to chemotherapy in the first-line treatment of extensive SCLC resulted in significantly longer overall survival (OS) and progression-free survival than chemotherapy alone (2). Almost all patients experience disease relapse within 3 months (3). Although SCLC-targeted therapy research has progressed, in contrast to non-small cell lung cancer (NSCLC) no personalized targeted therapy options have been derived so far. Thus, further research into the mechanism of SCLC and the exploration of new therapeutic targets for SCLC are indispensable (4).

A new promising target is Delta-like protein 3 (DLL3), a transmembrane protein found in most high-grade neuroendocrine carcinomas of the lung, including SCLC. Growing evidence supports a tumor-suppressor role for Notch-1 signaling in neuroendocrine tumors (5).

It is shown that the NOTCH receptor is mainly downregulated by DLL3, thereby inhibiting the NOTCH signaling pathway within the cell. Inactivation of Notch directs the lung stem cell to a neuroendocrine precursor cell and contributes via biallelic p53/RB loss to the onset of primary SCLC (6). In this context, the achaete-scute homolog 1 (Ascl1) gene transcription factor plays a major role. It controls crucial cellular mechanisms in SCLC such as cell growth and survival. DLL3 expression is understood as a direct downstream target of Ascl1, which interacts with the DLL3 gene promoter (7). This suggests that, during evolution of SCLC, Notch1 is inactivated, and Ascl1 and DLL3 are both activated and are, thus, counterparts to Notch1.

Abbreviations: Ascl1, Achaete-scute homolog 1; DLL3, Delta-like protein 3; IHC, Immunohistochemistry; NSCLC, Non-small cell lung cancer; OS, overall survival; Rova-T, Rovalpituzumab tesirine; SCLC, Small cell lung cancer; SI, staining intensity; TPS, Tumor proportion score.

Therefore, one can assume that DLL3 could also be used in cancer chemotherapy to target and suppress tumor cells (8). Rovalpituzumab tesirine (Rova-T) is an antibody–drug conjugate composed of SC16, a humanized IgG1 antibody against DLL3. Rova-T selectively binds to DLL3 on target-expressing cells, is internalized, and upon proteolytic cleavage, releases the toxin pyrrolobenzodiazepine (PBD) leading to cell death (9).

In a phase I clinical trial, Rova-T was more effective in SCLC with DLL3 overexpression (defined as expression in at least 50% of cancer cells by immunohistochemistry) compared with SCLC with a low level of DLL3 expression (5). Hence, DLL3 might be a promising predictive marker for treatment of SCLC with Rova-T (8). Rova-T is currently under development for patients with SCLC positive for DLL3 (3).

Methods to evaluate DLL3 expression assessed via immunohistochemistry are not standardized so far. In the current study, the two applied methods (tumor proportion score and H-score) were previously described in literature, including in the above mentioned trial (5, 10) and compared with each other.

Although most SCLC recur after initial response to chemotherapy, relapsed tumors are usually not biopsied. The aim of our study was, therefore, to investigate the expression of DLL3 on chemorelapsed SCLC samples and to compare its expression to chemonaive counterparts. Differences in DLL3 expression between matched samples would suggest therapy-associated changes in the tumor cells. In case of a loss of DLL3 expression in chemorelapsed SCLC samples one could assume that a therapy with Rova-T is not promising. The results of the study could be used to derive which material should be tested in case of planned therapy with Rova-T in the recurrence situation.

MATERIALS AND METHODS

Cohort

In this multi-institutional retrospective study, tissue samples from chemonaive SCLC and paired recurrent SCLC after chemotherapy as well as from metastatic SCLC were collected. The final cohort included 42 patients and consisted of 30 paired chemonaive-chemorelapsed, 5 paired chemonaive primary-metastatic, and 7 unpaired chemorelapsed SCLC without a chemonaive counterpart. In the latter, from 3 patients, we had

one sample each (only deriving from the primary site) and from 4 patients, we had several (up to 4) samples deriving from the primary site as well as from distant metastases (brain, lymph node, adrenal, liver, bone, contralateral lung). In the paired chemonaive-chemorelapsed subcohort, chemorelapsed tissue derived from local recurrences in 10 cases, from distant metastases in 19 cases (skin, brain, lymph node, bone, pleura, pericardium, breast, pancreas), and in one case, the location of the biopsied recurrent tumor was unknown. Chemonaive metastatic samples derived from adrenals, bone, liver, pleura, skin, and contralateral lung.

Patient Characteristics

The median age in the whole cohort was 63 years (range, 47–83 y), 27 (64.3%) patients were male, 15 (35.7%), were female. All patients received a platin-based chemotherapy, whereas none of the patients had received therapy with Rova-T or other therapeutic agents for example in the context of an immunotherapy. Follow-up data for 33 out of the 42 patients were available. From these, at time of last follow-up, 19 patients were deceased, and 14 were alive. Samples from 4 patients derived from autopsies. The basic clinicopathological data of our study cohort are summarized in **Table 1**.

This study was approved by the internal review board of the University of Luebeck (file number 16-277) and the respective local ethical committees.

Statistical Analyses

For the statistical analyses and data visualization, R software (version 4.0.2, R Foundation, Vienna, Austria; http://www.R-project.org) was used. To investigate differences of DLL3 expression between the group of chemonaive and chemorelapsed samples a Wilcoxon signed-rank test was used. To test if the two evaluation methods (TPS vs. H-score) give equivalent results, Pearson correlation was applied. The Wilcoxon rank-sum test was applied to correlate the site of the recurrent tumor and DLL3 expression. To analyze for correlation of DLL3 expression with clinicopathological characteristics, Fisher's exact test was used. Kaplan–Meier curves were used to illustrate OS in dependency of DLL3 expression and statistically proved by log-rank tests. A p-value of <0.05 was considered significant.

Immunohistochemistry (IHC)

IHC staining was performed according to the manufacturer's instructions, using the Ventana Discovery (Ventana Medical System) automated staining system. In brief, slides were incubated with the primary antibody DLL3 (clone SP347, Ventana, SN 678, RTU). Representative tumor blocks from FFPE tissue were cut in 4-μm thick sections.

DLL3 staining was considered positive if staining was membranous in at least 1% of tumor cells. Protein expression of DLL3 was assessed in two different ways: on the one hand by estimating the percentage of positive tumor cells from all tumor cells (tumor proportion score, TPS, range 0–100%) as previously described (5) and, on the other hand, semi-quantitatively using the H-score method according to Yan et al. by converting the staining intensity (SI) (range 0–3) and the TPS (range 0–100)

TABLE 1 | Patients' baseline characteristics.

	Total	Subcohort paired chemonaive-chemorelapsed
Patients		
Male	27	20
Female	15	10
Survival status		
Alive	14	8
Deceased	19	15
Unknown	9	7
Age at first diagnosis (years)		
Mean	63.6	63.8
Median	63	63
Range	47–83	47–79
Time span between diagnosis and last follow-up (days)		
Min.	13	121
Max.	2.728	1.436
Chemotherapy regime (partially known)		
Cisplatin + etopside	14/23 (60.9%)	8/16 (50%)
Carboplatin + etopside	9/23 (39.1%)	8/16 (50%)
Mean duration (days)	87.2	90.9
Min. duration (days)	30	30
Max. duration (days)	284	284
Palliative intention	21/23	15/16 (94%)
Adjuvant intention	1/23	0
Neoadjuvant intention	1/23	1/16 (6%)
Time span between chemonaive and chemorelapsed sample (days)		
Min.		48
Max.		1.294
Mean		404.1
Median		249
Time span between therapy initiation and relapse (days)		
Min.	15	92
Max.	1.297	1.297
Mean	430.9	421.7
Median	333.5	248
Tumor site		
Primary tumor + recurrent tumor same site	14	10
Primary tumor + recurrent tumor different site	27	19
Unknown	1	1
DLL3 expression (chemonaive vs. chemorelapsed sample)		
TPS 0%		4 vs. 6
TPS <1–49%		10 vs. 5
TPS ≥50%		16 vs. 19
H-Score 0		4 vs. 6
H-Score <150		16 vs. 8
H-Score ≥150		10 vs. 16
DLL3 expression dynamics		
Stable expression		19 (63.3%) with TPS vs. 17 (56.6%) with H-Score
Higher expression in chemonaive sample		4 (13.3%) with TPS vs. 4 (13.3%) with H-Score
Higher expression in chemorelapsed sample		7 (23.3%) with TPS vs. 9 (30%) with H-Score

to a H-score (range, 0–300) (10). SI was indicated as strongly positive (SI 3), moderately positive (SI 2), weakly positive (SI 1) and negative (SI 0). To dichotomize samples into positive and negative staining, TPS $< 50\%$ and H-score ≤ 150 were defined as DLL3 low expression (DLL3-low), and TPS $\geq 50\%$ and H-score > 150 were defined as DLL3 high expression (DLL3-high) (5, 10).

RESULTS

Expression Pattern of DLL3 Protein in Unpaired Chemorelapsed SCLC Samples

In seven cases of the whole cohort, we had solely chemorelapsed samples without a chemonaive counterpart. Of these, from three patients, we had one sample each (only deriving from the primary site), and from four patients, we had several (up to four) samples deriving from the primary site as well as from distant metastases. From the three cases with one sample, two were DLL3-high and one was DLL3-low, assessed by TPS. From the four cases with several samples, three (75%) showed a concordant DLL3 expression between the samples (two DLL3-low, one DLL3-high), and the other one showed high-DLL3 expression in the primary tumor and low-DLL3 expression in the metastatic site. Considering only the staining result of the first sample of each patient, four were DLL3-high and three DLL3-low. One of the two cases with concordant DLL3-low expression derived from an autopsy so that loss of expression may originate from autolysis.

Expression Pattern of DLL3 Protein in Paired Chemonaive Primary and Metastatic SCLC Samples

Three of the five cases with paired chemonaive primary and metastatic SCLC samples showed a concordant DLL3-high

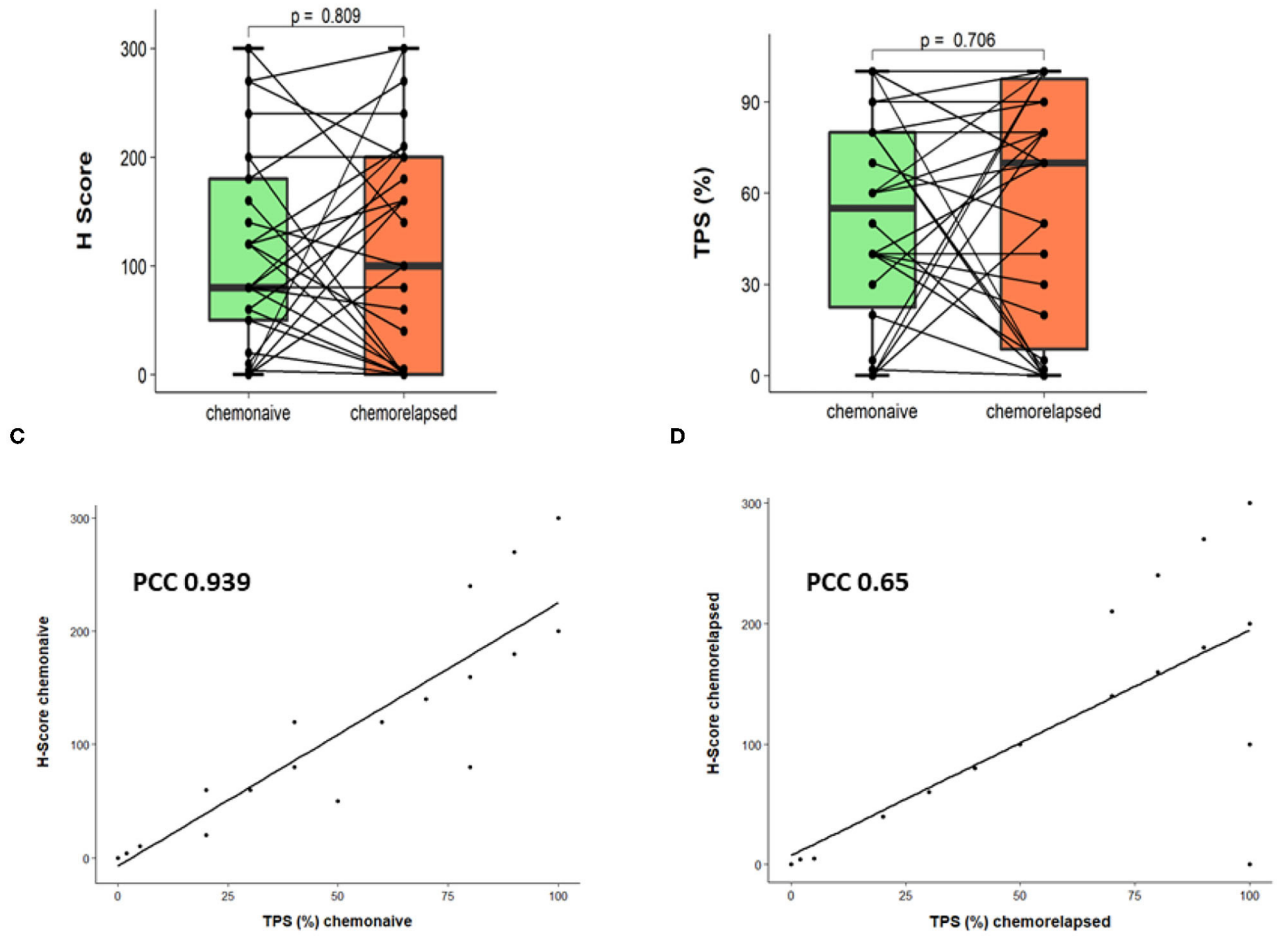

FIGURE 1 | Comparison of DLL3 expression in paired chemonaive-chemorelapsed SCLC samples. **(A)** DLL3 expression assessed by H-score. **(B)** DLL3 expression assessed by TPS. **(C)** Pearson correlation showing application of TPS and H-score on chemonaive SCLC samples. **(D)** Pearson correlation showing application of TPS and H-score on chemorelapsed SCLC samples.

staining pattern, and in two cases, we observed a high-DLL3 expression in the primary tumor and a low expression in the metastatic site, assessed by TPS. One case derived from an autopsy, and here, we investigated four samples deriving from different sites (adrenal, bone, liver, contralateral lung), all showing concordant low DLL3 expression. Here, concordant low expression might also be due to autolytic changes of the tissue.

Expression Pattern of DLL3 Protein in Paired Chemonaive-Chemorelapsed SCLC Samples

Considering only the chemonaive group, using the H-score method, 20 (66.6 %) out of 30 samples were DLL3-low, and 10 (33.3%) were DLL3-high. Out of the DLL3-low samples, four were negative (H-score 0). In the chemorelapsed group, 14 (46.6 %) were DLL3-low and 16 (53.3%) were DLL3-high. Here, out of the DLL3-low samples, 6 were negative (H-score 0). DLL3 expression between the chemonaive and chemorelapsed groups was not significantly different (Wilcoxon signed-rank test $p = 0.809$; **Figure 1A**). Concordant staining, either DLL3-low or DLL3-high in paired chemonaive-chemorelapsed specimens, was observed in 17 out of 30 (56.6%) SCLCs. From those, in 11 cases (64.7%), both samples were DLL3-low, and 6 (35.9%) were DLL3-high. In 13 cases (43.4%) staining was not concordant, meaning that, in 9 cases, the chemonaive sample was DLL3-low and the chemorelapsed sample was DLL3-high ("DLL3 up") and that in 4 cases, the chemonaive sample was DLL3-high, and the chemorelapsed sample was DLL3-low ("DLL3 down").

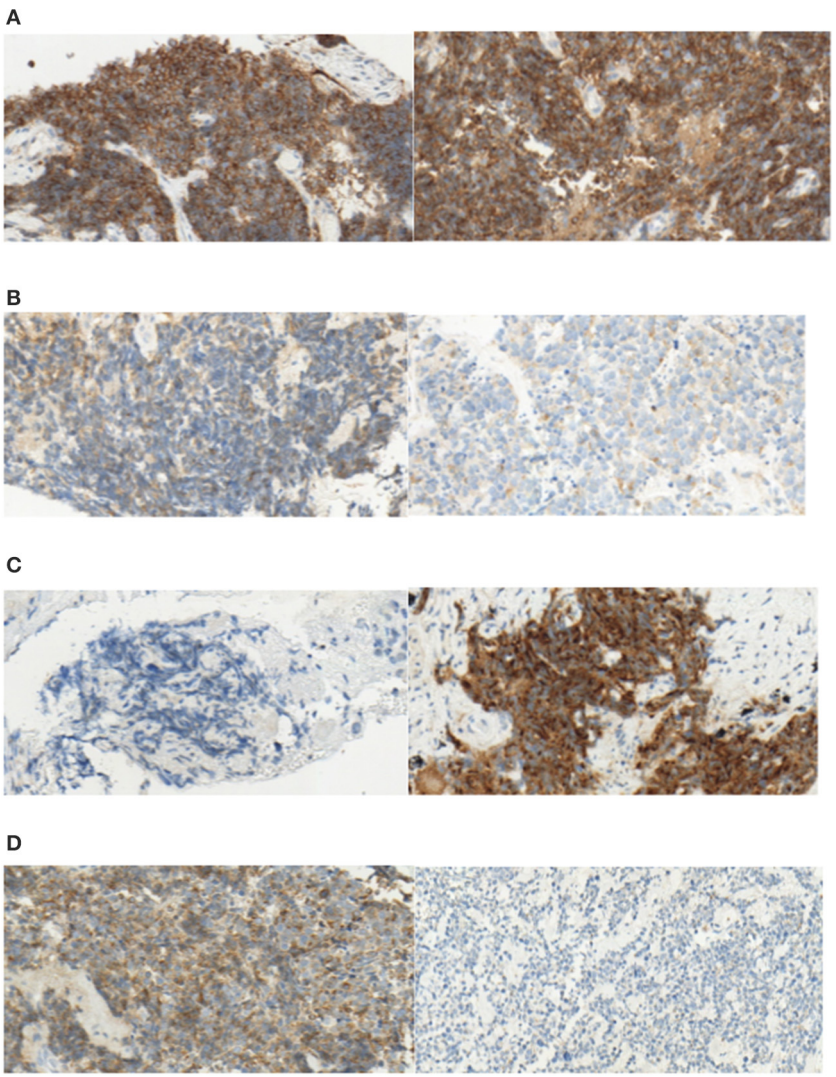

FIGURE 2 | Exemplary pictures of DLL3 staining patterns in paired chemonaive (left) and chemorelapsed (right) SCLC samples. **(A)** Both high DLL3 expression (TPS > 50%, H-score > 150), **(B)** Both low DLL3 expression (TPS < 50%, H-score < 150), **(C)** "DLL3 up" [low expression in chemonaive sample (TPS < 50%, H-score < 150) and high expression in chemorelapsed sample (TPS > 50%, H-score > 150)], **(D)** "DLL3 down" [low expression in chemorelapsed sample (TPS < 50%, H-score < 150) and high expression in chemonaive sample (TPS > 50%, H-score > 150); original magnification ×40].

With regard to TPS, 14 (46.6%) chemonaive samples were DLL3-low, and 16 (53.4%) were DLL3-high. In the chemorelapsed group, 11 (36.6%) samples were DLL3-low and 19 (63.3%) were DLL3-high. Negative samples (TPS <1%) within DLL3-low samples were identical to evaluation with H-score (4 in the chemonaive and 6 in the chemorelapsed groups, respectively). Again, DLL3 expression between the chemonaive and chemorelapsed group was not significantly different (Wilcoxon signed-rank test $p = 0.706$; **Figure 1B**). In the chemonaive group, mean TPS was 52.2%, ranging from 0 to 100%. In the chemorelapsed group, mean TPS was 57.6%, ranging from 0 to 100%. With regard to expression dynamics, 7 out of 30 samples (23.3%) showed equally low DLL3 expression, and 12 (40%) showed equally high expression, meaning that, in 63.3%, TPS was stable between chemonaive and chemorelapsed samples. In 36.7% ($n = 11$), DLL3 expression between the matched samples was different. In 7 cases (23.3%), the chemorelapsed sample had a high TPS, and the chemonaive counterpart a low TPS (DLL3 up), and in 4 cases (13.3%) the dynamic was the other way around (DLL3 down). DLL3 expression data are summarized in **Table 1**, and representative images of DLL3 protein expression assessed by IHC are provided in **Figure 2**.

Two of the cases originated from autopsies. Of these, one case showed a DLL3-down expression pattern assessed with the H-score method as well as with TPS. Again, this could be due to autolytic changes of the tissue. However, the other case showed an equally low expression without the chemorelapsed sample being completely negative (TPS 20%, SI2). Therefore, it cannot be stated in general that DLL3 expression is lost in autopsy material.

To assess both evaluation methods, we correlated TPS and H-score. Pearson correlation provided a linear dependency (PCC 0.939 for chemonaive samples, PCC 0.65 for chemorelapsed samples, **Figures 1C,D**), which proved that both methods were equally applicable. Because the TPS is easier to use in everyday diagnostic practice and probably shows less interobserver variability, only TPS was used for further statistical analysis.

We next evaluated if there was a correlation between tumor site and DLL3 expression. We found no significant differences between local pulmonal and distant recurrences (Wilcoxon rank-sum test $p = 0.32$; **Figure 3**).

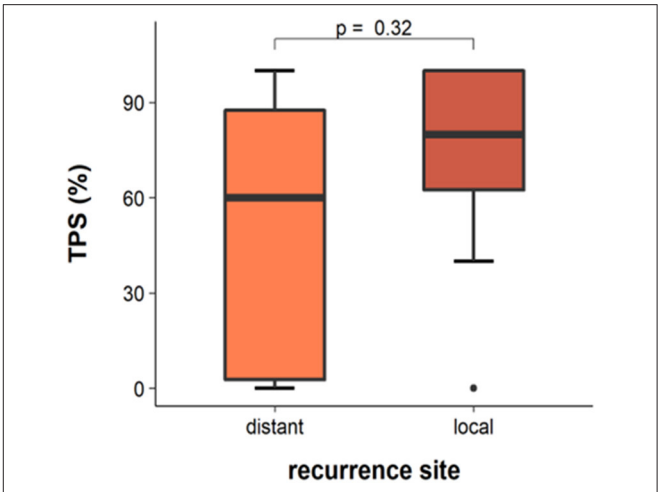

FIGURE 3 | DLL3 expression in chemorelapsed samples in dependency of site of recurrent tumor.

Correlation of DLL3 With Clinicopathological Characteristics in the Paired Chemonaive-Chemorelapsed SCLC Cohort

There was no significant correlation of DLL3 expression level estimated in chemonaive samples with regard to gender, T-status, N-status, M-status, UICC-status, or time to recurrence. The only significant result was shown with regard to age: DLL3-high SCLCs were more frequent in younger patients (median age 57 years) and SCLC with low DLL3 expression more frequent in older patients (median age 67) ($p = 0.024$) (**Table 2**). We performed the same analysis for the DLL3 expression level estimated in chemorelapsed samples and, however, found no significant result for any of the above mentioned parameters (not shown).

Correlation of DLL3 With OS in the Paired Chemonaive-Chemorelapsed SCLC Cohort

The median age of this subcohort was 63 years (range, 47–79), 20 (66.6%) were male, 10 (33.3%), were female. From 23 out of the 30 patients, data concerning survival status was available. The median follow-up time for the patients with SCLCs was 354 days (range, 121–1,436). At the time of last follow-up, 15 patients were deceased and eight were alive.

We analyzed whether DLL3 expression (TPS low vs. high) in chemorelapsed or chemonaive samples could predict OS. Although results are not significant, Kaplan–Meier curves show a trend for better OS if DLL is highly expressed in chemorelapsed samples (log-rank $p = 0.57$) and less expressed in chemonaive samples (log-rank $p = 0.42$) (**Figures 4A,B**), whereas a low DLL3 status in chemorelapsed samples and a high DLL3 expression status in chemonaive samples seem to be more unfavorable. Next, we aimed to analyze if the dynamics of DLL3 expression during therapy has an impact on OS. As the above mentioned results already suggest, upregulation of DLL3 expression in matched samples after therapy reveals a trend for a better OS, whereas the worst survival rates were seen in cases with a downregulated DLL3 expression (log-rank test $p = 0.56$; **Figure 4C**). Survival curves indicating cases in which DLL3 expression stayed stable, either both low or high, lay in between the two curves indicating an upregulated or downregulated DLL3-status and show also a trend for a more favorable survival in high DLL3 expressing tumors.

DISCUSSION

SCLC is one of the most aggressive tumors with so far very limited therapeutic options (5, 9). Essentially all patients with

TABLE 2 | Association analysis between DLL3 expression assessed in chemonaive samples and clinicopathological characteristics of paired chemonaive-chemorelapsed SCLC cohort.

DLL3 expression assessed in chemonaive sample	Total ($n = 30$)	TPS ≧ 50% ($n = 16$)	TPS < 50% ($n = 14$)	*p*-value
Gender				0.26
Male	20 (66.7%)	9 (56.2%)	11 (78.6%)	
Female	10 (33.3%)	7 (43.8%)	3 (21.4%)	
Age				0.024
Missing	1	1	0	
Median (IQR)	65 (57, 70)	57 (55, 68)	67 (61, 75)	
T-Stage				0.58
Missing	16	8	8	
T(1, 2)	4 (28.6%)	3 (37.5%)	1 (16.7%)	
T(3,4)	10 (71.4%)	5 (62.5%)	5 (83.3%)	
N-Status				1
Missing	16	8	8	
N–	2 (14.3%)	1 (12.5%)	1 (16.7%)	
N+	12 (85.7%)	7 (87.5%)	5 (83.3%)	
M-Status				1
Missing	16	8	8	
M–	4 (28.6%)	2 (25.0%)	2 (33.3%)	
M+	10 (71.4%)	6 (75.0%)	4 (66.7%)	
UICC-Stage				1
Missing	16	8	8	
<IV	4 (28.6%)	2 (25.0%)	2 (33.3%)	
IV	10 (71.4%)	6 (75.0%)	4 (66.7%)	
Time to recurrence (months)				0.693
Missing		1	0	
Mean (SD)	12.8 (11.6)	10.4 (7.6)	15.4 (14.5)	
Median (IQR)	8 (5, 16)	8 (6, 14)	8.5 (4, 23.5)	

extensive-stage SCLC and the majority of patients with limited-stage SCLC suffer relapse within months of completing initial standard therapy (11). As SCLC is rarely biopsied following the initial diagnosis, dynamics of expression of therapeutically relevant biomarkers in relapsed disease are poorly understood. Because DLL3 is largely expressed in SCLC and regarded as a potential biomarker for response to Rova-T treatment (8), we aimed to investigate DLL3 expression in chemorelapsed SCLC samples and to compare its expression with matched chemonaive SCLC samples, correlate its expression with clinicopathological data, and perform survival analysis stratified according to DLL3-high or DLL3-low status and dynamics of DLL3 expression during the course of therapy. Possible differences in expression may further indicate if chemonaive or chemorelapsed SCLC specimens should be investigated in cases of a planned therapy with Rova-T. To our knowledge, there are hardly any published studies that investigated DLL3 expression in chemorelapsed SCLC samples and paired chemonaive-chemorelapsed SCLC samples, respectively.

In line with data from the literature, we as well found DLL3 expression in the majority of our SCLC samples. The evaluation method to assess DLL3 expression is not standardized, and there are so far no international standards for cut-off values to determine expression of DLL3 (4).

When comparing the DLL3 expression data of our study with those from the literature, it is important to consider not only the evaluation method, but also the diversity of the DLL3 antibodies used. Brcic et al. (12) investigated four different DLL3 antibodies (VenA (clone SP347; Ventana, Roche, Tucson, AZ, USA), NovA (NBP2–24669; Novus Biological, Littleton, CA, USA), TherA (PA5–26336; Thermo Fisher Scientific, Waltham, MA, USA), and AbcA (ab103102; Abcam, Cambridge, MA, USA)) for their reliability to detect DLL3 expression in high-grade neuroendocrine tumors of the lung. Comparison of VenA [the antibody used in the current study and in the clinical trial (5)] with the other three antibodies demonstrated poor results for overall agreement, positive and negative agreement, and Kappa values. The authors concluded that using VenA as a reference antibody, none of the other three antibodies can reliably be used for the DLL3 test. This, of course, makes comparison of DLL3 expression data between studies difficult. **Table 3** gives an overview of some recent studies dealing with DLL3 expression in SCLC, including their cohort sizes, evaluation methods, used

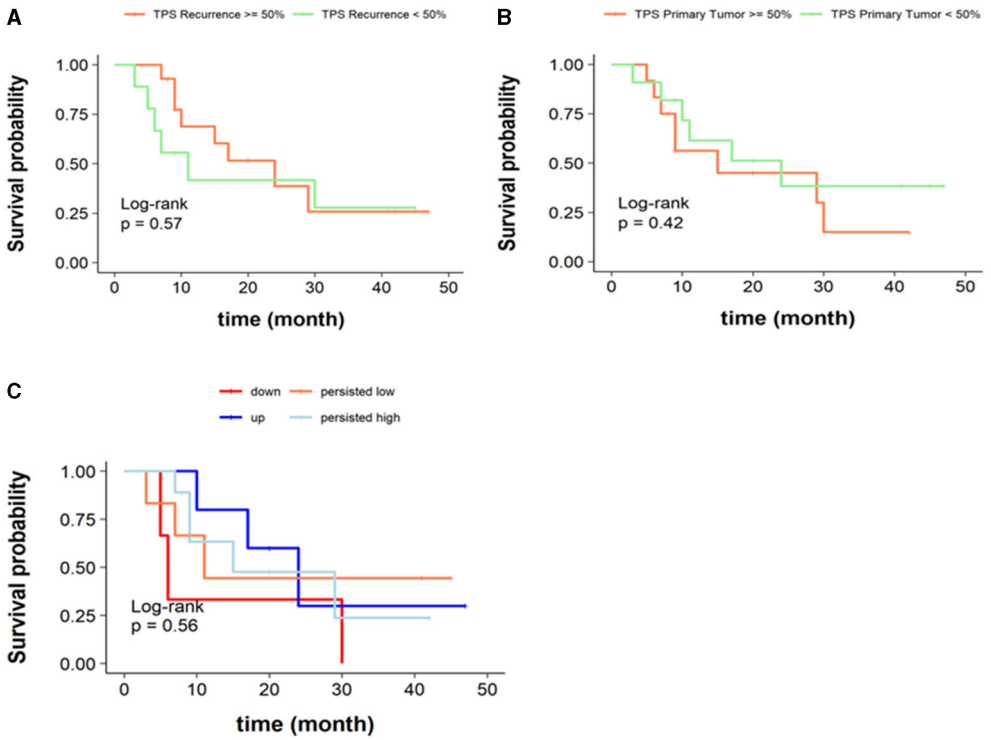

FIGURE 4 | Overall survival according to DLL3 expression status. **(A)** Kaplan–Meier curves stratified according to DLL3-high or DLL3-low status assessed with TPS in chemorelapsed specimens (log-rank $p = 0.57$). **(B)** Kaplan–Meier curves stratified according to DLL3-high or DLL3-low status assessed with TPS in chemonaive specimens (log-rank $p = 0.42$). **(C)** Kaplan–Meier curves stratified according to dynamics of DLL3 expression in the course of therapy. Persisted DLL3-low was defined as TPS < 50% in chemonaive and chemorelapsed samples, persisted DLL3-high was defined as TPS ≥50% in chemonaive and chemorelapsed samples, "up" was defined as a switch from TPS < 50% to ≥ 50%, and "down" was defined as a switch from TPS ≥50% to <50% in the course of therapy (log-rank test $p = 0.56$).

DLL3 antibodies, used cutoffs, and assessed expression data of DLL3 in SCLC.

We assessed DLL3 expression in two different ways, using the H-score and TPS, both known from prior studies (5, 10). We adopted 50% as the cutoff for TPS from a phase I trial conducted by Rudin et al. (5) and, with that, found expression of DLL3 in majority of chemonaive samples (86.6%) out of which 46.6% were DLL3-low and 53.4% DLL3-high. In the study from Rudin et al. (5), the range was higher with 74.4% being highly positive (29/39) and 25.6% (10/39) being weakly positive. The same cutoff was used by Tanaka et al., who investigated 63 presumably chemonaive SCLC samples and found 83% (52/63) positive for DLL3 with 20 samples (32%) being highly positive (3). The data in the literature vary; nevertheless, overall, a quite high rate of highly DLL3 expressing SCLC can be observed. In the group of chemorelapsed SCLC, we found similar DLL3 expression to that in the chemonaive group with 80% being positive, but with a slightly higher proportion of DLL3-high cases (63.3%, 19/30). DLL3 expression between chemonaive and chemorelapsed was stable in more than half of the cases (63.3%) and shifted from low to high or vice versa in 36.7%. However, DLL3 expression between chemonaive and chemorelapsed SCLC samples was not significantly different (Wilcoxon signed-rank test $p = 0.706$; **Figure 1B**) indicating no essential therapy-induced differences.

For evaluation with H-score, we adopted the cutoff of 150 from Yan et al. (10), who investigated 335 presumably chemonaive (*de novo*) SCLC samples and found a low expression (H-score ≤ 150) in 37.6% and a high expression (H-score > 150) in 62.4%. We found contrasting results with this method with a low expression in 66.6% (20/30) in the chemonaive group and a high expression in 33.3% (10/30) in the chemorelapsed group. In the chemorelapsed group instead, expression data were then again similar to those from above mentioned study with a shift to more highly positive SCLC cases [(53.3%, 16/30) vs. 46.6% (14/30) DLL3 low expressing samples]. However, the data are hardly comparable due to the significant differences in the size of the cohorts (335 vs. 30).

Concordant staining in paired chemonaive-chemorelapsed specimens, either both DLL3-low or DLL3-high, was found in only approximately half of the cases (56.6%), meaning that a significant portion (43.4%) showed a shift of DLL3 expression during course of therapy. However, also with this method, we found no significantly different DLL3 expressions between the two groups (Wilcoxon signed-rank test $p = 0.809$; **Figure 1A**).

With both evaluation methods, the proportion of matched samples showing deviating DLL3 expression, meaning a shift from low to high expression or vice versa, during course of therapy was considerable (43.4% with H-score, 36.7% with

TABLE 3 | Overview of recent studies on DLL3 expression in SCLC.

Study	Tissue related to therapy	Cohort size (*n*)	DLL3 antibody	Evaluation method	Cutoff	DLL 3 expression
Yan et al. (10)	Chemonaive (*"de novo"*)	335	ab103102; Abcam, Cambridge, UK	H-Score	≤150 low vs. > 150 high	37.6% low (126/335) 62.4% high (209/335)
Tanaka et al. (3)	not applicable Presumably Chemonaive	63	Stemcentrx, South San Francisco, CA, USA	TPS	<1%, 1–49%, ≥50%	<1%: 17% negative (11/63) 1–49%: 51% (32/63) ≥50%: 32% (20/63)
Xie et al. (13)	not applicable	44	Clone SP346, Ventana-Roche Diagnostics, Indianapolis, IN, USA	TPS plus four-level SI, but cut-off based on TPS	<50% low, ≥50% high	20.5% low (9/44) 79.5% high (35/44)
Regzedmaa et al. (8)	Chemonaive	38	No SAB1302862, Sigma-Aldrich, Shanghai, China	TPS scored as 1 (≤25%), 2 (26–50%), 3 (51–75%), 4 (>75%) multiplied with four-level SI	Median	47.4% low (18/38) 52.6% high (20/38)
Huang et al. (14)	Chemonaive ("firstly diagnosed")	72	ab103102, Abcam, Cambridge, MA, USA	TPS scored as 1 (1–9%), 2 (10–49%), 3 (50–79%), 4 (≥80%) multiplied with four-level SI	<6 low, ≥6 high	68% low (49/72) 32% high (23/72)
Furata et al. (15)	Chemonaive ("primary")	93	SP347; Spring Bioscience, Pleasanton, CA	TPS	<75% low, ≥75% high	53% low (49/93) 47% high (44/93)
Rudin et al. (5)	not applicable	39	Stemcentrx, South San Francisco, CA, USA	TPS	<50% low, ≥50% high	25.6% low (10/39) 74.4% high (29/39)
Rojo et al. (16)	Diverse (independent and paired)	1,050	Clone SP347, Ventana, Tucson	TPS Negative (0–24%), positive (≥25%), non-high positive (25–74%), high positive (≥75%)	Positive (≥25 %)	15% negative (155/1050) 85% positive (895/1050)

TPS). This indicates that DLL3 expression might be influenced by therapy and cannot be considered as stable. Unlike other predictive biomarkers, such as, e.g., PD-L1 with a required TPS of 50% for therapy of NSCLC with Pembrolizumab, so far, a high (≥50%) DLL3 expression of SCLC is not implemented as a prerequisite for therapy with Rova-T. However, if this were the case, our data demonstrate that it does matter which samples are chosen to assess DLL3 expression. There is only a little literature concerning DLL3 expression in paired chemonaive-chemorelapsed SCLC samples. Rojo et al. (16) investigated, in addition to a huge number of independent SCLC samples, also 36 paired SCLC samples, defining "paired" as two specimens from the same patient and same primary disease site or as a first specimen obtained at diagnosis and the second obtained at relapse/recurrence. Of these, only two samples corresponded to paired chemonaive-chemorelapsed samples as we had examined. Moreover, they used a different cutoff than we did with ≥25% positive tumor cells defined as positive DLL3 expression (**Table 3**). With that, they found 88% concordance between paired specimens without specifically addressing the paired chemonaive-chemorelapsed samples. Due to the significant deviation in size of the cohorts, results of this study are hardly comparable with our results.

To our knowledge, the above mentioned study by Yan et al. (10) is the only one using the H-score method with a cutoff of 150. Furthermore, combining a four-level SI and TPS to a H-score should show higher interobserver variability than just using TPS. We, therefore, assessed the two evaluation methods, and after Pearson correlation provided a linear dependency that indicated equality, we have then focused on TPS for further analyses.

We next investigated if the site of the biopsied recurrent tumor has an impact on DLL3 expression. In 33.3% (10/30) chemorelapsed tissue derived from local pulmonal recurrences and in 63.3% (19/30) from distant metastases. Concordant with

the literature (3, 10), we found no significant differences of DLL3 expression between local pulmonal and distant recurrences (Wilcoxon rank-sum test $p = 0.32$; **Figure 3**). Yan et al., for instance, compared intertumoral expression of DLL3 on the basis of 37 paired biopsies of primary and metastatic sites and found concordant staining in all cases (10).

Apart from age when considering the chemonaive samples, we found no association of DLL3 expression with clinicopathological data in our cohort (**Table 2**). Our observation that DLL3 expression actually does not associate with clinicopathological data broadly fit with those from the literature. For instance, Tanaka et al. (3) also found no significant association between DLL3 expression and age, sex, smoking history, or disease stage, and Yan et al. (10) found no significant association with age, distant metastasis status, or TNM stage. In the latter study, DLL3 expression was higher in TTF-1 expressing SCLC samples ($p = 0.006$), smokers ($p = 0.023$), and males ($p = 0.041$), whereas high DLL3 expression was associated with female sex ($p = 0.03$) in a study conducted by Xie et al. (13). Furata et al. found that DLL3-high expression (defined as TPS $\geq$ 75%) was significantly more prevalent in patients with lymph node metastases and advanced c-stage (15). These few significant correlations found in our study and in the literature are, due to their diversity, primarily a coincidence and might not have a causal relationship.

We next investigated if DLL3 expression has an impact on OS. Kaplan–Meier curves do not show significant results, but a trend for a better OS if DLL is highly expressed in chemorelapsed samples (log-rank $p = 0.57$) and low expressed in chemonaive samples (log-rank $p = 0.42$) (**Figures 4A,B**), whereas a low DLL3 status in chemorelapsed samples and a high DLL3 expression status in chemonaive samples seem to be more unfavorable. Several other studies also analyzed the relationship of DLL3 expression and OS, and the corresponding results are partly contradictory. Some studies found no statistically significant difference of OS between DLL3 low and high expressing tumors (3, 15), whereas Regzedmaa et al. found that high expression of DLL3 assessed on chemonaive SCLC correlated significantly with poorer patient outcomes ($p = <0.001$) (8). Yan et al. also found that patients with chemonaive SCLC having a high DLL3 expression level exhibited a lower OS compared with patients with DLL3-low expressing SCLC ($p = 0.007$). In this study, expression of DLL3 and TTF-1 was investigated in combination, and additionally, it was found that the group of SCLC with low expression of DLL3 in combination with missing TTF-1 expression showed improved OS (10). Huang et al. also found a high level of DLL3 to be correlated with low OS rate ($p < 0.01$) (14). Despite lacking significance, our survival curves also indicate that there is a trend for better survival if chemonaive samples show low DLL3 expression (**Figure 4B**). Xie et al. found that high DLL3 expression was associated with better OS in SCLC ($p = 0.049$). At first glance, the results seem contradictory. However, in this study, only a few cases showed low DLL3 expression, and after adjusting for age, tumor size, and stage, DLL3 expression was no longer associated with OS (13).

Due to our samples being matched, we then analyzed if the dynamics of DLL3 expression in the course of therapy associates with survival. As the above mentioned results already suggest, upregulation of DLL3 expression in matched samples after therapy reveals a trend for better overall survival, whereas the worst survival rates were seen in cases with a downregulated DLL3 expression (log-rank test $p = 0.56$; **Figure 4C**). Survival curves indicating cases in which DLL3 expression was concordant in chemonaive and chemorelapsed samples, either both low or high, lay in between the two curves, indicating survival in dependency of an upregulated or downregulated DLL3-status. Here, a trend that stable high expression is associated with a more favorable survival than stable low expression can be derived. This might suggest that DLL3 expression assessed in chemorelapsed samples is more meaningful regarding OS due to beforehand we could show that a low expression in chemonaive samples and a high expression of DLL3 only in chemorelapsed samples indicated a better OS (**Figures 4A,B**).

In a study from Tendler et al. (7), it was found that subjects with Notch1 low expressing chemorelapsed SCLC samples showed a better prognosis and higher sensitivity to chemotherapy. Assuming that Notch1 and DLL3 are opponents during the evolution of SCLC, one could expect a high DLL3 expression if Notch 1 shows a low expression. Thus, our result for a trend for better prognosis in DLL3 high expressing chemorelapsed SCLC is in line with that of Tendler et al.

To our knowledge, our study is the first investigating DLL3 expression in a large cohort of paired chemonaive-chemorelapsed SCLC samples, which is why our results concerning OS in relation to the dynamics of DLL3 expression cannot be compared with data in the literature. Our survival data is not significant. This might be due to the relatively small cohort size, which, at the same time, represents a limitation of our study. However, against the background that, in most cases, recurrent SCLC is not biopsied at all, our cohort is exceptional. Another limitation of our study is that recent literature (17, 18) on DLL3 seems to diminish its value as a potential therapeutic agent, which also weakens the value of the present work.

To sum up, the current study delivers, for the first time, data concerning DLL3 expression in a large cohort of rare paired chemonaive and chemorelapsed SCLC samples, which is exceptional due to relapsed SCLC are usually not being biopsied. However, investigation of chemorelapsed tumor tissue is essential because it might provide hints why early recurrences, characteristic for SCLC, occur. As the first, we show that, in a large proportion of paired chemonaive-chemorelapsed SCLC samples, DLL3 expression is not stable during the course of therapy, indicating therapy-associated alterations. This demonstrates that it is worth assessing protein expression of biomarkers in general and here, especially of DLL3 in chemorelapsed samples, meaning in the latest tumor tissue. This should, at the same time, be an incentive to gain tumor tissue by biopsy in relapses. Due to the manner of assessing expression of DLL3 not being standardized, we tested two evaluation methods and applied TPS and H-score. Both approaches delivered comparable results, but because TPS should be more practical in routine diagnostics than the H-score method, we have continued working with TPS. As in other studies, we found that the majority of SCLC samples expressed DLL3 and also did not find any

profound correlations with clinicopathological data or tumor site. Concordant with data from the literature, our survival analysis revealed a trend for a better OS if DLL is low expressed (<50%) in chemonaive samples. Interestingly, this does not seem to apply to chemorelapsed SCLC because, for those, we could observe a trend for a more favorable survival in the event of a high expression (≥50%). In line with that, cases showing a shift from a low to a high expression of DLL3 during the course of therapy indicated the most favorable survival data. These results should not be overstated due to the size of our cohort not being powered to detect association with survival data. However, the study definitely shows the importance of research of chemorelapsed tumor tissue.

DATA AVAILABILITY STATEMENT

The raw data supporting the conclusions of this article will be made available by the authors, without undue reservation.

AUTHOR CONTRIBUTIONS

SP and CK planned the research project and evaluated the samples. ED performed the immunohistochemical stainings. TJ performed the statistical analysis. F-OP, CH, BK, SBo, BM, MA, SBe, MT, HB, and FF provided patients' follow-up data. CK, TJ, RK, F-OP, CH, BM, JR-I, CI, MA, SBe, MT, HB, FF, BK, SBo, VS, JK, and SP wrote and/or revised the manuscript. All authors have read and agreed to the published version of the manuscript.

FUNDING

This research was supported with funds from the Section of Medicine at the University of Luebeck J18-2020.

ACKNOWLEDGMENTS

The authors thank ED for the excellent technical assistance.

REFERENCES

1. Saunders LR, Bankovich AJ, Anderson WC, Aujay MA, Bheddah S, Black K, et al. A DLL3-targeted antibody-drug conjugate eradicates high-grade pulmonary neuroendocrine tumor-initiating cells *in vivo*. *Sci Transl Med*. (2015) 7:302ra136. doi: 10.1126/scitranslmed.aac9459
2. Horn L, Mansfield AS, Szczesna A, Havel L, Krzakowski M, Hochmair MJ, et al. First-Line Atezolizumab plus chemotherapy in extensive-stage small-cell lung cancer. *N Engl J Med*. (2018) 379:2220–9. doi: 10.1056/NEJMoa1809064
3. Tanaka K, Isse K, Fujihira T, Takenoyama M, Saunders L, Bheddah S, et al. Prevalence of Delta-like protein 3 expression in patients with small cell lung cancer. *Lung Cancer Amst Neth*. (2018) 115:116–20. doi: 10.1016/j.lungcan.2017.11.018
4. Chen B, Li H, Liu C, Wang S, Zhang F, Zhang L, et al. Potential prognostic value of delta-like protein 3 in small cell lung cancer: a meta-analysis. *World J Surg Oncol*. (2020) 18:226. doi: 10.1186/s12957-020-02004-5
5. Rudin CM, Pietanza MC, Bauer TM, Ready N, Morgensztern D, Glisson BS, et al. Rovalpituzumab tesirine, a DLL3-targeted antibody-drug conjugate, in recurrent small-cell lung cancer: a first-in-human, first-in-class, open-label, phase 1 study. *Lancet Oncol*. (2017) 18:42–51. doi: 10.1016/S1470-2045(16)30565-4
6. Leonetti A, Facchinetti F, Minari R, Cortellini A, Rolfo CD, Giovannetti E, et al. Notch pathway in small-cell lung cancer: from preclinical evidence to therapeutic challenges. *Cell Oncol Dordr*. (2019) 42:261–73. doi: 10.1007/s13402-019-00441-3
7. Tendler S, Kanter L, Lewensohn R, Ortiz-Villalón C, Viktorsson K, De Petris L. The prognostic implications of Notch1, Hes1, Ascl1, and DLL3 protein expression in SCLC patients receiving platinum-based chemotherapy. *PLoS ONE*. (2020) 15:e0240973. doi: 10.1371/journal.pone.0240973
8. Regzedmaa O, Li Y, Li Y, Zhang H, Wang J, Gong H, et al. Prevalence of DLL3, CTLA-4 and MSTN expression in patients with small cell lung cancer. *OncoTargets Ther*. (2019) 12:10043–55. doi: 10.2147/OTT.S216362
9. Morgensztern D, Besse B, Greillier L, Santana-Davila R, Ready N, Hann CL, et al. Efficacy and safety of rovalpituzumab tesirine in third-line and beyond patients with DLL3-expressing, relapsed/refractory small-cell lung cancer: results from the phase II TRINITY study. *Clin Cancer Res*. (2019) 25:6958–66. doi: 10.1158/1078-0432.CCR-19-1133
10. Yan L-X, Liu Y-H, Li Z, Luo D-L, Li Y-F, Yan J-H, et al. Prognostic value of delta-like protein 3 combined with thyroid transcription factor-1 in small-cell lung cancer. *Oncol Lett*. (2019) 18:2254–61. doi: 10.3892/ol.2019.10538
11. Pietanza MC, Byers LA, Minna JD, Rudin CM. Small cell lung cancer: will recent progress lead to improved outcomes? *Clin Cancer Res*. (2015) 21:2244–55. doi: 10.1158/1078-0432.CCR-14-2958
12. Brcic L, Kuchler C, Eidenhammer S, Pabst D, Quehenberger F, Gazdar AF, et al. Comparison of four DLL3 antibodies performance in high grade neuroendocrine lung tumor samples and cell cultures. *Diagn Pathol*. (2019) 14:549–61. doi: 10.1186/s13000-019-0827-z
13. Xie H, Boland JM, Maleszewski JJ, Aubry MC, Yi ES, Jenkins SM, et al. Expression of delta-like protein 3 is reproducibly present in a subset of small cell lung carcinomas and pulmonary carcinoid tumors. *Lung Cancer Amst Neth*. (2019) 135:73–9. doi: 10.1016/j.lungcan.2019.07.016
14. Huang J, Cao D, Sha J, Zhu X, Han S. DLL3 is regulated by LIN28B and miR-518d-5p and regulates cell proliferation, migration and chemotherapy response in advanced small cell lung cancer. *Biochem Biophys Res Commun*. (2019) 514:853–60. doi: 10.1016/j.bbrc.2019.04.130
15. Furuta M, Sakakibara-Konishi J, Kikuchi H, Yokouchi H, Nishihara H, Minemura H, et al. Analysis of DLL3 and ASCL1 in surgically resected small cell lung cancer (HOT1702). *Oncologist*. (2019) 24:e1172–9. doi: 10.1634/theoncologist.2018-0676
16. Rojo F, Corassa M, Mavroudis D, Öz AB, Biesma B, Brcic L, et al. International real-world study of DLL3 expression in patients with small cell lung cancer. *Lung Cancer Amst Neth*. (2020) 147:237–43. doi: 10.1016/j.lungcan.2020.07.026
17. Blackhall F, Jao K, Greillier L, Cho BC, Penkov K, Reguart N, et al. Efficacy and safety of rovalpituzumab tesirine compared with topotecan as second-line therapy in DLL3-high SCLC: results from the phase 3 TAHOE study. *J Thorac Oncol*. (2021) 16:1547–58. doi: 10.1016/j.jtho.2021.02.009
18. Johnson ML, Zvirbule Z, Laktionov K, Helland A, Cho BC, Gutierrez V, et al. Rovalpituzumab tesirine as a maintenance therapy after first-line platinum-based chemotherapy in patients with extensive-stage-SCLC: results from the phase 3 MERU study. *J Thorac Oncol*. (2021) 16:1570–81. doi: 10.1016/j.jtho.2021.03.012

Conflict of Interest: SP is a consultant of Ventana, Roche, Novartis, Astellar, Astrazeneca, Bristol-Myers Squibb, Merck Serono and MSD. JK is a consultant of Roche, Novartis, BMS and MSD. BM received an honorary from AbbVie for a one-time consulting activity.

The remaining authors declare that the research was conducted in the absence of any commercial or financial relationships that could be construed as a potential conflict of interest.

Publisher's Note: All claims expressed in this article are solely those of the authors and do not necessarily represent those of their affiliated organizations, or those of the publisher, the editors and the reviewers. Any product that may be evaluated in this article, or claim that may be made by its manufacturer, is not guaranteed or endorsed by the publisher.

frontiers in Medicine

PERSPECTIVE
published: 27 October 2021
doi: 10.3389/fmed.2021.744697

SARS-CoV2 Infection and the Importance of Potassium Balance

*Helen C. Causton**

Department of Pathology and Cell Biology, Columbia University Irving Medical Center, New York, NY, United States

SARS-CoV2 infection results in a range of symptoms from mild pneumonia to cardiac arrhythmias, hyperactivation of the immune response, systemic organ failure and death. However, the mechanism of action has been hard to establish. Analysis of symptoms associated with COVID-19, the activity of repurposed drugs associated with lower death rates or antiviral activity *in vitro* and a small number of studies describing interventions, point to the importance of electrolyte, and particularly potassium, homeostasis at both the cellular, and systemic level. Elevated urinary loss of potassium is associated with disease severity, and the response to electrolyte replenishment correlates with progression toward recovery. These findings suggest possible diagnostic opportunities and therapeutic interventions. They provide insights into comorbidities and mechanisms associated with infection by SARS-CoV2 and other RNA viruses that target the ACE2 receptor, and/or activate cytokine-mediated immune responses in a potassium-dependent manner.

Keywords: electrolyte, renin-angiotensin system, drug repurposing, SARS-CoV-2 infection, potassium

OPEN ACCESS

Edited by:
Ihsan Ullah,
Khyber Medical University, Pakistan

Reviewed by:
Yan Li,
Oregon Health and Science University, United States
Ignacija Vlašić,
Rudjer Boskovic Institute, Croatia

***Correspondence:**
Helen C. Causton
hc2415@cumc.columbia.edu

Specialty section:
This article was submitted to Pathology, a section of the journal Frontiers in Medicine

Received: *20 July 2021*
Accepted: *30 September 2021*
Published: *27 October 2021*

Citation:
Causton HC (2021) SARS-CoV2 Infection and the Importance of Potassium Balance. Front. Med. 8:744697. doi: 10.3389/fmed.2021.744697

INTRODUCTION

SARS-CoV2 infects cells *via* interaction with the ACE2 receptor which is found primarily on the surface of the heart, liver, kidney, and lungs (1). ACE2 is a negative regulator of the renin-angiotensin system (RAS) that acts in conjunction with ion transporters and the insulin receptor to protect against hypertension, diabetes, cardiovascular disease, and organ damage (2). It does this by regulating electrolyte balance and blood pressure, cell volume, intercellular signaling, filtering of urine in the kidney, membrane potential, and the firing rate of electrically active cells (3, 4). Binding of ACE2 by the SARS-CoV2 virus and the processes of viral entry and replication, enhance degradation of the receptor, which decreases inhibition of the classical RAS system. The net result is increased reabsorption of sodium and water, and raised blood pressure (5). Hypokalemia/low intracellular potassium can also lead to cellular hyperpolarity, increased resting potential, and depolarization in cardiac and lung cells that can trigger ventricular arrhythmia and respiratory dysfunction (6). In parallel, expression of the viral viroporin, Orf3a protein actively promotes potassium efflux, and stimulates activation of the innate immune response. It does so by triggering

the cell-intrinsic Nod-like receptor family, pyrin domain-containing 3 (NLRP3) inflammasome (7–9), which promotes cytokine release. Inflammasome responses play fundamental roles in clearing viruses and promoting tissue repair (10), however, hyperactivation of this immune response, gives rise to the devastating "cytokine storm" that is associated with severe infection, and a major cause of death (11).

This mini-perspective discusses the effects of electrolyte and potassium imbalance in SARS-CoV2 infection, describes how a number of comorbidities of COVID-19 affect ion homeostasis and, identifies some drugs effective against SARS-CoV2 *in vivo* that have also been shown to affect pH or K+ balance. Collectively, these findings highlight the importance of maintaining, and promoting electrolyte homeostasis. They also provide a framework for beginning to understand the broad, and seemingly unrelated, range of symptoms associated with COVID-19 and possibly other RNA viruses, that target the ACE2 receptor and/or those that activate the NRPL3 inflammasome in a potassium-dependent manner.

POTASSIUM IMBALANCE IS COMMON AMONG PATIENTS WITH SEVERE SARS-CoV2 INFECTION

Potassium homeostasis is maintained at a systemic level, in the balance between dietary intake (∼100 mmol/day) and excretion (95% *via* the kidney; 5% *via* the colon) and *via* internal balance of K^+ between intracellular and extracellular fluid compartments (4). Hypokalemia, typically defined as <3.5 mmol/L in plasma, shares many of the features of SARS-CoV2 infection, including muscle weakness, palpitations, cardiac dysrhythmias, and poor diabetic control (4, 12).

In the course of SARS-CoV2 infection, hypokalemia is primarily caused by elevated aldosterone, which promotes excretion of potassium in urine (13). One study involving 1,415 patients, found electrolyte imbalance and hypokalemia were associated with disease severity (Weighted Mean Difference:0.12 mmol/L [95% CI: −0.18 to −0.07 mmol/ L], I21/433%) (14). Another found that hypokalemia around the time of admission was associated with a requirement for invasive mechanical ventilation (15), while a smaller study observed that although only 54% of the patients ($n = 175$) had low potassium levels, of the severely ill patients 85% had hypokalemia (13). A case-controlled study of three emergency rooms in France found that hypokalemia and hyponatremia (sodium <135 mmol/L) were independently associated with COVID-19 infection, but that low sodium, and not potassium levels were associated with ICU admission (16). Disease severity is also related to the degree of response to potassium replacement as mildly ill COVID-19 patients with hypokalemia in the Chen study achieved normokalemia within 5–8 days of potassium replacement (3 g potassium chloride or 40 mEq/day), whereas, it took 10–14 days to achieve homeostasis potassium in severely ill patients (13). Severe hypokalemia may be harder to correct as it is associated with alkalosis (29% had a ≥ pH 7.45) (13). This is due to hydrogen-potassium exchange between the intra and extracellular fluid (4). Patients with COVID-19 are also susceptible to pro-arrhythmic effects (17).

A NUMBER OF COMORBIDITIES FOR COVID-19 AFFECT ION HOMEOSTASIS

Patients with severe symptoms of COVID-19 are more likely to have kidney or cardiovascular disease, hypertension, diabetes mellitus (DM) or other comorbidities than those with milder symptoms (18–22). The association between COVID-19 and a number of these comorbidities is bidirectional (23, 24): patients with diabetes are more likely to develop severe symptoms or die of COVID-19 (12, 22) and acute diabetes or acid-ketosis can develop as a result of SARS-CoV2 infection (25–28). High levels of insulin are found in the olfactory bulb in the brain. Insulin modulates the voltage-dependent potassium channel, Kv1.3, and suppresses the Kv1.3-contributed current in cultured olfactory bulb neurons (OBNs) of rodents (29, 30),while deletion of the Kv1.3 channel results in "super smeller" mice (31). There is little data on the effect of decreased insulin production on the Kv1.3 channel, however it may contribute to the anosmia experienced by some COVID-19 patients (32).

A NUMBER OF REPURPOSED DRUGS EFFECTIVE AGAINST SARS-CoV2 AFFECT POTASSIUM BALANCE

It has been hard to obtain insights into the mechanism by which SARS-CoV2 acts, based on the diversity of symptoms identified in infected individuals. Likewise, FDA approved drugs that act *in vitro* to reduce viral replication and plaque formation, increase cell viability, or are associated with lower death rates in patients target a range of host factors. These drugs are used for a wide range of purposes from treatment of malaria to pancreatitis and diabetes (33–36) (**Table 1**). However, some patterns are emerging: 17 of 66 FDA approved drugs with anti-viral activity were found to target the Sigma-1 receptor (σ1-R) and sigma-2 receptor (σ2-R) (SIGMAR1/SIGMAR2) (34). Sigma receptors are ubiquitously expressed in mammalian tissues and are involved in cellular signaling in a number of conditions including retinal and neurodegenerative disorders (37, 38). A number of σ1-R and σ2-R receptor agonists have been found to inhibit Kv2.1 potassium channel activity in a receptor-independent manner (39), suggesting that they act to modulate potassium currents directly. Another 7 of the 69 drugs inhibit protein synthesis (34). Although the mechanism is not known, protein synthesis, and potassium abundance are inversely correlated in systems as diverse as yeast, algae, and mouse fibroblasts (40–43), such that inhibition of protein synthesis would be expected to result in greater intracellular potassium abundance. A further 17 drugs have been shown to affect osmotic or ion homeostasis. Agonists of potassium channels, angiotensin II, and protein synthesis were also found to be enriched among drugs with anti-SARS-CoV2 activity in an independent study (35).

TABLE 1 | Repurposed drugs with anti-viral activity that also affect potassium balance.

Drug	Human target	Anti-viral activity	Indication	Affects	Reference
Camostat	Cell Entry	(44, 45)	Pancreatitis	Elevates Na+:K+ ratio	(46)
Chloroquine	Cell Entry	(47)	Malaria, immune modulation	Blocks hERG K+ channels	(48)
Hydroxy chloroquine	Cell Entry	(34, 47)	Malaria, immune modulation	Blocks hERG K+ channels	(48)
Loratadine	SLC6A15	(49)	Antihistamine	Kv1.5, outward current	(50, 51)
Nafamostat	Cell Entry	(52)	Pancreatitis	Can induce hyperkalemia, by suppressing the Na-K ATPase dependent pathway	(53)
Pioglitazone	CISD1	(54)	Diabetes	Remodeling of Kv1.5 & Kv4.2	(55)
YH-1238	H+, K+ ATPase Proton Pump	(35)	Phase I	H^+,K^+-ATPase (ATP4A, ATP4B)	(35)

Some of these repurposed drugs many act to reduce disease severity *via* their effects on the immune system. Sex hormones, such as progesterone, promote immune tolerance, and anti-inflammatory responses and that may account for lower COVID-related disease severity and mortality in women and during pregnancy (56, 57). Clinical studies of drug efficacy also point to the key role of the renin-angiotensin system and electrolyte balance in influencing patient outcomes. A retrospective study of COVID-19 patients taking famotidine, an antiacid, found that hospitalized patients taking the drug were more than twice as likely to survive (33). Famotidine was also identified in a computational screen of drugs likely to have anti-SARS-CoV2 activity (36). Another drug, Nafamostat, acts on potassium balance by reducing urinary excretion of potassium *via* the Na+/K+ ATPase-dependent pathway (58, 59). These data support the idea that restoring potassium balance promotes a better host response against viral infection. Conversely some of these drugs pose a risk as they promote hyperkalemia (48, 60). This is a complication found in a number of patients who die of COVID-19 (37% of those who died (n = 113) compared with 14% (n = 161) of those who recovered (61).

Potassium dysregulation is also likely to form part of the mechanism that promotes viral pathogenicity. A study that ectopically expressed the SARS-CoV2 envelope (E) protein in HEK 293 and NIH3T3 cells found that it formed a pH-dependent ion channel permeable to potassium and sodium ions (62). Only a small proportion of the E protein ends up in the viral envelope and most is localized to the endoplasmic reticulum-Golgi complex where it multimerizes to form a virioporin, that promotes an increase in intra-golgi pH (62, 63). The E protein channel is critical for infectivity and for the pathogenicity of SARS-CoV2, as it is for other coronaviruses, and thus presents a good target for therapeutic intervention (63, 64).

DISCUSSION

Taken together, these observations drawn from comorbidities, clinical features of disease and the possible targets of drugs that are effective against viral infection show that symptoms associated with low intracellular potassium are similar to those that result from SARS-CoV2 infection, and that potassium efflux can promote hyperactivation of the innate immune response. Although we do not yet understand how SARS-CoV2 acts in detail, potassium balance is likely to be important for both the propagation and pathogenicity of the virus, *via* effects on both the virus, and on homeostatic mechanisms in the host.

It is likely that this line of enquiry will have relevance for understanding the consequences of viral infection more broadly. Ion disturbance, mediated by virioporins, is central to the mechanism of action of a range of viruses from influenza, and rhinovirus to COVID-19 and HIV (8), and a number of RNA viruses modulate activity of the NLRP3 inflammasome in a potassium-dependent manner (65, 66). In bats, dampening of the inflammasome and proinflammatory responses confers tolerance to a range of RNA viruses, suggesting that modulating the inflammasome may prove a useful therapeutic target for reducing disease severity in humans too (10).

Similarities between SARS-CoV2 and other coronaviruses offer further mechanistic insight and opportunities for drug repurposing. SARS-CoV1 also enters the cell *via* the ACE2 receptor and can cause acute lung failure, cardiac arrhythmia, gastrointestinal disorders, hyperkalemia and diabetes (4, 5, 67, 68). Nafamostat, which induces hyperkalemia, inhibits the activity of SARS-CoV1, 2 and MERS-CoV (52, 53, 60, 69). Approximately 50 FDA-approved drugs are known to have activity against all 3 viruses (70). These results present a strong argument for gaining a fundamental understanding of how electrolyte balance functions in both the healthy host and in response to viral infection. This knowledge is expected to identify strategies for diagnosis and therapeutic intervention in patients suffering from a number of virally induced diseases.

DATA AVAILABILITY STATEMENT

The original contributions presented in the study are included in the article/supplementary material, further inquiries can be directed to the corresponding author/s.

AUTHOR CONTRIBUTIONS

The author confirms being the sole contributor of this work and has approved it for publication.

REFERENCES

1. Hamming I, Timens W, Bulthuis ML, Lely AT, Navis G, van Goor H. Tissue distribution of ACE2 protein, the functional receptor for SARS coronavirus. A first step in understanding SARS pathogenesis. *J Pathol.* (2004) 203:631–7. doi: 10.1002/path.1570
2. Cheng H, Wang Y, Wang GQ. Organ-protective effect of angiotensin-converting enzyme 2 and its effect on the prognosis of COVID-19. *J Med Virol.* (2020) 92:726–730. doi: 10.1002/jmv.25785
3. Santos RA, Ferreira AJ, Simoes AC. Recent advances in the angiotensin-converting enzyme 2-angiotensin(1-7)-Mas axis. *Exp Physiol.* (2008) 93:519–27. doi: 10.1113/expphysiol.2008.042002
4. Unwin RJ, Luft FC, Shirley DG. Pathophysiology and management of hypokalemia: a clinical perspective. *Nat Rev Nephrol.* (2011) 7:75–84. doi: 10.1038/nrneph.2010.175
5. Kuba K, Imai Y, Rao S, Jiang C, Penninger JM. Lessons from SARS: control of acute lung failure by the SARS receptor ACE2. *J Mol Med.* (2006) 84:814–20. doi: 10.1007/s00109-006-0094-9
6. Bielecka-Dabrowa A, Mikhailidis DP, Jones L, Rysz J, Aronow WS, Banach M. The meaning of hypokalemia in heart failure. *Int J Cardiol.* (2012) 158:12–7. doi: 10.1016/j.ijcard.2011.06.121
7. Chen IY, Moriyama M, Chang MF, Ichinohe T. Severe acute respiratory syndrome coronavirus viroporin 3a activates the NLRP3 inflammasome. *Front Microbiol.* (2019) 10:50. doi: 10.3389/fmicb.2019.00050
8. Farag NS, Breitinger U, Breitinger HG, El Azizi, MA. Viroporins and inflammasomes: a key to understand virus-induced inflammation. *Int J Biochemistr Cell Biol.* (2020) 122:105738. doi: 10.1016/j.biocel.2020.105738
9. Xu H, Chitre SA, Akinyemi IA, Loeb JC, Lednicky JA, McIntosh MT, Bhaduri-McIntosh S. SARS-CoV-2 viroporin triggers the NLRP3 inflammatory pathway, *BioRxiv* (2020). doi: 10.1101/2020.10.27.357731
10. Nagaraja S, Jain D, Kesavardhana S. Inflammasome regulation in driving COVID-19 severity in humans and immune tolerance in bats. *J Leukoc Biol.* (2021) 21:93. doi: 10.1002/JLB.4COVHR0221-093RR
11. Hu B, Huang S, Yin L. The cytokine storm and COVID-19. *J Med Virol.* (2021) 93:250–256. doi: 10.1002/jmv.26232
12. Docherty A, Harrison E, Green C, Hardwick H, Pius R, Norman L, et al. Features of 20133 UK patients in hospital with covid-19 using the ISARIC WHO clinical characterisation protocol: prospective observational cohort study. *BMJ*. (2020) 369:m1985.
13. Chen D, Li X, Song Q, Hu C, Su F, Dai J, et al. Assessment of hypokalemia and clinical characteristics in patients with coronavirus disease 2019 in Wenzhou, China. *JAMA Netw Open.* (2020) 3:e2011122. doi: 10.1001/jamanetworkopen.2020.11122
14. Lippi G, South AM, Henry BM. Electrolyte imbalances in patients with severe coronavirus disease 2019 (COVID-19). *Ann Clin Biochem.* (2020) 57:262–265. doi: 10.1177/0004563220922255
15. Moreno-Perez O, Merino E, Leon-Ramirez JM, Andres M, Ramos JMJ, et al. CA.r. group, Post-acute COVID-19 syndrome. Incidence and risk factors: A Mediterranean cohort study. *J Infect.* (2021) 82:378–383. doi: 10.1016/j.jinf.2021.01.004
16. De Carvalho H, Richard MC, Chouihed T, Goffinet NQ, Freund Y, Kratz A, et al. Electrolyte imbalance in COVID-19 patients admitted to the emergency department: a case-control study. *Intern Emerg Med.* (2021) 6:32. doi: 10.1007/s11739-021-02632-z
17. Wu CI, Postema PG, Arbelo E, Behr ER, Bezzina CR, Napolitano C, et al. SARS-CoV-2, COVID-19, and inherited arrhythmia syndromes. *Heart Rhythm.* (2020) 17:1456–62. doi: 10.1016/j.hrthm.2020.03.024
18. Cheng Y, Luo R, Wang K, Zhang M, Wang Z, Dong L, et al. Kidney disease is associated with in-hospital death of patients with COVID-19. Kidney Int (2020) 97:829-838. doi: 10.1016/j.kint.2020.03.005
19. Dworakowska D, Grossman AB. Renin-angiotensin system inhibitors in management of hypertension during the COVID-19 pandemic. *J Physiol Pharm*acol (2020) 71:20. doi: 10.26402/jpp.2020.2.01
20. Lim JH, Jung HY, Choi JY, Park SH, Kim CD, Kim YL, et al.. Hypertension and Electrolyte Disorders in Patients with COVID-19. *Electrolyte Blood Press.* (2020) 18:23–30. doi: 10.5049/EBP.2020.18.2.23
21. Zhou F, Yu T, Du R, Fan G, Liu Y, Liu Z, et al. Clinical course and risk factors for mortality of adult inpatients with COVID-19 in Wuhan, China: a retrospective cohort study. *Lancet.* (2020) 395:1054–1062. doi: 10.1016/S0140-6736(20)30566-3
22. Zhu L, She ZG, Cheng X, Qin JJ, Zhang XJ, Cai J, et al. Association of Blood Glucose Control and Outcomes in Patients with COVID-19 and Pre-existing Type 2 Diabetes. *Cell Metabolism.* (2020) 31:1068–1077. doi: 10.1016/j.cmet.2020.04.021
23. Pal R, Bhadada SK. COVID-19 and diabetes mellitus: an unholy interaction of two pandemics. *Diabetes Metab Syndr.* (2020) 14:513-517. doi: 10.1016/j.dsx.2020.04.049
24. Nishiga M, Wang DW, Han Y, Lewis DB, Wu JC. COVID-19 and cardiovascular disease: from basic mechanisms to clinical perspectives. *Nat Rev Cardiol.* (2020) 17:543–558. doi: 10.1038/s41569-020-0413-9
25. Bornstein SR, Rubino F, Khunti K, Mingrone G, Hopkins D, Birkenfeld AL, et al. Practical recommendations for the management of diabetes in patients with COVID-19. *Lancet Diab. Endocrinol.* (2020) 8:546–550. doi: 10.1016/S2213-8587(20)30152-2
26. Chee YJ S.Ng JH, Yeoh E. Diabetic ketoacidosis precipitated by Covid-19 in a patient with newly diagnosed diabetes mellitus. *Diabet Res Clinic Pract.* (2020) 164:108166. doi: 10.1016/j.diabres.2020.108166
27. Li J, Wang X, Chen J, Zuo X, Zhang H, Deng A. COVID−19 infection may cause ketosis and ketoacidosis. *Diabet Obesity Metabol.* (2020) 22:1935–41. doi: 10.1111/dom.14057
28. Rubino F, Amiel SA, Zimmet P, Alberti G, Bornstein S, Eckel RH, et al. New-onset diabetes in Covid-19. *N Engl J Med.* (2020) 383:789–90. doi: 10.1056/NEJMc2018688
29. Fadool DA, Tucker K, Phillips JJ, Simmen JA. Brain insulin receptor causes activity-dependent current suppression in the olfactory bulb through multiple phosphorylation of Kv1.3. *J Neurophysiol.* (2000) 83:2332–48. doi: 10.1152/jn.2000.83.4.2332
30. Das P, Parsons AD, Scarborough J, Hoffman J, Wilson J, Thompson RN, et al. Electrophysiological and behavioral phenotype of insulin receptor defective mice. *Physiol Behav.* (2005) 86:287–96. doi: 10.1016/j.physbeh.2005.08.024
31. Fadool DA, Tucker K, Perkins R, Fasciani G, Thompson RN, et al. Kv1.3 channel gene-targeted deletion produces "Super-Smeller Mice" with altered glomeruli, interacting scaffolding proteins, biophysics. *Neuron.* (2004) 41:389–404. doi: 10.1016/S0896-6273(03)00844-4
32. Lechien JR, Chiesa-Estomba DR, Horoi MSD, Le Bon D, Rodriguez A, Dequanter D, et al. Olfactory and gustatory dysfunctions as a clinical presentation of mild-to-moderate forms of the coronavirus disease (COVID-19): a multicenter European study. *Eur Arch Otorhinolaryngol.* (2020) 277:2251–2261. doi: 10.1007/s00405-020-05965-1
33. Freedberg D, Conigliaro J, Wang T, Tracey K, Callahan M, Abrams J, et al. Famotidine use is associated with improved clinical outcomes in hospitalized covid-19 patients: a propensity score matched retrospective cohort study. *Gastroenterology.* (2020) 159:1129–31. doi: 10.1053/j.gastro.2020.05.053
34. Gordon DE, Jang GM, Bouhaddou M, Xu J, Obernier K, et al. A SARS-CoV-2 protein interaction map reveals targets for drug repurposing. *Nature*. (2020) 583:459–68. doi: 10.1038/s41586-020-2286-9
35. Riva L, Yuan S, Yin X L. Martin-Sancho, Matsunaga N, Pache LS, et al. Discovery of SARS-CoV-2 antiviral drugs through large-scale compound repurposing. *Nature.* (2020) 586:113-119. doi: 10.1038/s41586-020-2577-1
36. Wu C, Liu Y, Yang Y, Zhang P, Zhong W, Wang Y, et al. Analysis of therapeutic targets for SARS-CoV-2 and discovery of potential drugs by computational methods. *Acta Pharm Sin B.* (2020) 10:766–88. doi: 10.1016/j.apsb.2020.02.008
37. Wang J, Saul A, Roon P, Smith SB. Activation of the molecular chaperone, sigma 1 receptor, preserves cone function in a murine model of inherited retinal degeneration. *Proc Natl Acad Sci U S A.* (2016) 113:E3764–72. doi: 10.1073/pnas.1521749113
38. Maurice T, Goguadze N. Sigma-1 (sigma1) receptor in memory and neurodegenerative diseases. *Handbook Experiment Pharmacol.* (2017) 244:81–108. doi: 10.1007/164_2017_15
39. Liu X, Fu Y, Yang H, Mavlyutov T, Li J, McCurdy CR, et al. Potential independent action of sigma receptor ligands through inhibition of the Kv2.1 channel. *Oncotarget*. (2017) 8:59345–59358. doi: 10.18632/oncotarget.19581
40. Mahmoud S, Planes MD, Cabedo M, Trujillo C, Rienzo A, Caballero-Molada M, Sarma SC, Montesinos C, et al. TOR complex 1 regulates the yeast plasma membrane proton pump and pH and potassium homeostasis. *FEBS Lett.* (2017) 591:1993–2002. doi: 10.1002/1873-3468.12673

41. Primo C, Ferri-Blazquez, Leowith R, Yenush L. Reciprocal regulation of target of rapamycin complex 1 and potassium accumulation. *J Biol Chem.* (2017) 292:563–574. doi: 10.1074/jbc.M116.746982
42. O'Neill JS, Hoyle NP, Robertson JB, Edgar R, Frezza C, Day JH, et al. Eukaryotic cell biology is temporally coordinated to support the energetic demands of protein homeostasis. *Nat Commun.* (2020) 14:955521. doi: 10.1101/2020.05.14.095521
43. Stangherlin A, Wong D, Barbiero S, Watson J, Zeng A, Seinkmane E, et al. Compensatory ion transport buffers daily protein rhythms to regulate osmotic balance and cellular physiology. *BioRxiv preprint.* (2020) 28:118398. doi: 10.1101/2020.05.28.118398
44. Sun G, Sui Y, Zhou Y, Ya J, Yuan C, Jiang L, Huang M. Structural Basis of Covalent Inhibitory Mechanism of TMPRSS2-Related Serine Proteases by Camostat. *J Virol.* (2021) 95:e0086121. doi: 10.1128/JVI.00861-21
45. Hoffmann MH, Smith JC, Kruger N, Arora P, Sorensen LK, Sogaard OS, et al. Camostat mesylate inhibits SARS-CoV-2 activation by TMPRSS2-related proteases and its metabolite GBPA exerts antiviral activity. *EBioMedicine.* (2021) 65:103255. doi: 10.1016/j.ebiom.2021.103255
46. Kitamura K, Tomita K. Proteolytic activation of the epithelial sodium channel and therapeutic application of a serine protease inhibitor for the treatment of salt-sensitive hypertension. *Clin Exp Nephrol.* (2012) 16:44–8. doi: 10.1007/s10157-011-0506-1
47. Rakedzon S, Neuberger A, Domb AJ, Petersiel N, Schwartz E. From hydroxychloroquine to ivermectin: what are the anti-viral properties of anti-parasitic drugs to combat SARS-CoV-2? *J Travel Med.* (2021) 28:5. doi: 10.1093/jtm/taab005
48. Szendrey M, Guo J, Li W, Yang T, Zhang S. COVID-19 drugs chloroquine and hydroxychloroquine, but not azithromycin and remdesivir, block hERG potassium channels. *J Pharmacol Experiment Therapeut.* (2021) 377:265–72. doi: 10.1124/jpet.120.000484
49. Hou Y, Ge S, Li X, Wang C, He H, He L. Testing of the inhibitory effects of loratadine and desloratadine on SARS-CoV-2 spike pseudotyped virus viropexis. *Chem Biol Interact.* (2021) 338:109420. doi: 10.1016/j.cbi.2021.109420
50. Lacerda AE, Roy ML, Lewis EW, Rampe D. Interactions of the nonsedating antihistamine loratadine with a Kv1.5-type potassium channel cloned from human heart. *Mol Pharmacol.* (1997) 52:314–22. doi: 10.1124/mol.52.2.314
51. Crumb WJ. Rate-dependent blockade of a potassium current in human atrium by the antihistamine loratadine. *Br J Pharmacol.* (1999) 126:575–80. doi: 10.1038/sj.bjp.0702273
52. Hoffmann M, Schroeder SH, Kleine-Weber H, Muller MA, Drosten C, Pohlmann S. Nafamostat mesylate blocks activation of SARS-CoV-2: new treatment option for COVID-19. *Antimicrob Agents Chemotherap.* (2020) 64:20. doi: 10.1128/AAC.00754-20
53. Ookawara S, Tabei K, Sakurai T, Sakairi Y, Furuya H, Asano Y. Additional mechanisms of nafamostat mesilate-associated hyperkalaemia. *Eur J Clin Pharmacol.* (1996) 51:149–51. doi: 10.1007/s002280050176
54. Imamura K, Sakurai Y, Enami T, Shibukawa R, Nishi Y, Ohta A, Shu T, et al. iPSC screening for drug repurposing identifies anti-RNA virus agents modulating host cell susceptibility. *FEBS Open Bio.* (2021) 11:1452–1464. doi: 10.1002/2211-5463.13153
55. Gu J, Hu W, Liu X. Pioglitazone improves potassium channel remodeling induced by angiotensin II in atrial myocytes. *Med Sci Monit Basic Res.* (2014) 20:153–60. doi: 10.12659/MSMBR.892450
56. Slowik A, Lammerding L, Zendedel A, Habib P, Beyer C. Impact of steroid hormones E2 and P on the NLRP3/ASC/Casp1 axis in primary mouse astroglia and BV-2 cells after in vitro hypoxia. *J Steroid Biochem Mol Biol.* (2018) 183:18–26. doi: 10.1016/j.jsbmb.2018.05.003
57. Pinna G, Sex and COVID-19: a protective role for reproductive steroids. *Trends Endocrinol Metab.* (2021) 32:3–6. doi: 10.1016/j.tem.2020.11.004
58. Muto S, Imai M, Asano Y. Mechanisms of the hyperkalaemia caused by nafamostat mesilate: effects of its two metabolites on Na+ and K+ transport properties in the rabbit cortical collecting duct. *Br J Pharmacol.* (1994) 111:173–8. doi: 10.1111/j.1476-5381.1994.tb14040.x
59. Muto S, Sebata K, Watanabe H, Shoji F, Yamamoto Y, Ohashi M, Yamada T, et al. Effect of oral glucose administration on serum potassium concentration in hemodialysis patients. *Am J Kidney Dis.* (2005) 46:697–705. doi: 10.1053/j.ajkd.2005.06.013
60. Okajima M, Takahashi Y, Kaji T, Ogawa N, Mouri H. Nafamostat mesylate-induced hyperkalemia in critically ill patients with COVID-19: Four case reports. *World J Clin Cases.* (2020) 8:5320–5325. doi: 10.12998/wjcc.v8.i21.5320
61. Chen T, Wu D, Chen H, Yan W, Yang D, et al. Clinical characteristics of 113 deceased patients with coronavirus disease 2019: retrospective study. *BMJ.* (2020) 368:m1091. doi: 10.1136/bmj.m1091
62. Cabrera-Garcia D, Bekdash R, Abbott GW, Yazawa M, Harrison NL, he envelope protein of SARS-CoV2 increases intra-Golgi pH and forms a cation channel that is regulated by pH. *J Physiol.* (2021) 599:2851–68. doi: 10.1113/JP281037
63. Trobec T. The role of the SARS-CoV-2 envelope protein as a pH-dependent cation channel. *J Physiol.* (2021) 599:3435–3436. doi: 10.1113/JP281785
64. Singh Tomar PP, Arkin IT. SARS-CoV-2 E protein is a potential ion channel that can be inhibited by Gliclazide and Memantine. *Biochem Biophys Res Commun.* (2020) 530:10–14. doi: 10.1016/j.bbrc.2020.05.206
65. da Costa LS, Outlioua A, Anginot A, Akarid K, Arnoult D. RNA viruses promote activation of the NLRP3 inflammasome through cytopathogenic effect-induced potassium efflux. *Cell Death Dis.* (2019) 10:346. doi: 10.1038/s41419-019-1579-0
66. Choudhury S, Ma X, Abdullah SW, Zheng H. Activation and Inhibition of the NLRP3 Inflammasome by RNA Viruses. *J Inflamm Res.* (2021) 14:1145–1163. doi: 10.2147/JIR.S295706
67. Tsang OT, Chau TN, Choi KW, Tso EY, Lim W, Chiu MC, et al. Coronavirus-positive nasopharyngeal aspirate as predictor for severe acute respiratory syndrome mortality. *Emerg Infect Dis.* (2003) 9:1381–7. doi: 10.3201/eid0911.030400
68. Yang JK, Lin SS, Ji XJ, Guo LM. Binding of SARS coronavirus to its receptor damages islets and causes acute diabetes. *Acta Diabetol.* (2010) 47:193–9. doi: 10.1007/s00592-009-0109-4
69. Yamamoto M, Matsuyama S, Li X, Takeda M, Kawaguchi Y, Inoue JI et al. Identification of nafamostat as a potent inhibitor of Middle East Respiratory Syndrome coronavirus S protein-mediated membrane fusion using the split-protein-based cell-cell fusion assay. *Antimicrob Agents Chemotherap.* (2016) 60:6532–39. doi: 10.1128/AAC.01043-16
70. Weston S, Coleman C, Haupt R, Logue J, Matthews K, Frieman M. Broad anti-coronaviral activity of FDA approved drugs against SARS-CoV-2 in vitro and SARS-CoV in vivo. *J.Virol.* (2020) 94:e01218–20. 25:8482. doi: 10.1101/2020.03.25.008482

Conflict of Interest: The author declares that the research was conducted in the absence of any commercial or financial relationships that could be construed as a potential conflict of interest.

frontiers in Medicine

CASE REPORT
published: 29 November 2021
doi: 10.3389/fmed.2021.789250

Case Report: Syphilitic Hepatitis–A Rare and Underrecognized Etiology of Liver Disease With Potential for Misdiagnosis

Hiba A. Al Dallal[1†], Siddharth Narayanan[2†], Hanah F. Alley[3], Michael J. Eiswerth[4], Forest W. Arnold[5], Brock A. Martin[1] and Alaleh E. Shandiz[1]*

[1] Department of Pathology and Laboratory Medicine, University of Louisville, Louisville, KY, United States, [2] Department of Pediatrics, Nationwide Children's Hospital, Columbus, OH, United States, [3] Department of Neurology, University of Louisville, Louisville, KY, United States, [4] Department of Internal Medicine, University of Louisville, Louisville, KY, United States, [5] Division of Infectious Diseases, University of Louisville, Louisville, KY, United States

Syphilitic hepatitis (SH) in adults is a rare condition that can be easily misdiagnosed. Clinical and histopathologic manifestations of SH can mimic other infectious and non-infectious conditions, and the diagnosis should be considered in all at-risk patients with abnormal liver function tests. We present an unusual case of SH presenting with seizures and multiple liver lesions. This case report, in line with other newly published reports, promotes awareness of SH as a rare manifestation of treponemal infection and highlights the importance of including SH in the differential diagnosis for patients at risk for sexually transmitted infections and presenting with liver enzyme abnormalities. From a hospital quality control and socioeconomic perspective, our case adds to the growing body of evidence that demonstrates an increasing incidence of patients suffering from venereal diseases and injection drug use disorders, and the burden these conditions place on the healthcare system. Recognition of the clinicopathologic features of SH is required to prevent missed diagnosis and to foster systematic crosstalk between healthcare staff and public health personnel managing this problem.

Keywords: syphilis, drug abuse, hepatitis, seizure, liver enzymes, infection

OPEN ACCESS

Edited by:
Alessandro Vanoli, University of Pavia, Italy

Reviewed by:
Hwajeong Lee, Albany Medical College, United States
Irina Khamaganova, Pirogov Russian National Research Medical University, Russia

***Correspondence:**
Alaleh E. Shandiz
alaleh.shandiz@louisville.edu

[†]These authors share first authorship

Specialty section:
This article was submitted to Pathology, a section of the journal Frontiers in Medicine

Received: *04 October 2021*
Accepted: *09 November 2021*
Published: *29 November 2021*

Citation:
Al Dallal HA, Narayanan S, Alley HF, Eiswerth MJ, Arnold FW, Martin BA and Shandiz AE (2021) Case Report: Syphilitic Hepatitis–A Rare and Underrecognized Etiology of Liver Disease With Potential for Misdiagnosis. Front. Med. 8:789250. doi: 10.3389/fmed.2021.789250

INTRODUCTION

Syphilis is a disease caused by the non-hepatotropic bacterium *Treponema pallidum* and is associated with high-risk sexual activity. The stages of syphilis are well-defined, but the clinical manifestations can greatly vary between these stages (1, 2). In comparison to the first two stages (primary/secondary), untreated tertiary syphilis can present years after initial infection to cause devastating multi-organ system manifestations (3). While the overall incidence of syphilitic hepatitis (SH) is low, SH may occur in an estimated 3% of secondary syphilis cases (1). The incidence of tertiary syphilis presenting as SH is much less common.

Syphilitic hepatitis is usually asymptomatic or presents with non-specific symptoms. Non-hepatic manifestations of secondary syphilis, such as a characteristic diffuse maculopapular rash, are usually more helpful in pointing to the diagnosis than any hepatic signs or symptoms. The diagnosis of SH typically requires biochemical evidence of liver injury in the setting of confirmed treponemal serology, after exclusion of alternative causes of hepatic dysfunction (4). The pattern

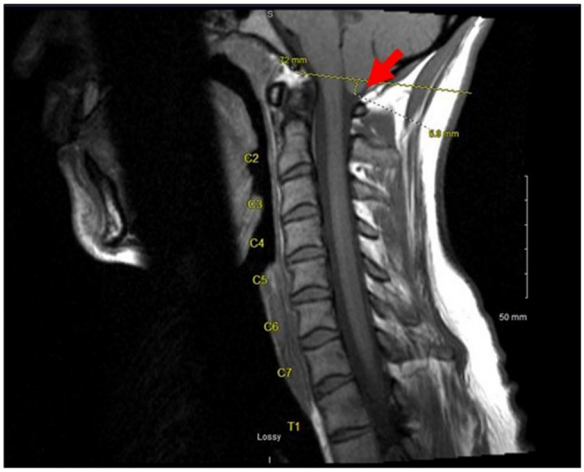

FIGURE 1 | A magnetic resonance imaging of the cervical spine showing a Chiari I malformation (red arrow) with a 5.8 mm displacement of the cerebellar vermis through the foramen magnum.

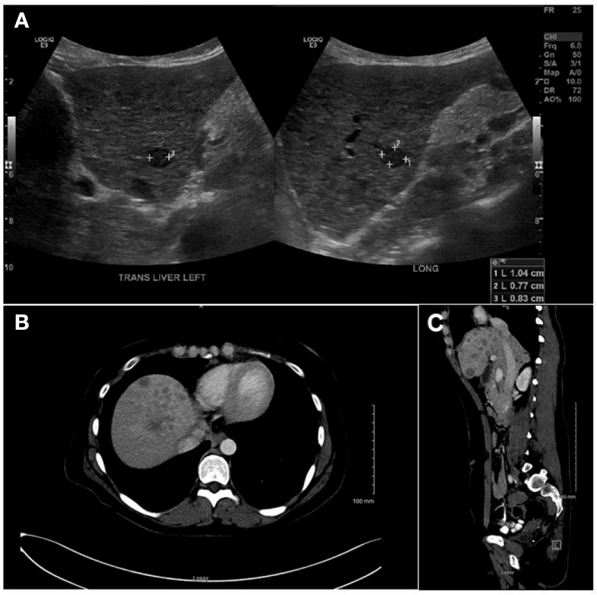

FIGURE 2 | (A) Liver ultrasound showing multiple hypo-echoic lesions ranging between 0.5 and 3.3 cm. **(B)** A liver computerized tomography scan showing multiple hypo-echoic lesions with peripheral rim of increased enhancement. **(C)** A magnetic resonance imaging (sagittal view) showing same as **(A,B)**.

of liver enzyme abnormalities is often cholestatic with altered alkaline phosphatase (ALP) levels and mildly elevated transaminases and bilirubin. Liver biopsy is often not required for diagnosis as response to antimicrobial therapy serves as a useful confirmatory finding.

We present an unusual case of an incarcerated adult female with a history of injection drug use (IDU) and multiple sexual partners who presented to our hospital with a constellation of neurological deficits and multiple liver lesions on imaging. After a comprehensive workup, she was diagnosed with tertiary SH with hepatic gummatous lesions but left against medical advice after only completing 4 days of penicillin treatment.

CASE REPORT

A 36-year-old incarcerated female with a history of polysubstance abuse and multiple sexual partners was found exhibiting seizure-like activity in her cell. On arrival at our hospital, she was unresponsive with convulsions of all extremities. Upon physical examination, she had upper motor neuron symptoms, including dilated pupils, rigidity of the lower extremities, and clonus, and a rectal temperature of 103°F. The patient was administered benzodiazepine to control the convulsions and intubated for airway protection. A computerized tomography (CT) scan of her head and neck was unremarkable, and magnetic resonance imaging (MRI) of the cervical spine demonstrated Chiari I malformation (**Figure 1**). An electroencephalogram of the brain confirmed seizure activity. Chest radiographs showed no evidence of an acute pulmonary process. Based on the initial presentation, a broad differential diagnosis was considered, including drug/toxin-induced neurological manifestations, infection, paraneoplastic syndrome, and metabolic (e.g., vitamin B12) deficiency.

An extensive workup was performed that included complete blood count, liver function tests, toxicology screens, and testing for multiple infectious diseases. Her white blood cell count was highly elevated (16×10^9 cells/L). Liver function tests revealed mildly elevated aspartate aminotransaminase (35 units/L, normal 8–34 units/L), alanine aminotransaminase (47 units/L, normal 7–24 units/L), and alkaline phosphatase (112 units/L, normal 25–105 units/L) with normal bilirubin. Vitamin B12 level was within the normal range. Urine toxicology was positive for cannabinoids, amphetamines, and benzodiazepines. An HIV screen was negative; however, the patient tested positive for *Treponema pallidum* antibodies (titer of 1:1,024) as well as hepatitis B surface antigen and DNA (PCR confirmation). A lumbar puncture for a cerebrospinal fluid culture and analysis was deferred due to the risk of herniation because of her Chiari I malformation.

Empiric treatment with intravenous penicillin G was initiated for a presumed diagnosis of neurosyphilis. However, the patient continued to exhibit unexplained, medically refractory severe nausea and vomiting, prompting abdominal imaging. An ultrasound assessment revealed multiple bilobar hypoechoic hepatic lesions (**Figure 2A**) which were confirmed as multiple hypoenhancing lesions on subsequent abdominal CT and MRI (**Figures 2B,C**). These additional imaging results raised consideration for atypical hepatic abscesses vs. metastatic malignancy, and a targeted liver core biopsy was performed.

Histologic sections of the biopsy showed involvement of the liver parenchyma by a dense mixed lymphoplasmacytic and granulocytic inflammatory infiltrate associated with

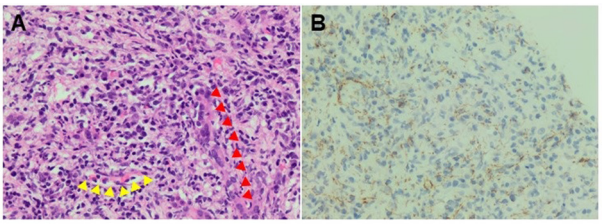

FIGURE 3 | (A) A H&E stain of the liver biopsy (400 X) showing mixed inflammatory infiltrate composed predominantly of lymphocytes and plasma cells and smaller numbers of neutrophils and eosinophils. The bile duct (red arrows) and portal vessel (yellow arrows) are highlighted. **(B)** An Anti-*Treponema pallidum* immunohistochemical staining confirmed the presence of spirochetes and highlighted numerous microorganisms having an epitheliotropic and vasculotropic pattern. The IHC was performed on the same tissue area as for the H&E stain.

TABLE 1 | Liver biochemical profile of our patient before and after antimicrobial treatment.

Liver function test	Hospital: Day 0	Hospital: Day 13 (discharge)
ALP (normal: 25–105 units/L)	112	84
AST (normal: 8–34 units/L)	35	29
ALT (normal: 7–24 units/L)	47	47
Albumin (normal: 3.4–4.8 g/dL)	2.7	3.1
Total bilirubin (normal: 0.2–1.1 mg/dL)	0.6	0.5

ALP, alkaline phosphatase; AST, aspartate transaminase; ALT, alanine transaminase.

reactive fibrosis (**Figure 3A**), foci of necrosis, and clusters of epithelioid histiocytes, consistent with inflammatory pseudotumor. In addition, foci of vascular and biliary inflammatory injury were present (**Figure 3A**). While a Warthin-Starry stain on the sample was negative, immunohistochemistry for treponemal organisms confirmed the presence of *Treponema pallidum* (Biocare APA 135 AA) and the diagnosis of tertiary stage SH with hepatic gummas (**Figure 3B**). The patient's liver function tests were monitored daily and showed initial improvement (**Table 1**); however, she left against medical advice following completion of only 4 days of the recommended 10–14-day course of intravenous penicillin for neurosyphilis.

DISCUSSION

Syphilis constantly challenges healthcare providers due to its multi-organ involvement, overlapping clinical stages, protean presentation, and it is an under-recognized etiology of liver dysfunction. In a retrospective study, liver enzyme abnormalities were common in patients with early syphilis (39%), yet only a small fraction (2.7%) were diagnosed with SH (5). Some authors have previously proposed clinical diagnostic criteria for SH (6), although diagnosis is still limited by the known clinical heterogeneity and lack of specific features of the disease (7).

The clinical manifestations of SH tend to be non-specific in adults. Common symptoms including low-grade fever, abdominal pain, sore throat, headache, weight loss, arthralgia or myodynia, splenomegaly, lymphadenopathy, and uveitis (7). Moderate elevations in liver enzymes, as well as markedly increased ALP and gamma-glutamyl transpeptidase levels, are reported in patients with SH (1, 2, 4). While the classic symmetric maculopapular rash of secondary syphilis, which involves the trunk and extremities including palms and soles, is a strong clue to the diagnosis of SH as a cause of liver enzyme abnormalities (8), it is not uniformly observed in all patients. Liver involvement represents spirochete dissemination (9) but can occur at any stage of the disease. In a systematic review of SH, the vast majority of patients (88.9%) presented with early stage (i.e., primary or secondary) disease; whereas, a small minority presented with latent (4.9%) or tertiary (6.3%) stage disease (10) when classic signs and symptoms of syphilis may be less apparent.

The histopathologic features of SH are likewise non-specific. Cases typically show mixed lymphoplasmacytic and granulocytic portal inflammation with variable bile duct injury and associated granulomas (9). A vasculotropic and epitheliotropic pattern of inflammation may be seen in some cases, but this is not etiologically specific and overlaps with other, more common inflammatory liver diseases. Although identification of spirochetes in the tissue by special stain or immunohistochemistry is diagnostic in the appropriate setting (11), false negative staining is not uncommon in the setting of disseminated treponemal disease, reaffirming the need for close clinicopathologic correlation to make the diagnosis in most cases. In the absence of known or reported risk factors for SH, the diagnosis is likely to be missed. Furthermore, potentially misleading clinical and imaging findings may prompt consideration and additional testing for other infectious, autoimmune, or neoplastic diseases, leading to delayed or misdiagnosis.

Our case emphasizes the importance of maintaining a broad differential diagnosis for hepatic enzyme abnormalities, including a comprehensive review of patient risk factors for common and uncommon causes of hepatitis. Despite an initial presentation with only mild liver enzyme elevations and multiple confounding and potentially misleading clinical and imaging findings, careful clinicopathologic correlation and appropriate diagnostic investigation eventually facilitated a conclusive diagnosis of tertiary SH.

Most cases of SH resolve with antibiotic medications for treponemal infection. Heightened clinical awareness and recognition of patients at risk for the disease are necessary to facilitate timely diagnosis and treatment. Risk factors including unprotected sexual activity, polysubstance abuse and IDU attribute to notably high rates of coinfection, increased hospital costs and a massive burden on the healthcare system (2, 12, 13). The incidence of primary and secondary syphilis are on the rise (1), and the identification and treatment of syphilis cases prevents progression to tertiary syphilis in affected individuals and the spread to other individuals.

Therefore, increased attention to the diagnosis of SH by care providers and pathologists is essential for achieving positive patient outcomes as well as hospital quality control and socioeconomic goals.

CONCLUSIONS

SH can be easily overlooked and misdiagnosed because of non-specific signs and symptoms at the presentation and mild hepatic manifestations, in addition to non-specific and overlapping histopathologic findings. The diagnosis of tertiary SH is particularly problematic as other clinical signs and symptoms of disseminated treponemal disease may be absent or inapparent. Given the availability of effective treatment, timely diagnosis can greatly decrease morbidity and mortality associated with this condition. Even in the absence of non-hepatic manifestations, SH should be considered in high-risk patients with altered liver function tests. Multi-disciplinary efforts from healthcare and regulatory bodies are needed to reduce its growing incidence.

DATA AVAILABILITY STATEMENT

The raw data supporting the conclusions of this article will be made available by the authors, without undue reservation.

ETHICS STATEMENT

This case report was reviewed by the IRB and determined that it did not meet the common rule requirements and was deemed Non-Human Subjects Research (NHSR). No personal health identifiers are included in this case report. The patient consent was obtained.

AUTHOR CONTRIBUTIONS

HAA collected the data and interpreted the diagnosis. SN analyzed the literature and wrote the manuscript. HFA and ME helped in collecting the data and edited the manuscript. FA, BM, and AS provided framework for the study, reviewed, and edited the manuscript. All authors have read and agreed to the final version of the manuscript.

REFERENCES

1. Alemam A, Ata S, Shaikh D, Leuzzi B, Makker J. Syphilitic hepatitis: a rare cause of acute liver injury. *Cureus.* (2021) 13:e14800. doi: 10.7759/cureus.14800
2. Narang N, Al-Jashaami L, Patel N. Spirochetes in the liver: an unusual presentation of a common STI. *Case Rep Med.* (2019) 2019:1012405. doi: 10.1155/2019/1012405
3. Ghanem KG, Ram S, Rice PA. The modern epidemic of syphilis. *N Engl J Med.* (2020) 382:845–54. doi: 10.1056/NEJMra1901593
4. Horn CL, Jalali S, Abbott J, Stein M. A surprising diagnosis: syphilitic gastritis and hepatitis. *Am J Med.* (2018) 131:1178–81. doi: 10.1016/j.amjmed.2018.03.023
5. Adachi E, Koibuchi T, Okame M, Sato H, Kikuchi T, Koga M, et al. Liver dysfunction in patients with early syphilis: a retrospective study. *J Infect Chemother.* (2013) 19:180–2. doi: 10.1007/s10156-012-0440-5
6. Mullick CJ, Liappis AP, Benator DA, Roberts AD, Parenti DM, Simon GL. Syphilitic Hepatitis in HIV-Infected Patients: A Report of 7 Cases and Review of the Literature. *Clin Infect Dis.* (2004) 39:e100–5. doi: 10.1086/425501
7. Huang J, Lin S, Wang M, Wan B, Zhu Y. Syphilitic hepatitis: a case report and review of the literature. *BMC Gastroenterol.* (2019) 19:191. doi: 10.1186/s12876-019-1112-z
8. Kaya A, Kaya SY. Management of syphilitic hepatitis. *BMC Gastroenterol.* (2020) 20:379. doi: 10.1186/s12876-020-01496-5
9. Pizzarossa AC, Rebella M. Hepatitis in patients with syphilis: an overlooked association. *BMJ Case Rep.* (2019) 12:226918. doi: 10.1136/bcr-2018-226918
10. Huang J, Lin S, Wan B, Zhu Y. A systematic literature review of syphilitic hepatitis in adults. *J Clin Transl Hepatol.* (2018) 6:306–9. doi: 10.14218/JCTH.2018.00003
11. Hoang MP, High WA, Molberg KH. Secondary syphilis: a histologic and immunohistochemical evaluation. *J Cutan Pathol.* (2004) 31:595—9. doi: 10.1111/j.0303-6987.2004.00236.x
12. Elnazeir M, Narayanan S, Badugu P, Hussain A, Stephens CB, Bhagat R, et al. Neurological manifestations associated with synthetic cannabinoid use–a case series. *Open Neurol J.* (2020) 14:53–8. doi: 10.2174/1874205X02014010053
13. Al Dallal HA, Narayanan S, Jones CM, Lockhart SR, Snyder JW. First case report of an unusual fungus (sporopachydermia lactativora) associated with a pulmonary infection in a drug injection user. *Clin Pathol.* (2021) 14:2632010X211029970. doi: 10.1177/2632010X211029970

Author Disclaimer: The findings and conclusions in this manuscript are those of the authors alone and do not necessarily represent the official position of the Centers for Disease Control and Prevention.

Conflict of Interest: The authors declare that the research was conducted in the absence of any commercial or financial relationships that could be construed as a potential conflict of interest.

Publisher's Note: All claims expressed in this article are solely those of the authors and do not necessarily represent those of their affiliated organizations, or those of the publisher, the editors and the reviewers. Any product that may be evaluated in this article, or claim that may be made by its manufacturer, is not guaranteed or endorsed by the publisher.

frontiers in Medicine

ORIGINAL RESEARCH
published: 09 February 2022
doi: 10.3389/fmed.2022.778489

Long-Term Persisting SARS-CoV-2 RNA and Pathological Findings: Lessons Learnt From a Series of 35 COVID-19 Autopsies

*Umberto Maccio[1], Annelies S. Zinkernagel[2], Reto Schuepbach[3], Elsbeth Probst-Mueller[4], Karl Frontzek[5], Silvio D. Brugger[2], Daniel Andrea Hofmaenner[3], Holger Moch[1] and Zsuzsanna Varga[1]**

[1] Department of Pathology and Molecular Pathology, University Hospital of Zürich, University of Zurich, Zurich, Switzerland, [2] Department of Infectious Diseases and Hospital Epidemiology, University Hospital of Zürich, University of Zurich, Zurich, Switzerland, [3] Institute of Intensive Care, University Hospital Zurich, University Hospital of Zürich, Zurich, Switzerland, [4] Department of Immunology, University Hospital of Zürich, Zurich, Switzerland, [5] Institute of Neuropathology, University Hospital Zurich, Zurich, Switzerland

OPEN ACCESS

Edited by:
Weiren Luo,
The Second Affiliated Hospital of Southern University of Science and Technology, China

Reviewed by:
Tracy Fischer,
Tulane University, United States
Paulo Hilario Nascimento Saldiva,
University of São Paulo, Brazil

***Correspondence:**
Zsuzsanna Varga
zsuzsanna.varga@usz.ch

Specialty section:
This article was submitted to Pathology, a section of the journal Frontiers in Medicine

Received: 17 September 2021
Accepted: 04 January 2022
Published: 09 February 2022

Citation:
Maccio U, Zinkernagel AS, Schuepbach R, Probst-Mueller E, Frontzek K, Brugger SD, Hofmaenner DA, Moch H and Varga Z (2022) Long-Term Persisting SARS-CoV-2 RNA and Pathological Findings: Lessons Learnt From a Series of 35 COVID-19 Autopsies. Front. Med. 9:778489. doi: 10.3389/fmed.2022.778489

Background: Long-term sequelae of coronavirus disease 2019 (COVID-19), including the interaction between persisting viral-RNA and specific tissue involvement, pose a challenging issue. In this study, we addressed the chronological correlation (after first clinical diagnosis and postmortem) between severe acute respiratory syndrome coronavirus 2 (SARS-CoV-2) RNA and organ involvement.

Methods: The presence of postmortem SARS-CoV-2 RNA from 35 complete COVID-19 autopsies was correlated with the time interval between the first diagnosis of COVID-19 and death and with its relationship to morphologic findings.

Results: Severe acute respiratory syndrome coronavirus 2 (SARS-CoV-2) RNA can be evident up to 40 days after the first diagnosis and can persist to 94 hours after death. Postmortem SARS-CoV-2 RNA was mostly positive in lungs (70%) and trachea (69%), but all investigated organs were positive with variable frequency. Late-stage tissue damage was evident up to 65 days after initial diagnosis in several organs. Positivity for SARS-CoV-2 RNA in pulmonary swabs correlated with diffuse alveolar damage ($p = 0.0009$). No correlation between positive swabs and other morphologic findings was present. Cerebral ($p = 0.0003$) and systemic hemorrhages ($p = 0.009$), cardiac thrombi ($p = 0.04$), and ischemic events ($p = 0.03$) were more frequent in the first wave, whereas bacterial pneumonia ($p = 0.03$) was more prevalent in the second wave. No differences in biometric data, clinical comorbidities, and other autopsy findings were found.

Conclusions: Our data provide evidence not only of long-term postmortem persisting SARS-CoV-2 RNA but also of tissue damage several weeks after the first diagnosis of SARS-CoV-2 infection. Additional conditions, such as concomitant bacterial pulmonary superinfection, lung aspergillosis, thromboembolic phenomena, and hemorrhages can further worsen tissue damage.

Keywords: COVID-19, long-COVID, SARS-CoV-2 RNA PCR, postmortal swabs, pulmonary superinfections, histopathology, autopsy

INTRODUCTION

Coronavirus disease 2019 (COVID-19), caused by the beta coronavirus severe acute respiratory syndrome coronavirus 2 (SARS-CoV-2), has been spreading dramatically worldwide since first being reported in Wuhan, China in December 2019 (1).

More than 1 year and a half after the beginning of the pandemic, long-term health consequences of COVID-19 due to persisting SARS-CoV-2 and tissue damage represent an emerging problem, although the pathogenetic mechanisms and the epidemiology of the phenomenon are still largely unknown (2, 3).

COVID-19 can occur with a varying degree of severity (4, 5). Approximately, 33% of patients are asymptomatic (4). Of those who develop symptoms, around 81% experience mild disease, 14% a more severe disease (with respiratory distress), whereas a subset of around 5% of patients progresses to a critical condition (with respiratory insufficiency and/or multi-organ dysfunction) (5). Although the respiratory tract is the most commonly involved organ system (6), patients can also develop cardiovascular complications (7), thromboembolic phenomena (8) including thromboangiitis obliterans (9), several neurologic complications (10), gastroenterological symptoms (11), exuberant inflammatory manifestations (12, 13), and secondary infections (14–17), suggesting that COVID-19 is a systemic disease. The general infection fatality rate is estimated to be 0.68% (18), but it is strongly variable across studies and increases with age and underlying comorbidities (such as arterial hypertension and diabetes) (19, 20).

Long-COVID, in general, used to describe the persistence of symptoms in patients who have recovered from COVID-19, and which cannot be explained by an alternative diagnosis, is thought to occur in up to 10% of cases (21). However, proposals for new classifications aiming to differentiate between acute post-COVID, long post-COVID, and persistent long-COVID are emerging (22).

The pathogenesis of COVID-19 is not fully understood. The angiotensin-converting enzyme 2 (ACE2) and transmembrane protease serine 2 (TMPRSS2) have been shown to be the main receptor and the cofactor for the entry of the virus into the cells (23), but also basigin (CD147) as a receptor (24) and furin as a cofactor (25) play a pivotal role. After the viral attack, complex interplays between humoral and cellular immunity complement activation, cytokines, and coagulation-induced organ damage (26–29). As possible explanations for Long-COVID, several pathogenetic mechanisms, including persistent inflammatory damage, direct viral toxicity in tissues, and post-intensive care syndrome, have been proposed (3, 21).

Autopsies of patients who died from COVID-19 are crucial to gain a better understanding of how SARS-CoV-2 induces damage in human tissues and to consequently improve patient management and therapeutic strategies (30). At the beginning of the pandemic, only few autopsies were performed due to concerns about aerosolization and infectivity of the virus (31). More recently, in compliance with biosafety recommendations of several international regulatory agencies, including the World Health Organization (32), the Centers for Disease Control and Prevention (CDC) (33), and the European Center for Disease Prevention and Control (34), rapidly expanding autopsy literature has become available (35). Nevertheless, although some reports of late histological findings of patients with COVID-19 in the form of single case studies exist, to our knowledge, no autopsy-based studies focusing on the persistence of tissue damage and long-term consequence of SARS-CoV-2 infection have been reported (36).

Additionally, although some clinical studies comparing the first and the second waves of the COVID-19 pandemic exist (37, 38), no detailed autopsy-based studies analyzing the clinical and morphologic differences between the patients who died from COVID-19 in the first compared to the second pandemic wave have been published yet. Moreover, the use of postmortem swabs for detecting the presence of SARS-CoV-2 RNA in autoptic tissues, the postmortem viral distribution, their correlation with the time interval between diagnosis and death, as well as their correlation with morphologic findings have not been extensively studied (39–42).

In view of the foregoing, the aims of our study are: (1) To describe morphologic findings in different organs and tissues and investigate their prevalence. (2) To detect the prevalence of pulmonary superinfection caused by bacteria, viruses, or fungi in patients who died from COVID-19. (3) To analyze possible differences in all those findings between patients who died during the first or second wave of the pandemic. (4) To describe the distribution of SARS-CoV-2 RNA in different organs through postmortem swabs. (5) To correlate the positivity of the postmortem swabs with the time interval between diagnosis of SARS-CoV-2 and death, the incidence of the autoptic morphologic findings with the time interval between diagnosis and death, and the morphologic findings with the positivity of the swabs in the corresponding organs.

MATERIALS AND METHODS

Autopsy Cohort

Overall, 35 autopsies of patients with pre-mortem PCR-confirmed COVID-19 disease were performed at the Department of Pathology and Molecular Pathology of the University Hospital of Zürich, Switzerland.

Seven autopsies (7/35, 20%) were performed during the "first wave" of the COVID-19 pandemic, corresponding to deaths between March 2020 and May 2020. No COVID-19 autopsy was performed between June 2020 and September 2020. The other 28 autopsies (28/35, 80%) were performed during the "second wave" of the COVID-19 pandemic, corresponding to deaths from October 2020 to April 2021. This arbitrary distinction between first and second waves was based on the official classification of the Swiss Federal Office of Public Health and is currently used for comparative purposes by other studies (43, 44).

No cases attributable to any variants of concerns of SARS-CoV-2 according to the WHO definition belonged to this autopsies cohort (45).

Consent to perform the autopsy was given in all cases and the institutional review board (Department of Pathology and Molecular Pathology of the University Hospital Zurich, Switzerland) approved the study. Ethical aspects of research on autopsy tissue of deceased patients, postmortem diagnostics, and molecular analyses were covered in accordance with the Swiss Federal Research Regulations (BASEC Nr. 2020.1316).

Postmortem Examination and Swabs

All postmortem examinations were conducted in a biosafety Level 3 postmortem facility within an average of 33 hours after death (range, 3–93 hours). After a careful macroscopic examination and photographic documentation, several tissue sites were systematically sampled using a standardized protocol for histological, immunohistochemical, immunofluorescence, and ultrastructural examinations.

Samples for histology and immunohistochemistry were routinely taken from the brain, lungs, heart, liver, spleen, gut, kidney, bone marrow, testicle or ovary, and endocrine organs (pituitary, thyroid, and adrenal glands) and immediately fixed in 4% buffered formalin for 24 hours. Of one patient of the second wave, the brain was not examined according to the declared will of the corresponding relatives.

After paraffin inclusion and microtome sectioning, every histologic sample was processed with conventional stain (hematoxylin and eosin, H&E). Subsequently, the samples were independently examined by two experienced pathologists (U.M. and Z.V.) for major morphological alterations (e.g., inflammation type and distribution, distribution and type of thrombi, infarcts or ischemic changes, signs of superinfection, such as fungal elements or nuclear inclusion suspect of viral infection, major reactive changes, such as metaplasia or hyperplasia of pneumocytes type 2). There was perfect agreement between the two pathologists for every finding in all examined samples (Cohen's kappa coefficient = 1).

During autopsies of the "second wave," postmortem swabs for SARS-CoV-2-RNA PCR assays from different organs were performed. Postmortem swabs were obtained from a predefined selection of organs: one swab from tracheal secretions, two from the lung parenchyma (one per each lower lobe), one from the myocardium (left ventricle), one from the liver, one from the kidney, one from the small intestine, one from the spleen, and one from the testicles or ovaries. Of one patient, no postmortem swabs were performed, and of another patient only swabs from the lung, heart, and liver were available.

Additional postmortem swabs from the brain (superior frontal gyrus, right) of six patients and from the lamina cribrosa of four patients were available.

During the gross examination, the swabs were taken from each organ after a small sterile incision prior to the dissection of the organ. Access to tracheal fluid was obtained through a small sterile incision of the membranous tracheal part.

Samples were immediately collected in a viral transport medium (cobas® PCR Media, Roche Nr. 06466281190, serving as a nucleic acid stabilizing transport and a storage medium for human specimens) and transported to the Laboratory of Immunology of the University Hospital Zurich, where the presence of SARS-CoV-2 RNA was assessed *via* a real-time reverse PCR assay (cobas® SARS-CoV-2, Roche Nr. 09175431190), a fully automated test for nucleic acid extraction and purification followed by real-time PCR (RT-PCR). Together with the nucleic acid from the sample, the added internal control was simultaneously extracted by adding proteinase and lysis reagent. During the PCR, a sequence of the ORF1 a/b, which is unique to SARS-CoV-2, and a conserved region in the envelope E gene were amplified. The product generated can be measured by detecting the fluorescence. In case of a positive result, the Ct-value (cycle threshold) was indicated (**Supplementary Table 1**). The Ct-value refers to the number of cycles needed to amplify the viral RNA to reach the predetermined threshold. The lower the Ct value, the more viral RNA was in the sample. The threshold of Ct-value (ORF1 a/b), under which a sample was interpreted as positive, was 40.

In addition, clinical history (including main comorbidities), biometric data [age, gender (male/female)], and body mass index (BMI, in kg/m^2) of each patient who died during the first and second waves were recorded. Data were obtained from the hospital clinical charts or from the external clinical history submitted to the autopsy (**Table 1**).

Statistical Analyses

Demographic and biometric data from the first and second waves were compared using Student's *t*-test (for age and body mass index, after having found those data to be normally distributed using the Shapiro-Wilk's test, where $p > \alpha$, setting a significance level [α] of 0.05) or Fisher's exact test (for gender, applying this simple 2 x 2 contingency table with one degree of freedom: first vs. second wave/male vs. female) as statistical hypothesis tests.

A Student's *t*-test was also performed to compare the time interval between COVID-19 diagnosis and death between patients who died in the first and second waves (after having found the data to be normally distributed using the Shapiro-Wilk's test, where $p > \alpha$, setting a significance level [α] of 0.05).

TABLE 1 | General characteristic, comparison of the two different cohorts (first vs. second wave) and detailed autopsies' findings.

	Patients from first wave of pandemic ($n = 7$)	**Patients from second wave of pandemic ($n = 28$)**	***p*-value**
Age (years)	69 (range 45–81)	71 (range 22–89)	0.71
M/F	4/7 (57%)	21/28 (75%)	0.38
BMI (kg/m^2)	27.9 (21.6–37.8)	27.4 (17.6–43.6)	0.85
Main clinical comorbidities	Cancer (5/7, 71%)	Cancer (9/28, 32%)	0.089
	Arterial hypertension (5/7, 71%)	Arterial hypertension (19/28, 68%)	1.0
	Pulmonary disease (2/7, 28%)	Pulmonary disease (12/28, 43%)	0.68
	Diabetes mellitus (3/7, 43%)	Diabetes mellitus (4/28, 14%)	0.12
	Solid organ transplantation (2/7, 29%)	Solid organ transplantation (2/28, 7%)	0.17
	Bone Marrow transplantation (0/7, 0%)	Bone Marrow transplantation (2/28, 7%)	1.0
	Overweight (3/7, 43%)	Overweight (11/28, 39%)	1.0
	Obesity (2/7, 28%)	Obesity (7/28, 25%)	1.0
Time interval between diagnosis and death (days)	12 (2–20)	18 (1–65)	0.39
DAD	6/7 (86%)	18/28 (64%)	0.39
Bacterial Pneumonia	2/7 (29%)	21/28 (75%)	**0.03**
Lung aspergillosis	0/7 (0%)	6/28 (21%)	0.31
Viral Pneumonia	0/7 (0%)	1/28 (4%) (HSV1+CMV)	1.0
Macroscopic thrombi	General incidence (3/7, 43%)	General incidence (13/28, 46%)	1.0
	Cardiac ventricle (3/7, 43%)	Cardiac ventricle (2/28, 7%)	**0.04**
	Pulmonary central (0/7, 0%)	Pulmonary central (1/28, 4%)	1.0
	Pulmonary paracentral (0/7, 0%)	Pulmonary paracentral (7/28, 25%)	0.30
	Pulmonary peripheral (0/7, 0%)	Pulmonary peripheral (9/28, 32%)	0.1
	Peripheral veins (0/7, 0%)	Major peripheral vessels (3/28, 11%)	1.0
Microscopic fibrin thrombi	General incidence (4/7, 57%)	General incidence (13/28, 46%)	0.69
	Myocardial vessels (1/7, 14%)	Myocardial vessels (2/28, 7%)	0.50
	Pulmonary vessels (2/7, 29%)	Pulmonary vessels (12/28, 43%)	0.68
	Renal (0/7, 0%)	Renal (1/28, 4%)	1.0
	Cerebral vessels (1/7, 14%)	Cerebral vessels (2/28, 7%)	0.5
	Skin (1/7, 14%)	NA	
Leucocytes thrombi	General incidence (3/7, 43%)	General incidence (14/28, 50%)	1.0
	Cardiac (1/7, 14%)	Cardiac (4/28, 14%)	1.0
	Pulmonary (3/7, 43%)	Pulmonary (12/28, 43%)	1.0
	Hepatic (1/7, 14%)	Hepatic (0/28, 0%)	0.20
	Mesenterial (1/7, 14%)	Mesenterial (1/28, 4%)	0.36
Hemorrhages	General incidence (7/7, 100%)	General incidence (12/28, 43%)	**0.009**
	Brain microhemorrhages (6/7, 86%)	Brain microhemorrhages (3/28, 11%)	**0.0003**
	Subarachnoid (1/7, 14%)	Subarachnoid (2/28, 7%)	0.50
	Subdural hematoma (0/7, 0%)	Subdural hematoma (3/28, 11%)	1.0
	Lung (3/7, 43%)	Lung (5/28, 18%)	0.3
Infarcts/Ischemia	General incidence (6/7, 86%)	General incidence (10/28, 36%)	**0.03**
	Cardiac (1/7, 14%)	Cardiac (3/28, 11%)	1.0
	Lung (0/7, 0%)	Lung (5/28, 18%)	0.56
	Small intestine (2/7, 29%)	Small intestine (5/28, 18%)	0.61
	Liver (1/7, 14%)	Liver (8/28, 29%)	0.65
	Cerebral (2/7, 29%)	Cerebral (2/27, 7%)	0.18

M, male; F, female; DAD, diffuse alveolar damage; BMI, body mass index; HSV1, herpes simplex virus 1; CMV, cytomegalovirus; NA, not available. Bold values are the statistically significant results.

Fisher's exact test was also applied to compare the presence of relevant clinical comorbidities (such as cancer history, chronic pulmonary diseases, interstitial lung disease, chronic obstructive pulmonary disorder, pulmonary hypertension, diabetes mellitus, or arterial hypertension) and pathological findings (such as the presence of pulmonary superinfection, cerebral bleedings, etc., as listed in **Table 1**) between the two waves, applying a simple 2 x 2 contingency table with one degree of freedom (first vs. second wave/the presence of a specific pathologic finding vs. the absence of the same).

Point-Biserial Correlation calculator was applied to compare the positivity of postmortem swabs in each analyzed organ with the time interval between diagnosis and death as well as to compare the incidence of morphologic findings with the time interval between diagnosis and death.

Fisher's exact test was performed to correlate the morphologic findings with the positivity of the swabs in the corresponding organs (positive vs. negative swab/the presence of a specific finding in the organ vs. the absence of the same).

Given the exploratory nature of these analyses, no adjustment for multiple testing was performed.

RESULTS

Findings in Patients From the "First Wave"

The average age of the patients was 69 years (range, 45–81 years; standard deviation, 13 years). Four (4/7, 57%) were male, and three (3/7, 43%) were female. The mean time between diagnosis of COVID-19 disease and death was 12 days (range, 2–20 days; standard deviation, 7 days). All patients (7/7, 100%) had one or more chronic comorbidities (arterial hypertension, diabetes mellitus, cancer, overweight, and/or obesity the most common). Two (2/7, 29%) were normal weight (with a BMI between 18.5 and 24.9 kg/m^2, according to the current WHO classification), three (3/7, 43%) were overweight (BMI between 25.1 and 29.9 kg/m^2), one (1/7, 14%) was obese Grade I (BMI between 30 and 34.9 kg/m^2) and one (1/7, 14%) obese Grade II (BMI between 35 and 39.9 kg/m^2). Average BMI was 27.9 kg/m^2 (range, 21.6–37.8 kg/m^2; standard deviation, 5.9 kg/m^2). Two patients (2/7, 29%, all of whom were male) were solid organ transplant recipients (kidney transplantation 7 and 17 years before death, respectively). One patient was diagnosed with SARS-CoV-2-associated pneumonia 2 months before death, and was successfully treated with conservative therapy and did not require oxygen supplementation, but 1 month after the negativity of SARS-CoV-2 PCR developed a reactivation or reinfection with rapid progression to respiratory insufficiency and death.

Regarding neurological manifestations, one patient had a cerebellar hemorrhage during hospitalization (1/7, 14%), one a severe diffuse brain ischemia 2 days before death (1/7, 14%), and one had recurrent seizures 6 months before death (1/7, 14%). The other four patients (4/7, 57%) had no neurological disorders.

Autopsies were performed on average 33 hours after death (range, 18–56 hours).

The cause of death in six patients (6/7, 86%) was diffuse alveolar damage (DAD), whereas the patient with reactivation/reinfection (1/7, 14%) was found to have massive bacterial pneumonia but no DAD.

Altogether, histopathologic findings consistent with bacterial pneumonia were found in two patients (2/7, 29%), but no fungal or viral pneumonia could be demonstrated.

Three patients (3/7, 43%) had intraventricular macroscopic thrombi. Microscopic fibrin thrombi [in the coronary arteries (1/7, 14%), pulmonary capillaries (2/7, 29%), skin capillaries (1/7, 14%), and cerebral capillaries (1/7, 14%)] as well as leukocytes thrombi [in pulmonary (3/7, 43%), cardiac (1/7, 14%), hepatic (1/7, 14%), and mesenterial capillaries (1/7, 14%)] were also common.

Several patients were also found to have hemorrhages [brain microhemorrhages (6/7, 86%), subarachnoid (1/7, 14%), and pulmonary (3/7, 43%)] and infarcts [small intestine (2/7, 29%) and liver (1/7, 14%)].

Constant adjunctive findings in the lungs were also, to a different degree, endotheliitis of capillaries, alveolar capillary macrophages, prominent hyperplasia of pneumocytes type 2, squamous metaplasia, interstitial edema, lymphocytic and histiocytic inflammation, fibrin-rich alveolar edema, and capillary stasis.

Details are summarized in **Table 1**. Representative images of the most important histopathological findings are shown in **Figures 1**, **2**, and **Supplementary Figure 1**.

Findings in Patients From the "Second Wave"

The average age of patients was 71 years (range, 22–89 years; standard deviation, 15 years). Twenty-one (21/28, 75%) were male, and seven (7/28, 25%) were female. The mean time between diagnosis of COVID-19 disease and death was 18 days (range, 1–65 days; standard deviation, 17 days). All patients (28/28, 100%) had one or more severe chronic comorbidities (arterial hypertension, chronic heart failure, cancer, diabetes mellitus, chronic lung disease [COPD (chronic obstructive pulmonary disease) and idiopathic pulmonary fibrosis], autoimmune diseases, chronic kidney disease, asthma, chronic liver disease, and overweight or obesity the most common.

Concerning neurological disorders, four patients had a history of previous ischemic strokes (4/28, 14%), three Alzheimer's disease or unspecified dementia (3/28, 11%), one mild cognitive impairment (1/28, 4%), two multiple cerebral metastases (2/28, 7%), two developed critical-illness neuromyopathy during hospitalization (2/28, 7%), two had a history of previous brain trauma (2/28, 7%), one developed diffuse hypoxic encephalopathy during hospitalization (1/28, 4%), and thirteen had no neurological disorders (13/28, 46%).

Two patients (2/28, 7%) were underweight (BMI $<$ 18.5 kg/m^2, according to current WHO classification), eight (8/28, 29%) normal weight (BMI between 18.5 and 24.9 kg/m^2), 11 (11/28, 39%) overweight (with a BMI between 25.1 and 29.9 kg/m^2), three (3/28, 11%) obese Grade I (BMI between 30. and 34.9 kg/m^2), one (1/28%, 3%) obese Grade II (BMI between 35. and 39.9 kg/m^2), and three (3/28, 11%) were obese Grade III (BMI $>$ 40 kg/m^2). Average BMI was 27.4 kg/m^2 (range, 17.6–43.6 kg/m^2; standard deviation, 7.2 kg/m^2).

All patients but one (27/28, 96%) were more than 55 years old at the time of death.

Autopsies were performed on average 33 hours after death (range, 3–93 hours).

Most important, autopsy findings in patients who died in the second wave were diffuse alveolar damage (DAD, 18/28, 64%), macrothrombi (general incidence, 13/28, 46%), microscopic fibrin thrombi (general incidence, 13/28, 46%), and leucocyte thrombi (general incidence, 14/28, 50%), hemorrhages

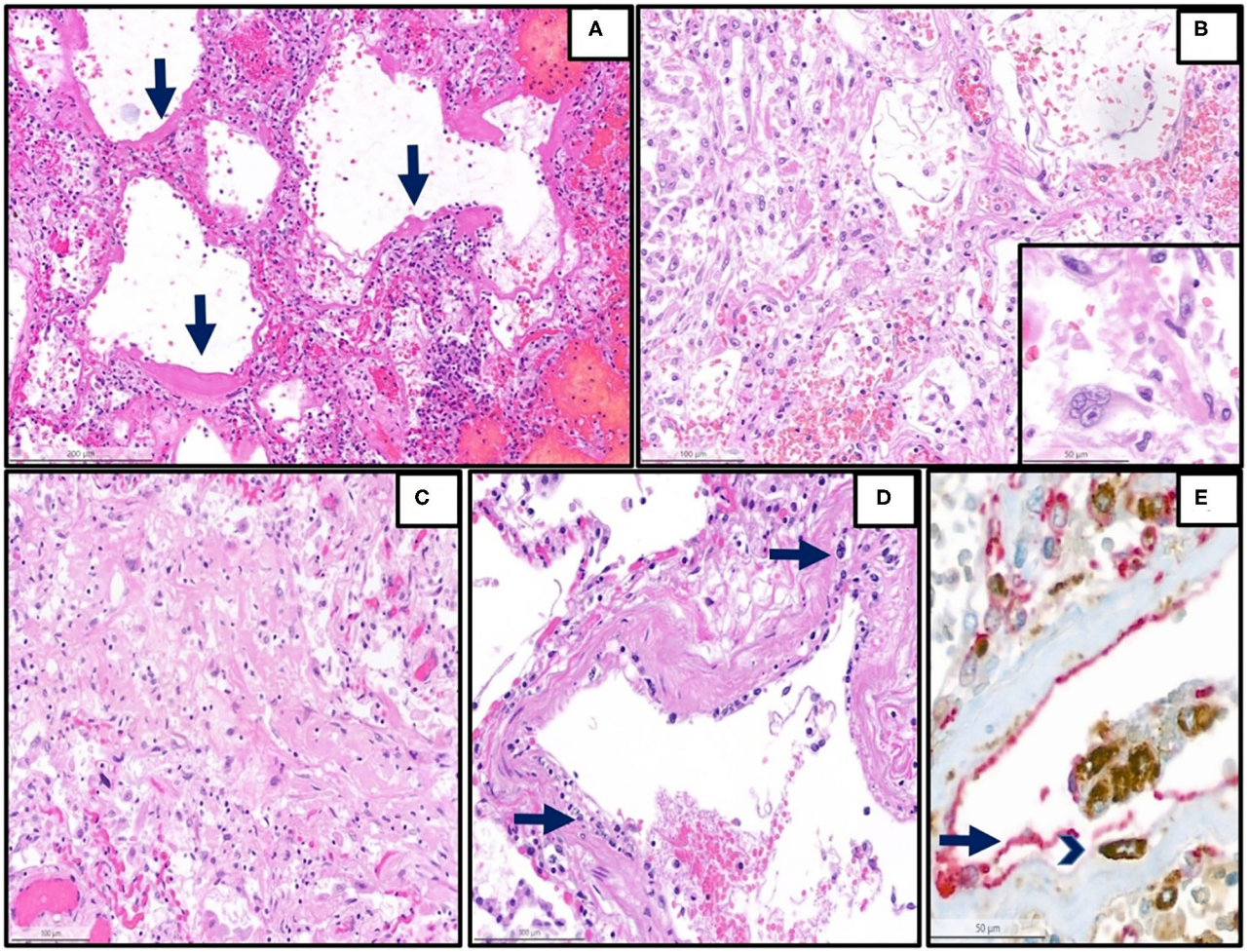

FIGURE 1 | Representative histopathological findings in autopsies from the first wave. **(A)** Lung tissue with diffuse alveolar damage in the exudative phase (hematoxylin and eosin (H&E), magnification 13 x, arrow: hyaline membranes). **(B)** Lung tissue with diffuse alveolar damage in the proliferative phase, which is defined by the presence of organization of the intra-alveolar and interstitial exudate, infiltration with chronic inflammatory cells, and interstitial myofibroblastic reaction. Proliferation and reactive atypias of type II cells are also noted (H&E, magnification 20 x). Inset: reactive pneumocytes type II, magnification 40 x). **(C)** Lung tissue with diffuse alveolar damage in the proliferative phase, showing an excessive collagen deposition (H&E, magnification 20 x). **(D)** Lung arterioles with endotheliitis, which is defined by the presence of subendothelial mononuclear inflammatory infiltrates (arrows) and damage of the endothelium (H&E, magnification 25 x) **(E)** Double immunohistochemistry [red: CD31 (endothelial marker), brown: CD68 (monocytic/macrophage marker)] of another representative case with endotheliitis shows endotheliitis of a venule in the lung with endothelial damage (arrow) and detachment with an associated mononuclear infiltrate (arrowhead) (H&E, magnification 28 x).

(in particular in cerebral parenchyma, subarachnoid and in the lung, with a general incidence of 12/28, 43%), lung infarcts (5/28, 18%), ischemia of small intestine (5/28, 18%, one among those also with angioinvasive candidiasis of the gut as complication), liver necrosis (8/28, 29%), and cerebral infarcts (2/27, 7%). Similar to patients who died in the first wave, constant adjunctive findings in the lungs were also, to a different degree, endotheliitis of capillaries, alveolar capillary macrophages, prominent hyperplasia of pneumocytes type 2, squamous metaplasia, interstitial edema, lymphocytic and histiocytic inflammation, fibrin-rich alveolar edema, and capillary stasis.

Details are summarized in **Table 1**. Representative images of the most important histopathological findings are shown in **Figures 3**, **4**. Additional details of the histopathological findings of this cohort are graphically illustrated in **Figures 5**, **6**.

Postmortem Swabs for SARS-CoV-2 RNA

Altogether, postmortem swabs were positive for SARS-CoV-2 RNA in the following organs/tissues with the following frequencies: trachea (18/26, 69%), lung (19/27, 70%), heart (8/27, 30%), liver (13/27, 48%), spleen (10/26, 38%), gut (9/26, 35%), kidney (13/26, 50%), testicles (9/19, 47%), ovary (1/7, 14%), brain (2/6, 33%), lamina cribrosa (3/4, 75%). Swabs for SARS-CoV-2 RNA were positive up to 39 days after the first diagnosis of COVID-19 (average, 18 days; range, 1–39 days) and up to 93 hours after deaths (average, 30 hours; range, 3–93 hours).

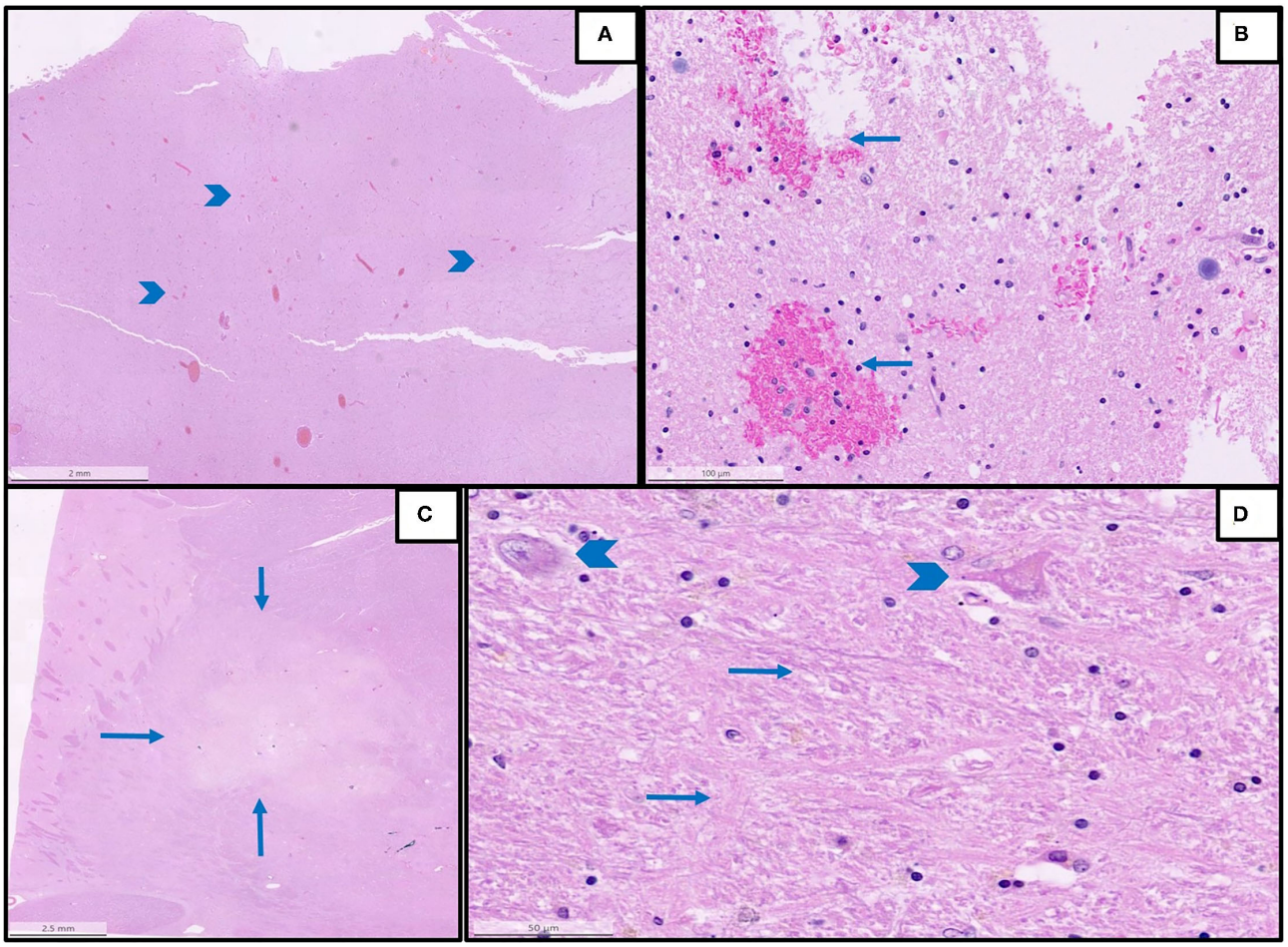

FIGURE 2 | Representative histopathological findings in autopsies from the first wave. **(A)** An overview of multifocal intracerebral microhemorrhages (arrowheads) in a sample from the brain stem (H&E, magnification 1.2 x). **(B)** The detail of image A with microhemorrhages (magnification 25 x, arrows: microhemorrhages). **(C)** An overview of acute brain infarction (arrows) in a sample from basal ganglia (H&E, magnification.62 x). **(D)** Details of image C showing red neurons (arrowheads) and beginning necrosis (arrows) of brain tissue (H&E, magnification 40 x).

Details are graphically shown in **Figures 7–9**, and information on Ct-values is provided in **Supplementary Table 1**.

Comparison Between the Two Waves

Demographic and Biometric Data

No difference concerning age ($p = 0.71$), time interval between diagnosis and death ($p = 0.39$), body mass index ($p = 0.86$), or gender ($p = 0.38$) between patients from the first and second waves could be demonstrated.

Clinical Comorbidities

An important comorbidity in patients who died in the first and second waves was a malignancy. Five patients from the first wave (5/7, 71%) and nine from the second wave (9/28, 32%) had an active or treated oncologic disease. Although cancer prevalence was slightly higher in the patients who died in the first than in the patients who died in the second wave, no statistically significant difference between the two groups could be demonstrated ($p = 0.089$).

A history of arterial hypertension was present in five patients of the first wave (5/7, 71%) and in 19 patients of the second wave (19/28, 68%), without statistically significant differences between the patients of the two waves.

Two patients (2/7, 28%) of the first wave had some form of pulmonary disease (COPD and lung hypertension), whereas 12 patients of the second wave (12/28, 43%) had a positive history of pulmonary disease [COPD, ILD (interstitial lung disease), lung hypertension or asthma)], but no difference in the prevalence of lung diseases between the two waves could be demonstrated ($p = 0.68$).

Three patients of the first wave (3/7, 43%) and four of the second wave (4/28, 14%) had diabetes mellitus. Although diabetes was slightly more common in the patients of the first wave, no statistically significant difference in the prevalence of diabetes between the two waves was found ($p = 0.12$).

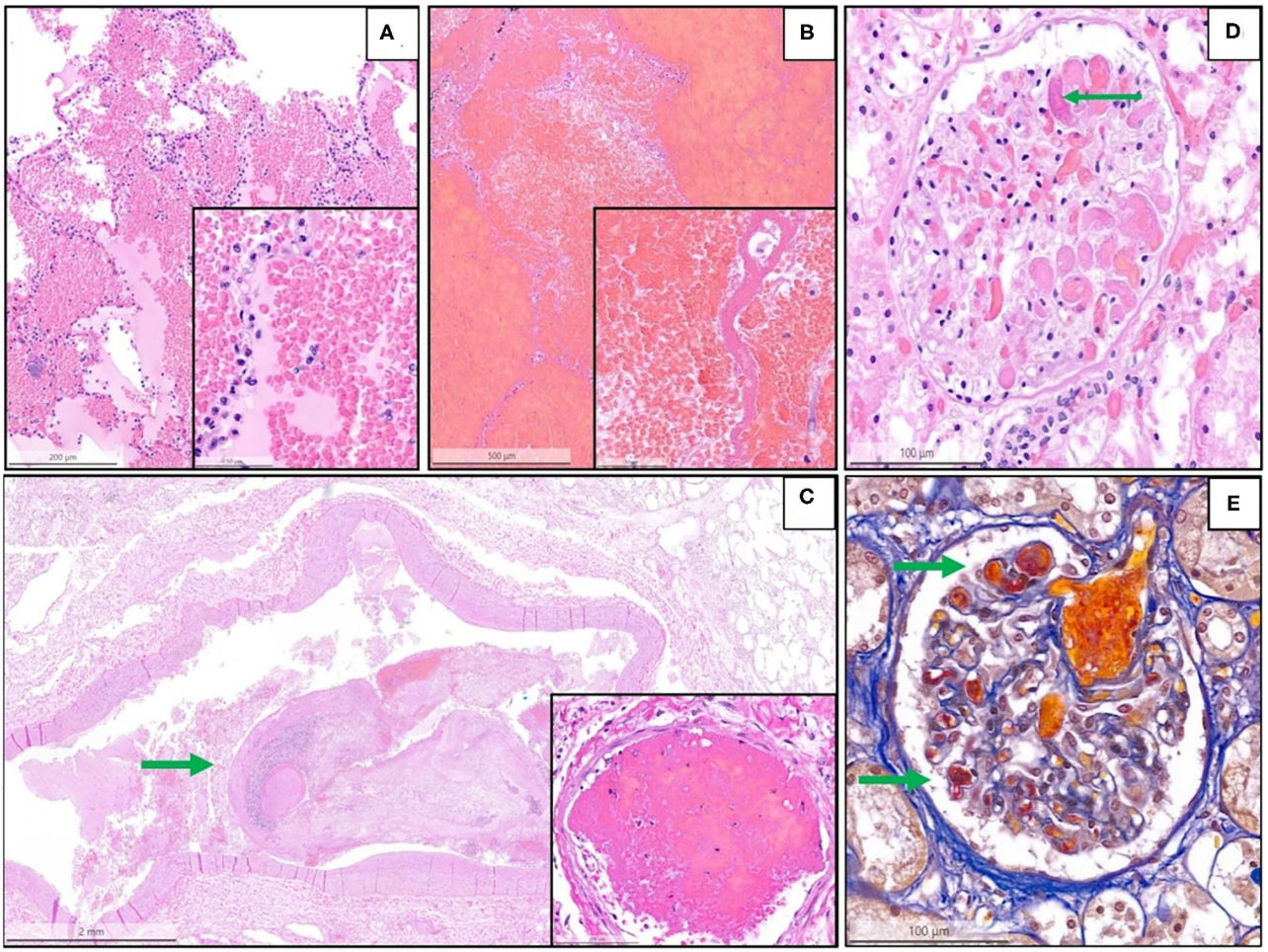

FIGURE 3 | Representative histopathological findings in autopsies from the second wave. **(A)** Acute pulmonary hemorrhage (H&E, magnification 10 x); the inset shows erythrocytes invading alveolar spaces (magnification 40 x). **(B)** Acute hemorrhagic pulmonary infarct (H&E, magnification 5 x); the inset shows a necrotic alveolar septum and hemorrhagic effusion in alveolar space (magnification 40 x). **(C)** Large thrombus (arrow) in a lung arteriole (H&E, magnification 1.4 x); the inset shows a fibrin thrombus in a lung capillary (magnification 28 x). **(D)** Glomerulus (kidney) with fibrin microthrombus (arrow) in a glomerular capillary (H&E, magnification 25 x). **(E)** Acid fuchsin orange G stain (AFOG-stain) shows several fibrin microthrombi (arrows) in the glomerular capillaries (magnification 25 x).

Autopsy Findings

No difference in the time interval between diagnosis of COVID-19 and death could be demonstrated between the patients who died in the first and in the second waves ($p = 0.39$). Moreover, although the finding of DAD was slightly more common in the patients who died in the first wave, no difference between the two cohorts could be identified ($p = 0.39$). Interestingly, the patients of the second wave showed significantly more often (21/28, 75%) bacterial pneumonia (defined histologically by the presence of a granulocytic inflammation with destruction of the lung parenchyma, with or without demonstrable microorganisms through Gram stain) than the patients of the first wave (2/7, 29%) ($p = 0.03$). Another important finding was lung aspergillosis, which was identified in six patients of the second wave (6/28, 21%) but none of the first wave (0/7, 0%), although the difference was not statistically significant ($p = 0.31$).

The general incidence of hemorrhages (independently from the organs considered) was significantly higher in the patients of the first wave (7/7, 100%) than in those of the second wave (14/28, 50%, $p = 0.009$). In more detail, microhemorrhages of the cerebral parenchyma were significantly more frequent among the patients of the first wave ($p = 0.0003$), but no statistically significant difference was observed with regard to hemorrhages in other organs. Similarly, the incidence of ischemic phenomena was significantly higher in the patients of the first wave (6/7, 86%) than in those of the second wave (10/28, 36%) ($p = 0.03$), although no statistically significant differences could be observed if the incidence of ischemic phenomena in the single organs or systems was considered. Intraventricular cardiac thrombi were also more frequent in the patients of the first wave ($p = 0.04$).

Details are demonstrated in **Table 1** and **Figure 10**.

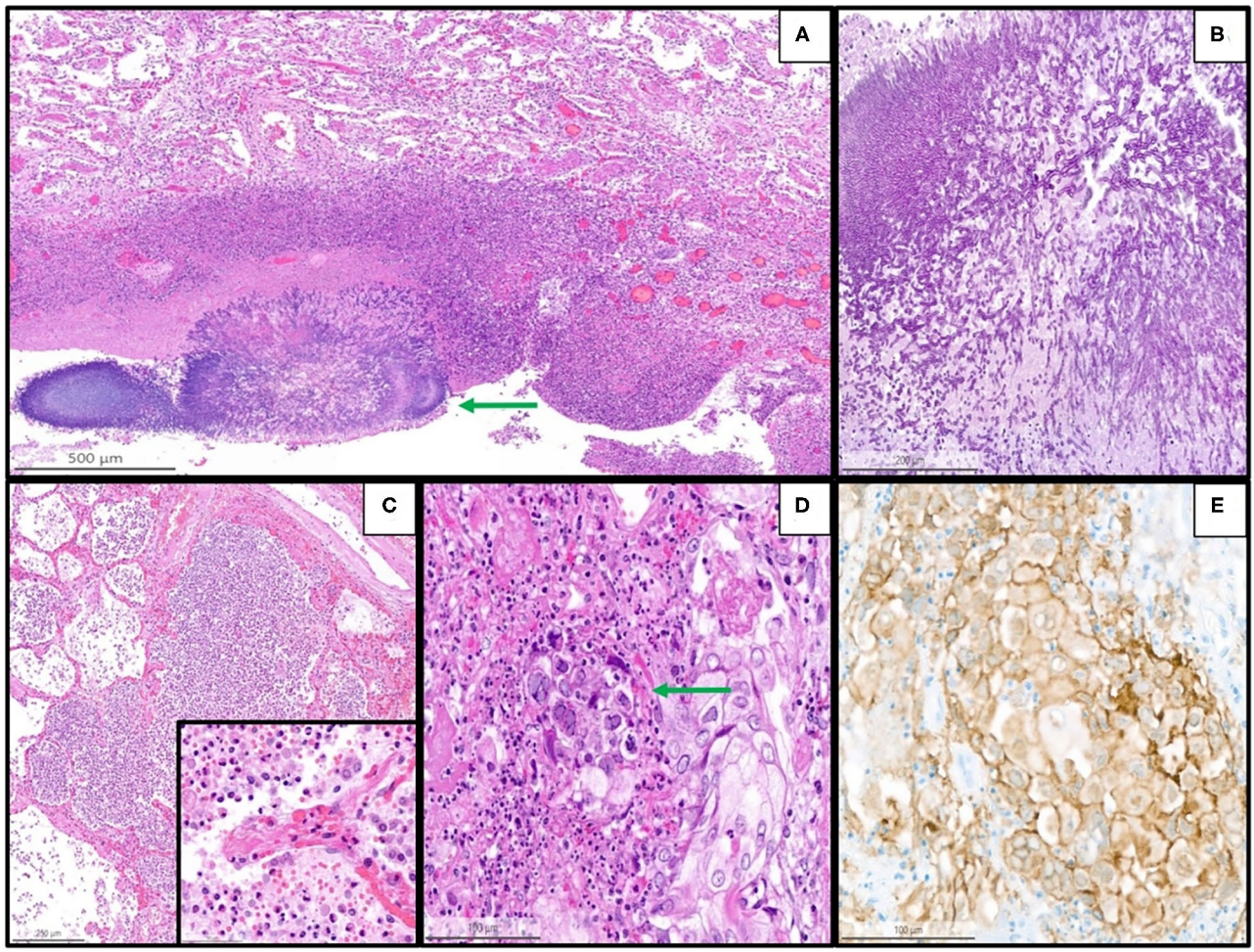

FIGURE 4 | Representative histopathological findings in autopsies from the second wave, illustrating examples of coinfections in the lung of the patients with coronavirus disease 2019 (COVID-19). **(A)** Lung tissue with aspergillosis (arrow) and surrounding acute inflammation (H&E, magnification 10 x). **(B)** Details of image A showing the typical hyphae of Aspergillus *spp*. (PAS, magnification 30 x). **(C)** Acute (bacterial) bronchopneumonia showing granulocytic exudate in the alveolar space and destruction of alveolar septa (H&E, magnification 6 x); the inset illustrates granulocytic inflammation with destruction of a septum (magnification 50 x). **(D)** Herpes simplex pneumonia exhibiting typical herpes-associated nuclear changes (molding, multinucleation, margination of chromatin, see the arrow) (H&E, magnification 25 x). **(E)** Immunohistochemistry for Herpes simplex virus demonstrates a granular cytoplasmic and nuclear positivity along with the typical nuclear changes (magnification 25 x).

Effect of Time Gap Between Diagnosis and Death

In the point-biserial correlation, a negative r between positivity of the postmortem swabs for SARS-CoV-2 RNA and the time interval between diagnosis and death was observed in all examined organs, but only in the lung ($p = 0.001$), trachea ($p = 0.02$), and liver ($p = 0.03$) this association was statistically significant (**Supplementary Table 2**).

A negative association between the time interval between diagnosis and death and the incidence of DAD and general incidence of infarcts (through a negative r in the point biserial correlation) could be demonstrated, although this difference was not statistically significant. In contrast, the association was positive (i.e., with increasing incidence by increasing the time interval between diagnosis and death) for bacterial pneumonia, lung aspergillosis, and general incidence of micro- and macrothrombi, and hemorrhages, but only the association with hemorrhages was statistically significant ($p = 0.012$) (**Supplementary Figure 2** and **Supplementary Table 3**).

The Effect of Positive Postmortem Swabs in Corresponding Organs

The correlation between morphologic findings and the presence of SARS-CoV-2 RNA in the corresponding postmortem tissues was statistically significant only for diffuse alveolar damage ($p = 0.0009$).

We have additionally divided the cases with a postmortem diagnosis of diffuse alveolar damage in two groups, according to the phase of diffuse alveolar damage (exudative vs. proliferative/organizing phase). No statistically significant

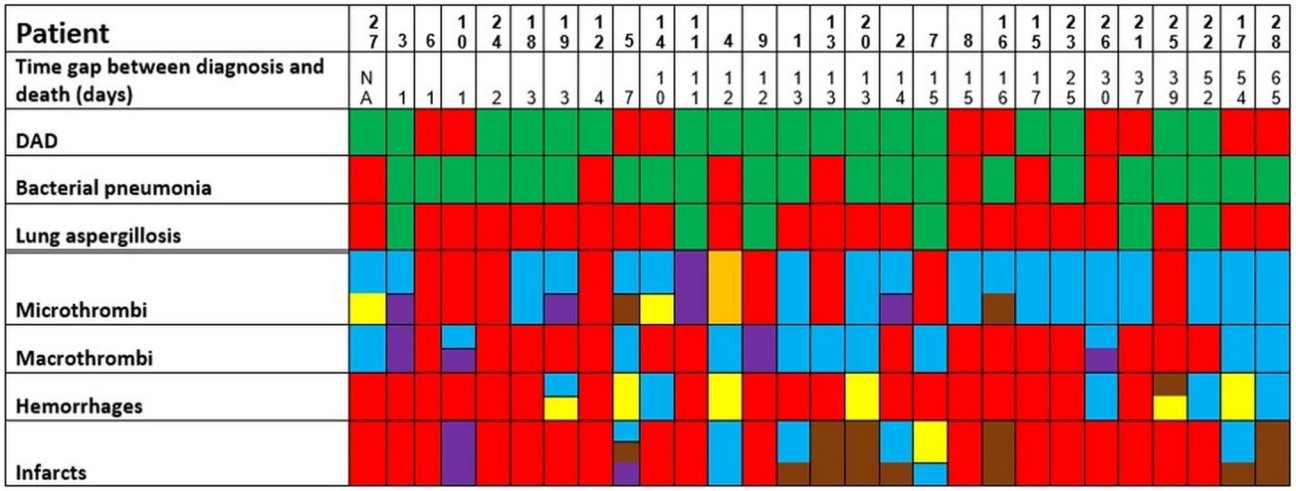

FIGURE 5 | Postmortem findings in the patients of the second wave (green: finding present, red: finding absent. Concerning micro- and macrothrombi, hemorrhages, and infarcts; the following colors to specify the anatomic localization are used: heart and/or major vessels = violet, lung = blue, brain/intracranial = yellow, liver/digestive tract = brown, kidney = orange). The patients are ordered from left to right in a crescent pattern based on the number of days between diagnosis of COVID-19 through nasopharyngeal swab and death. DAD, diffuse alveolar damage; NA, not available.

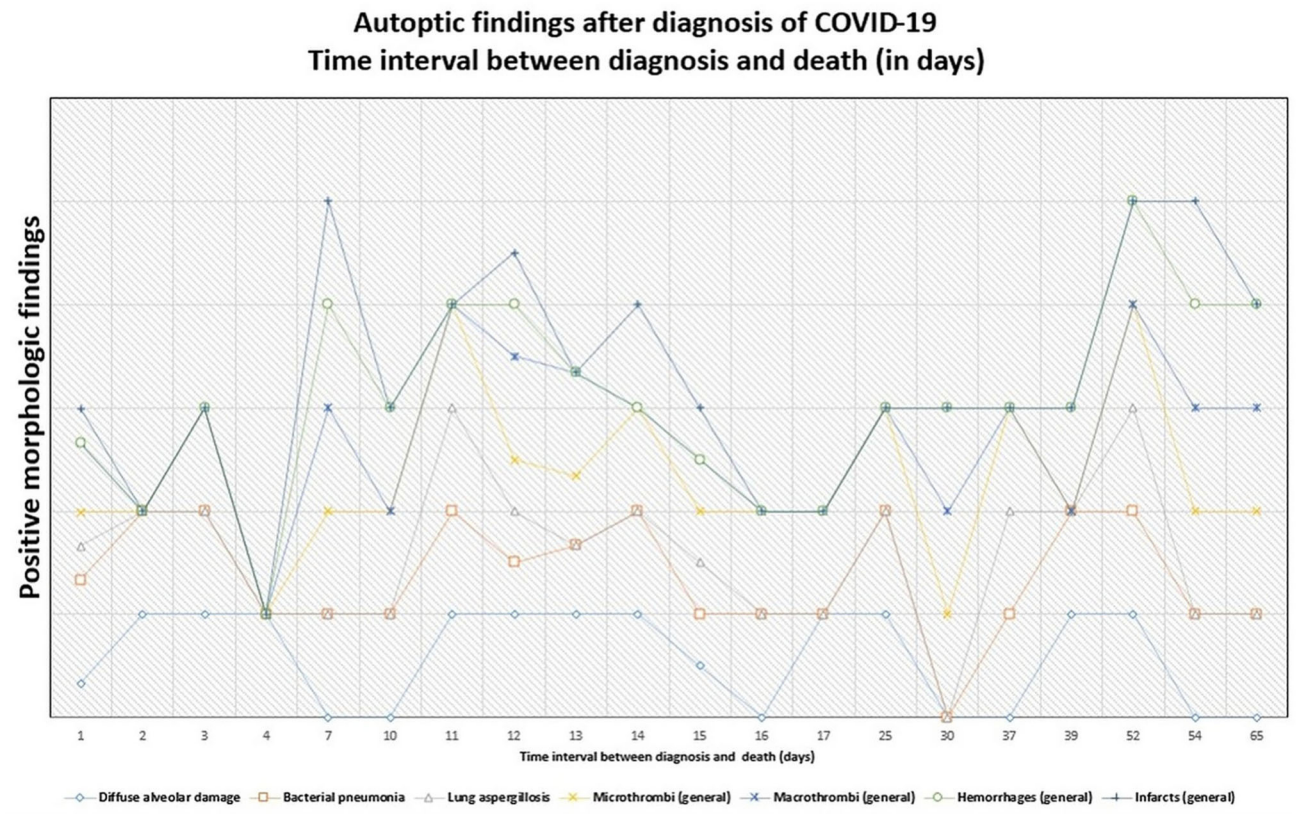

FIGURE 6 | Persistence of histopathologic findings in relation to the time interval between diagnosis and death (in days). The lines do not show absolute percentages but only the relative variation in prevalence of the findings. The different levels of the line along the y-axis are chosen to avoid their overlapping and to facilitate the visual interpretation but do not reflect an absolute percentage, for which we refer the reader to the text.

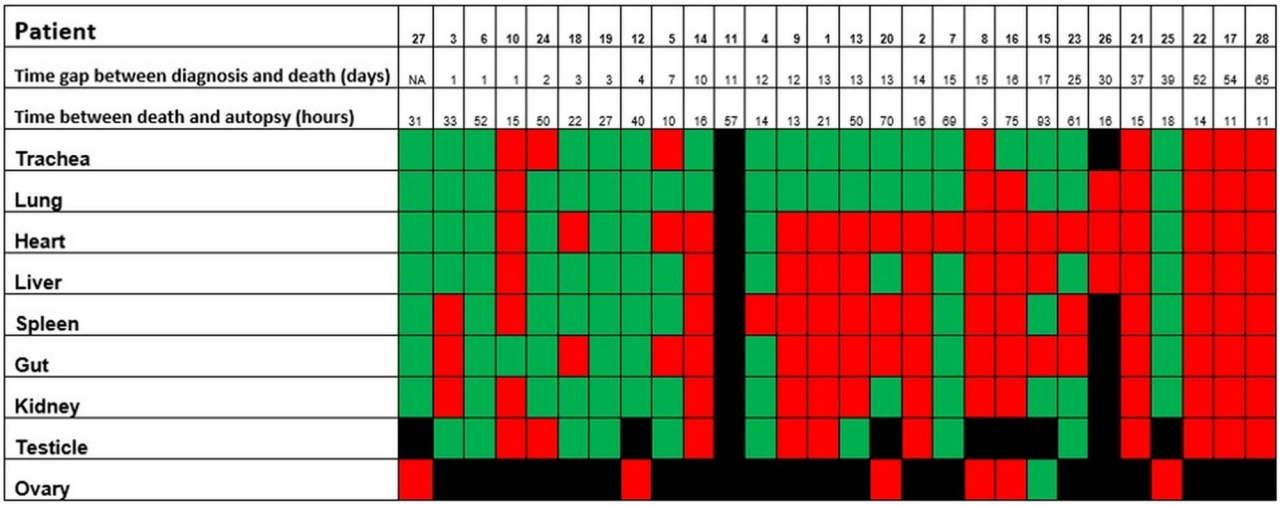

FIGURE 7 | Positivity of the postmortem swabs in the different organs (green: positive, red: negative, black: not available). The patients are ordered from left to right in a crescent pattern based on the number of days between diagnosis of COVID-19 through nasopharyngeal swab and death. Abbreviations: NA, not available.

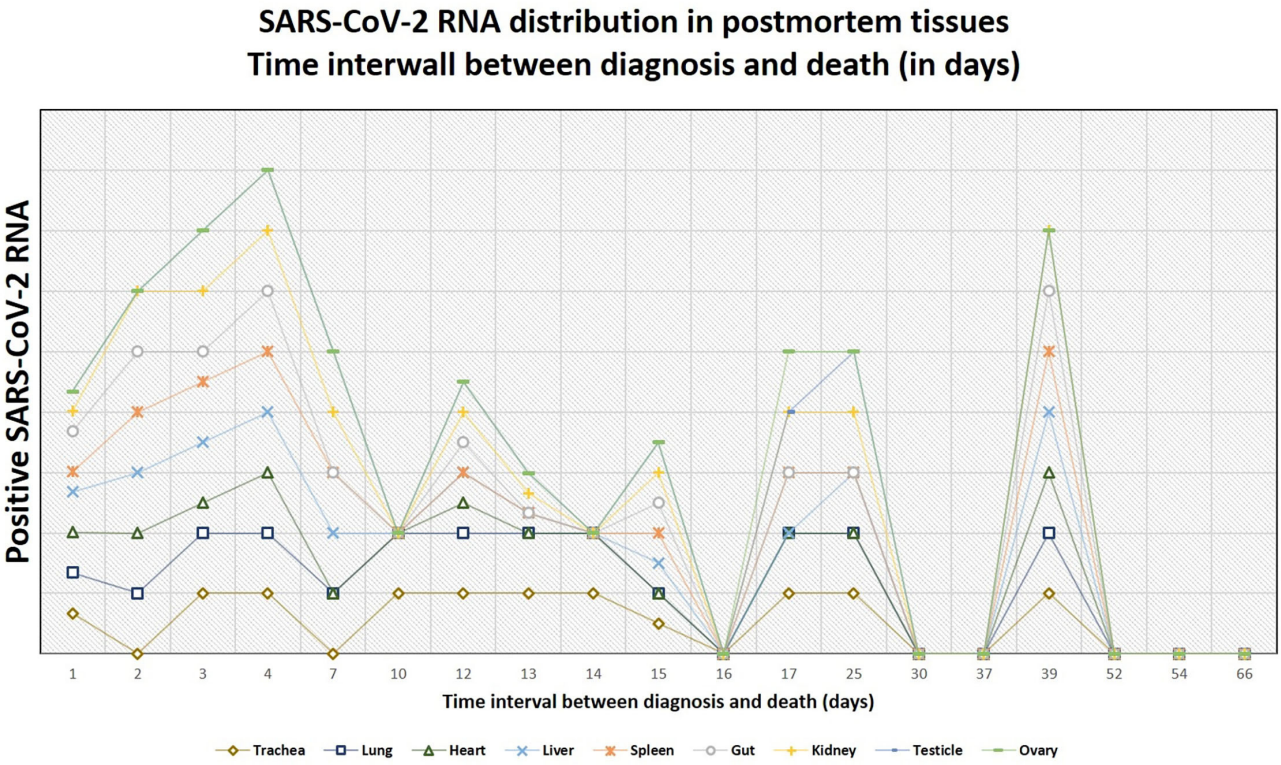

FIGURE 8 | The tendency of positivity of swabs for severe acute respiratory syndrome coronavirus 2 (SARS-CoV-2) RNA in relation to the time interval between diagnosis and death (in days). The lines do not show absolute percentages but only the relative variation in prevalence of the positivity for SARS-CoV-2 RNA. The different levels of the line along the y-axis are selected to avoid their overlapping and to facilitate the visual interpretation but do not reflect an absolute percentage, for which we refer the reader to the text.

association between the phase of diffuse alveolar damage and positivity for SARS-CoV-2 RNA in the lung tissue could be demonstrated (Fisher's exact test, $p = 0.53$). None of those patients had the fibrotic stage of diffuse alveolar damage.

(**Figure 5** and **Supplementary Tables 4, 5**).

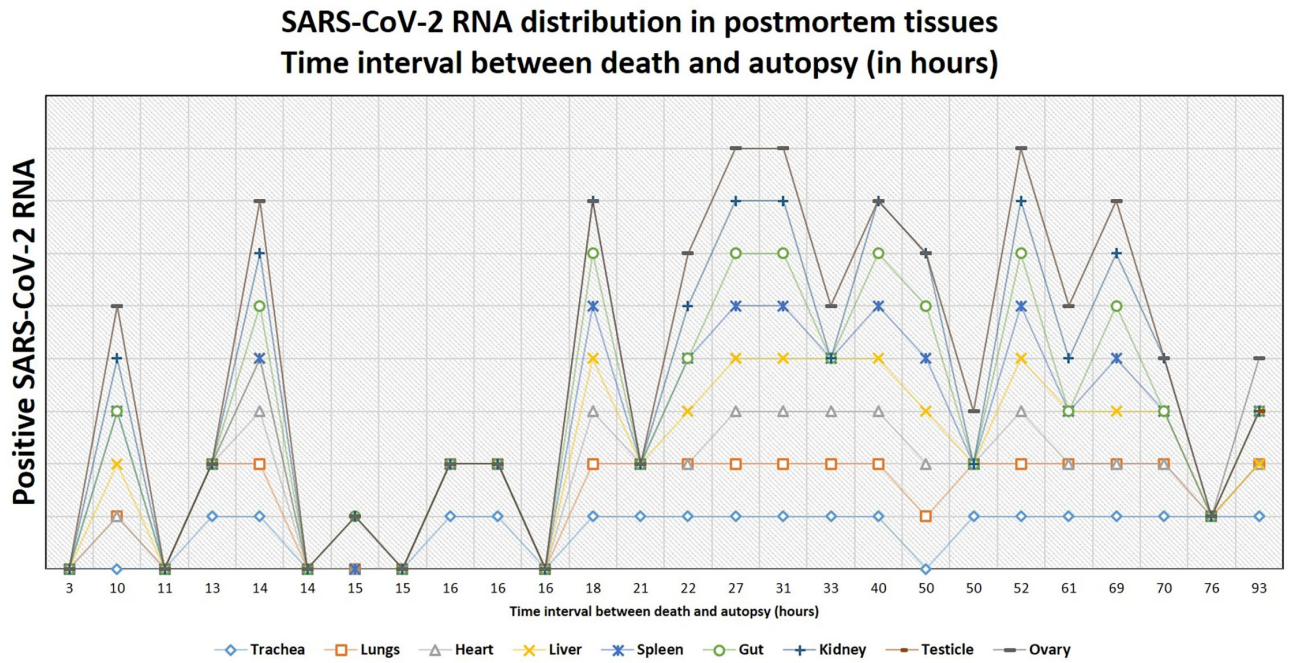

FIGURE 9 | The tendency of postmortem persistence and anatomical distribution of SARS-CoV-2 RNA in relation to the time interval between death and autopsy (postmortem interval, in hours). The lines do not show absolute percentages but only the relative variation in prevalence of the positivity for SARS-CoV-2 RNA. The different levels of the line along the y-axis are chosen to avoid their overlapping and to facilitate the visual interpretation but do not reflect an absolute percentage, for which we refer the reader to the text.

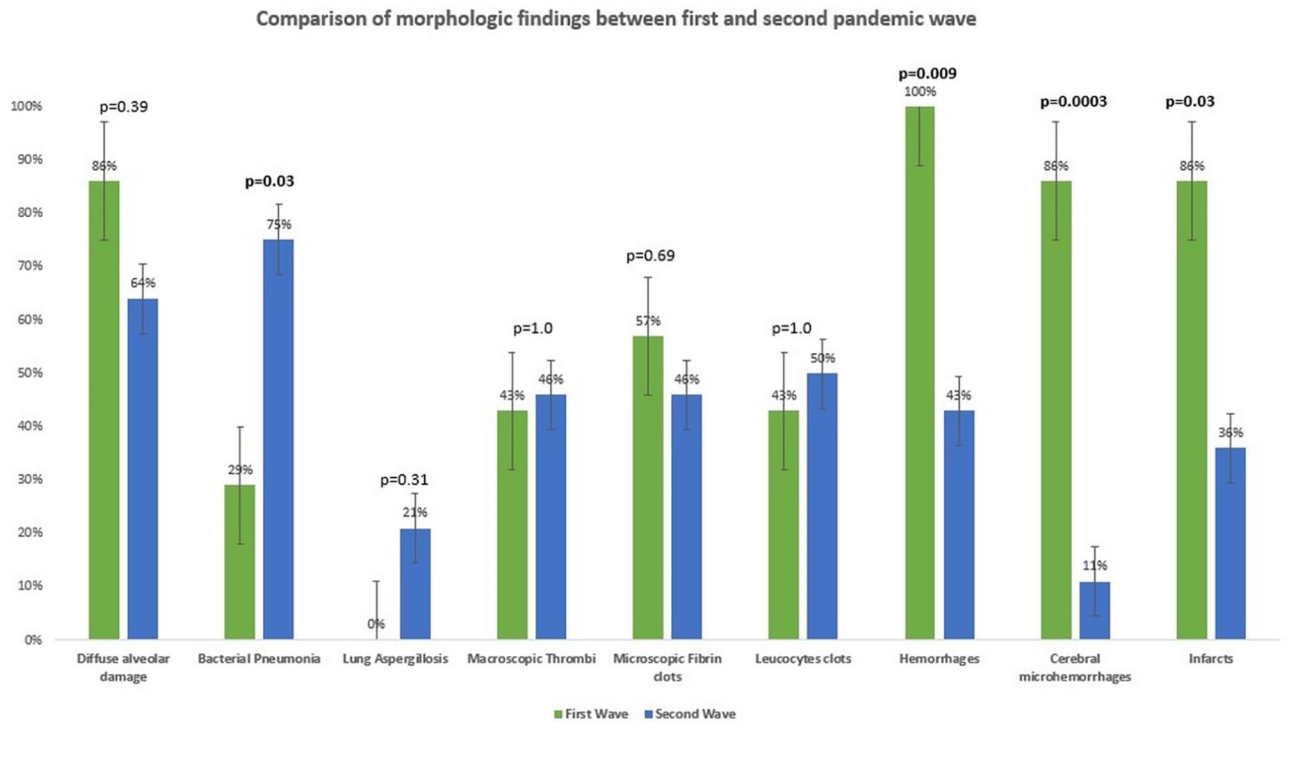

FIGURE 10 | Comparison of morphologic findings at autopsy between first and second pandemic waves.

DISCUSSION

Our data provide evidence of postmortem persisting SARS-CoV-2 RNA up to more than 1 month after the first COVID-19 diagnosis. Moreover, tissue damages, observed in this cohort as diffuse alveolar damage, systemic thromboembolic phenomena, ischemic damages, and hemorrhages, could also be demonstrated up to 2 months after the first diagnosis of SARS-CoV-2 infection. Of note, these morphologic findings can last longer than the persistence of SARS-CoV-2 RNA and can be frequently observed without evidence of SARS-CoV-2 RNA in the affected organs. There is a strong association between persistence of SARS-CoV-2 RNA in the lung and diffuse alveolar damage, but not between the persistence of SARS-CoV-2 RNA and other morphologic findings. In cases of diffuse alveolar damage, no statistically significant difference in the positivity of postmortem swabs for SARS-CoV-2 RNA in the lung could be observed between exudative and proliferative phases. Furthermore, we can show that additional conditions, such as concomitant bacterial pneumonia and lung aspergillosis, can occur at any point after the diagnosis of SARS-CoV-2 infection (ranging from very early, i.e., 1 day after diagnosis, to later, i.e., up to 2 months) and can worsen the tissue damage contributing to mortality and morbidity. Those findings together might suggest that tissue damage is not only and always dependent on direct viral effects but could also be mediated through several inflammatory mechanisms and may, therefore, corroborate the hypothesis of possible long-term persistence of COVID-19 in a subset of patients and thus contribute to the understanding of long-COVID disease. Nevertheless, we acknowledge that 35 autopsies represent a limited cohort compared to the total number of fatal cases of COVID-19 in our country, and that an autopsy-based cohort is exposed to too many biases (such as including just the patients with severe comorbidities in a hospital setting) to draw definitive conclusions on the pathogenesis of long-COVID. Moreover, additional studies are needed to explain how many of those morphologic findings (e.g., hemorrhages or infarcts) are directly related to SARS-CoV-2, to different therapies, or to the clinical settings of critically ill patients, as well as to better characterize harms and benefits of therapies.

This study shows that the most important autoptic findings in the patients who died from COVID-19 were diffuse alveolar damage (24/35, 69%) and concomitant bacterial pneumonia (23/35, 66%). Lung aspergillosis was also a relevant superinfection in many patients of the second wave (6/28, 21%), known as an important cause of death in critically ill patients. In general, the most important cause of death was diffuse alveolar damage, and, according to the interpretation provided in the autopsy report, SARS-CoV-2 was seen as the major responsible factor in death in most cases (26/35, 74%). In all other patients but one, bacterial pneumonia with or without concomitant lung aspergillosis was the main cause of death, and SARS-CoV-2 was a relevant comorbidity (8/35, 23%). Only one patient (1/35, 3%), aged 22, died from the complications of a myocardial infarction, and the concomitant SARS-CoV-2 infection did not contribute to mortality.

The biometric data, prevalence of clinical comorbidities, and morphologic findings of this autopsy-based cohort are in line with those reported in a recently published review by *Caramaschi et al.* on 58 studies on autopsies or biopsies of overall 662 patients with COVID-19, providing further confirmation of the spectrum and characteristics of this new disease (46).

To the best of our knowledge, no previous studies compared biometric and clinical data as well as autoptic findings between the first and second pandemic waves. Of note, only the general incidence of hemorrhages and of brain microhemorrhages was significantly higher among the patients of the first wave compared to those of the second wave (respectively, $p = 0.009$ and $p = 0.0003$). On this point, brain microhemorrhages in COVID-19 are well-known radiologic and autoptic findings (47–51) and are significantly more frequent in the patients with severe disease and in the ICU (intensive care unit) setting (52). According to the literature, their general incidence ranges from 6.9–54% (52), but, to our knowledge, no studies compare the incidence of cerebral microhemorrhages between the two waves. Nevertheless, caution is needed while interpreting these results; the first point to consider is a sampling bias, given the fact that the protocol for brain sampling was not as standardized as for other organs and the quantity of samples varies among autopsies.

Moreover, autopsy findings do not necessarily reflect the situation of critically ill patients, considering that an autoptic examination is performed only in a minor percentage of cases. However, the present result remains interesting and further confirms that COVID-19 is a systemic disease. Cerebral microhemorrhages are indeed a well-known complication in patients with severe COVID-19 and maybe associated with cerebral endotheliitis (35, 53), although they could also be observed in critically ill patients without COVID-19 in the context of critical illness-associated microbleeds (CRAM) (54). Again, those considerations are of utmost importance when evaluating the harms and benefits of different therapies in severe COVID-19.

The association between severe COVID-19 and bacterial superinfection as well as lung aspergillosis has already been reported in the literature, although the incidence varies among studies (55–57). In our cohort, the incidence of bacterial pneumonia was significantly higher in the second wave. Moreover, the patients of the second wave developed lung aspergillosis more frequently, but this difference was not statistically significant. Among others, a possible explication for these differences is the use of dexamethasone as standard therapy in severe COVID-19 during the second pandemic wave. Given the small number of patients of this cohort, only speculations are possible, and larger studies are necessary to validate this hypothesis.

Apart from that, no statistically significant difference between the patients of the first and of the second pandemic wave concerning age, gender prevalence, body mass index, time interval between diagnosis of SARS-CoV-2 and death, prevalence of main comorbidities, and of most autoptic findings was demonstrated. However, due to the small sample size of the entire cohort, no substantial differences between the first and second waves can be drawn and additional studies, in

particular, metanalyses might be necessary to better understand the epidemiologic differences between the pandemic waves.

In patients of the second wave, postmortem swabs were most positive in the lung (70%) and the trachea (69%). SARS-CoV-2 RNA could be detected up to 93 hours after death. The persistence of SARS-CoV-2 RNA several hours and even days after death is a described phenomenon in several organs (58–60), and has been detected up to 35 days after death according to one case report (61). A possible limitation in the interpretation of these results might be that positive SARS-CoV-2 RNA does not necessarily reflect the presence of the virus in the tissues. Actually, false-positive results are reported to occur in about 2% of cases in living patients (62), being contamination during collection procedures, extraction or amplification (e.g., through aerosolization in containment hood), or cross-reaction with other viruses (e.g., other Coronaviruses), some of the factors which might contribute to false-positive RT-PCR results (63). Postmortem RT-PCR for SARS-CoV-2 in tissues of the upper respiratory tract has shown a sensitivity of 96.8% and a specificity ranging from 94.2 to 97.5% (64), so that false-positive and false-negative results should be taken into account. Even a true positive result does not always reflect a viable virus. A surrogate estimating virus viability may be the ct-value of the RT-PCR test: a study by *Jaafar et al.* showed that the culture of the virus is successful up to a ct-value of 25 (70%), but at a ct-value of 30, this value drops to 20%, and values above 35 are associated with only a low likelihood of successful culture (3%) (65). In virtue of these considerations, additional studies to assess virus viability from autopsy tissues are needed.

Of note, in the second wave, typical histological signatures of COVID-19, such as endotheliitis, leucocytic- or fibrin-thrombi, could be demonstrated also in organs where no SARS-CoV-2 RNA was detected through postmortem swabs and in the patients in whom SARS-CoV-2 was not the main cause of death. Moreover, in our cohort, apart from diffuse alveolar damage, no significant correlation was found between swabs' positivity and morphologic findings. These findings further support the role of indirect and persisting viral damage rather than a direct viral effect of SARS-CoV-2 (27, 65, 66).

This result partially agrees with an autopsy-based study of *Skok et al.*, where no correlation between viral load and severity of organ damages at autopsy was found (41).

In our cohort, there was an inverse association between the time elapsed from diagnosis and death and the positivity of swabs in the organs (i.e., the more time passes, the less frequent positivity is observed), but this was statistically significant only for the lung, the trachea, and the liver. Despite this tendency, we found positive postmortem swabs in different organs also in the patients who were diagnosed with COVID-19 several days before, and one patient had positive swabs of trachea, lung, heart, gut, liver, and kidney even 39 days after the diagnosis. Importantly, we found a statistically significant correlation between SARS-CoV-2 RNA evidence in swabs in the lungs and the occurrence of diffuse alveolar damage ($p = 0.0009$), but the association between other morphologic findings and positivity of the swabs in the corresponding organs was not statistically significant.

Up to date, postmortem viral tropism and dynamics through swab examinations have not been characterized in detail. Two autopsy-based studies of *Skok et al.* investigated the presence of SARS-CoV-2 RNA on different organs at autopsy and found a systemic distribution of the virus (in the throat, lung, intestine, and brain) and morphologic findings in line with ours (41, 42).

Another autopsy-based study of *Deinhardt-Emmer et al.*, including 11 patients who died from COVID-19, described the viral distribution through postmortem swabs performed in a relatively short time interval after death (mean, 5.6 hours; range, 1.5–15 hours). The authors demonstrated a systemic involvement with the highest viral load in the lungs and hypothesized a topological correlation of viral load and histopathological damage in the lung (39).

In general, our results on postmortem swabs and morphologic findings are in line with the aforementioned autopsy-based studies, providing further confirmation of the systemic nature of COVID-19 and of the tropism of SARS-CoV-2 for different organs. Moreover, the lack of correlation between the presence of SARS-CoV-2 RNA in tissues and morphologic findings seems again to confirm an inflammatory-mediated process, rather than direct viral damage, as already postulated in the literature (66–70).

In summary, SARS-CoV-2 RNA persists in different organs several weeks after the first diagnosis of COVID-19. Macroscopic and histologic pieces of evidence of tissue damage in critically ill patients can be demonstrated up to 2 months thereafter both in organs with and without postmortem evidence of SARS-CoV-2 RNA. Cerebral microhemorrhages were statistically more frequent in the patients of the first pandemic wave. Postmortem SARS-CoV-2 RNA showed a systemic distribution, with the highest prevalence in the lungs and trachea. There is a significant correlation between the presence of SARS-CoV-2 RNA and diffuse alveolar damage in the lungs, but no other correlation with other autoptic findings.

DATA AVAILABILITY STATEMENT

The original contributions presented in the study are included in the article/**Supplementary Material**, further inquiries can be directed to the corresponding author.

ETHICS STATEMENT

The studies involving human participants were reviewed and approved by Swiss Ethics. The patients/participants provided their written informed consent to participate in this study.

AUTHOR CONTRIBUTIONS

UM designed the study, collected samples, analyzed morphologic data, performed statistical analyses, interpreted clinical and pathological data, and drafted the article. AZ designed the study, interpreted clinical and pathological data, and drafted the article. RS designed the study, interpreted clinical and pathological data, and drafted the article. EP-M performed PCR analyses on

postmortem swabs, interpreted clinical and pathological data, and drafted the article. KF, SB, and DH interpreted clinical and pathological data and drafted the article. HM designed the study, analyzed morphologic data, interpreted clinical and pathological data, and drafted the article. ZV designed the study, analyzed morphologic data, interpreted clinical and pathological data, drafted the article, and coordinated the cooperation among the authors. All the authors were involved in critical reading, writing the article, and had final approval of the submitted and published version.

FUNDING

The experiments were covered by the Internal University Research Funds of the Department of Pathology and Molecular Pathology, University Hospital Zurich Switzerland.

ACKNOWLEDGMENTS

The authors thank the following contributions to the study: Mrs. Daniela Meir, Mrs. Annabelle Marks, and Mr. Fabian Baron for the excellent technical assistance in the postmortem analyses and to all the patients' families who approved performing the autopsies.

SUPPLEMENTARY MATERIAL

The Supplementary Material for this article can be found online at: https://www.frontiersin.org/articles/10.3389/fmed.2022.778489/full#supplementary-material

Supplementary Figure 1 | Details of **Figures 2C,D** (cerebral tissue from basal ganglia). Inset 1: Luxol-stain demonstrates myelin loss (magnification 25 x). Inset 2: immunostaining for NF70/200 (magnification 25 x) demonstrates loss of axons: as such, myelin loss should be interpreted as secondary to infarction and not as demyelination. Inset 3: Luxol-stain in a control case from the same anatomical region (basal ganglia) without myelin loss. Inset 4: immunostaining for NF70/200 in a control case from the same anatomical region (basal ganglia) without loss of axons.

Supplementary Figure 2 | Comparison between morphologic findings and positivity of postmortem swabs in the corresponding organs. The patients are ordered from up to down in a crescent pattern based on the number of days between diagnosis of COVID-19 through nasopharyngeal swab and death. Interpretation: green = finding present with positive swab; blue = finding present with negative swab; red = finding absent with positive swab; black = finding absent with negative swab. NA, not available; DAD, diffuse alveolar damage; BP, bacterial pneumonia; LA, lung aspergillosis; MiT, microthrombi; MaT, Macrothrombi; LH, lung hemorrhages; LI, lung infarcts; MI, myocardial infarction.

REFERENCES

1. Zhu N, Zhang D, Wang W, Li X, Yang B, Song J, et al. A novel coronavirus from patients with pneumonia in China, 2019. *N Engl J Med.* (2020) 382:727–33. doi: 10.1056/NEJMoa2001017
2. Huang C, Huang L, Wang Y, Li X, Ren L, Gu X, et al. 6-month consequences of COVID-19 in patients discharged from hospital: a cohort study. *Lancet.* (2021) 397:220–32. doi: 10.1016/S0140-6736(20)32656-8
3. Nalbandian A, Sehgal K, Gupta A, Madhavan MV, McGroder C, Stevens JS, et al. Post-acute COVID-19 syndrome. *Nat Med.* (2021) 27:601–15. doi: 10.1038/s41591-021-01283-z
4. Oran DP, Topol EJ. The proportion of SARS-CoV-2 infections that are asymptomatic: a systematic review. *Ann Intern Med.* (2021) 174:655–62. doi: 10.7326/M20-6976
5. Wu Z, McGoogan JM. Characteristics of and important lessons from the coronavirus disease 2019. (COVID-19) outbreak in china: summary of a report of 72314 cases from the chinese center for disease control and prevention. *JAMA.* (2020) 323:1239–42. doi: 10.1001/jama.2020.2648
6. Grant MC, Geoghegan L, Arbyn M, Mohammed Z, McGuinness L, Clarke EL, et al. The prevalence of symptoms in 24,410 adults infected by the novel coronavirus (SARS-CoV-2; COVID-19): A systematic review and meta-analysis of 148 studies from 9 countries. *PLoS ONE.* (2020) 15:e0234765. doi: 10.1371/journal.pone.0234765
7. Wang D, Hu B, Hu C, Zhu F, Liu X, Zhang J, et al. Clinical characteristics of 138 hospitalized patients with 2019 novel coronavirus-infected pneumonia in Wuhan, China. *JAMA.* (2020) 323:1061–9. doi: 10.1001/jama.2020.1585
8. Helms J, Tacquard C, Severac F, Leonard-Lorant I, Ohana M, Delabranche X, et al. High risk of thrombosis in patients with severe SARS-CoV-2 infection: a multicenter prospective cohort study. *Intensive Care Med.* (2020) 46:1089–98. doi: 10.1007/s00134-020-06062-x
9. Luo W YH, Gou J, Li X, Sun Y, Li J, Liu L. Clinical pathology of critical patient with novel coronavirus pneumonia (COVID-19). *Preprints.* (2020).
10. Liotta EM, Batra A, Clark JR, Shlobin NA, Hoffman SC, Orban ZS, et al. Frequent neurologic manifestations and encephalopathy-associated morbidity in Covid-19 patients. *Ann Clin Transl Neurol.* (2020) 7:2221–30. doi: 10.1002/acn3.51210
11. Wiersinga WJ, Rhodes A, Cheng AC, Peacock SJ, Prescott HC. Pathophysiology, Transmission, Diagnosis, and Treatment of Coronavirus Disease 2019. (COVID-19): A Review. *JAMA.* (2020) 324:782–93. doi: 10.1001/jama.2020.12839
12. Huang C, Wang Y, Li X, Ren L, Zhao J, Hu Y, et al. Clinical features of patients infected with 2019 novel coronavirus in Wuhan, China. *Lancet.* (2020) 395:497–506. doi: 10.1016/S0140-6736(20)30183-5
13. Mehta P, McAuley DF, Brown M, Sanchez E, Tattersall RS, Manson JJ, et al. COVID-19: consider cytokine storm syndromes and immunosuppression. *Lancet.* (2020) 395:1033–4. doi: 10.1016/S0140-6736(20)30628-0
14. Bartoletti M, Pascale R, Cricca M, Rinaldi M, Maccaro A, Bussini L, et al. Epidemiology of invasive pulmonary aspergillosis among COVID-19 intubated patients: a prospective study. *Clin Infect Dis.* (2020).
15. Rawson TM, Moore LSP, Zhu N, Ranganathan N, Skolimowska K, Gilchrist M, et al. Bacterial and fungal coinfection in individuals with coronavirus: a rapid review To support COVID-19 antimicrobial prescribing. *Clin Infect Dis.* (2020) 71:2459–68. doi: 10.1093/cid/ciaa530
16. Sepulveda J, Westblade LF, Whittier S, Satlin MJ, Greendyke WG, Aaron JG, et al. Bacteremia and blood culture utilization during COVID-19 surge in New York City. *J Clin Microbiol.* (2020) 58. doi: 10.1128/JCM.00875-20
17. Buehler PK, Zinkernagel AS, Hofmaenner DA, Wendel Garcia PD, Acevedo CT, Gomez-Mejia A, et al. Bacterial pulmonary superinfections are associated with longer duration of ventilation in critically ill COVID-19 patients. *Cell Rep Med.* (2021) 2:100229. doi: 10.1016/j.xcrm.2021.100229
18. Meyerowitz-Katz G, Merone L, A. systematic review and meta-analysis of published research data on COVID-19 infection fatality rates. *Int J Infect Dis.* (2020) 101:138–48. doi: 10.1016/j.ijid.2020.09.1464
19. Zhou F, Yu T, Du R, Fan G, Liu Y, Liu Z, et al. Clinical course and risk factors for mortality of adult inpatients with COVID-19 in Wuhan, China: a retrospective cohort study. *Lancet.* (2020) 395:1054–62. doi: 10.1016/S0140-6736(20)30566-3
20. Onder G, Rezza G, Brusaferro S. Case-Fatality Rate and Characteristics of Patients Dying in Relation to COVID-19 in Italy. *JAMA.* (2020) 323:1775–6. doi: 10.1001/jama.2020.4683
21. Greenhalgh T, Knight M. A'Court C, Buxton M, Husain L. Management of post-acute Covid-19 in primary care. *BMJ.* (2020) 370:m3026. doi: 10.1136/bmj.m3026
22. Fernandez-de-Las-Penas C, Palacios-Cena D, Gomez-Mayordomo V, Cuadrado ML, Florencio LL. Defining post-COVID symptoms (Post-Acute

COVID, long COVID, persistent post-COVID): an integrative classification. *Int J Environ Res Public Health*. (2021) 18. doi: 10.3390/ijerph18052621
23. Hoffmann M, Kleine-Weber H, Schroeder S, Kruger N, Herrler T, Erichsen S, et al. SARS-CoV-2 cell entry depends on ACE2 and TMPRSS2 and Is blocked by a clinically proven protease inhibitor. *Cell*. (2020) 181:271–80 e8. doi: 10.1016/j.cell.2020.02.052
24. Wang K, Chen W, Zhang Z, Deng Y, Lian JQ, Du P, et al. CD147-spike protein is a novel route for SARS-CoV-2 infection to host cells. *Signal Transduct Target Ther*. (2020) 5:283. doi: 10.1038/s41392-020-00426-x
25. Walls AC, Park YJ, Tortorici MA, Wall A, McGuire AT, Veesler D. Structure, Function, and Antigenicity of the SARS-CoV-2 Spike Glycoprotein. *Cell*. (2020) 183:1735. doi: 10.1016/j.cell.2020.11.032
26. Chauhan AJ, Wiffen LJ, Brown TP. COVID-19: A collision of complement, coagulation and inflammatory pathways. *J Thromb Haemost*. (2020) 18:2110–7. doi: 10.1111/jth.14981
27. Hu B, Huang S, Yin L. The cytokine storm and COVID-19. *J Med Virol*. (2021) 93:250–6. doi: 10.1002/jmv.26232
28. Lee S, Channappanavar R, Kanneganti TD. Coronaviruses: innate immunity, inflammasome activation, inflammatory cell death, and cytokines. *Trends Immunol*. (2020) 41:1083–99. doi: 10.1016/j.it.2020.10.005
29. Lo MW, Kemper C, Woodruff TM. COVID-19: Complement, coagulation, and collateral damage. *J Immunol*. (2020) 205:1488–95. doi: 10.4049/jimmunol.2000644
30. Sekhawat V, Green A, Mahadeva U. COVID-19 autopsies: conclusions from international studies. *Diagn Histopathol (Oxf)*. (2021) 27:103–7. doi: 10.1016/j.mpdhp.2020.11.008
31. Salerno M, Sessa F, Piscopo A, Montana A, Torrisi M, Patane F, et al. No Autopsies on COVID-19 Deaths: A Missed Opportunity and the Lockdown of Science. *J Clin Med*. (2020) 9. doi: 10.3390/jcm9051472
32. Organisation WH. Infection prevention and control for the safe management of a dead body in the context of COVID-19: interim guidance, 24 March 2020. Available online at: https://appswhoint/iris/handle/10665/331538. (2020).
33. (CDC). CfDCaP. Collection and submission of postmortem specimens from deceased persons with known or suspected COVID-19, March 2020. (Interim guidance) (2020). Available online at: https://wwwcdcgov/coronavirus/2019-ncov/hcp/guidance-postmortem-specimenshtml (2020).
34. Control ECfDPa. Considerations related to the safe handling of bodies of deceased persons with suspected or confirmed COVID-19. Available online at: https://wwwecdceuropaeu/en/publications-data/considerations-related-safe-handling-bodies-deceased-persons-suspected-or (2020).
35. Satturwar S, Fowkes M, Farver C, Wilson AM, Eccher A, Girolami I, et al. Postmortem findings associated with SARS-CoV-2: systematic review and meta-analysis. *Am J Surg Pathol*. (2021) 45:587–603. doi: 10.1097/PAS.0000000000001650
36. Croci GA, Vaira V, Trabattoni D, Biasin M, Valenti L, Baselli G, et al. Emergency lung transplantation after COVID-19: immunopathological insights on two affected patients. *Cells*. (2021) 10. doi: 10.3390/cells10030611
37. Palmieri L, Palmer K, Lo Noce C, Meli P, Giuliano M, Floridia M, et al. Differences in the clinical characteristics of COVID-19 patients who died in hospital during different phases of the pandemic: national data from Italy. *Aging Clin Exp Res*. (2021) 33:193–9. doi: 10.1007/s40520-020-01764-0
38. Soriano V, Ganado-Pinilla P, Sanchez-Santos M, Gomez-Gallego F, Barreiro P, de Mendoza C, et al. Main differences between the first and second waves of COVID-19 in Madrid, Spain. *Int J Infect Dis*. (2021) 105:374–6. doi: 10.1016/j.ijid.2021.02.115
39. Deinhardt-Emmer S, Wittschieber D, Sanft J, Kleemann S, Elschner S, Haupt KF, et al. Early postmortem mapping of SARS-CoV-2 RNA in patients with COVID-19 and the correlation with tissue damage. *Elife*. (2021) 10. doi: 10.7554/eLife.60361
40. Dell'Aquila M, Cattani P, Fantoni M, Marchetti S, Aquila I, Stigliano E, et al. Postmortem swabs in the severe acute respiratory syndrome coronavirus 2 pandemic: report on 12 complete clinical autopsy cases. *Arch Pathol Lab Med*. (2020). 144(11):1298-302. doi: 10.5858/arpa.2020-0362-SA
41. Skok K, Stelzl E, Trauner M, Kessler HH, Lax SF. Post-mortem viral dynamics and tropism in COVID-19 patients in correlation with organ damage. *Virchows Arch*. (2021) 478:343–53. doi: 10.1007/s00428-020-02903-8
42. Skok K, Vander K, Setaffy L, Kessler HH, Aberle S, Bargfrieder U, et al. COVID-19 autopsies: Procedure, technical aspects and cause of fatal course. *Experiences from a single-center Pathol Res Pract*. (2021) 217:153305. doi: 10.1016/j.prp.2020.153305
43. Coronavirus ac. Available online at: https://www.bag.admin.ch/bag/en/home/krankheiten/ausbrueche-epidemien-pandemien/aktuelle-ausbrueche-epidemien/novel-cov.html
44. Wolfisberg S, Gregoriano C, Struja T, Kutz A, Koch D, Bernasconi L, et al. Comparison of characteristics, predictors and outcomes between the first and second COVID-19 waves in a tertiary care centre in Switzerland: an observational analysis. *Swiss Med Wkly*. (2021) 151:w20569. doi: 10.4414/smw.2021.20569
45. WHO. WHO. SARS-CoV-2 variants. (2021). Available online at: https://wwwwhoint/en/activities/tracking-SARS-CoV-2-variants/
46. Caramaschi S, Kapp ME, Miller SE, Eisenberg R, Johnson J, Epperly G, et al. Histopathological findings and clinicopathologic correlation in COVID-19: a systematic review. *Mod Pathol*. (2021). doi: 10.1038/s41379-021-00814-w
47. Chougar L, Shor N, Weiss N, Galanaud D, Leclercq D, Mathon B, et al. Retrospective observational study of brain MRI findings in patients with acute SARS-CoV-2 infection and neurologic manifestations. *Radiology*. (2020) 297:E313–E23. doi: 10.1148/radiol.2020202422
48. Egbert AR, Cankurtaran S, Karpiak S. Brain abnormalities in COVID-19 acute/subacute phase: A rapid systematic review. *Brain Behav Immun*. (2020) 89:543–54. doi: 10.1016/j.bbi.2020.07.014
49. Kantonen J, Mahzabin S, Mayranpaa MI, Tynninen O, Paetau A, Andersson N, et al. Neuropathologic features of four autopsied COVID-19 patients. *Brain Pathol*. (2020) 30:1012–6. doi: 10.1111/bpa.12889
50. Kremer S, Lersy F, de Seze J, Ferre JC, Maamar A, Carsin-Nicol B, et al. Brain MRI findings in severe COVID-19: A retrospective observational study. *Radiology*. (2020) 297:E242–E51. doi: 10.1148/radiol.2020202222
51. Lin E, Lantos JE, Strauss SB, Phillips CD, Campion TR. Jr., Navi BB, et al. Brain imaging of patients with COVID-19: findings at an academic institution during the height of the outbreak in New York City. *AJNR Am J Neuroradiol*. (2020) 41:2001–8. doi: 10.3174/ajnr.A6793
52. Choi Y, Lee MK. Neuroimaging findings of brain MRI and CT in patients with COVID-19: A systematic review and meta-analysis. *Eur J Radiol*. (2020) 133:109393. doi: 10.1016/j.ejrad.2020.109393
53. Kirschenbaum D, Imbach LL, Rushing EJ, Frauenknecht KBM, Gascho D, Ineichen BV, et al. Intracerebral endotheliitis and microbleeds are neuropathological features of COVID-19. *Neuropathol Appl Neurobiol*. (2021) 47:454–9. doi: 10.1111/nan.12677
54. Fanou EM, Coutinho JM, Shannon P, Kiehl TR, Levi MM, Wilcox ME, et al. Critical Illness-Associated Cerebral Microbleeds. *Stroke*. (2017) 48:1085–7. doi: 10.1161/STROKEAHA.116.016289
55. Nori P, Cowman K, Chen V, Bartash R, Szymczak W, Madaline T, et al. Bacterial and fungal coinfections in COVID-19 patients hospitalized during the New York City pandemic surge. *Infect Control Hosp Epidemiol*. (2021) 42:84–8. doi: 10.1017/ice.2020.368
56. Dudoignon E, Camelena F, Deniau B, Habay A, Coutrot M, Ressaire Q, et al. Bacterial pneumonia in COVID-19 critically ill patients: a case series. *Clin Infect Dis*. (2021) 72:905–6. doi: 10.1093/cid/ciaa762
57. Lansbury L, Lim B, Baskaran V, Lim WS. Co-infections in people with COVID-19: a systematic review and meta-analysis. *J Infect*. (2020) 81:266–75. doi: 10.1016/j.jinf.2020.05.046
58. El Bouzidi K, Howard M, Ali H, Khan M, Harris A, Zuckerman M. 'Test, test, test' even after death: persistence of SARS-CoV-2 RNA in postmortem nasopharyngeal swabs. *J Clin Pathol*. (2020). doi: 10.1136/jclinpath-2020-207091
59. Sawant OB, Singh S, Wright RE. 3rd, Jones KM, Titus MS, Dennis E, et al. Prevalence of SARS-CoV-2 in human post-mortem ocular tissues. *Ocul Surf*. (2021) 19:322–9. doi: 10.1016/j.jtos.2020.11.002
60. Servadei F, Mauriello S, Scimeca M, Caggiano B, Ciotti M, Anemona L, et al. Persistence of SARS-CoV-2 Viral RNA in nasopharyngeal swabs after death: an observational study. *Microorganisms*. (2021). 9. doi: 10.3390/microorganisms9040800
61. Beltempo P, Curti SM, Maserati R, Gherardi M, Castelli M. Persistence of SARS-CoV-2 RNA in post-mortem swab 35 days after death: A case report. *Forensic Sci Int*. (2021) 319:110653. doi: 10.1016/j.forsciint.2020.110653
62. Braunstein GD, Schwartz L, Hymel P, Fielding J. False positive results with SARS-CoV-2 RT-PCR tests and how to evaluate a RT-PCR-positive test for the

possibility of a false positive result. *J Occup Environ Med.* (2021) 63:e159–e62. doi: 10.1097/JOM.0000000000002138
63. Skittrall JP, Wilson M, Smielewska AA, Parmar S, Fortune MD, Sparkes D, et al. Specificity and positive predictive value of SARS-CoV-2 nucleic acid amplification testing in a low-prevalence setting. *Clin Microbiol Infect*. (2021). 27:469 e9–e15. doi: 10.1016/j.cmi.2020.10.003
64. Hall JA, Harris RJ, Emmett HE, Lowe B, Singanayagam A, Twohig KA, et al. On the sensitivity and specificity of postmortem upper respiratory tract testing for SARS-CoV-2. *J Infect Dis.* (2021) 224:389–94. doi: 10.1093/infdis/jiab270
65. Jaafar R, Aherfi S, Wurtz N, Grimaldier C, Van Hoang T, Colson P, et al. Correlation between 3790 quantitative polymerase chain reaction-positives samples and positive cell cultures, including 1941. Severe acute respiratory syndrome coronavirus 2 isolates. *Clin Infect Dis.* (2021) 72:e921. doi: 10.1093/cid/ciab531
66. England JT, Abdulla A, Biggs CM, Lee AYY, Hay KA, Hoiland RL, et al. Weathering the COVID-19 storm: Lessons from hematologic cytokine syndromes. *Blood Rev*. (2021) 45:100707. doi: 10.1016/j.blre.2020.100707
67. Karki R, Sharma BR, Tuladhar S, Williams EP, Zalduondo L, Samir P, et al. Synergism of TNF-alpha and IFN-gamma triggers inflammatory cell death, tissue damage, and mortality in SARS-CoV-2 infection and cytokine shock syndromes. *Cell*. (2021). 184:149–68 e17. doi: 10.1016/j.cell.2020.11.025
68. Nicosia RF, Ligresti G, Caporarello N, Akilesh S, Ribatti D. COVID-19 Vasculopathy: mounting evidence for an indirect mechanism of endothelial injury. *Am J Pathol.* (2021). doi: 10.1016/j.ajpath.2021.05.007
69. Ragab D, Salah Eldin H, Taeimah M, Khattab R, Salem R. The COVID-19 cytokine storm; what we know so far. *Front Immunol.* (2020) 11:1446. doi: 10.3389/fimmu.2020.01446
70. Zhang J, Wu H, Yao X, Zhang D, Zhou Y, Fu B, et al. Pyroptotic macrophages stimulate the SARS-CoV-2-associated cytokine storm. *Cell Mol Immunol.* (2021) 18:1305–7. doi: 10.1038/s41423-021-00665-0

Conflict of Interest: The authors declare that the research was conducted in the absence of any commercial or financial relationships that could be construed as a potential conflict of interest.

Publisher's Note: All claims expressed in this article are solely those of the authors and do not necessarily represent those of their affiliated organizations, or those of the publisher, the editors and the reviewers. Any product that may be evaluated in this article, or claim that may be made by its manufacturer, is not guaranteed or endorsed by the publisher.

frontiers in Medicine

ORIGINAL RESEARCH
published: 21 February 2022
doi: 10.3389/fmed.2022.841550

Lymphatic Vessel Invasion in Routine Pathology Reports of Papillary Thyroid Cancer

Costanza Chiapponi[1], Hakan Alakus[1], Matthias Schmidt[2], Michael Faust[3], Christiane J. Bruns[1], Reinhard Büttner[4], Marie-Lisa Eich[4] and Anne M. Schultheis[4]*

[1] Department of General, Visceral, Cancer and Transplant Surgery, University Clinic of Cologne, Cologne, Germany, [2] Department for Nuclear Medicine, University Clinic of Cologne, Cologne, Germany, [3] Policlinic for Endocrinology, Diabetes and Prevention Medicine, University Clinic of Cologne, Cologne, Germany, [4] Institute for Pathology, University Clinic of Cologne, Cologne, Germany

Purpose: It is not mandatory to report lymphatic vessel invasion in pathology reports of papillary thyroid cancer (PTC) according to the current Union for International Cancer Control (UICC) TNM (tumor, nodes, and metastases) classification. However, there is some evidence for its correlation with lymph node metastasis (LNM) and prognosis. The aim of this study was to explore the clinical implication of lymphatic vessel invasion documentation of PTC because pathology reports play a pivotal role in postsurgical clinical decision-making in endocrine tumor boards.

Methods: Patients undergoing postoperative radioiodine treatment for PTC at the University Hospital of Cologne, Germany between December 2015 and March 2020 were identified. Pathology reports were screened for documentation of lymphatic vessel invasion. Demographics and clinicopathologic data of patients documented, including lymphatic vessel invasion and lymph nodal involvement were analyzed.

Results: A total of 578 patients were identified and included. Lymphatic vessel invasion was reported in pathology reports of 366 (63.3%) and omitted in 112 (36.7%) patients. Positive lymphatic vessel invasion (L1) was diagnosed in 67 (18.3%) of 366 patients and was documented as absent (L0) in 299 (81.7%) patients. Lymph nodal (N) status was positive (N+) in 126 (45.6%) and negative (N0) in 150 (54.3%) of these patients. In 54 (80.6%) L1 cases N+ status and in 137 (65.6%) L0 cases N0 status was diagnosed. In 13 (19.4%) cases with L1 status, there were no LNMs (L1 N0). In total, 72 (34.4%) patients had LNM despite L0 status (L0 N+). The sensitivity and specificity of LVI reporting for LNM were 0.42 and 0.91, respectively.

Conclusion: In routine pathology reports of PTC used for indication to postoperative radioiodine treatment by a German endocrine tumor board, lymphatic vessel invasion was found to be reported inconsistently and mostly as L0. L1 diagnoses, however, reliably correlated with reported LNM and might, thus, be relevant for clinical decision-making. For this reason, we advocate for standardized pathologic reassessment of lymphatic vessel invasion, in particular for cases where lymph nodes are not included in the pathologic specimen and if L0 is documented.

Keywords: papillary thyroid cancer, lymph node metastasis, lymph vascular invasion, nodal involvement of papillary thyroid cancer, L0, L1, lymph vessel

OPEN ACCESS

Edited by:
Andrey Bychkov, Kameda Medical Center, Japan

Reviewed by:
Kennichi Kakudo, Izumi City General Hospital, Japan
Tetiana Bogdanova, National Academy of Sciences of Ukraine, Ukraine

****Correspondence:***
Costanza Chiapponi
costanza.chiapponi@uk-koeln.de

Specialty section:
This article was submitted to Pathology, a section of the journal Frontiers in Medicine

Received: *22 December 2021*
Accepted: *20 January 2022*
Published: *21 February 2022*

Citation:
Chiapponi C, Alakus H, Schmidt M, Faust M, Bruns CJ, Büttner R, Eich M-L and Schultheis AM (2022) Lymphatic Vessel Invasion in Routine Pathology Reports of Papillary Thyroid Cancer. Front. Med. 9:841550. doi: 10.3389/fmed.2022.841550

INTRODUCTION

Papillary thyroid cancer (PTC) has a very good prognosis. For this reason, the extent of surgery and prophylactic lymphadenectomy are controversial issues. The European Society of Endocrine Surgery (ESES) recommends prophylactic lymphadenectomy in patients with tumor stages T3 or T4, in patients older than 45 years or younger than 15 years, of the male gender, with bilateral or multifocal tumors, and known involved lateral lymph nodes (1). The British Thyroid Association (BTA) advocates for it in aggressive histopathological subtypes, in patients older than 44 years, with multifocality and tumors sized >4 cm at their largest diameter (2). Also, according to the American Thyroid Association (ATA) "prophylactic central-compartment neck dissection (ipsilateral or bilateral) should be considered in patients with papillary thyroid carcinoma with clinically uninvolved central neck lymph nodes (cN0) who have advanced primary tumors (T3 or T4) or clinically involved lateral neck nodes (cN1b), or if the information will be used to plan further steps in therapy" (3). The European Society of Medical Oncologists (ESMO) underlines that it facilitates the precise staging of the disease and guides subsequent treatment and follow-up, although there is controversial evidence supporting the improvement of recurrence or mortality rate (4). Moreover, the Japanese Association of Endocrine Surgeons (JAES) recommends it for all patients with PTC, excluding papillary microcarcinoma of the thyroid (5). Personalized approaches are required, taking into account the context of the patient, the tumor biology, the experience of the thyroid surgeon, and the benefit/risk ratio (6). In a recent meta-analysis including 9,369 PTCs, lymph node metastasis (LNM) was identified in 31.7% of patients (7). Significant risk factors were age (<45 years), gender (male), multifocality, tumor size (>1 cm), tumor location (upper third of the thyroid), capsular invasion, and extrathyroidal extension (ETE) (7). However, not negligible rates of LNM have been reported for pT1a tumors (8, 9). The clinical significance of lymph nodal involvement in pT1a and pT1b tumors is controversial. Although a recent study reports rates of 11% for PTCs incidentally diagnosed during autopsy (10), there is also some evidence for an increased risk of recurrence (11) and for compromised overall survival in patients with nodal involvement (12), making this issue very relevant for young patients. For this reason, the diagnosis of LNM leads to radioiodine treatment and suppressive TSH treatment during follow-up, even in pT1a patients in Germany. Since pT1a or even pT1b tumors can be diagnosed incidentally in patients undergoing thyroidectomy for multinodular goiter, many of these patients do not undergo lymphadenectomy.

Lymphatic vessel invasion (LVI) has been shown to correlate with LNM and with patients' prognoses in several tumor entities (13–16). In a recent study, it was found to be the only independent prognostic factor of disease free survival (DFS) in patients with lymph node-negative superficial esophageal squamous cell carcinoma (17). Even its documented absence (L0) might play some predictive role: a multicenter retrospective analysis found that no LNMs were identified in women with low-risk cervical cancer and no LVI. L0 was suggested as a possible argument for omitting prophylactic lymphadenectomy in these patients (18). Although there is some evidence that LVI in PTC correlates with LNMs (19–22) and with outcomes of patients (6, 23, 24), LVI does not play any concrete role in clinical decision-making. Vascular invasion instead is included among those crucial histologic variables for initial risk stratification and clinical management of PTC, alongside ETE, margin status (R), and the number of metastatic lymph nodes (pN-status) (25–27). LVI (L-status; L1 = invasion and L0 = no invasion) is not regularly included in pathology reports in PTC in Europe, as it is not mandatory to report LVI according to the current TNM classification (28). One possible explanation is that LVI in PTC is often not easily identified in thyroid parenchyma (**Figure 1**) (29).

Lymphatic vessel invasion is defined as "*tumor deposits within lymphatic spaces*" that may manifest "*as psammoma bodies alone within these spaces*" (27, 30, 31). However, often the invaded lymph vascular channels are overgrown by the tumor, as evidenced by the absence of lymphatic channels in the central part of most PTCs with lymph node metastases (29). The thin walls of the lymphatic vascular channels and the invasive nature of the tumors are factors, which can make LVI detection challenging (**Figure 1**). In addition, LVI assessment is not sufficiently standardized in our experience: for the most part, only representative tumor sections are embedded and H&E staining of representative sections are deemed sufficient for reporting the lack of LVI (L0). However, LVI is not only limited to the tumor itself and tumor interface but could be manifested by the spread of PTC in the ipsilateral and even contralateral lobe seen as psammomas and/or (usually subcapsular) "tumor seeds." Additional immunohistochemical stains or additional tissue sectioning might help detect LVI. Both, generally, are not routinely performed in the clinical setting (**Supplementary Figure 1**).

The aim of this study was to critically question the LVI documentation in routine pathology reports of papillary thyroid cancer. Tumors that were deemed worth treating with radioiodine therapy by the multidisciplinary endocrine tumor board of the university were included and the impact of LVI documentation on clinical and pathological parameters was explored. We also investigated if LVI documentation might be helpful for identifying nodal involvement in pT1a tumors.

METHODS

Patients

Patients who underwent postoperative radioiodine therapy between December 2015 and March 2020 (4 years and 3 months) for PTC as judged by the interdisciplinary tumor board for endocrine tumors at the University Hospital Cologne, Germany were identified and included. In Germany, national guidelines advise for radioiodine therapy in PTC pT1b and higher, and in selected cases of pT1a (e.g., unfavorable histology, lymph node involvement, etc.). Postoperative tumor board recommendations are generally based on pathology reports besides clinical information delivered by the presenting physician.

Surgery was performed as thyroidectomy with or without central lymph node dissection depending on the time of

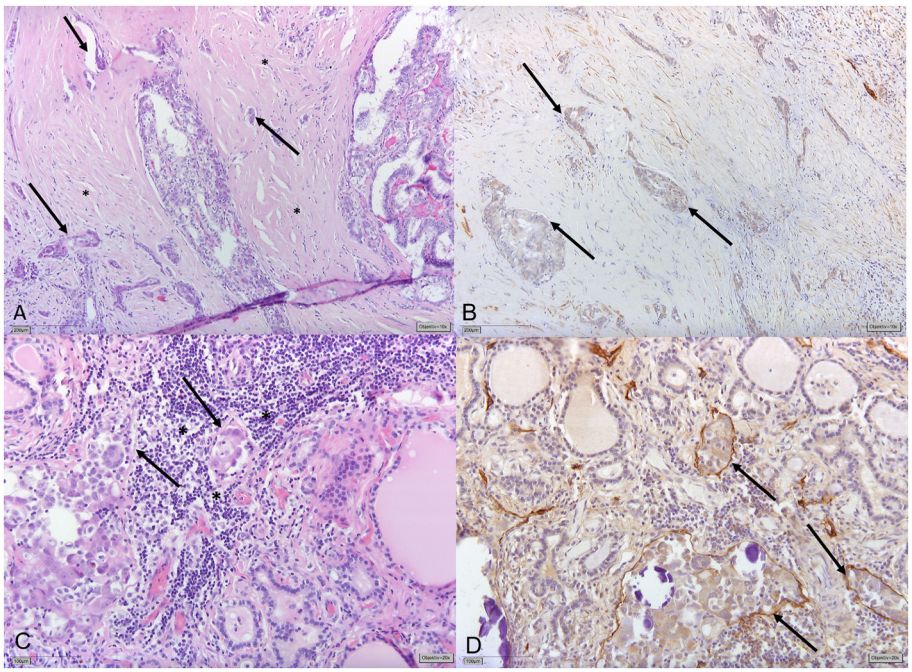

FIGURE 1 | (A) Papillary thyroid carcinoma (PTC) displaying significant stromal desmoplasia (*) with small tumor foci surrounded by slit-like spaces (→) indicating vascular invasion. **(B)** Immunohistochemical staining for Podoplanin/D2-40 shows that slit-like spaces lack circumferential staining for D2-40 (→) indicating the presence of retraction artifacts and not lymphatic vessel invasion (LVI). **(C)** Different tumor areas of the same PTC show small tumor nodules with discrete slit-like spaces (→) surrounded by lymphocytes (*). **(D)** Circumferential D2-40-positivity confirming LVI (→).

diagnosis (pre- or postoperatively) and the experience of surgeon, as recommended by the German Guidelines (32). In some cases, lateral lymph node dissection was also performed, when the preoperative radiologic diagnosis suggested lymph node involvement, according to the current German Guidelines (32).

Histopathology

In our pathologic institute, the resected specimens were fixed in 4% phosphate-buffered formalin and embedded in Paraffin. For each cm of the tumor (largest diameter), one tumor section was embedded. A 3-cm large tumor would be analyzed using three tumor sections, ideally comprising one entire diametrical section of the tumor. Three micron thick sections were cut and stained with H&E. Diagnoses were made according to the, at that time, current (2009 and 2017) WHO classification of Tumors of Endocrine Organs. Shortly, H&E-stained sections were routinely screened for signs of LVI. These included the presence of tumor tissue and/or psammoma bodies in lymphatic spaces, including lymphatic spaces within the tumor, but also at the periphery of the tumor, or somewhere else in the resection specimen, as described by Mete et al. (27) and Wittekind (28). Additional immunohistochemical staining was not routinely performed, but only in a subset of cases, which were deemed unclear. Staging, including the assessment of the Nodal Status and LVI, was performed according to the 2018 International Union Against Cancer (UICC) TNM classification system (28). In addition to the number of the resected and metastatic lymph nodes, the number of metastatic lymph nodes with extracapsular extension (ece+) was also determined.

In instances where patients were only referred for radioiodine treatment to our University Hospital, only pathology reports were obtained and included.

Additionally, in order to find out if LVI identification might be helpful for identifying nodal involvement in pT1a tumors, 22 specimens of papillary microcarcinomas with confirmed nodal involvement were retrospectively reassessed with H&E and D2-40 immunohistochemistry (IHC) by two experienced pathologists, according to the criteria defined above (28) (presence of tumor tissue and/or psammoma bodies in lymphatic spaces, including lymphatic spaces within the tumor, but also at the periphery of the tumor, or somewhere else in the resection specimen).

Data Collection, Analysis, and Ethic

Electronic and paper data of the University Hospital of Cologne were retrospectively collected and analyzed. Data were analyzed using Excel 365 and IBM SPSS Statistics for Windows, Version 25.0, Armonk, NY, USA. This study was approved by the ethics committee of the University Hospital Cologne (Approval ID 20-1724).

RESULTS

Characteristics of Patients

Between December 2015 and March 2020, 740 patients received radioiodine treatment at our institution. Forty (5.4%) cases were

excluded due to incomplete data. Five hundred and seventy-eight (82.6%) reports described papillary thyroid carcinomas (PTC) and were included in the present analysis. They corresponded to 175 (30.2%) males and 403 (69.8%) females. The median age of male patients was 50 years (range 17–82 years) and that of female patients 47 years (range 11–85 years) ($p < 0.05$). Advanced tumor stages (pT3/T4) were diagnosed more frequently ($p < 0.05$) in men (42 of 175 cases, 42%) than in women (63 of 403, 15.6%).

Lymphatic Vessel Invasion Report

In 366 (63.3%) of 578 pathology reports, the LVI status was described. The frequency of LVI reporting was not associated with gender of patients ($p = 0.54$), age ($p = 0.37$), tumor size ($p = 0.11$), PTC variant ($p = 0.57$), or pT status ($p = 0.66$). LVI status was more often reported in patients without N-reporting (Nx, $p < 0.05$) (**Table 1**).

Lymphatic Vessel Invasion Status

Lymphatic vessel invasion absence (L0) was documented in 299 (81.7%) and positive lymph vascular invasion (L1) in 67 (18.3%) of 366 pathology reports. Lymph vascular invasion (L1) was more frequently detected in male patients ($p = 0.01$), greater tumor size ($p < 0.05$), higher pT- ($p < 0.01$), and pN-status ($p < 0.01$). Whereas, lymph vascular invasion (L1) was seen in only 5% of patients with a pT1a status, the frequency of L1 increased to 23.5% in pT2, 32% in pT3 and 66.7% in pT4 ($p < 0.01$). Similarly, lymph vascular invasion (L1) was reported in only 8.7% patients with pN0 and in 42.8% patients with pN+ ($p < 0.01$). In Nx patients L1 was reported in only 4.4% of cases ($p < 0.01$) (**Table 2**).

Lymphatic Vessel Invasion and Lymph Node Metastasis (LNM)

In 454 (78.5%) of 578 PTC pathology reports the N-status was reported either as negative 256 (N0, 56.4%) or positive 198 (N+, 43.6%). In 276 (60.8%) reports, a LVI and a pN-status were also documented (**Table 2**).

Patients with nodal involvement showed significantly more often an L1 diagnosis (80.6 vs. 19.4%, $p < 0.01$) and an advanced pT status (pT4 88.9 vs. 11.1%, $p < 0.05$) in their pathology report (**Supplementary Table 1**). They were significantly more frequently male (63.8 vs. 36.2%; $p < 0.01$), younger (median age 41 years, range 11–84 vs. 51, range 18–85; $p < 0.01$) and had a higher number of harvested lymph nodes (21.3 ± 15.8 vs. 14.5 ± 13.9, $p < 0.01$) (**Supplementary Table 1**). The independent variables LVI, pT status, gender, age, and the number of harvested lymph nodes, which were significant in univariate analysis, were then entered into the regression model for multivariate logistic regression analysis. The results showed that LVI, male gender, younger age, a larger number of harvested lymph nodes were significant risk factors for LNM (**Supplementary Table 2**).

Positive LVI (L1) was described in 67 (24.3%) patients. Among them, 54 (80.6%) also had positive pN-status (L1pN+) and 13 (19.4%) had a pN0-status (L1pN0).

L0 was documented in 209 (57.1%) patients. Among them, 137 (65.6%) had a pN0-status (L0pN0), whereas in 72 (34.4%) patients a pN+ status was documented (L0pN+). Most L0pN+ cases were found in pT1b (39.2%), followed by pT2 (24.3%) and pT1a (17.5%).

TABLE 1 | Lymphatic vessel invasion (LVI) report and clinicopathologic variables (*p-values are calculated for LVI reported vs. non-reported).

		LVI report		
	$\sum$ $n = 578$	LVI reported $n = 366$ (81.7%)	LVI non-reported $n = 212$ (18.3%)	p*
Age				
Median (range)	47.5 (11–85)	48 (11–85)	49 (18–82)	n.s.
Gender				
Male	175 (30.3%)	113 (64.6%)	62 (35.4%)	n.s.
Female	403 (69.7%)	253 (62.7%)	150 (37.3%)	
Tumor size				
Median (mm)	18.5 (11–79)	20 (11–75)	18 (11–79)	n.s.
PTC variant				
Conventional	495 (85.6%)	315 (63.6%)	180 (36.3%)	
Follicular	7 (12.6%)	45 (61.6%)	28 (38.4%)	
Tall cell	6 (1.0%)	3 (50.0%)	3 (50.0%)	n.s.
Columnar	3 (0.5%)	3 (100.0%)	0	
Cribriform morular	1 (0.2%)	0	1 (100.0%)	
pT status				
1a	135 (23.3%)	79 (58.6%)	56 (41.4%)	
1b	205 (35.4%)	127 (62.0%)	78 (38.0%)	
2	133 (23%)	98 (73.7%)	35 (26.3%)	n.s.
3	88 (15.2%)	53 (60.2%)	35 (39.8%)	
4	17 (2.9%)	9 (53.0%)	8 (47.0%)	
pN category				
N0	256 (44.3%)	150 (58.6%)	106 (41.4%)	
N+	198 (34.2%)	126 (63.6%)	72 (36.3%)	<0.05
No lymph nodes resected	124 (21.4%)	90 (72.6%)	34 (27.4%)	

Tumor size was calculated for the non-pT1a tumors. Next to the median values, the ranges are reported. n.s., non-significant.

Additionally, 22 pT1a tumors with nodal involvement were reassessed using H&E and D2-40 IHC (**Supplementary Figure 1**). They had been diagnosed as L0 in 13 (61.9%) cases and as L1 in 2 (9%) cases. In 7 (31.8%) cases, L status was not documented. Retrospective reassessment using both H&E and D2-40 IHC performed by two independent, experienced pathologists delivered no tumor tissue and/or psammoma bodies in lymphatic spaces, including lymphatic spaces within the tumor, but also at the periphery of the tumor, or somewhere else in the resection specimen, and L0 was reassessed according to this definition in all cases (**Supplementary Table 2**).

Predictive Value of LVI Report for Lymph Node Metastasis

The positive assessment of LVI (L1) correlated in 80.6% of cases with lymph node metastases. The documented absence of LVI (L0) was correlated in 65.5% of cases with tumor-free lymph nodes. The sensitivity and specificity of the LVI report for lymph nodal involvement in this study were 0.41 and 0.92, respectively.

TABLE 2 | LVI presence (L1) and absence (L0) and clinicopathologic variables (*p-values are calculated for L0 vs. L1).

		LVI status		
	∑ *n* = 366	L0 *n* = 299 (75.7%)	L1 *n* = 67 (24.3%)	*p**
Age				
Median (range)	48 (11–85)	48 (17–85)	46 (11–76)	n.s.
Gender				
Male	113 (30.9%)	84 (74.3%)	29 (25.7%)	<0.01
Female	253 (69.1%)	215 (84.9%)	38 (15.0%)	
Tumor size				
Median (mm)	20 (11–75)	18 (11–64)	25.5 (11–75)	<0.05
PTC variant				
Conventional	315 (81.4%)	255 (80.9%)	60 (19%)	
Follicular	45 (12.2%)	41 (91.1%)	4 (8.9%)	
Tall cell	3 (0.8%)	2 (66.7%)	1 (33.3%)	
Columnar	3 (0.8%)	1 (33.3%)	2 (66.7%)	n.s.
Cribriform morular	0 (0.0%)	0	0	
pT status				
1a	79 (21.5%)	75 (94.9%)	4 (5.0%)	
1b	127 (34.6%)	110 (86.6%)	17 (13.4%)	
2	98 (26.8%)	75 (76.5%)	23 (23.5%)	<0.01
3	53 (14.5%)	36 (68.0%)	17 (32.0%)	
4	9 (2.5%)	3 (33.3%)	6 (66.7%)	
pN category				
N0	150 (41.0%)	137 (91.3%)	13 (8.7%)	
N+	126 (34.4%)	72 (57.2%)	54 (42.8%)	<0.01
No lymph nodes resected	90 (24.6%)	86 (95.6%)	4 (4.4%)	

Tumor size was calculated for the non-pT1a tumors. Next to the median values, the ranges are reported. n.s., non-significant.

The positive and the negative predictive value were 0.80 and 0.65, respectively.

As described above, reported LVI was a significant independent risk factor for LNM in the multivariate analysis ($p = 0.001$, **Supplementary Table 2**).

DISCUSSION

In several tumor entities, LVI has been shown to correlate with LNMs and with prognoses of patients (13–18). Similar data are available for PTC (6, 19–24). However, LVI does not play a role in clinical decision-making according to all major guidelines and is not mandatory in pathology reports of PTC according to the current TNM classification (28). In Australia, it has been shown to be routinely reported and is only omitted in 15.8% of cases (33). In this study, the data of a German academic endocrine center were explored in order to identify the extent of LVI documentation in routine pathology reports of papillary thyroid cancer and estimate its role as a possible predictor for LNM, especially in cases that generally do not require lymphadenectomy like microcarcinomas <1 cm.

Lymphatic vessel invasion was reported in 63.3% of pathology reports of patients with PTCs, who underwent postoperative radioiodine treatment at our institute. The presence of LVI increased expectedly alongside with higher stage, from 5% in pT1a, 13.4% in pT1b, 23.5% in pT2, 32% in pT3 to 66.7% in pT4 (**Table 2**). Similarly, the rate of LNM rose from 42.5% in pT1a, 40.8% in pT1b, 44.2% in pT2, 53.5% in pT3, to 88.9% in pT4 (**Supplementary Table 1**).

Our data confirm that L1 documented in pathology report quite reliably correlated with a diagnosis of lymph node metastases (pN+). A total of 54 (80.6%) patients with reported positive LVI also had a diagnosis of LNM. On the other hand, 13 (19.4%) patients with positive LVI (L1) had a pN0-status in the initial histopathologic report. These L1pN0 cases might be due to the fact that the surgeon performing a prophylactic lymphadenectomy might have missed deeper or lateral lymph nodes, in order to avoid complications in a procedure performed for a cancer, which generally has an excellent prognosis. Eleven (84.6%) of these 13 patients achieved biochemical and radiological cure in a mean follow-up of 27.6 ± 16 months after radioiodine treatment. One 59-year-old woman with a pT1b pN0 (0/1), L1 tumor, and a 31-year-old woman with a pT2 pN0 (0/1), L1 tumor instead have not been cured by initial surgery and radioiodine therapy (RAIT). In the first case, there are elevated and slowly increasing thyroglobulin levels with currently no evidence of structural disease in repeated iodine and PET-CT scan. The second patient underwent repeated cervical surgery delivering eight PTC metastases in 40 resected lymph nodes.

In 72 (34.4%) cases, LNM was reported despite L0 status indicating a concrete risk of lymph node involvement even in L0 reporting. Thirteen of these patients had a pT1a tumor. Pathologic reassessment of 22 specimens including 13 L0, 2 L1, and seven tumors with no LVI documentation was performed by two independent, experienced pathologists. No cases showed LVI diagnosis according to the current definition [presence of tumor tissue and/or psammoma bodies in lymphatic spaces, including lymphatic spaces within the tumor, but also at the periphery of the tumor, or somewhere else in the resection specimen (29)], despite nodal involvement. Two cases, which had originally been reported as L1 (**Supplementary Table 3**), could not be confirmed as L1. This underlines the difficulty of diagnosing lymph vessel invasion especially in smaller tumors, even with the additional use of IHC.

In the interpretation of the data presented in this study, the reliability of pathology reports needs to be discussed. The thin walls of the lymphatic vascular channels and the invasive nature of the tumors are likely elements masking the evidence of lymphatic invasion (30). Xu and Ghossein recently pointed out that features separating lymphatic from vascular invasion based on histology alone can be difficult (34). Lymphatic invasion is generally assessed by H&E staining method only. One major challenge of this method is to distinguish lymphatic invasion from the retraction artifacts caused by tissue handling and fixation (29) (**Figure 1**). The use of IHC staining methods can support the diagnosis: a meta-analysis on lymphatic invasion in

breast cancer showed detection rates ranging from 10 to 49% for H&E and a narrower range from 21 to 42% for IHC (35). In the daily practice, moreover, only representative parts of the tumor are sectioned and examined, and IHC is not used routinely, indicating a possibility of underdiagnosis of lymphatic invasion (**Supplementary Figure 1**). Since the CAP 2021 considers LVI as a core reporting element (27), the clear criteria for diagnosis, including direct and indirect LVI signs, should be more broadly implemented in routine pathologic protocols for PTC.

Another issue to consider is the variability in the number of harvested lymph nodes in lymph node dissections. Some pathology reports included only one lymph node and cases were signed out as "pN0" based on this singular, possibly unintended resected node. In several cases lymphadenectomy had not been performed, according to the German guidelines stating that the benefit of prophylactic lymphadenectomy is unclear and should be performed only by experienced thyroid surgeons, weighing the risk of morbidity and the possible benefit for the patient. If lymphadenectomy is performed, there are three main aspects influencing lymphadenectomy results. There are individual patient-associated anatomic aspects, like the normal number of lymph nodes in the central neck compartment varying between 2 and 44 lymph nodes (36). There are also technical aspects, which are relevant to the surgeons and some which are relevant to the pathologist. The surgeon must make sure that the extent of resection does not unnecessarily increase morbidity and the pathologist must be aware that smaller lymph nodes may be hard to detect within large dissection specimens and ideally embed the complete specimen (36). A retrospective Surveillance, Epidemiology, and End Results (SEER) analysis, including the results of 5,107 central lymphadenectomies for PTC, reported an average total number of lymph nodes removed of 4 (37). The significantly higher number reported in this study is possibly due to the fact that most patients receiving lymphadenectomy had been operated in specialized clinics. Additionally, according to the German guidelines, lateral lymphadenectomy is also warranted if the lymph nodes appear sonographically enlarged or suspicious. While evidence of LNMs can help the nuclear medicine specialist in correct staging and for adjusting the radioiodine activity to administer (38), a diagnosis of four tumor-free lymph nodes, instead, can hardly rule out lymph node involvement.

Several studies agree that LVI has a positive correlation with LNMs (19–22), and a negative impact on outcomes of patient (6, 23, 24), although single studies report no significant association with response to therapy (39). In this study, the positive correlation with LNMs can be confirmed. An additional finding is the remarkably high percentage of LNM (34.4%) in L0 tumors, which is also confirmed by the data of Pontius et al. (32.5%) (23). Given this high rate of LNMs, despite the lack of LVI and given the limits of the currently widely used methods (H&E staining of representative parts of the tumors only), the L0 report appears of poor clinical significance.

Some shortcomings of this study must be mentioned. First, the reference standard consisted of pathology reports, thus conclusions might be affected by the individual bias of pathologists, who initially signed out the specimens. So far, we did not routinely reassess specimens of patients referred for postoperative treatment at our institution. Based on the data presented, we plan to reassess lymph vessel invasion in the future, in order to investigate if this information might impact clinical decision-making. Second, long-term follow-up data for some of these patients are not included, hence we did not analyze systematically which of these patients developed metastases in the course of their disease or even radioiodine refractory disease. Finally, the patients included in this study were treated or referred to a university center (40). It also needs to be mentioned that active surveillance for low-risk PTC has shown to be safe and feasible in certain populations. However, in Europe and especially in the time lapse of this study, it is currently limited to clinical trials. Moreover, to the best of our knowledge, there are no data on active surveillance of nodal involvement.

CONCLUSION

We conclude that the presence of LVI (L1) documented in routine pathology reports delivers important information, as it likely correlates with LNM. The reported absence of LVI (L0) however, with the widely used H&E staining of a representative section of the tumor, does not reliably correlate with the absence of LNM and might suggest wrong assumptions. In the absence of lymph nodes in the surgical specimen, standardized pathologic reassessment of L0 diagnosis included in routine pathology reports might be helpful for better assessment of the risk of nodal involvement.

DATA AVAILABILITY STATEMENT

The raw data supporting the conclusions of this article will be made available by the authors, without undue reservation.

ETHICS STATEMENT

The studies involving human participants were reviewed and approved by the Ethic Board of the University Hospital of Cologne. Written informed consent for participation was not required for this study in accordance with the national legislation and the institutional requirements.

AUTHOR CONTRIBUTIONS

CC and AS designed the study, together with CJB and RB. CC, M-LE, and AS collected the data. CC, HA, M-LE, MS, MF, and AS contributed to the interpretation of the results. MS, HA, CJB, RB, and MF contributed critical feedback and helped shape the research, analysis, and manuscript. CC and AS wrote the first draft of the manuscript. All authors critically revised the manuscript, approved the final version of the manuscript, decided to submit this study, and agreed to be accountable for all aspects of the work as recommended by the International Committee of Medical Journal Editors (ICMJE) authorship criteria.

ACKNOWLEDGMENTS

We would like to thank Mrs. Caitlin Czarniecki for language editing.

SUPPLEMENTARY MATERIAL

The Supplementary Material for this article can be found online at: https://www.frontiersin.org/articles/10.3389/fmed.2022.841550/full#supplementary-material

Supplementary Figure 1 | Representative cases of papillary thyroid carcinoma depicting the need for standardized LVI evaluation. **(A)** Papillary thyroid carcinoma (PTC; pT1b) without evidence of lymphovascular invasion (LVI) on H&E-stained section of the primary tumor. However, psammoma bodies can be appreciated (∗) sometimes surrounded by slit-like spaces. No additional staining was performed. The case was signed out as L1 as a lymph node metastasis was detected [pN1 (4/5)]. **(B)** Hereinafter performed Podoplanin (D2-40) immunohistochemistry (IHC) showed very few lymphovascular channels (→) at the periphery of the tumor; no evidence for LVI. **(C)** PTC (pT1a) with small tumor nodules at the periphery, some of which are surrounded by slit-like-spaces potentially suggesting LVI on HE stained sections. The case was signed out as L0 without further analysis and showed lymph node metastases [pN1 (2/33)]. **(D)** Subsequently performed D2-40 staining depicts vascular channels at the periphery of the tumor without tumor cell invasion supporting the absence of LVI. **(E)** PTC (pT1b) with small foci of tumor nodules surrounded by slit-like spaces at the periphery (∗) suggesting LVI. The case was signed out as L1. No lymph node metastases were detected [pN0 (0/6)]. **(F)** LVI could not be confirmed by D2-40 staining.

Supplementary Table 1 | Patients with L- and N status. Lymph nodal involvement was significantly more frequent in younger patients, in men and in patients with a higher number of harvested lymph nodes, higher pT status, and lymphatic vessel invasion (LVI) documented in the pathology report. Tumor size was not significant ($p = 0.47$).

Supplementary Table 2 | Results of a multivariate analysis including the independent variables gender, age, pT status, LVI and number of harvested lymph nodes, which had been found significant in **Supplementary Table 1**. The results showed that LVI, gender, age, and a number of harvested lymph nodes were significant risk factors for lymph node metastasis. B, β coefficient; SIG, statistical significance, *p*-value.

Supplementary Table 3 | Pathology reassessment of 22 cases of pT1a pN1 papillary thyroid carcinoma (PTCs), including 13 L0, 2 L1, and 7 cases in which LVI had not been documented. LVI could not be diagnosed in any case, also in the two cases in which it had been reported.

REFERENCES

1. Sancho JJ, Lennard TWJ, Paunovic I, Triponez F, Sitges-Serra A. Prophylactic central neck disection in papillary thyroid cancer: a consensus report of the European Society of Endocrine Surgeons (ESES), Langenbecks. *Arch Surg.* (2014) 399:155–63. doi: 10.1007/s00423-013-1152-8
2. Perros P, Boelaert K, Colley S, Evans C, Evans RM, Gerrard Ba G, et al. Guidelines for the management of thyroid cancer. *Clin Endocrinol.* (2014) 81(Suppl 1):1–122. doi: 10.1111/cen.12515
3. Haugen BR, Alexander EK, Bible KC, Doherty GM, Mandel SJ, Nikiforov YE, et al. 2015 American Thyroid Association Management Guidelines for adult patients with thyroid nodules and differentiated thyroid cancer: the American Thyroid Association Guidelines Task Force on thyroid nodules and differentiated thyroid cancer. *Thyroid.* (2016) 26:1–133. doi: 10.1089/thy.2015.0020
4. Filetti S, Durante C, Hartl D, Leboulleux S, Locati LD, Newbold K, et al. Thyroid cancer: ESMO Clinical Practice Guidelines for diagnosis, treatment and follow-up. *Ann Oncol.* (2019) 30:1856–83. doi: 10.1093/annonc/mdz400
5. Ito Y, Onoda N, Okamoto T. The revised clinical practice guidelines on the management of thyroid tumors by the Japan Associations of Endocrine Surgeons: core questions and recommendations for treatments of thyroid cancer. *Endocr J.* (2020) 67:669–717. doi: 10.1507/endocrj.EJ20-0025
6. Sun W, Lan X, Zhang H, Dong W, Wang Z, He L, et al. Risk factors for central lymph node metastasis in CN0 papillary thyroid carcinoma: a systematic review and meta-analysis. *PLoS ONE.* (2015) 10:e0139021. doi: 10.1371/journal.pone.0139021
7. Luo Y, Jiang H, Xu W, Wang X, Ma B, Liao T, et al. Clinical, pathological, and molecular characteristics correlating to the occurrence of radioiodine refractory differentiated thyroid carcinoma: a systematic review and meta-analysis. *Front Oncol.* (2020) 10:549882. doi: 10.3389/fonc.2020.549882
8. Medas F, Canu GL, Cappellacci F, Boi F, Lai ML, Erdas E, et al. Predictive factors of lymph node metastasis in patients with papillary microcarcinoma of the thyroid: retrospective analysis on 293 cases. *Front Endocrinol.* (2020) 11:551. doi: 10.3389/fendo.2020.00551
9. Huang Y, Yin Y, Zhou W. Risk factors for central and lateral lymph node metastases in patients with papillary thyroid micro-carcinoma: retrospective analysis on 484 cases. *Front Endocrinol.* (2021) 12:640565. doi: 10.3389/fendo.2021.640565
10. Robenshtok E, Neeman B, Reches L, Ritter A, Bachar G, Kaminer K, et al. Adverse histological features of differentiated thyroid cancer are commonly found in autopsy studies: implications for treatment guidelines. *Thyroid.* (2021) 32:37–45. Online ahead of print. doi: 10.1089/thy.2021.0268
11. Kluijfhout WP, Drake FT, Pasternak JD, Beninato T, Vriens MR, Shen WT, et al. Incidental positive lymph nodes in patients with papillary thyroid cancer is independently associated with recurrent disease. *J Surg Oncol.* (2017) 116:275–80. doi: 10.1002/jso.24680
12. Adam MA, Pura J, Goffredo P, Dinan MA, Reed SD, Scheri RP, et al. Presence and number of lymph node metastases are associated with compromised survival for patients younger than age 45 years with papillary thyroid cancer. *J Clin Oncol.* (2015) 33:2370–5. doi: 10.1200/JCO.2014.59.8391
13. Wakayama A, Kudaka W, Matsumoto H, Aoyama H, Ooyama T, Taira Y, et al. Lymphatic vessel involvement is predictive for lymph node metastasis and an important prognostic factor in endometrial cancer. *Int J Clin Oncol.* (2018) 23:532–8. doi: 10.1007/s10147-017-1227-6
14. Moy AP, Mochel MC, Muzikansky A, Duncan LM, Kraft S. Lymphatic invasion predicts sentinel lymph node metastasis and adverse outcome in primary cutaneous melanoma. *J Cutan Pathol.* (2017) 44:734–9. doi: 10.1111/cup.12969
15. Ishikawa Y, Aida S, Tamai S, Akasaka Y, Kiguchi H, Akishima-Fukasawa Y, et al. Significance of lymphatic invasion and proliferation on regional lymph node metastasis in renal cell carcinoma. *Am J Clin Pathol.* (2007) 128:198–207. doi: 10.1309/0FT8WTDKREFHHP4P
16. Lee YJ, Huh JW, Shin JK, Park YA, Cho YB, Kim HC, et al. Risk factors for lymph node metastasis in early colon cancer. *Int J Colorectal Dis.* (2020) 35:1607–13. doi: 10.1007/s00384-020-03618-7
17. Oguma J, Ozawa S, Kazuno A, Yamamoto M, Ninomiya Y, Yatabe K, Makuuchi H, Ogura G. Prognostic impact of lymphovascular invasion in lymph node-negative superficial esophageal squamous cell carcinoma. *Dis Esophagus.* (2019) 32:doz001. doi: 10.1093/dote/doz001
18. Minig L, Fagotti A, Scambia G, Salvo G, Patrono MG, Haidopoulos D, et al. Incidence of lymph node metastases in women with low-risk early cervical cancer (<2 cm) without lymph-vascular invasion. *Int J Gynecol Cancer.* (2018) 28:788–93. doi: 10.1097/IGC.0000000000001236
19. So YK, Kim MJ, Kim S, Son YI. Lateral lymph node metastasis in papillary thyroid carcinoma: A systematic review and meta-analysis for prevalence, risk factors, and location. *Int J Surg.* (2018) 50:94–103. doi: 10.1016/j.ijsu.2017.12.029
20. Aydin Buyruk B, Kebapci N, Yorulmaz G, Buyruk A, Kebapci M. An evaluation of clinicopathological factors effective in the development of central and lateral lymph node metastasis in papillary thyroid cancer. *J Natl Med Assoc.* (2018) 110:384–90. doi: 10.1016/j.jnma.2017.07.007

21. Lim II, Hochman T, Blumberg SN, Patel KN, Heller KS, Ogilvie JB. Disparities in the initial presentation of differentiated thyroid cancer in a large public hospital and adjoining university teaching hospital. *Thyroid.* (2012) 22:269–74. doi: 10.1089/thy.2010.0385
22. Sun W, Zheng B, Wang Z, Dong W, Qin Y, Zhang H. Meta-analysis of risk factors for CCLNM in patients with unilateral cN0 PTC. *Endocr Connect.* (2020) 9:387–95. doi: 10.1530/EC-20-0058
23. Pontius LN, Youngwirth LM, Thomas SM, Scheri RP, Roman SA, Sosa JA. Lymphovascular invasion is associated with survival for papillary thyroid cancer. *Endocr Relat Cancer.* (2016) 23:555–62. doi: 10.1530/ERC-16-0123
24. Shin CH, Roh JL, Song DE, Cho KJ, Choi SH, Nam SY, et al. Prognostic value of tumor size and minimal extrathyroidal extension in papillary thyroid carcinoma. *Am J Surg.* (2020) 220:925–31. doi: 10.1016/j.amjsurg.2020.02.020
25. Haddad RI, Nasr C, Bischoff L, Busaidy NL, Byrd D, Callender G, et al. NCCN guidelines insights: thyroid carcinoma, version 2.2018. *J Natl Compr Canc Netw.* (2018) 16:1429–40. doi: 10.6004/jnccn.2018.0089
26. Leenhardt L. et al., 2013 European Thyroid Association Guidelines for cervical ultrasound scan and ultrasound-guided techniques in the postoperative management of patients with thyroid cancer. *Eur Thyroid J.* (2013) 2:147–59. doi: 10.1159/000354537
27. Mete O, Seethala RR, Asa SL, Bullock MJ, Carty SE, Hodak SP, et al. *College of American Pathologists: Protocol for the Examination of Specimens From Patients With Carcinomas of the Thyroid Gland*. (2019). Available online at: https://documents.cap.org/protocols/cp-endocrine-thyroid-19-4200.pdf (accessed January 10, 2022).
28. Wittekind C. *TNM Klassifikation maligner Tumoren*. Berlin: Springer (2020).
29. Mai KT, Truong LD, Ball CG, Olberg B, Lai CK, Purgina B. Lymphatic endothelial cancerization in papillary thyroid carcinoma: hidden evidence of lymphatic invasion. *Pathol Int.* (2015) 65:220–30. doi: 10.1111/pin.12272
30. Kovacevic B, Vucevic D, Cerovic S, Eloy C. Peripheral versus intraparenchymal papillary thyroid microcarcinoma: different morphologies and PD-L1 expression. *Head Neck Pathol.* (2021). doi: 10.1007/s12105-021-01337-1
31. Cheng SP, Lee JJ, Chien MN, Kuo CY, Jhuang JY, Liu CL. Lymphovascular invasion of papillary thyroid carcinoma revisited in the era of active surveillance. *Eur J Surg Oncol.* (2020) 46:1814–9. doi: 10.1016/j.ejso.2020.06.044
32. Dralle H, Musholt TJ, Schabram J, Steinmüller T, Frilling A, Simon D, et al. German Association of Endocrine Surgeons practice guideline for the surgical management of malignant thyroid tumors. *Langenbecks Arch Surg.* (2013) 398:347–75. doi: 10.1007/s00423-013-1057-6
33. Kahn C, Simonella L, Sywak M, Boyages S, Ung O, O'Connell D. Postsurgical pathology reporting of thyroid cancer in New South Wales, Australia. *Thyroid.* (2012) 22:604–10. doi: 10.1089/thy.2011.0501
34. Xu B. and Ghossein R, Critical prognostic parameters in the anatomic pathology reporting of differentiated follicular cell-derived thyroid carcinoma. *Cancers.* (2019) 11:1100. doi: 10.3390/cancers11081100
35. Zhang S, Zhang D, Yi S, Gong M, Lu C, Cai Y, et al. The relationship of lymphatic vessel density, lymphovascular invasion, and lymph node metastasis in breast cancer: a systematic review and meta-analysis. *Oncotarget.* (2017) 8:2863–73. doi: 10.18632/oncotarget.13752
36. Hu JQ, Wen D, Ma B, Zhang TT, Liao T, Shi X. et al. The extent of lymph node yield in central neck dissection can be affected by preoperative and intraoperative assessment and alter the prognosis of papillary thyroid carcinoma. *Cancer Med.* (2020) 9:1017–24. doi: 10.1002/cam4.2762
37. Enyioha C, Roman SA, Sosa JA. Central lymph node dissection in patients with papillary thyroid cancer: a population level analysis of 14,257 cases. *Am J Surg.* (2013) 205:655–61. doi: 10.1016/j.amjsurg.2012.06.012
38. Nylén C, Eriksson FB, Yang A, Aniss A, Turchini J, Learoyd D, et al. Prophylactic central lymph node dissection informs the decision of radioactive iodine ablation in papillary thyroid cancer. *Am J Surg.* (2021) 221:886–92. doi: 10.1016/j.amjsurg.2020.08.012
39. Kim Y, Roh JL, Song D, Cho KJ, Choi SH, Nam SY, et al. Predictors of recurrence after total thyroidectomy plus neck dissection and radioactive iodine ablation for high-risk papillary thyroid carcinoma. *J Surg Oncol.* (2020) 122:906–13. doi: 10.1002/jso.26090
40. Alzahrani AS, Moria Y, Mukhtar N, Aljamei H, Mazi S, Albalawi L, et al. Course and predictive factors of incomplete response to therapy in low- and intermediate-risk thyroid cancer. *J Endocr Soc.* (2020) 5:bvaa178. doi: 10.1210/jendso/bvaa178

Conflict of Interest: The authors declare that the research was conducted in the absence of any commercial or financial relationships that could be construed as a potential conflict of interest.

Publisher's Note: All claims expressed in this article are solely those of the authors and do not necessarily represent those of their affiliated organizations, or those of the publisher, the editors and the reviewers. Any product that may be evaluated in this article, or claim that may be made by its manufacturer, is not guaranteed or endorsed by the publisher.

frontiers | Frontiers in Medicine

REVIEW
published: 06 April 2022
doi: 10.3389/fmed.2022.861909

Female Presidents of the "Royal College of Pathologists": Their Achievements and Contributions

Sarah E. Coupland[1,2], Lance N. Sandle[3] and Michael Osborn[4]*

[1] Department of Molecular and Clinical Cancer Medicine, University of Liverpool, Liverpool, United Kingdom, [2] Liverpool Clinical Laboratories, Liverpool University Hospitals NHS Foundation Trust, Liverpool, United Kingdom, [3] The Royal College of Pathologists, London, United Kingdom, [4] Department of Cellular Pathology, Charing Cross Hospital, North West London Pathology Hosted at Imperial College NHS Trust, London, United Kingdom

The Royal College of Pathologists (RCPath) celebrates its Diamond Jubilee in 2022 since its opening by Her Majesty Queen Elizabeth II in 1962. One of the main remits of RCPath is the overseeing of the training of pathologists and scientists working in pathology's 17 different specialties within the United Kingdom and across the globe. During its 60 years, three female Presidents have been elected: Dame Barbara Clayton (1984–1987), Dr. Suzannah (Suzy) Lishman CBE (2014–2017), and Prof. Joanne (Jo) Martin (2017–2020). Whilst Clayton specialised in Chemical Pathology and its relevance to public health, both Lishman and Martin are diagnostic cellular histopathologists with differing areas of expertise. This article reviews the contributions of these three distinguished and inspirational female pathologists to Pathology ("the science behind the cure"), to healthcare, public health and education, medical research, and to teaching. It highlights their qualities as leaders and mentors for those not only in medicine but in other career settings.

Keywords: Royal College of Pathologists, Chemical Pathology, diagnostic histopathology, Dame Barbara Clayton, Dr. Suzy Lishman, Prof. Jo Martin, leadership in Pathology

OPEN ACCESS

Edited by:
Sabrina Battista,
Istituto per l'Endocrinologia e l'Oncologia "Gaetano Salvatore" (CNR), Italy

Reviewed by:
Darren Treanor,
Leeds Teaching Hospitals NHS Trust, United Kingdom
Karin Oien,
University of Glasgow, United Kingdom

****Correspondence:***
Sarah E. Coupland
s.e.coupland@liverpool.ac.uk

Specialty section:
This article was submitted to Pathology, a section of the journal Frontiers in Medicine

Received: *25 January 2022*
Accepted: *14 March 2022*
Published: *06 April 2022*

Citation:
Coupland SE, Sandle LN and Osborn M (2022) Female Presidents of the "Royal College of Pathologists": Their Achievements and Contributions. Front. Med. 9:861909. doi: 10.3389/fmed.2022.861909

INTRODUCTION

The Royal College of Pathologists (RCPath) is celebrating its 60th anniversary in 2022. The College was founded on June 21st, 1962. It received its Royal Charter in February 1970. Its first substantive premises were at two Carlton House Terrace, a Grade I listed Georgian Townhouse located in the heart of Westminster, London. It was opened on 16th December that year by its Royal patron, Her Majesty Queen Elizabeth II. In November 2018, RCPath moved to its new premises, a bespoke award-winning building designed by Bennetts Associates in Alie Street, Aldgate, East London.

The College is a charity with over 11,000 members worldwide. RCPath oversees the training of pathologists and scientists working in 17 different specialties, including cellular pathology, clinical biochemistry, haematology, medical microbiology and virology, immunology, forensic, and veterinary pathology. Most members are medical, scientific, dental, or veterinary practitioners working mainly in United Kingdom hospitals and universities. The Trustee Board of the College includes its Honorary Officers, comprising amongst others the elected President of the College

and three Vice-Presidents (Communications; Teaching and Learning; and Professionalism). The President and Vice-Presidents have 3-year terms, and they undertake these unremunerated roles in addition to their routine diagnostic work. The first President of the College was Sir Roy Cameron, from 1962 to 1966. During its 60 years, three female Presidents have been elected: *Dame Barbara Clayton* (1984–1987), *Dr. Suzannah (Suzy) Lishman CBE* (2014–2017), and *Prof. Joanne (Jo) Martin* (2017–2020). The aim of the following article is to review the contributions of these three distinguished female pathologists to Pathology ("the science behind the cure"), to healthcare, and to medical research and teaching.

DAME BARBARA EVELYN CLAYTON (1984–1987)

Prof. Dame Barbara Clayton was born in Liverpool, United Kingdom, on September 2nd, 1922, to her parents Constance Evelyn (née Caine) and William Clayton, who then moved to Orpington, London (1). Her father was a food scientist who is renowned for inventing salad cream. Dame Barbara was educated at St Nicholas Preparatory School in Orpington, and subsequently at nearby Bromley County School for Girls, where she was head girl. She then studied medicine at the University of Edinburgh and the Edinburgh Royal Infirmary, qualifying in 1946. Following graduation, she commenced a Ph.D. in the Medical Research Council Clinical Endocrinology Unit in Edinburgh, on the topic of oestrogens (1, 2). After completing this in 1949, Clayton returned to London and became the Holden Research Fellow at St Thomas's Hospital Medical School for 7 years, before she was promoted to Clinical Lecturer in Chemical Pathology. Her research on hormones – e.g., adrenocorticotropic hormone (ACTH), parathyroid hormone and its interactions with Vitamin D, as well as ascorbic acid metabolism – and the development of new biochemical techniques – brought her well-deserved recognition.

In 1959, she moved to Great Ormond Street Hospital (GOSH) where she was a consultant pathologist and continued to do research, particularly in the genetic metabolic disorders suffered by newborn babies. She pursued a passion for improving childrens' healthcare and was renowned for her expertise in the diagnosis of phenylketonuria – the special diet that Clayton designed continues to be in common use today (3, 4).

In 1964, Prof. Clayton and others were very concerned with the high levels of lead found in some children's blood, and this led to her writing a landmark paper entitled "Lead poisoning in children" in 1964 (5), highlighting the detrimental effects lead has on the growth and development of their nervous systems. Whilst a member of the "Royal Commission on Environmental Pollution" in the 1980s, she campaigned for and lobbied the United Kingdom government to enforce a ban on lead in petrol, paint, and other products.

In 1978, after the sudden death of her husband (William [Bill] Klyne), Clayton moved to the new medical school at the University of Southampton as Prof. of Chemical Pathology and Human Metabolism (*its first female Prof.*) and honorary consultant chemical pathologist at the University hospital. She was Dean of Medicine at the University from 1983 to 1986, and honorary consultant chemical pathologist at the Southampton General Hospital. Appointed Emeritus Prof. in 1987, she continued her work on nutrition, but this time looking at the needs of the elderly, particularly those in care homes, about which there was little information and under resourcing.

Over her career, Clayton published about 200 academic papers, which addressed basic and translational research as well as hospital-based and community screening/care of metabolic disorders. She also served on more than 30 expert committees, several of which she chaired. These included the British Nutrition Foundation, the Association of Clinical Biochemists, the Biomedical Sciences Section of the British Association for the Advancement of Science, the Society for the Study of Inborn Errors of Metabolism, the British Nutrition Foundation, and the medical/scientific panel of the Leukaemia Research Fund. Clayton served on Royal Commission on Environmental Pollution from 1981 to 1996 and chaired the enquiry into the Camelford water pollution incident in 1988. The latter dealt with the inadvertent addition of aluminium sulphate to the water supply, raising the concentration to 3,000 times the then admissible level.

Relevant to this article, *Clayton was the first female President of the Royal College of Pathologists* her term being 1984–1987. Her College portrait now located in the new RCPath building in Alie Street shows her not with microscope or a learned tome on her lap but with a simple cup of tea – a symbol of her convivial personality and her ability to solve problems with diplomacy (**Figure 1**). She was also President of the National Society for Clean Air and Pollution (1995–1997) and the British Dietetic Association (1989–2008).

She received several Honours including a CBE in 1983 and DBE in 1988 for "outstanding contributions on the importance of diet and nutrition and in Chemical Pathology." In 1999, she was awarded the "British Medical Association's Gold Medal" for distinguished merit (a rarely awarded honour), and was conferred an Honorary Fellow of the Institute of Biology as well as an Honorary Fellow of the Royal College of Paediatrics and Child Health.

Dame Barbara Clayton was an inspiration and believed that women just had to be better than men to succeed. She was both sociable and private, never shouting about her own achievements.

DR. SUZANNAH (SUZY) CLAIRE LISHMAN, CBE (2014–2017)

Dr. Suzy Lishman was born in 1967 into a medical family (grandfather and father, both GPs; aunt, respiratory physician; mother and both grandmothers, all nurses), in Beverley in the East Riding of Yorkshire and was educated at Wakefield Girls' High School, The King's School Ely and the Neale Wade Community College in March, Cambridgeshire (6). She grew up in Yorkshire and the Fens in England. She was inspired by her aunt Angela, who showed her that women can have good careers in medicine, and so she followed her footsteps to Girton College,

FIGURE 1 | Prof. Dame Barbara Clayton.

FIGURE 2 | Dr. Suzy Lishman, CBE.

Cambridge and the London Hospital Medical College to study Medicine, qualifying in 1992. After completing house jobs in East London, Lishman applied to University College Hospital to specialise in histopathology; she completed this specialist training in 1999. Her first consultant job was at Hinchingbrooke Hospital in Huntingdon, and she moved to Peterborough District Hospital in 2006. The hospitals merged in 2017 to form North West Anglia NHS Foundation Trust. Lishman is currently a consultant cellular pathologist and lead medical examiner at this Trust. She has an interest in colorectal pathology and is pathology lead for the Bowel Cancer Screening Programme.

Lishman was involved with the College very early even as a Trainee in Histopathology, attending trainees' committee meetings. Between 2005 and 2017, she held every honorary office of the Royal College of Pathologists (except Treasurer), as Assistant Registrar (2005–2009), Registrar (2009–2011), Vice-President (Communications; 2011–2014), and President (2014–2017) (**Figure 2**). During this time, Dr. Lishman raised the profile of the speciality tremendously by introducing public engagement initiatives such as National Pathology Week and International Pathology Day. She has closely collaborated with the Science Museum, Royal Institution, Royal Society, and Cheltenham Science Festival, amongst many other venues and organisations. She has also contributed to numerous television documentaries, talking on a range of topics from the health of Henry VIII to the hidden dangers in the Tudor, Victorian, and Edwardian home. Lishman is active on social media with the Twitter and Instagram handles of "@ilovepathology." She uses various media to achieve outreach: in particular, Lishman is renowned for the development of "Living Autopsy" events, which involve a talk and simulation about what happens during a post-mortem examination. The format employs a "living model," who "acts" as a dead body whilst the pathologist talks through how they would perform an autopsy, showing the real instruments used and then drawing on the chest of the model's body to explain where incisions are made, the location of major organs and what tests would be carried out. The aim of the 60–90 min demonstration is to give a scientifically accurate and sensitive account of this important medical examination. The film of Dr. Lishman performing "The Living Autopsy" has received well over a million views on the RCPath YouTube channel (7). Dr. Lishman has often adapted her Living Autopsy demonstration to incorporate various themes of cultural and local interest. Previous events have explored the bubonic plague, Richard III's death, and what would happen if one died in space. Her public engagement work led to some amusing situations, including "being filmed for television demonstrating the effect of wearing a tight corset on a male model at Griff Rhys Jones' London home; performing a virtual brain autopsy at Latitude Festival (complete with blancmange brain); and being interviewed by actor Larry Lamb about the pathology faced by soldiers in WWI trenches). In 2013, she was named one of the fifty most inspirational women in healthcare by the "Health Service Journal," which described her as the "public face of pathology" and "the most outward facing person from that specialism." Dr. Lishman was awarded the Royal College of Pathologists' Medal in 2010 and the Royal Society Kohn Award in 2012 for her public engagement work.

Ultimately, Dr. Lishman was elected President of the Royal College of Pathologists, commencing in November 2014, *as the College's second female (and youngest) president*. As

President, she passionately represented the views of members, working closely with other specialist societies, and forging links with parliamentarians and other policy makers to ensure that pathology is considered in health-related discussions. She continued performing her living autopsies and talking to school groups in between presidential duties. A quote from Lishman is: "One of the joys of being a College officer is working with a diverse group of people from different regions, specialties and professional backgrounds for the benefit of members and patients."

Following her Presidential term, Dr. Lishman was appointed to (and remains) Chair of the RCPath Medical Examiners' Committee and national training lead for medical examiners. Medical examiners are senior medical doctors, who are trained in the legal and clinical elements of death certification processes. The Committee overseas a national system of medical examiners that is currently being rolled out in England and Wales to provide much-needed support for bereaved families and to improve patient safety. Dr. Lishman has delivered training to over 1400 medical examiners so far and is currently co-chairing joint training sessions for medical examiners and coroners and organising the second annual medical examiners conference. She is also one of the editors of the first textbook for medical examiners, which will be published in 2022.

In addition to her work on death certification reform, Dr. Lishman is a member of Council of the Royal Veterinary College and chairs their Ethics and Welfare Committee. She has chaired the Scientific Advisory Committee of the charity Bowel Cancer United Kingdom since 2017 and is a trustee of National Enquiry into Patient Outcome and Death (NCEPOD) and the Association for Art History. She has served as a non-executive director of the Medical Protection Society and is on the national Lynch Syndrome Steering group. Dr. Lishman regularly gives talks to schools through "Speakers for Schools" and "Inspiring the Future" and mentors disadvantaged students through the Social Mobility Foundation. She is a regular contributor to several leadership courses, particularly for women.

Dr. Lishman has won several awards: she was nominated one of the top 100 Pathologists of the Power List in 2015 (8, 9) and 2018. In 2018, she also received a CBE for services to pathology. She has an honorary doctorate (DSc) from Swansea University, is an honorary member of the Royal Colleges of Physicians of London, Edinburgh, and Ireland and is an honorary fellow of Girton College, Cambridge. Dr. Lishman was appointed to the David Jenkins memorial Chair in Forensic and Legal Medicine in 2019 and is an honorary fellow of that organisation.

FIGURE 3 | Prof. Jo Martin.

PROF. JOANNE (JO) ELIZABETH MARTIN (2017–2020)

Prof. Jo Martin was born into a modest background, with a stimulating, happy family in Hertfordshire. Her education was supported by a county scholarship to the local girls' school. She moved to Uppingham School for A levels for the science teaching, and she applied to Cambridge University for Medicine and was accepted. She was the first of her family to go to university. She qualified *via* Cambridge University and the London Hospital Medical College in 1984 and, following House appointments at Guy's and then St Thomas' Hospitals, she returned to the London Hospital to train in pathology. Martin was awarded an MRC Training Fellowship in 1988, an MRC Fellowship in 1990 and Wellcome Trust Advanced Research Training Fellowship in 1991. She gained her MRCPath (as it was then) in 1993. She was awarded a Ph.D at the University of London in 1997 in "The cellular pathology of the lower motor neuron in motor neuron disease," before becoming established at Queen Mary University of London. She was appointed Clinical Senior Lecturer/Consultant Histopathologist in 1996 and subsequently, Prof. of Neuropathology in 1997 at Queen Mary University of London. She was the only clinician in a major international programme of genetics related to neurodegeneration and neurological disorders, and as part of this designed the "SHIRPA" protocol which has been used in models ever since (10). She has published over 130 papers, including in Nature group and Science journals. She is a practising histopathologist, with a particular expertise in neuromuscular disease of the gut and renal pathology.

Prof. Martin has wide experience of healthcare management and leadership in a range of positions, including Acting Medical Director (January–June 2010), Deputy Medical Director (June 2010–December 2011), Interim Chief Medical Officer (July 2015–January 2016), and Director of Academic Health Sciences at

BOX 1 | Citations from RCPath's former female Presidents.
Prof. Dame Barbara Clayton: "I usually get my own way when I want it."
Dr. Suzy Lishman CBE: "If you see an inspirational person who's done what you hope to do, ask if they'll be your mentor. Don't be afraid to ask – people are generally pleased to share their experience to help others."
Prof. Jo Martin: "Do whatever you can to make it better – we can all make a positive difference."

Barts Health NHS Trust. She negotiated the entry of Barts and Queen Mary into UCLPartners, an Academic Health Science partnership, as founding partners. She was Executive lead for both the Clinical Research Network North Thames, and the Collaboration for Leadership in Applied Health Research and Care (CLAHRC) North Thames, involving multiple acute, primary care and third sector organisations and higher education establishments across a very wide complex organisational region. She led education and research across Barts Health NHS Trust, and created App-based training tools for staff, students, patients, and carers, including eCPD which has delivered over 50,000 free modules. She also acquired further degrees at University of London Master's degree in Leadership (2005), and as part of her involvement in pathology benchmarking, became an Honorary Lecturer in Healthcare Management, Keele University. Additionally, from 2013 to 2016, Prof. Martin was National Clinical Director for Pathology for NHS England.

Prof. Martin was elected the third female President of the Royal College of Pathologists from November 2017 until November 2020 (**Figure 3**). During her Presidency, she worked across programmes and projects in all the 17 pathology disciplines within the College including genetics, transfusion, digital pathology, data, networks, and with many professional bodies and patient groups. She also visited labs all over the United Kingdom to meet pathologists and learn about their needs and expertise. In particular, she championed expansion of, and support for, workforce, and investment into laboratory information management systems, many of which are obsolete, and roll out of digital pathology. All three of these programmes are now funded and being rolled out, with her support from NHSE/I as National Speciality Advisor, as she Chairs the National Pathology Board and Pathology Workforce Board.

Since March 2021, she has been Director of the Blizard Institute, part of the Whitechapel campus of The Faculty of Medicine and Dentistry of Queen Mary University London and is a world class biomedical research institute that integrates all stages of research from basic science through to clinical studies across a diverse range of fields including genomics, cell biology, translational immunology, neuroscience, and trauma. She has chaired the Research Advisory Board of the Motor Neurone Disease Association since 2018, with involvement in that organisation dating back to 1997. In 2021, she took up post as the Deputy Vice Principal Health at Queen Mary University London.

Finally, Prof. Martin is RCPath lead in a partnership with Health Education England on the innovative Pathology Portal project. The Pathology Portal, to be formally launched in June 2022, will deliver a platform to host high-quality training materials in all pathology disciplines that can be customised to individual needs covering flexible training, return-to-work training, and testing to support learning. The aim is to expand the platform to cover all pathology specialties, providing trainees with an adaptive learning approach, to support development of proficiency in general and specialist areas and to provide flexible and equitable access to content.

For her dedication to Pathology, exceptional service to healthcare, research, and education, Prof. Martin has received numerous awards, including Innovation Trust of the Year NHSIL (2012); Innovation of the Year, Barts Health NHS Trust (2018); she was nominated to be one of the top 100 Pathologists of the Power List in 2018 and was number 3 on this list (11). Her eCPD app won the Education App of the year 2019 at the United Kingdom App awards. She has received the Israel Doniach Lifetime Achievement Award Pathological Society (2018) (12); IBMS Honorary Fellowship (2020; a rare and prestigious honour); Honorary Fellowship of the Royal College of Physicians of Ireland (2020) and Honorary Fellowship of the Faculty of Public Health (2021), in recognition of her work during the COVID pandemic.

SUMMARY

Each of RCPath's former female Presidents represent inspirational and formidable women, each having differing strengths, contributing in differing ways to Pathology, healthcare, medical teaching, and research, all with steely determination, stamina, and great leadership skills. Their lifepaths were/are ones of commitment and determination, where they have made the absolute best of the "cards they had been dealt" at each stage and have created clearer paths for those following behind them. They are mentors for future generations of women in not only a career in medicine, but one in all areas of life. In the **Box 1** below is a quote from each of them, which may provide guidance for future generations.

As part of the College's 60th Birthday year, we celebrate what Clayton, Lishman, and Martin have achieved as Leaders and what they have contributed to this speciality.

AUTHOR CONTRIBUTIONS

All authors listed have made a substantial, direct, and intellectual contribution to the work, and approved it for publication.

ACKNOWLEDGMENTS

The authors thank Mr. Shane Johns for providing the photos (www.shanejohns.com).

REFERENCES

1. Richmond, C. *Lancet Obituary*. (2011) 377:23–9.
2. Munksroll. *Munks Roll Details for Barbara Evelyn (Dame) Clayton*. London: The Roll of the Royal College of Physicians (2018).
3. Casemore DP, Armstrong M, Jackson B, Gordon Nichols, Thom BT. Screening for cryptosporidium in stools. *Lancet*. (1984) 1:734–5. doi: 10.1016/s0140-6736(84)92245-1
4. Clayton BE. Phenylketonuria. *J Med Genet*. (1971) 8:37–40. doi: 10.1136/jmg.8.1.37
5. Moncrieff AA, Koumides OP, Clayton BE, Patrick AD, Renwick AG, Roberts GE. Lead poisoning in children. *Arch Dis Child*. (1964) 39:1–13.
6. Suzy Lishman: grateful to the air bubble. *BMJ*. (2015) 351:h3458. doi: 10.1136/bmj.h3458
7. Youtube. *Living Autopsy | Dr Suzy Lishman | Discovery Day at Home*. (2020). Available online at: https://www.youtube.com/watch?v=rGwJQuKZjpI (accessed Sep 26, 2020).
8. The Pathologist. *The Power List*. (2015). Available online at: https://thepathologist.com/power-list/the-power-list-2015/7-suzy-lishman (accessed January 25, 2022).
9. Government Digital Service. *"New Year's Honours 2018" (PDF)*. London: Government Digital Service (2017). p. 17.
10. Rogers DC, Fisher EM, Brown SD, Peters J, Hunter AJ, Martin JE. Behavioral and functional analysis of mouse phenotype: SHIRPA, a proposed protocol for comprehensive phenotype assessment. *Mamm Genome*. (1997) 8:711–3.
11. The Pathologist. *The Power List*. (2018). Available online at: https://thepathologist.com/power-list/2018/3-jo-martin (accessed January 25, 2022).
12. Pathological Society. *Chronological list of Doniach Lecturers*. Edinburgh: Pathological Society (2011).

Conflict of Interest: The authors declare that the research was conducted in the absence of any commercial or financial relationships that could be construed as a potential conflict of interest.

frontiers | Frontiers in Medicine

CASE REPORT
published: 03 June 2022
doi: 10.3389/fmed.2022.841441

Case Report: Extensive Tumor Profiling in Primary Neuroendocrine Breast Cancer Cases as a Role Model for Personalized Treatment in Rare and Aggressive Cancer Types

Dörthe Schaffrin-Nabe[1]*, *Stefan Schuster*[2], *Andrea Tannapfel*[3] and *Rudolf Voigtmann*[1]

[1] Praxis für Hämatologie und Onkologie, Bochum, Germany, [2] Datar Cancer Genetics Europe GmbH, Eckersdorf, Germany, [3] Institute of Pathology, Ruhr-University Bochum, Bochum, Germany

Neuroendocrine breast cancer (NEBC) is a rare entity accounting for <0.1% of all breast carcinomas and <0.1% of all neuroendocrine carcinomas. In most cases treatment strategies in NEBC are empirical in absence of prospective trial data on NEBC cohorts. Herein, we present two case reports diagnosed with anaplastic and small cell NEBC. After initial therapies failed, comprehensive tumor profiling was applied, leading to individualized treatment options for both patients. In both patients, targetable alterations of the PI3K/AKT/mTOR pathway were found, including a PIK3CA mutation itself and an STK11 mutation that negatively regulates the mTOR complex. The epicrisis of the two patients exemplifies how to manage rare and difficult to treat cancers and how new diagnostic tools contribute to medical management.

Keywords: extensive tumor profiling, rare cancer therapy, primary endocrine breast cancer, personalized treatment, targeted therapies

OPEN ACCESS

Edited by:
Lorenzo Memeo,
Mediterranean Institute of Oncology (IOM), Italy

Reviewed by:
Pablo Gajate,
Ramón y Cajal University Hospital, Spain
Deepika Sirohi,
The University of Utah, United States

***Correspondence:**
Dörthe Schaffrin-Nabe
josten-nabe@onkologie-bochum.com

Specialty section:
This article was submitted to Pathology, a section of the journal Frontiers in Medicine

Received: *22 December 2021*
Accepted: *25 April 2022*
Published: *03 June 2022*

Citation:
Schaffrin-Nabe D, Schuster S, Tannapfel A and Voigtmann R (2022) Case Report: Extensive Tumor Profiling in Primary Neuroendocrine Breast Cancer Cases as a Role Model for Personalized Treatment in Rare and Aggressive Cancer Types. Front. Med. 9:841441. doi: 10.3389/fmed.2022.841441

INTRODUCTION

Primary neuroendocrine breast cancer (NEBC) comprises a heterogeneous group of tumors with a low incidence (0.1%) among all breast cancer subtypes (1). In the literature, NEBCs are generally associated with poor long-term survival and with rapid resistance development (1–3). Therapeutic guidelines have not been established to date. The diagnosis of NEBC is often challenging as other neuroendocrine tumors, but also lung, gastrointestinal, and pancreatic cancers, need to be excluded (4, 5).

Currently, surgical intervention is the mainstay of the therapeutic approach (5, 6).

Treatment strategies are chosen dependent on Classification of Malignant Tumors (TNM) status, aggressiveness, age, general condition, and comorbidities of the patient (7). If (neo-)adjuvant chemotherapy is necessary, NEBC is being treated either analog to adenocarcinomas of the breast or SCLC (8, 9). Previously, Ki67 was used as a decision tool in NEBC; Ki67 < 15% led to a breast cancer analog therapy, i > 15% of the therapy was orientated to SCLC/neuroendocrine treatment (7). Promising results were seen when a combination of surgery, radiotherapy, and chemotherapy was applied (6).

There are no guidelines for staging and therapy in the metastatic setting, leaving the treating oncologist to opt for suitable systemic treatments (10, 11).

The development of molecular tumor profiling in recent years increasingly provides the opportunity for the use of targeted therapies, taking into account the involved activation and inhibition of the signal transduction pathways (12–14). This tool is particularly useful for rare tumors without existing therapy guidelines and for tumors that are refractory to therapy.

We want to illustrate the diagnostic and therapeutic challenges presenting the epicrisis of two patients diagnosed with NEBC in these above-mentioned situations.

PATIENT 1

The first patient was a 67-year-old female (**Figure 1**), who had a primary NEBC of the small cell subtype confirmed by histopathology. The definitive tumor stage was pT2, pN1a, L1, V0, G3, and Ki67 at 60%. She underwent modified radical mastectomy with axillary dissection and adjuvant administration of six cycles of Carboplatin and Etoposide, followed by radiotherapy. There was no indication for radiotherapy of the neurocranium as performed in SCLC.

Two years later, pronounced bilateral pleural metastasis without effusion was detected and one brain metastasis on the left occipital side was surgically removed. Both are related to the previously described NEBC. Considering micrometastases of the brain, the patient received Topotecan.

Further brain metastases, progressive lung metastasis with effusion, and metastatic spread to bone and thyroid gland were discovered by MRI 2 months afterward during ongoing chemotherapy.

Consequently, tumor profiling was performed with the exacta® test using peripheral blood to detect genetic alterations by NGS, targetable markers by immunocytochemistry staining, pharmacogenetics of tumor specific medication, and chemotherapy sensitivity testing using circulating tumor associated cells (**Table 1**) (15–17).

PATIENT 2

The second 51-year-old female patient suffered from an NEBC anaplastic large cell subtype (**Figure 2**). After breast-conserving therapy and sentinel lymphonodectomy, the definitive tumor stage was pT2, pN0, G3, Ki 67 40%, L0, V0, Pn0, ER 30%, PR neg, and Her2/neu neg. In the adjuvant setting, carboplatin and etoposide were applied with extremely poor clinical tolerability.

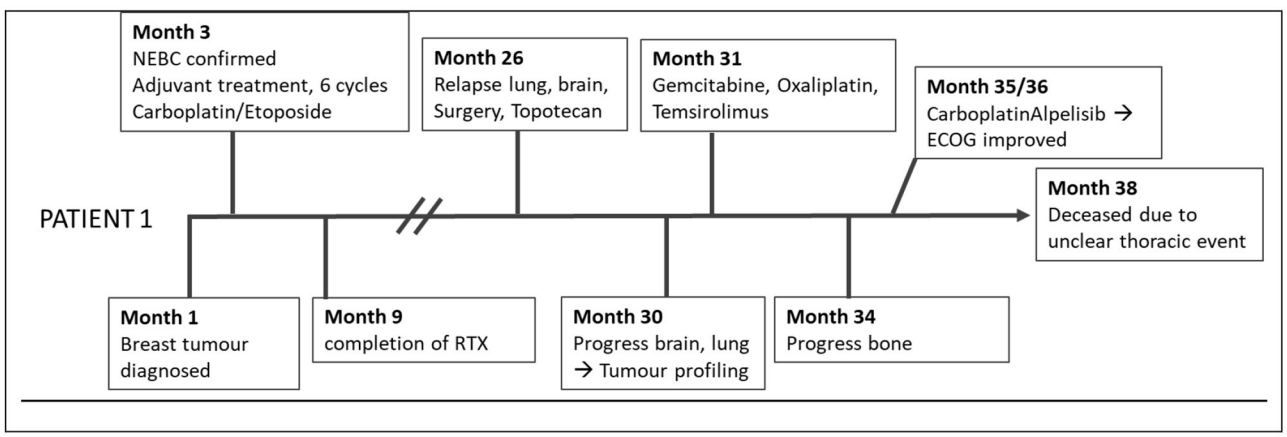

FIGURE 1 | Timeline of patient 1.

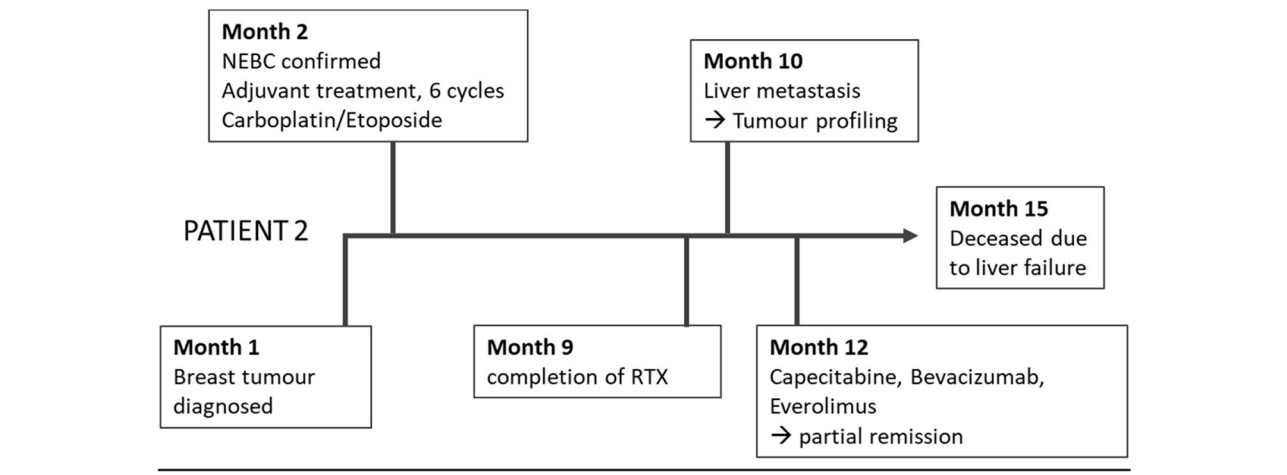

FIGURE 2 | Timeline of Patient 2.

Shortly after completion of adjuvant radiotherapy, hepatic filiae appeared in the right liver lobe. The planned atypical liver resection was rejected, because of intraoperatively detected diffuse spread into the left lobe.

Histopathologic confirmation revealed highly proliferating liver metastasis with a Ki67 of 80%, poorly differentiated, associated with the known NEBC.

Tumor profiling was performed using exacta® analysis this time based on a tumor biopsy together with a blood sample (**Table 1**). Simultaneous to this analysis, a diffuse bone metastasis with infiltration of the spinal canal with corresponding clinical signs was observed and radiotherapy was applied.

DISCUSSION

The reported aggressive scenario in both patients is consistent with high grading and high proliferation index (Ki67 > 60%). The initial chemotherapies failed and raised the question of novel therapeutic strategies. Dotatate-based PET-CT as an experimental diagnostic and therapeutic alternative was rejected (18). Both cases required the use of newly available diagnostic tools like NGS considering that recommendations for genomic alterations in specific tumor types exist, but not in NEBC or other neuroendocrine tumors (NET). At no stage, guidelines or clinical trials were available, only the individual approach was left.

In the case of the first patient, exacta® revealed an activating mutation of PIK3CA p.E545K, which is one of the most mutated genes and has been found to play a crucial role in several cancer types, but information about the incidence in NEBC is inconsistent in the literature (19–21). The PI3K/AKT/mTOR pathway is highly important for proliferation, migration, and cell survival and alterations are quite frequent in other NETs (22). The mutation, therefore, suggested a therapeutic benefit from mTOR and PIK3CA inhibition. Due to extended metastasis (pleura, neurocranium, and bone) and high Ki67, Gemcitabine and Oxaliplatin were added based on the chemosensitivity result to the mTOR inhibitor Temsirolimus (16, 23). Even though the therapy was tailored to individual tumor characteristics, the patient progressed, developing new pulmonary metastasis and lymphangitis, as well as pronounced pleural effusion. No response was seen despite molecular genetic evidence, together with an upregulation at the messenger RNA (mRNA) level of AKT, an important activator of mTOR, thus, suggesting a potential benefit from mTOR inhibitors. Resistance mechanisms to mTOR inhibitors, for example, caused by disruption of the negative feedback loop between SGK1 and PI3K signaling, followed by AKT activation, could explain treatment failure (24–26). Furthermore, RHEB (RAS homolog enriched in brain) as an mTOR activator was downregulated, together with mTOR downstream activating pathway components, like eIF4B (eukaryotic initiation factor 4B) and S6 (ribosomal subunit S6 = RPS6) (27, 28).

In this case, activation of mTOR seemed to have a lesser impact concerning tumor cell proliferation. Subsequently, she underwent pleurodesis on both sides. TROP2 overexpression relating to Sacituzumab-Govitecan (29, 30), or biomarkers for immune checkpoint inhibitors, were not observed.

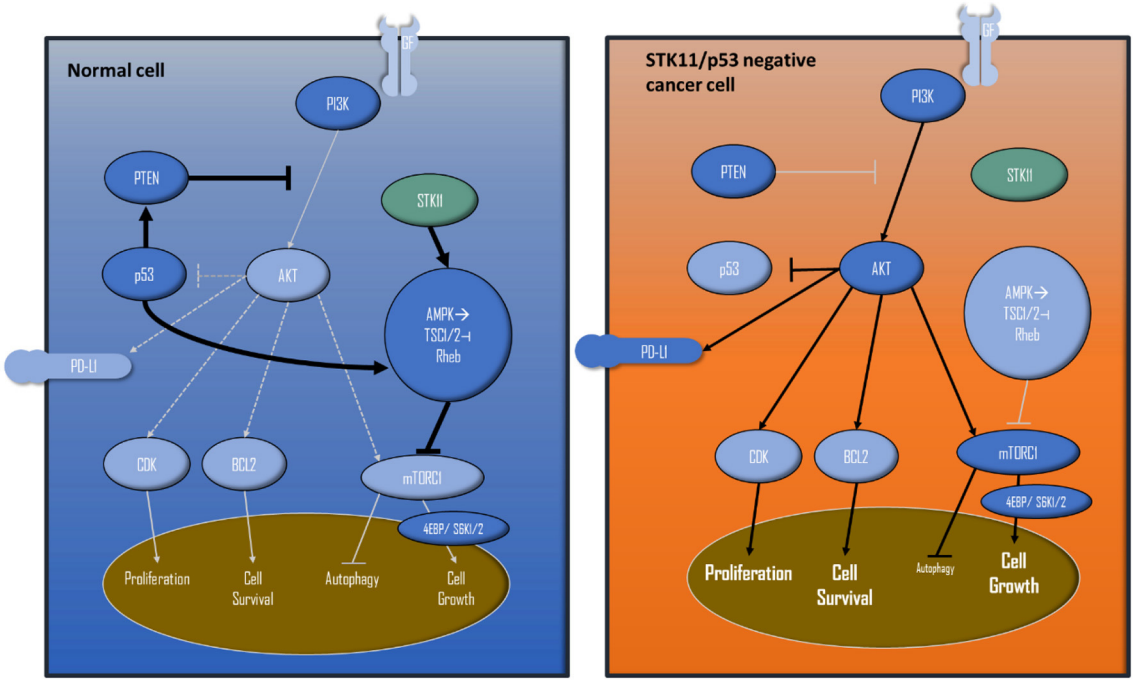

FIGURE 3 | Simplified PIK3/AKT/mTOR pathway and interactions with STK11 and p53. The left shows a wild-type cell, the right cell displays how STK11 and p53 loss of function leads to extensive proliferation/cell survival and cell growth, because of the missing negative feedbacks and activations.

TABLE 1 | Main results of the tumor profiling.

	Case 1	Case 2
Genetic Mutations/Amplifications	PIK3CA p.E545K	TP53 p.R290fs; STK11 p.Y131; NOTCH1 pQ1155; PIK3CG/D; FGFR2 amplification
Pathway Modeling (mRNA based)	Decreased DHFR signaling, increased HIF1 signaling	Increased signaling of TUBB2A, PGF, VEGFA, HIF1
Chemosensitivity Cell Death Rate [%]	Gemcitabine 72%	Gemcitabine +Carboplatin 85%
	Oxaliplatin 59%	Etoposide 79%
	Vinblastine 58%	Gemictabine 60%
	Etoposid < 25%	5-Fluoruracil 56%
	Topotecan < 25%	Carboplatin 55%
IHC Staining (PD-L1, EGFR, VEGFA, mTOR)	EGFR	-
MMR/MSI	Negative	MSI stable
Tumour Mutational Burden	0, 59 mutations/Mb blood-based	2, 21 mutations/Mb tissue based
Pharmacogenomics (altered metabolism)	ERCC1, NT5C2, UGT1A1, ABCB1	ERCC1, CYP2D6, UGT1A1, FCGR2A

Since NGS revealed PIK3CA as the only targetable alteration and AKT together with transcription factors, such as BCL2 were upregulated, it appeared that the proliferation promoting influence was not triggered via the mTOR pathway. The therapy was focused on the PIK3CA mutation, again (**Figure 3**). We evaluated intrinsic resistance factors for PIK3CA inhibitors, no PTEN loss nor amplification of FGFR1 could be detected (25, 31).

The analysis of the PI3K pathway, including the peripheral effector components involved at the molecular and mRNA levels, indicated that the use of the PI3K inhibitor Alpelisib would not suffice to inhibit the complete PI3K/AKT pathway. This assumption is supported by the fact that important components of tumor metabolism like PEPCK (phosphoenol-pyruvate-carboxykinase), cell cycle progression like CDK20, Myc, and factors of cell survival like Mcl1, Bim were not upregulated. In addition, IRS family member 4, which constitutively hyperactivates the PI3K/AKT pathway, was downregulated on the mRNA level. Components of the cross-linked oncogenic pathway, such as Rat Sarcoma Virus (RAS), were not upregulated, therefore, inhibition of this pathway did not appear promising (32). To address this issue and to take into account the high proliferation rate, a cytostatic agent was administered in analogy to the study NCT04215003, together with Alpelisib.

For the first time, a remarkable therapeutic effect was observed. From ECOG II, the patient changed toward ECOG 0 within 3 weeks, also because oxygenation improved from 57 to 70 mm/Hg. Sonographically, the effusion was not traceable anymore. Seven weeks later she suffered from an etiologically unclear thoracic pain event and died.

The second patient presented herself with hepatic progress shortly after completing adjuvant therapies. Tumor profiling was performed based on a liver biopsy together with a blood sample. An STK11p.Y131* mutation with clinical relevance was found. STK11/LKB1 mutations are reported in neuroendocrine tumors, such as large cell subtypes (33–35), but rare in breast cancers with an incidence of 0,2–1,0 % (35). STK11 alterations are associated with a lack of PDL1 expression, and the patient had a low TMB. Being MSI stable, no efficacy of checkpoint inhibitors was predicted (29).

The detected STK11mutation is considered to be a loss-of-function mutation resulting in activation of mTOR, as it is additionally induced by the detected p53 alteration (**Figure 3**). Functional loss of p53 activity can contribute to higher activities of the PI3K/AKT/mTOR pathways (36, 37).

To evaluate further the mTOR effect, we investigated additional peripheral effectors at the mRNA level.

Due to STK11 loss, the mTOR activation was most likely triggered *via* S6K1/2 (ribosomal S6 protein kinase 1/2), which was partially upregulated, stimulating proliferation by eIF4B and S6. Consequently, we applied the mTOR inhibitor, Everolimus, in this situation (35, 38–40).

Everolimus, itself, is approved by the Food and Drug Administration (FDA) for hormone receptor-positive and Her2 negative breast cancer. It is also the standard of care for NETs in National Comprehensive Cancer Network (NCCN) guidelines (41).

But mTOR inhibition as monotherapy based on allosteric inhibitors of mTORC1, like Everolimus, may lead to decreased therapeutic efficacy due to several resistance mechanisms: this could be incomplete inhibition of mTORC1, suppression of negative feedback loops, for example via increased IRS 1, which activates PI3K/AKT, ERK pathway activation, just to mention only a few of resistance factors (22, 25, 42). There is evidence of potential synergism with angiogenetic inhibitors. Taking into account the presence of upregulation of VEGFA and HIF-alpha-pathway, Bevacizumab was added to Everolimus (43–45).

Due to the highly proliferating disease and extent of metastasis, Capecitabine was administered in accordance with the test results (46). This is not surprising as Capecitabine is the standard of care to treat breast cancer, it is also mentioned in German guidelines for colorectal NETs or of NETs pancreatic origin. The therapy combination of Everolimus, Bevacizumab, and Capecitabine was well-tolerated. Imaging showed partial remission for 3 months. Then, the tumor progressed dramatically, and the patient died soon due to liver insufficiency.

CONCLUSION

To date, molecular profiling is used especially in breast, lung, colorectal, prostate, and gastric cancer (47). Here we demonstrate two patients with a rare tumor entity as a role models to illustrate the benefit to which a broader molecular tumor profiling can offer a significant contribution not only to diagnosis but also to the therapeutic regime.

Therapy-relevant mutations were uncovered, analyzing numerous tumor-relevant genes (>400) and pharmacogenomics. Specifically, the intelligent combination of immunocytochemistry/-histochemistry, chemosensitivity testing on tumor cells, DNA alterations, and expression profiles, could be detected and delivered valuable insights to tailor therapy.

Hence the rate of ineffective and cost-intensive therapies can be diminished and will improve the already available personalized, targeted therapies. Currently, application of solitary genetic testing delivers advantages only to a minority of patients (48–50). The first basket trials especially like the SHIVA trial largely failed because molecular filters were applied (48). Newer trials like the RESILIENT trial had beneficial outcomes even in late-stage patients with several previous therapies applying enhanced molecular analysis comprising also cytological features and other cancer characteristics (15).

Promising new options are especially needed for rare tumor entities, exemplified by NEBC, which remains a major diagnostic and therapeutic challenge today. From the start, there are numerous pitfalls in diagnosing NEBC, because it is itself a heterogeneous group of tumors. The rarity of this tumor type makes it imperative to apply sensitive diagnostic tools for effective treatment options.

It is also important for patients, for whom empirical therapy showed no efficiency and potential therapies based on tumor-specific profiles, respecting possible resistance mechanisms are explored. Viewed in isolation, not only the targets may be considered for the choice of therapy, but, if possible, the context of the whole pathway network together with other biomarkers too.

Questions that we need to ask, is whether the therapeutic effect justified the application of comprehensive tools in these cases. In both heavily pre-treated patients, actionable targets were discovered together with findings from ICC, chemosensitivity, and pathway modeling leading to a treatment that was well-tolerated and an improvement in the overall situation. However, both patients suffered from a highly aggressive subtype and were already in the metastatic situation where curative treatment is virtually not possible and the effects of the treatment did not last longer than a few months. Especially in rare cancers, where the prognosis is worse from the start, we should think about using tailored therapies based on comprehensive tumor characteristics earlier, because, only then, can we know whether this approach will provide a benefit. Trials to combine several rare cancer types and extensive profiling could hold the key to a successful treatment.

DATA AVAILABILITY STATEMENT

The datasets presented in this article are not readily available because of ethical and privacy restrictions. Requests to access (no. E-MTAB-11703) the datasets should be directed to the corresponding author.

ETHICS STATEMENT

Ethical review and approval was not required for the study on human participants in accordance with the local legislation and institutional requirements. The patients/participants provided their written informed consent to participate in this study.

AUTHOR CONTRIBUTIONS

DS-N: counseling of patients, clinical management, data analysis, data interpretation, and manuscript writing. RV: counseling of patients, data interpretation, and manuscript review. AT: data interpretation and manuscript review. SS: data analysis and manuscript writing. All authors contributed to the article and approved the submitted version.

REFERENCES

1. Roininen N, Takala S, Haapasaari K-M, Jukkola-Vuorinen A, Mattson J, Heikkilä P, et al. Primary neuroendocrine breast carcinomas are associated with poor local control despite favourable biological profile: a retrospective clinical study. *BMC Cancer.* (2017) 17:72. doi: 10.1186/s12885-017-3056-4
2. Wang J, Wei B, Albarracin CT, Hu J, Abraham SC, Wu Y. Invasive neuroendocrine carcinoma of the breast: a population-based study from the surveillance, epidemiology and end results (SEER) database. *BMC Cancer.* (2014) 14:147. doi: 10.1186/1471-2407-14-147
3. Cloyd JM, Yang RL, Allison KH, Norton JA, Hernandez-Boussard T, Wapnir IL. Impact of histological subtype on long-term outcomes of neuroendocrine carcinoma of the breast. *Breast Cancer Res Treat.* (2014) 148:637–44. doi: 10.1007/s10549-014-3207-0
4. Angarita FA, Rodríguez JL, Meek E, Sánchez JO, Tawil M, Torregrosa L. Locally-advanced primary neuroendocrine carcinoma of the breast: case report and review of the literature. *World J Surg Onc.* (2013) 11:128. doi: 10.1186/1477-7819-11-128
5. Inno A, Bogina G, Turazza M, Bortesi L, Duranti S, Massocco A, et al. Neuroendocrine carcinoma of the breast: current evidence and future perspectives. *Oncologist.* (2016) 21:28–32. doi: 10.1634/theoncologist.2015-0309
6. Salemis NS. Primary neuroendocrine carcinoma of the breast: a rare presentation and review of the literature. *Intractable Rare Dis Res.* (2020) 9:233–46. doi: 10.5582/irdr.2020.03046
7. Tsai T-H, Hsieh P-P, Hong Y-C, Yeh C-H, Yu LH-L, Yu M-S. Metastatic primary neuroendocrine carcinoma of the breast (NECB). *J Cancer Res Pract.* (2018) 5:38–42. doi: 10.1016/j.jcrpr.2017.10.003
8. Oberg K. Management of neuroendocrine tumours. *Ann Oncol.* (2004) 15 Suppl 4:iv293–298. doi: 10.1093/annonc/mdh942
9. Wei X, Chen C, Xi D, Bai J, Huang W, Rong L, et al. case of primary neuroendocrine breast carcinoma that responded to neo-adjuvant chemotherapy. *Front Med.* (2015) 9:112–6. doi: 10.1007/s11684-014-0345-z

10. Trevisi E, La Salvia A, Daniele L, Brizzi MP, De Rosa G, Scagliotti GV, et al. Neuroendocrine breast carcinoma: a rare but challenging entity. *Med Oncol.* (2020) 37:70. doi: 10.1007/s12032-020-01396-4
11. Salama JK, Milano MT. Radical irradiation of extracranial oligometastases. *J Clin Oncol.* (2014) 32:2902–12. doi: 10.1200/JCO.2014.55.9567
12. Cancer Genome Atlas Network. Comprehensive molecular portraits of human breast tumours. *Nature.* (2012) 490:61–70. doi: 10.1038/nature11412
13. André F, Ciruelos E, Rubovszky G, Campone M, Loibl S, Rugo HS, et al. Alpelisib for PIK3CA-mutated, hormone receptor-positive advanced breast cancer. *N Engl J Med.* (2019) 380:1929–40. doi: 10.1056/NEJMoa1813904
14. Lavigne M, Menet E, Tille J-C, Lae M, Fuhrmann L, Bonneau C, et al. Comprehensive clinical and molecular analyses of neuroendocrine carcinomas of the breast. *Mod Pathol.* (2018) 31:68–82. doi: 10.1038/modpathol.2017.107
15. Nagarkar R, Kohi S, Hirata K, Goggins M, Sato N. Encyclopedic tumor analysis for guiding treatment of advanced, broadly refractory cancers: results from the RESILIENT trial. *Oncotarget.* (2019) 10:27188. doi: 10.18632/oncotarget.27188
16. Crook T, Gaya A, Page R, Limaye S, Ranade A, Bhatt A, et al. Clinical utility of circulating tumor-associated cells to predict and monitor chemo-response in solid tumors. *Cancer Chemother Pharmacol.* (2020) 87:197–205. doi: 10.1007/s00280-020-04189-8
17. Crook T, Patil D, Gaya A, Plowman N, Limaye S, Ranade A, et al. Improved treatment outcomes by using patient specific drug combinations in mammalian target of rapamycin activated advanced metastatic cancers. *Front Pharmacol.* (2021) 12:631135. doi: 10.3389/fphar.2021.631135
18. Terlević R, Perić Balja M, Tomas D, Skenderi F, Krušlin B, Vranic S, et al. Somatostatin receptor SSTR2A and SSTR5 expression in neuroendocrine breast cancer. *Ann Diagn Pathol.* (2019) 38:62–6. doi: 10.1016/j.anndiagpath.2018.11.002
19. Ang D, Ballard M, Beadling C, Warrick A, Schilling A, O'Gara R, et al. Novel mutations in neuroendocrine carcinoma of the breast: possible therapeutic targets. *Appl Immunohistochem Mol Morphol.* (2015) 23:97–103. doi: 10.1097/PDM.0b013e3182a40fd1
20. McCullar B, Pandey M, Yaghmour G, Hare F, Patel K, Stein M, et al. Genomic landscape of small cell carcinoma of the breast contrasted to small cell carcinoma of the lung. *Breast Cancer Res Treat.* (2016) 158:195–202. doi: 10.1007/s10549-016-3867-z
21. Marchiò C, Geyer FC, Ng CK, Piscuoglio S, De Filippo MR, Cupo M, et al. The genetic landscape of breast carcinomas with neuroendocrine differentiation: Genetics of neuroendocrine breast cancer. *J Pathol.* (2017) 241:405–19. doi: 10.1002/path.4837
22. Yang J, Nie J, Ma X, Wei Y, Peng Y, Wei X. Targeting PI3K in cancer: mechanisms and advances in clinical trials. *Mol Cancer.* (2019) 18:26. doi: 10.1186/s12943-019-0954-x
23. Burstein HJ, Mangu PB, Somerfield MR, Schrag D, Samson D, Holt L, et al. American society of clinical oncology clinical practice guideline update on the use of chemotherapy sensitivity and resistance assays. *JCO.* (2011) 29:3328–30. doi: 10.1200/JCO.2011.36.0354
24. Li Z, Yang Z, Passaniti A, Lapidus RG, Liu X, Cullen KJ, et al. positive feedback loop involving EGFR/Akt/mTORC1 and IKK/NF-kB regulates head and neck squamous cell carcinoma proliferation. *Oncotarget.* (2016) 7:31892–906. doi: 10.18632/oncotarget.7441
25. Rozengurt E, Soares HP, Sinnet-Smith J. Suppression of feedback loops mediated by PI3K/mTOR induces multiple overactivation of compensatory pathways: an unintended consequence leading to drug resistance. *Mol Cancer Ther.* (2014) 13:2477–88. doi: 10.1158/1535-7163.MCT-14-0330
26. Vellai T. How the amino acid leucine activates the key cell-growth regulator mTOR. *Nature.* (2021) 596:192–4. doi: 10.1038/d41586-021-01943-7
27. Li S, Kong Y, Si L, Chi Z, Cui C, Sheng X, et al. Phosphorylation of mTOR and S6RP predicts the efficacy of everolimus in patients with metastatic renal cell carcinoma. *BMC Cancer.* (2014) 14:376. doi: 10.1186/1471-2407-14-376
28. Rutkovsky AC, Yeh ES, Guest ST, Findlay VJ, Muise-Helmericks RC, Armeson K, et al. Eukaryotic initiation factor 4E-binding protein as an oncogene in breast cancer. *BMC Cancer.* (2019) 19:491. doi: 10.1186/s12885-019-5667-4
29. Vranic S, Palazzo J, Sanati S, Florento E, Contreras E, Xiu J, et al. Potential novel therapy targets in neuroendocrine carcinomas of the breast. *Clin Breast Cancer.* (2019) 19:131–6. doi: 10.1016/j.clbc.2018.09.001
30. Bardia A, Mayer IA, Diamond JR, Moroose RL, Isakoff SJ, Starodub AN, et al. Efficacy and safety of Anti-Trop-2 antibody drug conjugate sacituzumab govitecan (IMMU-132) in heavily pretreated patients with metastatic triple-negative breast cancer. *JCO.* (2017) 35:2141–8. doi: 10.1200/JCO.2016.70.8297
31. Xie Y, Su N, Yang J, Tan Q, Huang S, Jin M, et al. FGF/FGFR signaling in health and disease. *Sig Transduct Target Ther.* (2020) 5:181. doi: 10.1038/s41392-020-00222-7
32. Khan AQ, Kuttikrishnan S, Siveen KS, Prabhu KS, Shanmugakonar M, Al-Naemi HA, et al. RAS-mediated oncogenic signaling pathways in human malignancies. *Semin Cancer Biol.* (2019) 54:1–13. doi: 10.1016/j.semcancer.2018.03.001
33. Rekhtman N, Pietanza MC, Hellmann MD, Naidoo J, Arora A, Won H, et al. Next-generation sequencing of pulmonary large cell neuroendocrine carcinoma reveals small cell carcinoma–like and non–small cell carcinoma–like subsets. *Clin Cancer Res.* (2016) 22:3618–29. doi: 10.1158/1078-0432.CCR-15-2946
34. Derks JL, Leblay N, Thunnissen E, van Suylen RJ, den Bakker M, Groen HJM, et al. Molecular subtypes of pulmonary large-cell neuroendocrine carcinoma predict chemotherapy treatment outcome. *Clin Cancer Res.* (2018) 24:33–42. doi: 10.1158/1078-0432.CCR-17-1921
35. Parachoniak CA, Rankin A, Gaffney B, Hartmaier R, Spritz D, Erlich RL, et al. Exceptional durable response to everolimus in a patient with biphenotypic breast cancer harboring an STK11variant. *Cold Spring Harb Mol Case Stud.* (2017) 3:a000778. doi: 10.1101/mcs.a000778
36. Levine AJ, Puzio-Kuter AM. The control of the metabolic switch in cancers by oncogenes and tumor suppressor genes. *Science.* (2010) 330:1340–4. doi: 10.1126/science.1193494
37. Nakanishi A, Kitagishi Y, Ogura Y, Matsuda S. The tumor suppressor PTEN interacts with p53 in hereditary cancer (review). *Int J Oncol.* (2014) 44:1813–9. doi: 10.3892/ijo.2014.2377
38. Laderian B, Mundi P, Fojo TE, Bates S. Emerging therapeutic implications of stk11mutation: case series. *Oncol.* (2020) 25:733–7. doi: 10.1634/theoncologist.2019-0846
39. Han D, Li S-J, Zhu Y-T, Liu L, Li M-X. LKB1/AMPK/mTOR signaling pathway in non-small-cell lung cancer. *Asian Pac J Cancer Prev.* (2013) 14:4033–9. doi: 10.7314/APJCP.2013.14.7.4033
40. Akeno N, Miller AL, Ma X, Wikenheiser-Brokamp KA. p53 suppresses carcinoma progression by inhibiting mTOR pathway activation. *Oncogene.* (2015) 34:589–99. doi: 10.1038/onc.2013.589
41. Shah MH, Goldner WS, Halfdanarson TR, Bergsland E, Berlin JD, Halperin D, et al. NCCN guidelines insights: neuroendocrine and adrenal tumors, version 2.2018. *J Natl Compr Canc Netw.* (2018) 16:693–702. doi: 10.6004/jnccn.2018.0056
42. Formisano L, Napolitano F, Rosa R, D'Amato V, Servetto A, Marciano R, et al. Mechanisms of resistance to mTOR inhibitors. *Crit Rev Oncol Hematol.* (2020) 147:102886. doi: 10.1016/j.critrevonc.2020.102886
43. Marton I, Knezevic F, Ramic S, Milosevic M, Tomas D. Immunohistochemical expression and prognostic significance of HIF-1α and VEGF-C in neuroendocrine breast cancer. *Anticancer Res.* (2012) 32:5227–32.
44. Pal K, Madamsetty VS, Dutta SK, Wang E, Angom RS, Mukhopadhyay D. Synchronous inhibition of mTOR and VEGF/NRP1 axis impedes tumor growth and metastasis in renal cancer. *NPJ Precis Oncol.* (2019) 3:31. doi: 10.1038/s41698-019-0105-2
45. Hobday TJ, Qin R, Reidy-Lagunes D, Moore MJ, Strosberg J, Kaubisch A, et al. Multicenter phase II trial of temsirolimus and bevacizumab in pancreatic neuroendocrine tumors. *JCO.* (2015) 33:1551–6. doi: 10.1200/JCO.2014.56.2082
46. Sabanathan D, Eslick GD, Shannon J. Use of neoadjuvant chemotherapy plus molecular targeted therapy in colorectal liver metastases: a

systematic review and meta-analysis. *Clin Colorectal Cancer*. (2016) 15:e141–7. doi: 10.1016/j.clcc.2016.03.007

47. Mosele F, Remon J, Mateo J, Westphalen CB, Barlesi F, Lolkema MP, et al. Recommendations for the use of next-generation sequencing (NGS) for patients with metastatic cancers: a report from the ESMO precision medicine working group. *Annals Oncol.* (2020) 31:1491–505. doi: 10.1016/j.annonc.2020.07.014
48. Le Tourneau C, Delord J-P, Gonçalves A, Gavoille C, Dubot C, Isambert N, et al. Molecularly targeted therapy based on tumour molecular profiling versus conventional therapy for advanced cancer (SHIVA): a multicentre, open-label, proof-of-concept, randomised, controlled phase 2 trial. *Lancet Oncol.* (2015) 16:1324–34. doi: 10.1016/S1470-2045(15)00188-6
49. Tsimberidou A-M, Hong DS, Ye Y, Cartwright C, Wheler JJ, Falchook GS, et al. Initiative for molecular profiling and advanced cancer therapy (IMPACT): an md anderson precision medicine study. *JCO Precis Oncol.* (2017) 2017:10. doi: 10.1200/PO.17.00002
50. Jovelet C, Ileana E, Le Deley M-C, Motte N, Rosellini S, Romero A, et al. Circulating cell-free tumor DNA analysis of 50 genes by next-generation sequencing in the prospective MOSCATO trial. *Clin Cancer Res.* (2016) 22:2960–8. doi: 10.1158/1078-0432.CCR-15-2470

Conflict of Interest: SS is employed by Datar Cancer Genetics Europe GmbH.

The remaining authors declare that the research was conducted in the absence of any commercial or financial relationships that could be construed as a potential conflict of interest.

frontiers | Frontiers in Medicine

TYPE Original Research
PUBLISHED 01 August 2022
DOI 10.3389/fmed.2022.933933

OPEN ACCESS

EDITED BY
Andrey Bychkov,
Kameda Medical Center, Japan

REVIEWED BY
Filippo Fraggetta,
Cannizzaro Hospital, Italy
Artyom Borbat,
State Research Center
Burnasyan, Russia
Doug Hartman,
University of Pittsburgh Medical
Center, United States

*CORRESPONDENCE
Lisa Browning
lisa.browning@ouh.nhs.uk

SPECIALTY SECTION
This article was submitted to
Pathology,
a section of the journal
Frontiers in Medicine

RECEIVED 01 May 2022
ACCEPTED 07 July 2022
PUBLISHED 01 August 2022

CITATION
Browning L, White K, Siiankoski D,
Colling R, Roskell D, Fryer E,
Hemsworth H, Roberts-Gant S,
Roelofsen R, Rittscher J and Verrill C
(2022) RFID analysis of the complexity
of cellular pathology workflow—An
opportunity for digital pathology.
Front. Med. 9:933933.
doi: 10.3389/fmed.2022.933933

RFID analysis of the complexity of cellular pathology workflow—An opportunity for digital pathology

Lisa Browning [1,2]*, Kieron White[1], Darrin Siiankoski[1], Richard Colling[1,3], Derek Roskell[1], Eve Fryer[1], Helen Hemsworth[1], Sharon Roberts-Gant[1], Ruud Roelofsen[4], Jens Rittscher[2,5] and Clare Verrill[1,2,3]

[1]Department of Cellular Pathology, Oxford University Hospitals NHS Trust, John Radcliffe Hospital, Oxford, United Kingdom, [2]NIHR Oxford Biomedical Research Centre, Oxford University Hospitals NHS Foundation Trust, Oxford, United Kingdom, [3]Nuffield Department of Surgical Sciences, John Radcliffe Hospital, University of Oxford, Oxford, United Kingdom, [4]Philips Digital and Computational Pathology, Precision Diagnosis Solutions, Best, Netherlands, [5]Department of Engineering Science, Institute of Biomedical Engineering, University of Oxford, Oxford, United Kingdom

Digital pathology (DP) offers potential for time efficiency gains over an analog workflow however, to date, evidence supporting this claim is relatively lacking. Studies available concentrate on specific workflow points such as diagnostic reporting time, rather than overall efficiencies in slide logistics that might be expected. This is in part a result of the complexity and variation in analog working, and the challenge therefore in capturing this. We have utilized RFID technology to conduct a novel study capturing the movement of diagnostic cases within the analog pathway in a large teaching hospital setting, thus providing benchmark data for potential efficiency gains with DP. This technology overcomes the need to manually record data items and has facilitated the capture of both the physical journey of a case and the time associated with relevant components of the analog pathway predicted to be redundant in the digital setting. RFID tracking of 1,173 surgical pathology cases and over 30 staff in an analog cellular pathology workflow illustrates the complexity of the physical movement of slides within the department, which impacts on case traceability within the system. Detailed analysis of over 400 case journeys highlights redundant periods created by batching of slides at workflow points, including potentially 2–3 h for a case to become available for reporting after release from the lab, and variable lag-times prior to collection for reporting, and provides an illustration of patterns of lab and pathologist working within the analog setting. This study supports the challenge in evidencing efficiency gains to be anticipated with DP in the context of the variation and complexity of the analog pathway, but also evidences the efficiency gains that may be expected through a greater understanding of patterns of working and movement of cases. Such data may benefit other departments building a business case for DP.

KEYWORDS

digital pathology, workflow, efficiency, time, analog, cost, radiofrequency identification (RFID), surgical pathology

Introduction

Digital pathology (DP) has taken center stage in the last few years within the setting of diagnostic pathology, and whilst to date only small numbers of laboratories worldwide have undergone a complete transition to DP for surgical pathology reporting, there are increasing numbers of departments embarking on the journey. The potential and actual benefits of adoption of DP are well-documented (1, 2); the promised utility of DP within diagnostic cellular pathology/surgical pathology services is many-fold (3), and includes the potential for time efficiency gains seen from a digital workflow as compared with the traditional "analog" workflow of glass slide microscopy. However, to date the evidence to support adoption of DP has necessarily been focused on proof of non-inferiority of digital diagnosis compared with traditional glass slides, with multiple large validation studies supporting the safety and quality aspects of DP for clinical diagnosis (4). Given the upfront financial investment needed to implement a DP set-up, the predicted cost-efficiencies associated with such gains become important within business cases put before funding bodies (3, 5, 6). Whilst generally it is claimed that DP is more time efficient and therefore has the potential to be more cost-efficient, much of the literature on this matter is subjective; there are very few published studies reporting on actual time efficiency or cost-benefit analyses of implementing DP and these parameters are difficult to capture and to compare due to inherent complexity of cellular pathology workflows, variability across centers and largely manual processes.

A report from a center in Granada, Spain (7) that has become fully digital, claims that since making the transition the pathologists are able to report on average 21% more cases per year. The detail of what facilitated this increase in productivity is not outlined in detail, but it would likely be related to more than just a change in the modality of reporting from glass to digital, and more a reflection of efficiency savings at multiple points within the journey of a case through the diagnostic laboratory. Few authors have attempted to break down the workflow pathway to analyze this in detail, and this is not surprising given its complexity. Ho et al. (8) sought to use contextual inquiry to gain an understanding of the complexities of the specimen journey, highlighting the concepts important to a pathologist within an analog workflow that would need to be considered during the development and transition to DP, in terms of how a pathologist approaches a case and progresses the case toward a diagnosis. This method was based upon observation of pathologists during a routine "sign-out service", during which time notes were made of activities performed in order to construct affinity diagrams and graphical models of aspects of the work process, and served to illustrate inefficiencies in the analog workflow within the "pathologist role" including technical interruptions, deficiencies of data needed to complete a case, and inefficiencies of manual interpretation of diagnostic parameters such as mitotic counts. However, this study did not investigate the wider analog workflow.

Reports in the literature which detail the impact on laboratory/diagnostic workflow associated with the adoption of diagnostic DP are mainly descriptive texts around the "journey" to DP (7, 9–14). There are a few studies which include data on the impact of DP on pathologist reporting times (analog vs. DP) (15, 16) or more broadly on the "value-added" potential of digital pathology, by way of its impact on operational measures such as cost, time, service quality (17). Whilst some authors claim that actual diagnostic reporting time for a pathologist is equivalent or even reduced on the digital platform (15), a recently reported comprehensive equivalency and efficiency study set within the clinical workflow (16), concluded that DP was associated with a median overall 19% decrease in efficiency per case compared with glass. However, these studies looked only at reporting time for a case, rather than comparison of time within the entire workflow, and as acknowledged by the authors of the latter study, time savings elsewhere within the workflow may offset the apparent increase they demonstrated in turnaround time associated with digitally reporting a case, again underscoring the complexity of capturing what an efficiency saving is.

There are only a handful of studies which have been dedicated to analyzing and/or evidencing the differences that may be expected between analog (glass slide-based) and digital pathology pathologist working in terms of aspects of the diagnostic workflow (18–21). For example, the time in motion study (18) detailed the components of the pathway analyzed within the lab (case entry and case assembly time) and the separate analysis of the components undertaken by the pathologist, which were broken down into slide review, reporting (i.e., report writing), workflow-related, and other. This study highlighted the potential for a 13.4% saving in pathologist time related to workflow factors which would be expected to be negated in a digital setting. This figure of 13.4% potential time efficiency saving has been quite frequently quoted within the literature related to "benefits of DP" and has been translated by the same group to provide a figure for potential increase in pathologist productivity (19).

It is recognized that the analog workflow is inherently inefficient, with numerous "stop points" which would potentially disappear within a digital workstream, and these studies to date highlight at least some of these inefficiencies, although none with an overview of the entire relevant workflow. However, as finances within healthcare are increasingly scrutinized, further evidence around aspects of the analog workflow that will be altered or removed with the transition to DP, in a variety of laboratory settings, will be important for business cases going forward and this must be balanced against steps that will be added with DP such as cleaning of slides, loading slides into scanners and the time slides spend in scanners—waiting to be

scanned, the scanning process (which in modern scanners is brief) and waiting to be unloaded.

We designed a novel study utilizing radiofrequency identification (RFID) technology to track the movement of surgical cases and personnel within a Cellular Pathology department over a set period of time, to analyze specific aspects of the workflow that we predicted could be at least partly negated in the move from an analog to a digital workflow. Through the unrestricted capture and analysis of both the physical movement of the slides and of personnel, and the duration of time for specific components of the workflow, we illustrate the complexity of the analog pathway and highlight areas of potential for efficiency savings and other significant gains in the digital workflow.

Methods

The study setting

The study was set in a large academic teaching hospital Cellular Pathology Department in 2019 prior to implementation of a fully digital pathology workflow for all surgical histology and referral cases which was completed in 2020 (13). The throughput is ∼340,000 surgical histology and immunohistochemistry slides per year, together with 4,100 extra-large slides, and 40,000 referral slides. With 29 consultant histopathologists, 2 specialty doctors, and 9 trainees we operate a specialized service divided into 11 subspecialties, including pediatric pathology (but excluding neuropathology and soft tissue/bone pathology which are served within other laboratories). There is pathology support for 28 multidisciplinary team (MDT) meetings. The departmental footprint is that of a laboratory in one area, but with consultant and other offices geographically spread across the hospital site.

The study was designed to analyze the post-laboratory (pathologist focused) journey of the glass slide from the lab, to the pathologist for reporting, and eventually back to storage/filing, and the associated movement of personnel. The rationale behind this was the anticipated shift in slide logistics with DP; we hypothesized that this part of the glass slide journey would be effectively removed with a digital workflow, as most glass slides would then need only to go from the automated H&E stainer to the "sign-out" bench in the lab, to the scanner, and then to be stored/filed whereas the laboratory processes with the exception of slide scanning would remain largely unchanged.

The study was conducted as a service evaluation audit of current practice without the need for ethics committee approval. Signed consent was sought from personnel within the department for their participation in the study related to the use of anonymized data and potential photographic images.

The RFID technology

Radiofrequency identification (RFID) technology uses electromagnetic fields to identify and track tags which can be embedded within an object. This negates the need for the object to be moved within the field of sight of a reader as would be necessary for a barcode, thus allowing the technology to be more discretely integrated with minimal impact on the system, in this case the laboratory workflow, being analyzed.

The use of RFID technology in healthcare is not new, with RFID technology deployed in a variety of settings such as the tracking of medical equipment/assets, tracking and managing drugs and patients, and tracking of blood supplies (22). Within pathology departments RFID technology has been utilized in recent years for quality improvement; to track pathology specimens and to ensure accurate patient identification (23–25). The technology for this study was therefore proven within the setting of a pathology laboratory, but within the literature to date had not been utilized specifically for analysis of time points within a pathology specimen workflow. The technology was selected for the ability to collect the complexity of data needed to track workflow in a cellular pathology laboratory.

Pre-study planning

Analysis of the workflow

The first step in the study was to gain a clear understanding of the analog laboratory workflow. This was necessary in order to decide; (i) which aspects of the workflow would be tracked, and (ii) how these would be tracked in an effective way with minimal disruption to both workflow and staff in a busy department.

We undertook a process mapping exercise to detail the journey of a surgical case from the laboratory to the pathologist and back to filing following provision of a histology report, and in so doing were able to identify a start and end point which would be consistent within both the analog and digital workflow, with the other steps in the process predicted to effectively disappear following this transition (Figure 1). The study would track the components that would be most significantly impacted by the transition from analog to digital working, both in terms of movement of cases ("assets") and personnel.

Optimal placement of the RFID readers was decided primarily on the basis of the workflow, although adjustments were necessary to minimize impact on the workflow itself, and to ensure technological success. Readers were placed at specific physical points which could be translated into an equivalent workflow point; at the start and end points of the workflow within the lab (the "sign-out" bench and "filing final", respectively) and then at points which would register specific tasks; the pigeon holes (PH) from where pathologists collected their cases, the secretarial office to track movement related to case distribution for teams operating a "pooled" system of cases

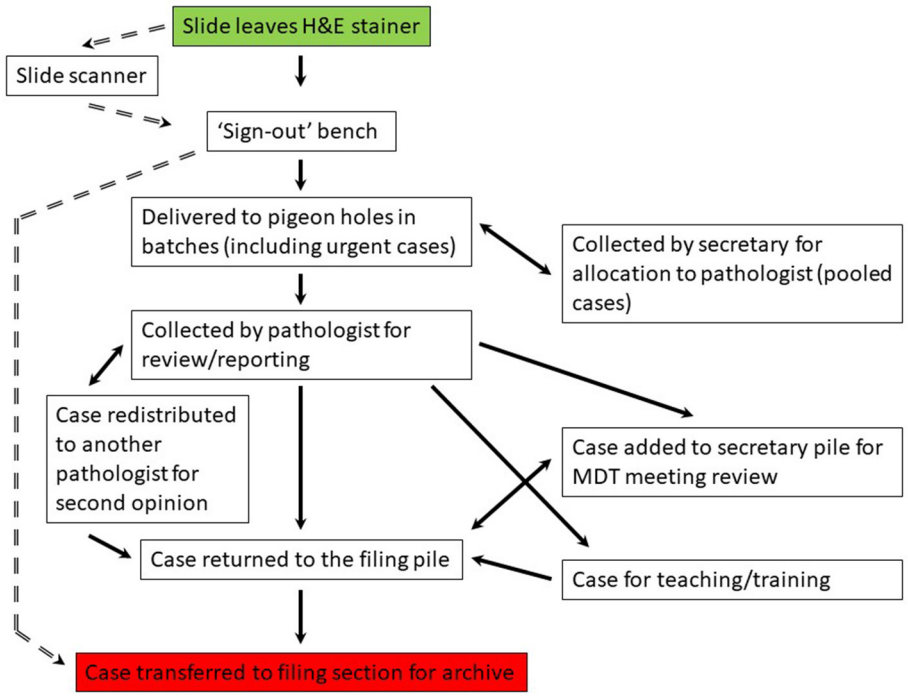

FIGURE 1
Process map for the laboratory workflow for a case from the point at which it is ready for pathology review to the return of the case for archiving following provision of a histology report. The analog workflow is on the right (solid arrows) and the predicted digital workflow is on the left (broken arrows). Start point (green) and end point (red) are the same for the analog and digital workflow. MDT, multidisciplinary team. Pigeon hole (PH) is the collection point for a diagnostic case by a pathologist, each having their own designated PH.

and for case movement related to multidisciplinary team (MDT) meetings, at pass points for pathologists as they relocated with the cases to their offices, the filing bench for return of reported cases by the PHs, and the final filing station within the lab from where slides would be archived. Slides are temporarily piled at the "filing pile" by the PH until they are relocated in batches by the laboratory technicians to the "filing final" bench within the lab from where they are returned to the archive.

The RFID equipment set-up

For the study we utilized a passive ultrahigh frequency (UHF) RFID system, with RFID tags for the tracking of cases, and RFID tags embedded in badges to be worn by personnel. Readers were installed for tracking of tags and for processing of the data and transmission to the data hub.

The RFID tags were individually attached to cardboard slide trays holding a surgical case—one case per tray in order to track movement of individual cases effectively. These trays were further identified with green labels in order that those handling the case (biomedical scientists, secretaries, pathologists) would be prompted to "register" the case on the desktop for specified fixed RFID tag readers (Figures 2A,B).

The RFID readers were either free-standing (Impinj, Seattle WA USA, Speedway xPortal^{TM} Integrated Portal Reader) to detect movement of a case or personnel, or designed to be placed under a desktop (Impinj, CS-777 Brickyard^{TM} Near-Field Antenna) to read tags associated with slide trays/cases placed onto a worksurface (Figures 2C,D). Placement of the RFID readers was based upon the understanding of the workflow. A period of testing ensured operability of the system (tracking of cases and transmission of the data to the hub), and importantly it ensured that the system was acceptable to users with minimal impact on the process being analyzed, and that there was no interference from the RFID system on laboratory equipment, such as temperature monitoring devices for refrigerators/freezers. Readers were placed at the start point where cases leave the lab from the sign out bench (in batches), at the doors at the end of the lab through which cases pass before they are distributed into the PH for collection by pathologists (designated PH doors), at several pass points within corridors and doors through which it was predicted that pathologists pass whilst transporting cases back to their workstations (offices) for review and reporting, at the filing pile by the PH where reported cases are routinely returned and are then batched and transported to the final filing bench back in the laboratory (Figure 3). The critical placement of the readers to ensure that they detected tags on cases at a specific workflow point and were not detecting tags of cases at another workflow point, meant that in areas

FIGURE 2
RFID tags attached to individual slide trays **(A)**, each tray designated for a single case. Tags could be detected by the RFID reader even when within piles of trays **(B)**. The position of the table top RFID reader (under the bench, see **C**) was indicated to the biomedical scientists by the placement of tape, within the bounds of which the tray was placed in order to "register" it **(D)**. This set up was present at the start and end point of the study at the sign-out bench and the filing final, respectively. Placement of RFID readers was on the basis of the process mapping of the workflow. The reader in D is that by the pigeon hole doors, placed to capture the movement of cases from the laboratory to the pigeon holes which was the point at which they were available to the pathologist. RFID, radiofrequency identification.

it was necessary to use surrogate locations for the readers (Supplementary Figure 1).

The RFID tags did not encode any patient identifiable data, and the RFID badges worn by personnel were anonymous; color-coded to the role of the wearer (lab technician vs. administrative staff vs. pathologist) and identified only by a number on the reverse.

The RFID data capture software (AUCXIS, Stekene Belgium, P-track) was installed on a laptop and this communicated with a database service (R-Connect). The RFID readers communicated over Wi-Fi with the R-Connect service through an access point. P-Track then visualized the raw data by means of a graphical user interface, providing the following output: (Time)—(EPC tag data)—(Tag Type) (Staff Badge or Tray Label) and (Reader Name) (location).

Case selection

We conducted the study over two separate time periods (study one = 21 days, 28 January to 17 February 2019, study two = 24 days, 4–27 March 2019) to allow sufficient time for most cases to follow the analog pathway (Figure 1), i.e., to leave the lab, undergo pathology review and reporting, and be returned to slide filing, allowing also for time for diversion from this pathway for example for MDT meeting review, second opinion, teaching.

The RFID labels were applied to slide trays for consecutive cases leaving the lab within the pathology specialties taking part in the study; urological pathology and gastrointestinal pathology (study 1), and breast pathology and dermatopathology (study 2). These specialties were selected due to; (i) the high-throughput of cases and turnaround times not impacted on for example by frequent requirements for ancillary tests associated with long lag-times such as molecular, and (ii) for specific workflow considerations such as the inclusion of the collation of cases in a pile in the secretarial office for the urology MDT meeting, or specialties operating a pooled system whereby biopsy cases were collected by a member of the secretarial staff once they had left the lab and then distributed evenly across pathologists within a specialty team, before being placed into the reporting pathologist's PH. These specialty-specific features would demonstrate the wider aspects of the analog workflow which would be transformed following transition to DP.

FIGURE 3
The "real-life" analog laboratory workflow which will effectively disappear with the transition to digital pathology. The cases leave the lab from the sign out bench **(A)** in batches, passing through the doors at the end of the lab (PH doors, **B**, see also Figure 2D) to be distributed into the PH **(C)** for collection by pathologists. Pathologists transport cases back to their workstations (offices) for review and reporting **(D)**, and then batch the cases prior to returning them to the filing bench (filing pile, **E**) from where they are collected several times daily and taken for filing at the "filing final" bench back in the laboratory **(F)**. The position of RFID readers in the images is indicated by the arrows. PH, pigeon holes.

Results

Study 1—Gastrointestinal pathology and urological pathology case workflow

There were 695 tagged cases for this study period which included focus on two specific workflow aspects which will not exist in a digital workflow;

- For one specialty the movement of biopsy cases from a "pool" by a secretary from the collection point at the PHs to their desk (in batches) for redistribution of the cases amongst the consultant team, and then placement back in the relevant consultant PH.
- The collation of cases for an MDT (urology)—cases piled at a specific location in the secretarial office which would be included in the weekly MDT meeting list for discussion,

and then returned after the MDT to the filing pile (and thence to filing final/archive).

The trace data from this study period clearly demonstrates the complexity of the pathway that a diagnostic case takes from the time it leaves the lab (*via* the PH doors) for diagnostic reporting to the time at which it is returned to filing. Figure 4A shows the numbers of cases logged at various workflow points and the route of a case between these workflow points. Specific workflow points of interest were those associated with the "reallocation of cases" amongst a specialty team, and the movement of a case to and from a "pile" for an MDT, and there were 74 and 35 readings at these workflow points, respectively. The detailed analysis revealed that of the 695 tagged cases, 93 cases (13%) had been traced from the start of the analog journey at the sign-out bench in the lab to the end point at the "filing final" point, with 9% of the cases being traced from sign-out bench to "pathologist" to "filing final". Whilst it is highly likely that a small proportion remained within the workflow at the end of the study period, particularly urological pathology cases which had been diverted to the pile of cases for the MDT meeting, it became apparent that technical tracking of tags was not optimal. This resulted in some traces not being complete and which was addressed prior to commencement of study period 2. The data from study 1 was then used to scope out the landscape of complexity of the pathway within the analog setting and inform subsequent analyses of the study 2 captured traces.

Study 2—Breast pathology and dermatopathology case workflow

Following study 1 the positioning of the RFID detectors was revised to ensure better data capture. There were 478 traced cases for this second study period. As for study 1, the workflow points captured by the RFID tags are illustrative of the complexity of the journey of a case (Figure 4B). In fact, there were 113 unique trace patterns identified which recorded different patterns of physical movement of a case through the workflow. The most common trace pattern was sign out bench—PH doors—filing pile—filing final (59 traces). A proportion of the cases did not complete the analog "journey" during the study period, as would be expected, or showed traces with an illogical sequence such as filing final as the first timestamp. In total, 33 traces were completely excluded from further analysis. There were 445 traces remaining, however given that a timestamp had not been registered at each of the workflow points for all traces they were analyzed individually to determine which timestamps were available and thus which data could be analyzed from each trace. The breakdown of trace analysis is given in Supplementary Figure 2.

For the analyses, the timestamp at the PH doors was used as a surrogate for availability of a case in the pathologist's PH for reporting; batching of cases at the sign out bench following the quality check meant that this (sign out bench) timestamp was not a reliable indicator of readiness for reporting.

Timestamps have been analyzed to determine aspects of the analog pathway that will be significantly impacted by a transition to DP, principally around time taken for a case that is ready to leave the lab to actually be available for a pathologist to report, and the time that a case remains out of the laboratory within the workflow and therefore potentially untraceable, as follows:

1. Sign out bench to PH doors
2. PH doors to pathologist
3. Sign out bench to return of case to filing pile
4. Sign out bench to return of case to filing final
5. Pathologist to return of case to filing final
6. Filing pile to filing final

The time data for workflow points 1, 3, 4, and 6 is presented in Table 1, with the more detailed analyses to include the "pathologist" timepoints (points 2 and 5) presented separately below.

Time taken for a case to become available for reporting (sign out bench to PH doors)

Once a case has been quality checked and is ready to leave the lab for reporting, it is batched at the sign out bench, and taken with other cases from the lab to be distributed within the PH. This activity is done in batches to make it time efficient within the analog pathway.

From Table 1 it can be seen that the median time a case would "wait" at the sign out bench was 5.5 min, and the mean time around an hour, however depending upon the time of day some cases would "wait" overnight to be delivered to the PH for reporting, with the longest delay being 40 h. Analysis of the timestamps for when cases were made available to pathologists (PH doors) is presented in Figure 5A. Whilst there is a spread of times that cases leave the lab during the day, it is seen that 45% of cases (125 of 280 with relevant traces) leave the lab before 14:00, although with few leaving the lab before 10:00, and that there is a peak between 15:00 and 18:00 when almost 50% of the cases leave the lab (138 of 280 cases). This is not unexpected given the pre-analytical laboratory steps for a case subsequent to routine overnight tissue processing (including block cutting, H&E staining, cover-slipping, slide labeling); tasks usually completed in the morning. It is noteworthy though that a third of cases left the lab after 16:00.

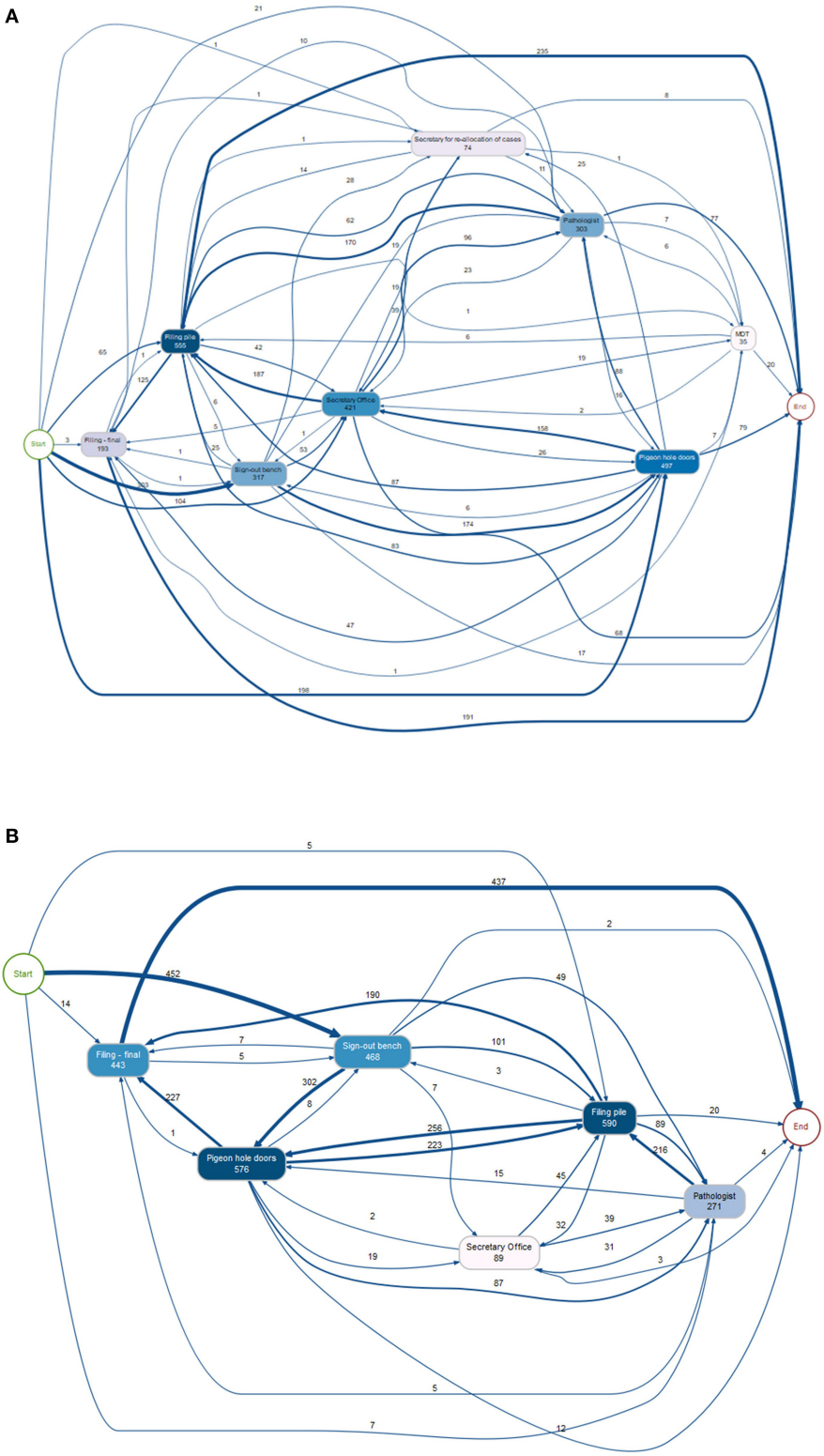

FIGURE 4
Diagrams showing the tracking of cases during the study period, with the number of cases following each pathway and being registered at each workflow point as shown, some being registered more than once at each point. **(A)** Study period 1 (695 cases). The movement of cases from the PH to the secretary for redistribution amongst a specialty team of pathologists, and then back to the PH for collection by a pathologist is shown (74 reads), as well as the movement of cases to the MDT pile for collation for the weekly meeting (35 reads), with 20 being returned to filing during the study period. **(B)** Study period 2 (478 cases). PH , pigeon holes; MDT, multidisciplinary team.

TABLE 1 Time taken between specified workflow points in the analog pathway.

	Number of available traces with the data	Range of time (minutes)	Mean time (minutes)	Median time (minutes)
Sign-out to PH doors	280	0.3–2,414.4	68.5	5.5
Sign-out to filing pile	387	3.6–29,014.6	5,855.8	3,912.8
Sign-out to filing final	402	214–27,047.6	7,134.9	4,395.3
Filing pile to filing final	396	1.2–20,185.7	1,461.8	1,069.2

PH, pigeon hole.

Time taken for a case to reach a pathologist (PH doors to pathologist)

There were 59 traces with the pathologist timestamp in the workflow which provided data to illustrate when cases were collected for reporting, and a means to demonstrate patterns in the way in which a pathologist works within the analog pathway (see also Supplementary material).

Sixty-nine percent of the cases (41 of 59) were collected by a pathologist on the same day that they left the lab, and by the end of day 2, 85% of cases had been collected (50 of 59). The remaining 15% were collected on or after day 3, with the longest interval until collection of a case being 8 days. The lag time for the 15% of cases not collected on day 1 or 2 will include weekends and potentially other days a pathologist was not available, due for example to less than fulltime working.

In terms of length of time taken for the cases to be collected by a pathologist after leaving the lab (for 59 cases), the range was 0–9,594 min (day 8), with a mean of 1,199 min (∼20 h) and a median of 125 min. Restricting the analysis to cases collected on day 1 (41 cases), the range was 0–1,320 min, with a mean of 118 min and a median of 79 min.

Figure 5B illustrates that there is a pattern to the time of day that pathologists appear to collect cases for reporting. Overall, of cases leaving the lab after 15:00 ($n = 29$), 15 (52%) are collected on day 1 but a further 8 (28%) are not collected until day 2, or later (20%). For cases collected on the same day as they have been made available from the lab (day 1), the peak time for cases to be collected by pathologists is between 14:00 and 18:00 (32 cases, 78%), with 22 cases (54%) being collected after 16:00 (Figure 5C). This appears to indicate that generally there is a lag of a couple of hours between the peak time at which cases are made available, and the time at which cases are collected. If this pattern holds true across all of the cases leaving the lab, then given that we have seen that a third of cases leave the lab after 16:00 it could be estimated that overall around 15% of cases per day will not be collected for diagnostic reporting until the following day if they are not "ready" from the lab for collection in the PH by 16:00.

Time that a case remains out of the laboratory within the diagnostic workflow (sign out bench to return to filing)

The analysis of time that a case has spent in different parts of the workflow provides additional detail in relation to time that a case is effectively "out of circulation"; periods during which the case would potentially be difficult to locate within the department should it be needed.

From analysis of the relevant trace data (Supplementary Figure 2) it is seen that once a case has left the lab (sign out bench), the average time before it is returned to the final filing point for archiving is 7,135 min (almost 5 days), with the shortest period being 214 min, and the longest period recorded being 27,048 min (almost 19 days, Table 1). This time period partly reflects turnaround time for a case for generation of a diagnostic report, and we have not specifically collected data on this for the purpose of this study, however it will also include time periods for which the cases have been diverted from the pathway for an MDT meeting, or for activities such as teaching. It is recognized that pathologists also tend to batch cases for return to limit the number of trips to the lab, and indeed the times of day that cases are logged back at the filing pile for archiving show similarity to the times at which cases are made available for collection by pathologists (Figure 6A) indicating perhaps an attempt by pathologists to optimize time efficiency by returning reported cases when new cases are collected.

Time taken for a case to reach the final filing station after it is returned to the lab

The onward return of the cases to filing final for archiving is an additional workflow inefficiency, as illustrated by the average wait of cases for 1,462 min (24 h) to be filed ready for archiving, although a good proportion of the cases were filed much faster than this (1st quartile = 114 min, data for 399 cases). The efficiency of this activity appears to be at least partly dependent

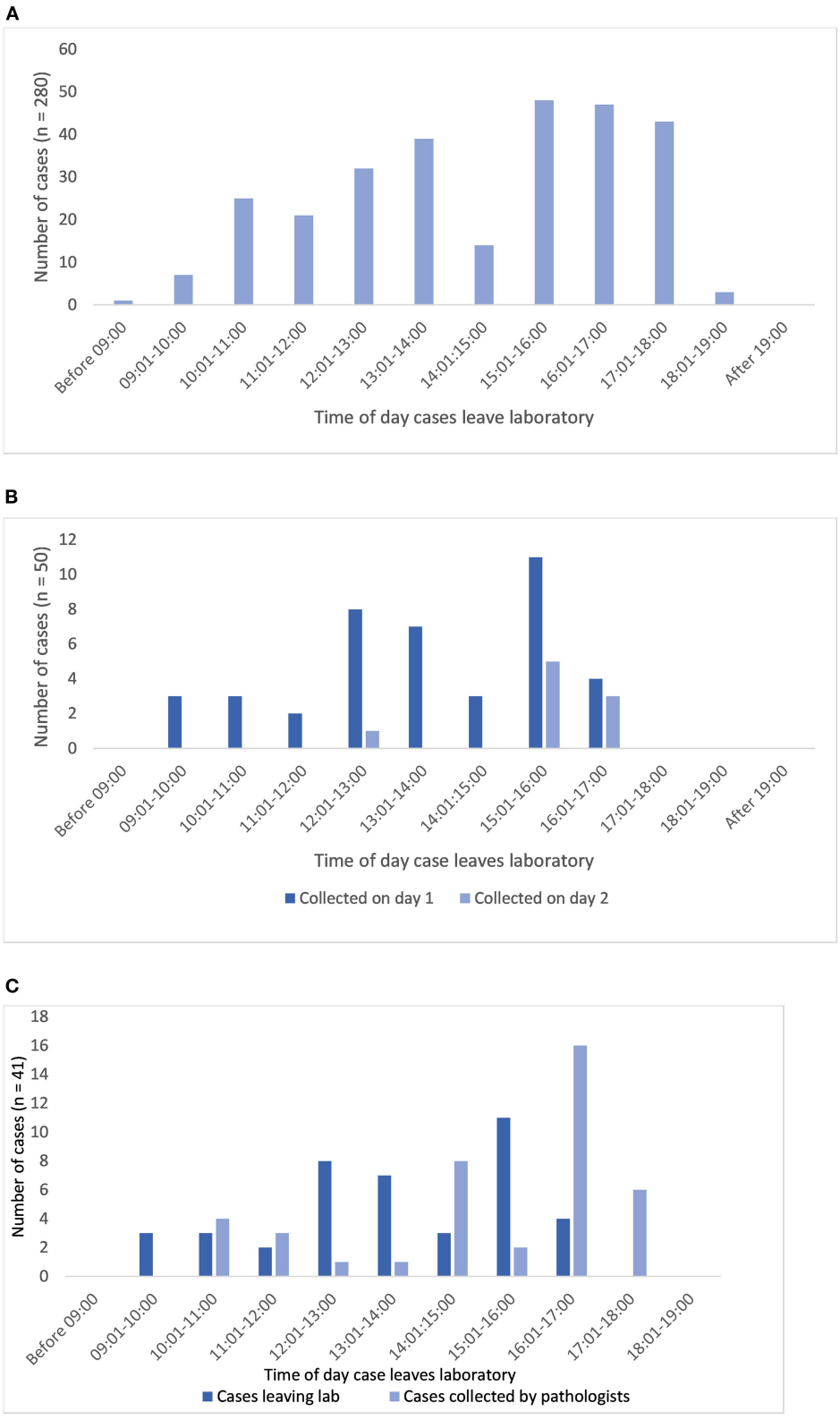

FIGURE 5
(A) Shows the distribution of times that diagnostic cases leave the lab *via* the pigeon hole doors at which point they are available for a pathologist to collect and report ($n = 280$ cases). **(B,C)** Show analysis limited to the traces with both PH doors and pathologist timestamps ($n = 59$ cases). **(B)** Shows the correlation of times that cases leave the lab and the times that pathologists collect cases (cases collected on day 1 or 2 only, $n = 50$). **(C)** Shows the time distribution of cases leaving the lab which were collected by pathologists on day 1 (same day, $n = 41$).

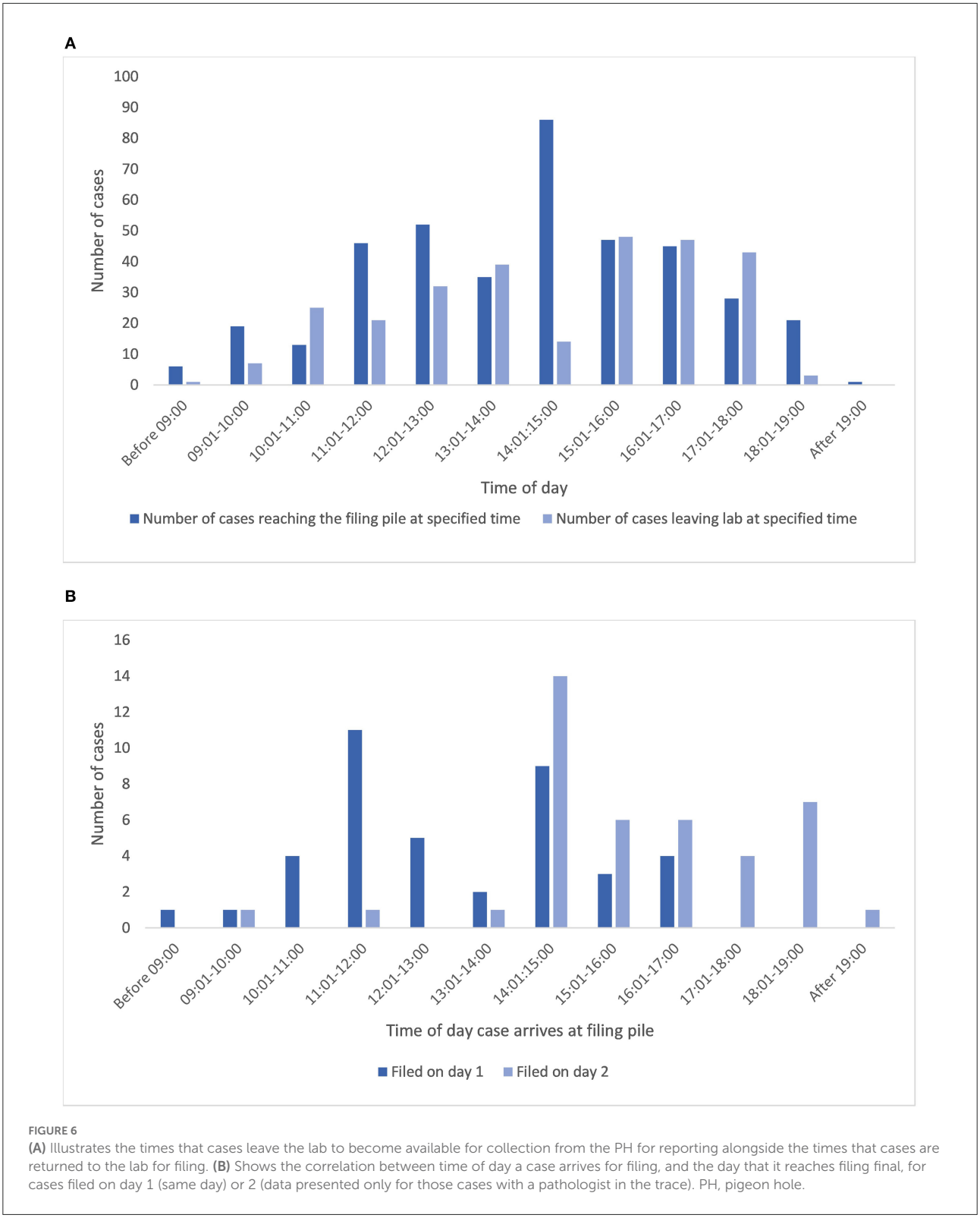

FIGURE 6
(A) Illustrates the times that cases leave the lab to become available for collection from the PH for reporting alongside the times that cases are returned to the lab for filing. **(B)** Shows the correlation between time of day a case arrives for filing, and the day that it reaches filing final, for cases filed on day 1 (same day) or 2 (data presented only for those cases with a pathologist in the trace). PH, pigeon hole.

upon the time that a case is returned for filing. Figure 6B illustrates the data related to this activity for traces which also included a pathologist and that were filed on day 1 or 2 after being returned, showing that 60% (24 of 40) of cases that reached the filing pile before 14:00 and 83% of those before 15:00 were filed (filing final) on the same day that they had reached the filing

pile, whereas of the 41 cases filed on day 2, 93% had reached the filing pile after 14:00. Overall of these cases, 44% of cases were returned to the final filing/archive bench on the same day as they were placed in the filing pile, and 90% had been returned to filing final by the end of day 2, with 98% of cases having been filed by the end of day 4, and the rest by day 6.

Movement of personnel

Movement of cases within the workflow was associated with movement of personnel, divided into the role categories of biomedical scientists, secretarial staff, and pathologists. For illustrative purposes we captured the movement of staff utilizing the RFID tagged badges they wore, detected at the same workflow points as the diagnostic cases. For study 2, 31 personnel wore RFID-tagged badges: 15 BMSs, 9 pathologists, 7 secretarial/administrative staff. Whilst the movement of individual personnel could be captured as they were registered at the various workflow points, the purpose of this part of the study was more to capture an overview of personnel movement; where different categories of personnel were at different times. This data (Figure 7), shows patterns in terms of the times of day that personnel are detected at various workflow points, with the PH doors (pigeonholes) being a particularly "busy" location, and patterns as to which locations people in particular roles are detected.

Discussion

Considerable evidence exists within the literature around the pathologist experience and quality assurance aspects of DP, mostly around the validation process and concordance between DP and glass. However, in spite of claims that DP is of potential benefit in improvement of laboratory and pathologist efficiency there is a dearth of evidence around this subject, and specifically in respect to the potential impact of DP on laboratory workflow and slide logistics. In fact, a recent review by Jahn et al. (2) comments that "there is no real-life cost-efficiency analysis for full DP implementation with sufficient (>5 years) follow-up". Most studies to date focus on operational savings as a whole rather than detailed analysis of existing workflows and the potential thereby to understand the elements that may benefit most from the transition to DP, not only through time efficiency gains, but in the wider context of patient safety and quality improvement. Baidoshvili et al. (20) undertook physical measurements of time taken within various aspects of an analog workflow, comparing this with a digital workflow in a laboratory setting in The Netherlands handling around 220 cases/day. They captured potential time efficiency savings in slide logistics of up to 1,147 min/day across five key workflows (>19 h), including case assembly and transfer to pathologists, slide archiving, MDT preparation. Their study provides an assessment of potential time efficiencies in components of the analog pathway, however it does not capture the real-life movement of cases within the analog workflow and the variability in this, nor the sheer complexity of the case journey, which has additional impact on routine working. It is the inherent difficulty in capturing the complexity of workflows that likely contributes to the lack of such available data, which we attempt to address in this novel study. Utilization of RFID technology has allowed automated and continuous tracking of cases throughout the entirety of the post-laboratory workflow, evidencing the actual movement of cases within the laboratory and wider department, and illustrating the pathways a case follows which are sometimes deviant from that expected, impacting potentially on case traceability. This technology has facilitated direct measurement of timestamps for cases at pivotal pathway points, allowing detailed observation of the analog workflow in a manner that is not easily captured with manual recording, although it was not issue free and adjustments were needed to capture the data more optimally.

A key aspect of the transition to DP often focused upon is the prediction of improved turnaround times (TAT) in diagnostic reporting. TAT is seen as a measure of quality within the practice of cellular pathology, which is influenced by a myriad of factors of which the laboratory need to be aware (26). Instinctively a shortened turnaround time would result from the instant availability of a case digitally after booking out from the lab, negating the need for the physical movement of a case to a pathologist, which in our department involves collection of cases from a designated location next to the lab, the "pigeon hole" (PH). Both the booking out of the cases from the lab at the sign out bench and the manual transportation of cases to the PH is typically done in batches, immediately conferring a delay in case availability. Our study has captured a mean lag time of around an hour for cases waiting in the lab to be taken to PHs, and a further lag time of around 2 h before pathologists collect cases from their PH for reporting. In our system therefore a digital workflow could potentially negate an average 2–3 h of "delay" in a case reaching a pathologist for reporting. Whilst there is accepted variability between laboratories in terms of workflow, this specific aspect of physically getting cases from the lab to the pathologist will be reproducible across laboratory settings to at least some extent and this data therefore offers an indication of a relevant efficiency gain that will be transferable. The study from Baidoshvili et al. (20) showed that similar workflow components (preparation of a case to leave the lab, batching, and transfer of cases to pathologist) took 640 min/day (for around 200 cases), and predicted that in the digital workflow this would be reduced to 36 min/day for the same number of cases. We also noted that whilst 52% of cases leaving the lab after 15:00 were still collected on the same day, a further 28% were not collected until the following day, or later (20%). Perhaps significantly, given that we demonstrated that around one third

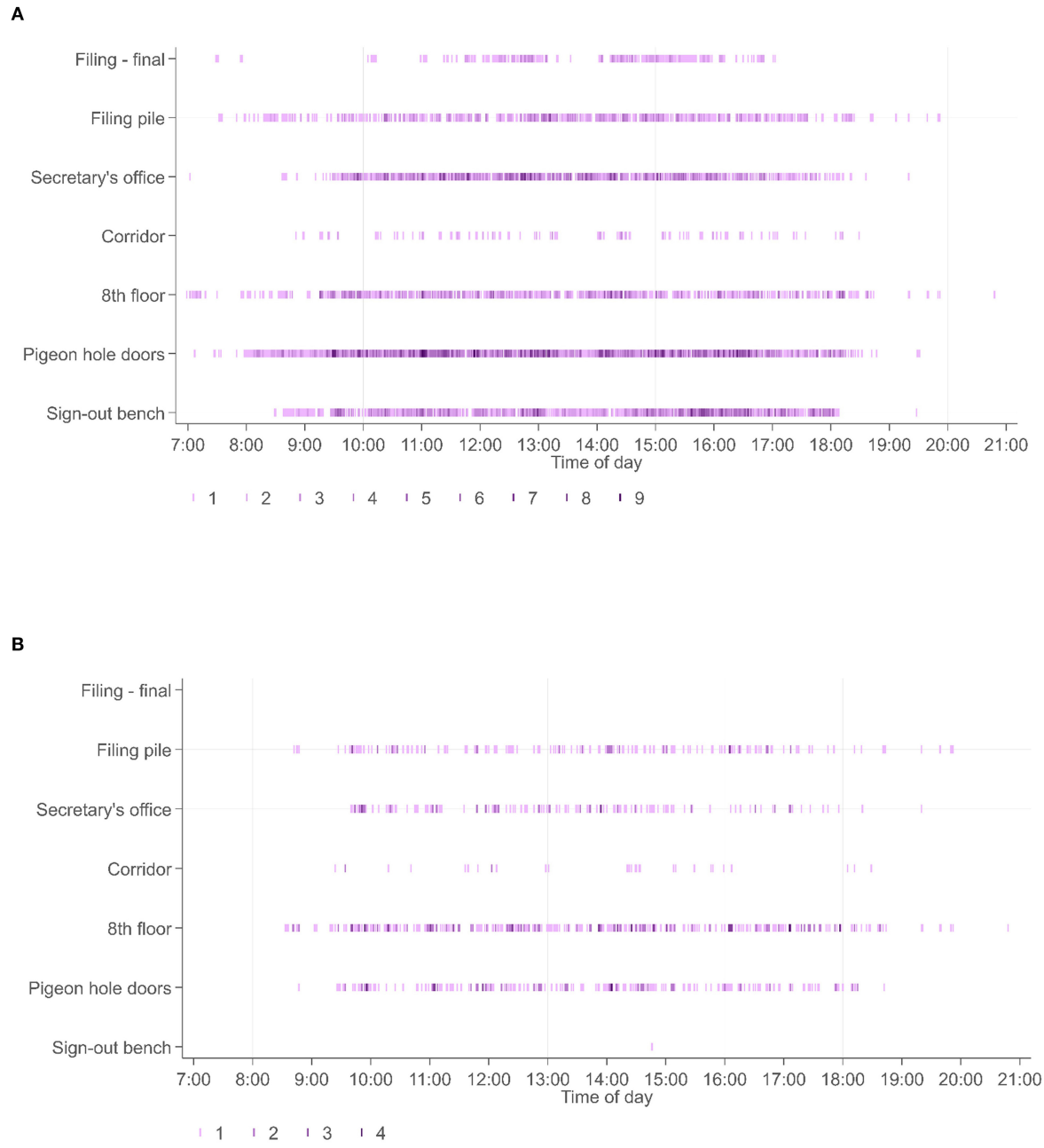

FIGURE 7
(A) Shows the timestamps at specific workflow points across all 31 personnel wearing RFID tagged badges (biomedical scientists, secretaries, pathologists), presented across the entire period for study 2. By contrast **(B)** shows the locations of pathologists within this workflow over the same time period. It is seen that pathologists do not spend time at the sign out bench or filing final pile (locations more frequently visited by biomedical scientists), and that the timestamps are related to readers associated with collection of cases (PH doors), relocation of cases to their offices (8th floor and corridor readers) or to return of cases (filing pile).

of cases leave the lab after 16:00, this potentially translates to 15% of cases not being collected for reporting on the same day that they leave the lab. These few hours "saved" through the instant digital access to a case could facilitate same day reporting of greater numbers of cases, or requests to the lab for extra work, also having potential impact on case turnaround time which is increasingly important as a performance indicator in addition to the direct benefit on patient management pathways. Furthermore, whilst not captured in detail in our study, the time taken for pathologists to physically collect and return cases

and the interruptions in the working day needed to do this, will be an additional important efficiency saving with DP. The concept of the pathologist as an operator or machine who can only undertake one task at one time is described in a previous study of workflow scheduling in pathology laboratories (27).

In all of these assumptions it must be acknowledged that these potential savings will be dependent upon the set-up/order of workflow in a digital pathway. Furthermore, it should also be considered that in the overall TAT for a case within the workflow (from receipt to authorization of a diagnostic report), there will be an impact from the scanning time *per se*, and the loading of cases onto the scanner, as well as the quality control process (which is likely to vary between labs in terms of where it falls within the pathway). However, by contributing an understanding of the real-life journey of a case and the working patterns of both the lab and the pathologist within the existing analog workflow, this study may aide the design of a digital workflow to optimize efficiency gains.

The physical delivery of glass slide cases in batches for a pathologist to report, the "push" approach, does not generally allow ready identification of cases within the pile according to their clinical urgency nor does it accommodate variation in pathologist availability (28). We have shown there is a variation in lag time from the earliest opportunity that a case is available from the lab to the time it is collected for reporting, which includes extended periods likely accounted for by flexible working patterns. Indeed, whilst there was a median time interval of around 2 h (mean time interval of 20 h) before a case was collected for reporting we saw that 15% of cases were collected on day 3 or later after being made available from the lab. We do not have specific details as to working patterns to account for these findings, but it illustrates the variation that exists. Pooling of cases for reallocation across a team is an option available in an analog workflow to accommodate such variation, however this introduces additional manual work into the system such as secretarial redistribution with associated additional movement of cases as we have shown in the first part of our study. A digital workflow offers the opportunity for any pathologist to see all cases that are ready for reporting, which can be tagged according to clinical urgency to enable prioritization of reporting. Cases can be "pulled" from this digital workflow and more easily distributed amongst a team and in accordance with availability, potentially offering a ready means to smooth the flow of work and turnaround times.

Perhaps the most compelling feature of the data presented is the complexity of the pathways that these diagnostic cases took. Whilst we had process-mapped the predicted pathways we had not anticipated the extent and variation of the physical movement of a case around the department between the time it was available for reporting and the time that it was returned to the final filing point from which it could be safely archived. Significantly, the time period that a case is out of the lab but not in filing, is one in which it is typically challenging to locate in current analog systems, which results in significant wasted time looking for slides if they are needed, and the inherent risk of a case going "missing". Whilst a case may be traceable when physically with a pathologist, we have shown that the cases spend significant redundant time at multiple other points within the pathway such as re-distribution by administrative personnel, in a pile for an MDT meeting, in a pre-archive filing pile, during which time the case is effectively out of circulation and would be difficult to locate if needed. In our study the average time that a case spent effectively "out of circulation" within the workflow (from sign out to return to filing final for archiving) was around 5 days, although the range was 214 min to 19 days. Part of this time was accounted for by a case waiting for an average of 24 h within a "pre-filing" pile to be transported to the filing station for archiving. By returning the glass slides to the archive after scanning, these remain accessible should they be needed, with the digital images freely accessible to those with access, whether this is for diagnostic reporting, teaching, MDT meetings, clinical trial review, etc.

Whilst we did not capture time taken by administrative staff to collate cases for an MDT meeting, as others have shown (20) this is also a point of potential time efficiency gain in the digital workflow, partly given that cases can evidently be out with the archive for long periods of time when they may be needed. Our own observations are echoed in a recent commentary on digital pathology experience from a Dutch group (14) which remarks in the context of preparation for an MDT meeting, that "*a resident would spend about a full day collecting slides from the archive or the desks of our 30 pathologists and residents*".

Finally, we were also able to capture the complexities of the movement of personnel with the RFID badges worn by study participants, which varied according to their role (pathologist vs. biomedical scientist vs. secretary). There were clearly busy locations in terms of the workflow points, and it is predicted that a digital workflow would negate a substantial amount of this personnel movement, creating another time efficiency that may otherwise not have been so easily evidenced. In the current setting of the pandemic, this movement is not without potential risk, and the impact of DP in this context (29, 30), will likely continue into the foreseeable future.

On the basis of the literature to date, we would regard our study as probably the longest in terms of duration, and the largest in terms of the number of cases for which data has been captured, and with analysis of activity of the broadest range and number of personnel. We acknowledge that some data is incomplete but overall the data presented offers a detailed analysis of the "post-laboratory" journey of a surgical case; to the best of the authors knowledge no other studies to date have reported on continuous capture of similar data over such a time period. As we have shown in our study, the complexity of the analog pathway cannot be under-estimated, and efficiencies gained within a digital workflow will be multifactorial and

not limited to saving time and potential improvements in turnaround times.

The potential inefficiencies seen in an analog workflow that could be addressed with digital pathology relate to batching with redundant time periods, physical movement of staff and cases, and loss or temporary unavailability of slides for which time is spent on locating them. Although concrete time efficiency savings are difficult to extrapolate in this study when moving from analog to digital, clear potential for improved patient safety aspects with DP are seen due to case traceability, and availability of slides for review and discussion at MDT, as well as potential for improvement in diagnostic reporting times resulting from more timely case availability.

Importantly, access to digital pathology underpins the potential benefit anticipated from the future integration of artificial intelligence into the workflow (31). It is challenging therefore to "pin down" exact cost savings that could be presented as part of a business case to support transition to DP as there are many "softer" savings and additional benefits that do not have direct cost implications. There is also the potential for revenue opportunities within the digital laboratory which may offset financial outlay in the longer term (6). Such opportunities may be within the context of increasing the caseload of a department enabled by digital working across sites, but also include contribution to more academic avenues such as image analysis and computational pathology. Indeed, in the UK there is an increasing recognition of the value of industry partnerships with the NHS and universities to aid the development of advanced diagnostics and ultimately improvement in patient care, which may also provide revenue back to the NHS.

Study limitations

The main limitation of our study in terms of the impact on the transferability of the potential efficiency gains that we have reported, is that it has been conducted within a single institution. This is not unique in terms of pre-existing studies looking at efficiency related to analog and digital workflows, but transferability of the study outcomes to other laboratory settings will be dependent upon the workflow which, as we have discussed, is typically variable across laboratories. We have however highlighted the aspects of our study data that we feel will be most transferable, and aspects such as complexity of the pathways that cases follow in the analog setting is likely to be a consistent feature across institutions.

We have acknowledged within our Section Results the limitations of our study in terms of the deficiencies of data collected during study period 1 in particular, which was attributed to technical issues related to the placement of readers which were set up within a functioning laboratory setting. In this respect the study was ambitious in the aim of capturing data with readers necessarily set within fairly close confines in the workplace, but we wanted to be able to operate the study within a real-life setting with as little impact on the system being analyzed as possible. In spite of this relative limitation, we still captured the movement of over 1,000 cases, and had detailed data from 400 case journeys to allow meaningful analysis of the analog workflow. The complexity of the case journey was underestimated, and whilst this provides strong evidence for aspects of potential safety and quality gains with a digital workflow, it necessitated detailed manual downstream data analysis, with unavoidable redundancy of some data which had been collected. We recognize that we have not captured data from our LIMS which could have provided additional timestamps for analysis, such as those related to cases being booked out of the lab, or to reports being authorized by pathologists. We appreciate that this may have further augmented the study, but we feel that we have illustrated sufficient detail in the analog pathway to benefit the understanding of the pinch points in the workflow, and foresee that this will be beneficial even to the optimization of existing analog workflows in departments who are yet to consider the digital transition. Finally, whilst we have not covered the entire range of subspecialties within the department we do not believe this to impact upon the validity of the main take home messages which are related to complexity of pathways and the pinch points, which we feel will be similar regardless of the specialty analyzed. Certainly in our own department the workflow from lab to pathologist and pathologist back to the lab, would not generally be specialty-specific.

Conclusion

In this study we have utilized a novel approach to capturing the glass slide-based (analog) cellular pathology workflow within a large teaching hospital setting, using RFID technology. The complexity of the workflow that we have illustrated is evidence of the challenge in capturing workflow data, which may in part explain the relative lack of evidence of efficiency savings by "going digital" and implementing digital pathology to date. We demonstrate the lag times in the analog workflow before a case reaches a pathologist for reporting, and the patterns of analog working that will be redundant with DP, and the potential for at least some unnecessary time in physical movement of slides and personnel around the department, and redundant time when cases are not moving through the workflow. Our intention is to reassess the workflow with DP fully implemented within our laboratory, however since the analog data was captured the unanticipated changes imposed on our working lives by the COVID-19 pandemic has meant that a future study will need to take into consideration the resultant change in work patterns, and significantly any remote working. Although we recognize that there may be differences in workflows between laboratories, this study is an attempt to provide evidence around potential

efficiencies within this specific but significant portion of the workflow of a surgical case which may benefit a business case for DP in other settings. Importantly having detailed tracking data gives us a baseline position and enables the creation of complementary lean workflows for pathologists and lab staff to optimize chances of cases being available as soon as possible and navigating pinch points.

Data availability statement

The raw data supporting the conclusions of this article will be made available by the authors, without undue reservation.

Author contributions

LB, KW, DS, and CV contributed to the conceptualization of the study and the study design. Technical input in relation to the RFID equipment and set-up, and the data acquisition and initial processing was provided externally, as detailed within the manuscript. LB led the analysis of the data with input from KW and CV. The manuscript was drafted by LB and reviewed and revised by CV. All authors contributed to the final drafting of the manuscript and approved the final paper.

Funding

This paper was supported by the PathLAKE Center of Excellence for Digital Pathology and Artificial Intelligence which was funded from the Data to Early Diagnosis and Precision Medicine strand of the HM Government's Industrial Strategy Challenge Fund, managed, and delivered by Innovate UK on behalf of UK Research and Innovation (UKRI). Grant Ref: File Ref 104689/Application Number 18181. CV and LB are part funded by the National Institute for Health Research (NIHR) Oxford Biomedical Research Center (BRC). CV also receives funding support from the Chinese Academy of Medical Sciences (CAMS) Innovation Fund for Medical Science (CIFMS), China (Grant Number: 2018-I2M-2-002). Philips (Amsterdam, Netherlands) provided the following funding for this study: the RFID equipment (Impinj, Seattle, WA, USA), data capture software (AUCXIS, Stekene, Belgium), and the preliminary data analysis which was commissioned from CQM (Consultants in Quantitative Medicine, Eindhoven, Netherlands).

Acknowledgments

With thanks to the digital pathology steering group in the department of Cellular Pathology at the John Radcliffe Hospital, Oxford for their support in setting up this study, and to the biomedical scientists, administrative staff, and pathologists who took part in the study. Manuel Salto-Tellez and Jacqueline A. James are Principal Investigators in PathLAKE at Queens's University Belfast, Nasir Rajpoot is Principal Investigators in PathLAKE at the University of Warwick, Emad Rakha is Principal Investigator in PathLAKE at the University of Nottingham and David Snead is Principal Investigator in PathLAKE at University Hospitals Coventry Warwickshire—all were involved in generating the PathLAKE program, including funding.

Conflict of interest

JR is a co-founder of Ground Truth Labs. CV is the principal investigator of a study evaluating Paige Prostate. University of Oxford and Oxford University Hospitals NHS Foundation Trust are part of the PathLAKE consortium. PathLAKE has received in kind industry investment from Philips. Philips (Amsterdam, Netherlands) provided the following funding for this study: the RFID equipment (Impinj, Seattle WA USA), data capture software (AUCXIS, Stekene Belgium), and the preliminary data analysis which was commissioned from CQM (Consultants in Quantitative Medicine, Eindhoven, Netherlands). RR has a role as Product Manager for Philips (Digital and Computational Pathology).

The remaining authors declare that the research was conducted in the absence of any commercial or financial relationships that could be construed as a potential conflict of interest.

Publisher's note

Author disclaimer

Views expressed are those of the authors and not necessarily those of the PathLAKE Consortium members, the NHS, Innovate UK or UKRI.

Supplementary material

The Supplementary Material for this article can be found online at: https://www.frontiersin.org/articles/10.3389/fmed.2022.933933/full#supplementary-material

References

1. Williams BJ, Bottoms D, Treanor D. Future-proofing pathology: the case for clinical adoption of digital pathology. *J Clin Pathol.* (2017) 70:1010–8. doi: 10.1136/jclinpath-2017-204644

2. Jahn SW, Plass M, Moinfar F. Digital pathology: advantages, limitations and emerging perspectives. *J Clin Med.* (2020) 9:3697. doi: 10.3390/jcm9113697

3. Hanna MG, Ardon O, Reuter VE, Sirintrapun SJ, England C, Klimstra DS, et al. Integrating digital pathology into clinical practice. *Mod Pathol.* (2022) 35:152–64. doi: 10.1038/s41379-021-00929-0

4. Azam AS, Miligy IM, Kimani PK, Maqbool H, Hewitt K, Rajpoot NM, et al. Diagnostic concordance and discordance in digital pathology: a systematic review and meta-analysis. *J Clin Pathol.* (2020). 74:448–55. doi: 10.1136/jclinpath-2020-206764

5. Williams BJ, Bottoms D, Clark D, Treanor D. Future-proofing pathology part 2: building a business case for digital pathology. *J Clin Pathol.* (2019) 72:198–205. doi: 10.1136/jclinpath-2017-204926

6. Lujan G, Quigley JC, Hartman D, Parwani A, Roehmholdt B, Meter BV, et al. Dissecting the business case for adoption and implementation of digital pathology: a white paper from the digital pathology association. *J Pathol Inform.* (2021) 12:17. doi: 10.4103/jpi.jpi_67_20

7. Retamero JA, Aneiros-Fernandez J, Del Moral RG. Complete digital pathology for routine histopathology diagnosis in a multicenter hospital network. *Arch Pathol Lab Med.* (2020) 144:221–8. doi: 10.5858/arpa.2018-0541-OA

8. Ho J, Aridor O, Parwani AV. Use of contextual inquiry to understand anatomic pathology workflow: implications for digital pathology adoption. *J Pathol Inform.* (2012) 3:35. doi: 10.4103/2153-3539.101794

9. Thorstenson S, Molin J, Lundström C. Implementation of large-scale routine diagnostics using whole slide imaging in Sweden: digital pathology experiences 2006-2013. *J Pathol Inform.* (2014) 5:14. doi: 10.4103/2153-3539.129452

10. Cheng CL, Azhar R, Sng SH, Chua YQ, Hwang JS, Chin JP, et al. Enabling digital pathology in the diagnostic setting: navigating through the implementation journey in an academic medical centre. *J Clin Pathol.* (2016) 69:784–92. doi: 10.1136/jclinpath-2015-203600

11. Evans AJ, Salama ME, Henricks WH, Pantanowitz L. Implementation of whole slide imaging for clinical purposes: issues to consider from the perspective of early adopters. *Arch Pathol Lab Med.* (2017) 141:944–59. doi: 10.5858/arpa.2016-0074-OA

12. Stathonikos N, Nguyen TQ, Spoto CP, Verdaasdonk MAM, van Diest PJ. Being fully digital: perspective of a Dutch academic pathology laboratory. *Histopathology.* (2019) 75:621–35. doi: 10.1111/his.13953

13. Colling R, Protheroe A, Sullivan M, Macpherson R, Tuthill M, Redgwell J, et al. Digital pathology transformation in a supraregional germ cell tumour network. *Diagnostics.* (2021) 11:2191. doi: 10.3390/diagnostics11122191

14. Stathonikos N, Nguyen TQ, van Diest PJ. Rocky road to digital diagnostics: implementation issues and exhilarating experiences. *J Clin Pathol.* (2021) 74:415–20. doi: 10.1136/jclinpath-2020-206715

15. Vodovnik A. Diagnostic time in digital pathology: a comparative study on 400 cases. *J Pathol Inform.* (2016) 7:4. doi: 10.4103/2153-3539.175377

16. Hanna MG, Reuter VE, Hameed MR, Tan LK, Chiang S, Sigel C, et al. Whole slide imaging equivalency and efficiency study: experience at a large academic center. *Mod Pathol.* (2019) 32:916–28. doi: 10.1038/s41379-019-0205-0

17. Isaacs M, Lennerz JK, Yates S, Clermont W, Rossi J, Pfeifer JD. Implementation of whole slide imaging in surgical pathology: a value added approach. *J Pathol Inform.* (2011) 2:39. doi: 10.4103/2153-3539.84232

18. Stratman C, Drogowski L, Ho J. *Digital Pathology in the Clinical Workflow: A Time & Motion Study [Conference Presentation]*. San Diego, CA: Pathology Visions (2010). Available online at: https://digitalpathologyassociation.org/pathology-visions-2010 (accessed January 28, 2022).

19. Ho J, Ahlers SM, Stratman C, Aridor O, Pantanowitz L, Fine JL, et al. Can digital pathology result in cost savings? A financial projection for digital pathology implementation at a large integrated health care organization. *J Pathol Inform.* (2014) 5:33. doi: 10.4103/2153-3539.139714

20. Baidoshvili A, Bucur A, van Leeuwen J, van der Laak J, Kluin P, van Diest PJ. Evaluating the benefits of digital pathology implementation: time savings in laboratory logistics. *Histopathology.* (2018) 73:784–94. doi: 10.1111/his.13691

21. Hanna MG, Reuter VE, Samboy J, England C, Corsale L, Fine SW, et al. Implementation of digital pathology offers clinical and operational increase in efficiency and cost savings. *Arch Pathol Lab Med.* (2019) 143:1545–55. doi: 10.5858/arpa.2018-0514-OA

22. Álvarez López Y, Franssen J, Álvarez Narciandi G, Pagnozzi J, González-Pinto Arrillaga I, Las-Heras Andrés F, et al. Technology for management and tracking: e-health applications. *Sensors.* (2018) 18:2663. doi: 10.3390/s18082663

23. Bostwick DG. Radiofrequency identification specimen tracking in anatomical pathology: pilot study of 1067 consecutive prostate biopsies. *Ann Diagn Pathol.* (2013) 17:391–402. doi: 10.1016/j.anndiagpath.2013.04.007

24. Pantanowitz L, Mackinnon AC, Jr., Sinard JH. Tracking in anatomic pathology. *Arch Pathol Lab Med.* (2013) 137:1798–810. doi: 10.5858/arpa.2013-0125-SA

25. Norgan AP, Simon KE, Feehan BA, Saari LL, Doppler JM, Welder GS, et al. Radio-frequency identification specimen tracking to improve quality in anatomic pathology. *Arch Pathol Lab Med.* (2020) 144:189–95. doi: 10.5858/arpa.2019-0011-OA

26. DeSimone Mi, Heher YK. A Framework for Utilization of Turnaround Time as a Quality Metric in Surgical Pathology. *AJSP Rev Reports.* (2022) 27:142–8. doi: 10.1097/PCR.0000000000000522

27. Azadeh A, Baghersad M, Farahani MH, Zarrin M. Semi-online patient scheduling in pathology laboratories. *Artif Intell Med.* (2015) 64:217–26. doi: 10.1016/j.artmed.2015.05.001

28. Bracey T. Digital pathology. Can scanning and storing the contents of microscope slides simplify the logistical challenges faced by pathologists today. *Bull Royal Coll Surg England.* (2017) 99:93–6. doi: 10.1308/rcsbull.2017.93

29. Browning L, Colling R, Rakha E, Rajpoot N, Rittscher J, James JA, et al. Digital pathology and artificial intelligence will be key to supporting clinical and academic cellular pathology through COVID-19 and future crises: the PathLAKE consortium perspective. *J Clin Pathol.* (2021) 74:443–7. doi: 10.1136/jclinpath-2020-206854

30. Lujan GM, Savage J. Shana'ah A, Yearsley M, Thomas D, Allenby P, et al. Digital pathology initiatives and experience of a large academic institution during the coronavirus disease 2019 (COVID-19) pandemic. *Arch Pathol Lab Med.* (2021) 145:1051–61. doi: 10.5858/arpa.2020-0715-SA

31. Rakha EA, Toss M, Shiino S, Gamble P, Jaroensri R, Mermel CH, et al. Current and future applications of artificial intelligence in pathology: a clinical perspective. *J Clin Pathol.* (2021) 74:409–14. doi: 10.1136/jclinpath-2020-206908

Advantages of publishing in Frontiers

OPEN ACCESS
Articles are free to read for greatest visibility and readership

FAST PUBLICATION
Around 90 days from submission to decision

HIGH QUALITY PEER-REVIEW
Rigorous, collaborative, and constructive peer-review

TRANSPARENT PEER-REVIEW
Editors and reviewers acknowledged by name on published articles

Frontiers
Avenue du Tribunal-Fédéral 34
1005 Lausanne | Switzerland

Visit us: www.frontiersin.org
Contact us: frontiersin.org/about/contact

REPRODUCIBILITY OF RESEARCH
Support open data and methods to enhance research reproducibility

DIGITAL PUBLISHING
Articles designed for optimal readership across devices

FOLLOW US
@frontiersin

IMPACT METRICS
Advanced article metrics track visibility across digital media

EXTENSIVE PROMOTION
Marketing and promotion of impactful research

LOOP RESEARCH NETWORK
Our network increases your article's readership